Production of Antibacterial Polyhydroxyalkanoates for Biomedical Applications

Piarali, S.

Production of Antibacterial Polyhydroxyalkanoates for Biomedical Applications

Sheila Azim Piarali

A thesis submitted to the University of Westminster in candidature for the award of the degree of Doctor of Philosophy

April 2020

I declare that the presented work was carried out in accordance with the Guidelines and Regulations of the University of Westminster. The work is original except where indicated by special reference in the text.

The submission as a whole or part is not substantially the same as any that I previously or am currently making, whether in published or unpublished form, for a degree, diploma or similar qualification at any university or similar institution.

Until the outcome of the current application to the University of Westminster is known, the work will not be submitted for any such qualification at another university or similar institution.

Any views expressed in this work are those of the author and in no way represent those of the University of Westminster.

Signed: Sheila Azim Piarali

Date: July 2019

First of all, I would like to thank God for giving me strength and courage to surpass all my difficulties during this project.

Being part of this project was indeed a challenge and overcoming it would not have been possible without the people and organisations listed here.

I cannot thank enough my previous supervisor, Dr. Moritz von Stosch, for advertising this PhD position to me and I am thankful for the financial support from the European Union's Horizon 2020 research and innovation program, Marie Skłodowska-Curie Grant Agreement No. 643050 (HyMedPoly Project).

I would like to express my sincere gratitude to my supervisors Prof. Ipsita Roy and Dr. Jochen Salber for always showing availability to support me and to guide me. For their will in seeing their students succeed and for always pushing us to deliver our best. For their kindness and patience.

In Westminster, I would like to acknowledge with appreciation Barbara and Rinat whose help and knowledge was crucial for the start of my project. I thank my colleagues Isabel, Alexandra, Elena, Pooja, Hima and Moyin, my colleagues in Bochum, Patricia and Ayesha and my colleagues from the HyMedPoly project for the great companionship throughout these years. I would like to especially thank my friends, Isabel, Patricia and Alexandra for supporting me when I most needed.

I am forever grateful for the help given by the staff at the University of Westminster, especially by Neville Antonio and for the help provided by the Department of Medical Microbiology, especially by Lennart, Felix, Jennifer and Martina.

I am thankful to Dr. Maxim Ryadnov from the National Physical Laboratory, for providing the antimicrobial peptides and Prof. Dr. Jürgen Groll from the Universität Würzburg, Germany for providing the six-armed star-shaped poly(ethylene oxide-stat-propylene oxide) containing isocyanate end groups, NCO-sP(EO-stat-PO). I would like to thank Prof. Dr. Axel Rosenhahn and her PhD student Wenfa Yu for their support with the water contact angle measurements, to PD DR. Sabine Seisel and Dr. Nicola Morden for their support with the scanning electron microscopy, to Phan Thanh Binh for her support with the GC-MS measurements and to Dr. Labrini for her help with the XPS measurements.

I would like to thank my friends, Marta, Rita, Beatriz, Duarte, Páscoa, Valter and Diogo for their time, for their curiosity, for their advices and for their will in motivating me. I would like to thank João Miguel, Hugo, Nicole, Jason, Ralf, Margarita, Tânia, Carolina and Fred for their moral support and for their friendship.

Finally, I am blessed for always having the support of my family, especially from my grandmother, Farida, my mother, Karima, my father, Azim, my sister, Sarah and my boyfriend João. Thank you for believing in me, for always being there when I needed, for all your love and all your prayers.

"Struggle is the meaning of life; defeat or victory is in the hands of God. But struggle itself is man's duty and should be his joy." - Sir Sultan Muhammad Shah Aga Khan III

The failure of implants is often linked to an early contamination by bacteria leading to biofilm formation, causing tissue-related infections or device-related infections. This, allied with the lack of efficacy of antibiotics against biofilms, emphasizes the need to develop new locally acting antibacterial materials in clinical and medical settings.

The main aim of this research project was to develop a novel class of polyhydroxyalkanoates with added antibacterial functionalities for biomedical applications. Polyhydroxyalkanoates were produced by bacterial fermentation using glucose as the carbon source. Poly(3-hydroxybutyrate), P(3HB), was obtained from *Bacillus subtilis* OK2 and poly(3-hydroxyoctanoate-co-3-hydroxydecanoate), P(3HO-co-3HD) was obtained from *Pseudomonas mendocina* CH50. A chemical characterisation was carried out to confirm the identity of the polymers produced. Furthermore, the physical characterisation identified P(3HB) as a stiff, strong and brittle material, and P(3HO-co-3HD) as a ductile, weak and soft material.

Considering the materials properties, P(3HB) was selected to improve the performance of medical devices by acting as an antibacterial coating while P(3HO-co-3HD) was selected to be processed as antibacterial tissue engineering fibre-based scaffold.

Novel films composed of P(3HB) and varying percentages of small molecule trans-cinnamaldehyde were developed for their potential use as bioactive materials. Evidence that trans-cinnamaldehyde was incorporated in P(3HB) films was supported by the chemical characterisation of the materials. In addition, the physical characterisation of the newly developed materials showed an improvement of the mechanical properties and an increased pore content in comparison to the pristine material.

The antibacterial characterisation of the materials confirmed their activity against Gram-positive and Gram-negative bacteria. Additionally, the materials with the highest loadings of trans-cinnamaldehyde were able to maintain a biocidal effect for a period of 7 consecutive days and prevent biofilm formation. Such promising results led to the formulation of new P(3HB)/trans-cinnamaldehyde solutions to coat polyurethane tubes as a preliminary experience which could later be translated into the coating of medical devices such as central venous catheters. Polyurethane tubes were dpi-coated with different solutions of P(3HB) and trans-cinnamaldehyde. Surface analysis was performed by evaluating different cross-sections of the materials and the results showed that that the extraluminal layer of the coating was

highly porous relative to that of the uncoated polyurethane and that the intraluminal layer became less smooth. The antibacterial properties were tested against *S. epidermidis* (ATCC® 35984™) and the results confirmed the antibacterial, anti-adhesive and anti-biofilm properties of the materials. Additionally, the materials showed a cytotoxic effect on L929 murine fibroblasts, however haemocompatibility studies confirmed a non-haemolytic effect of the coated materials on erythrocytes.

On the other hand, the development of P(3HO-co-3HD) based antibacterial materials was done by physically adsorbing antimicrobial peptides, AMP3, Nut2 and LL-37, individually, or biofilm-disrupting enzyme Dispersin B. The chemical characterisation performed on the films confirmed the presence of the agents on its surface. Wettability studies showed that the surface of the materials adsorbed with high molecular weight agents such as LL-37 and Dispersin B became more hydrophilic and that the surface of the materials adsorbed with lower molecular weight agents such as AMP3 and Nut2 remained similar to that of the original material. Furthermore, the antibacterial characterisation showed that the modified P(3HO-co-3HD) materials were able to reduce bacterial adhesion of Gram-positive and Gram-negative bacteria. Moreover, the cytotoxic evaluation of the materials showed that L929 murine fibroblasts were able to proliferate on all modified surfaces. In order to explore its potential as a fibrous tissue engineering scaffold with antibacterial properties, P(3HO-co-3HD) fibres were produced by electrospinning. Microscopy analysis showed the presence of aligned and beadless fibres. Two approaches were studied to add antibacterial functionalities to P(3HO-co-3HD) fibres, namely a physical adsorption process and a covalent coupling of the agents.

Since the surface properties of the materials such as wettability are known to play a critical role in the process of eukaryotic tissue cell adhesion, proliferation and differentiation as well as bacterial adhesion, the wettability properties of the newly developed materials were assessed as well as its cytotoxicity and antibacterial activity. Overall, the wettability properties changed significantly as the materials became hydrophilic, the fibre materials excellent cell viability and excellent anti-adhesive and anti-biofilm properties. In conclusion, a new class of antibacterial polyhydroxyalkanoates with added antibacterial, anti-adhesive and anti-biofilm functionalities was developed serving as potential alternatives and complementary strategies in many biomedical applications.

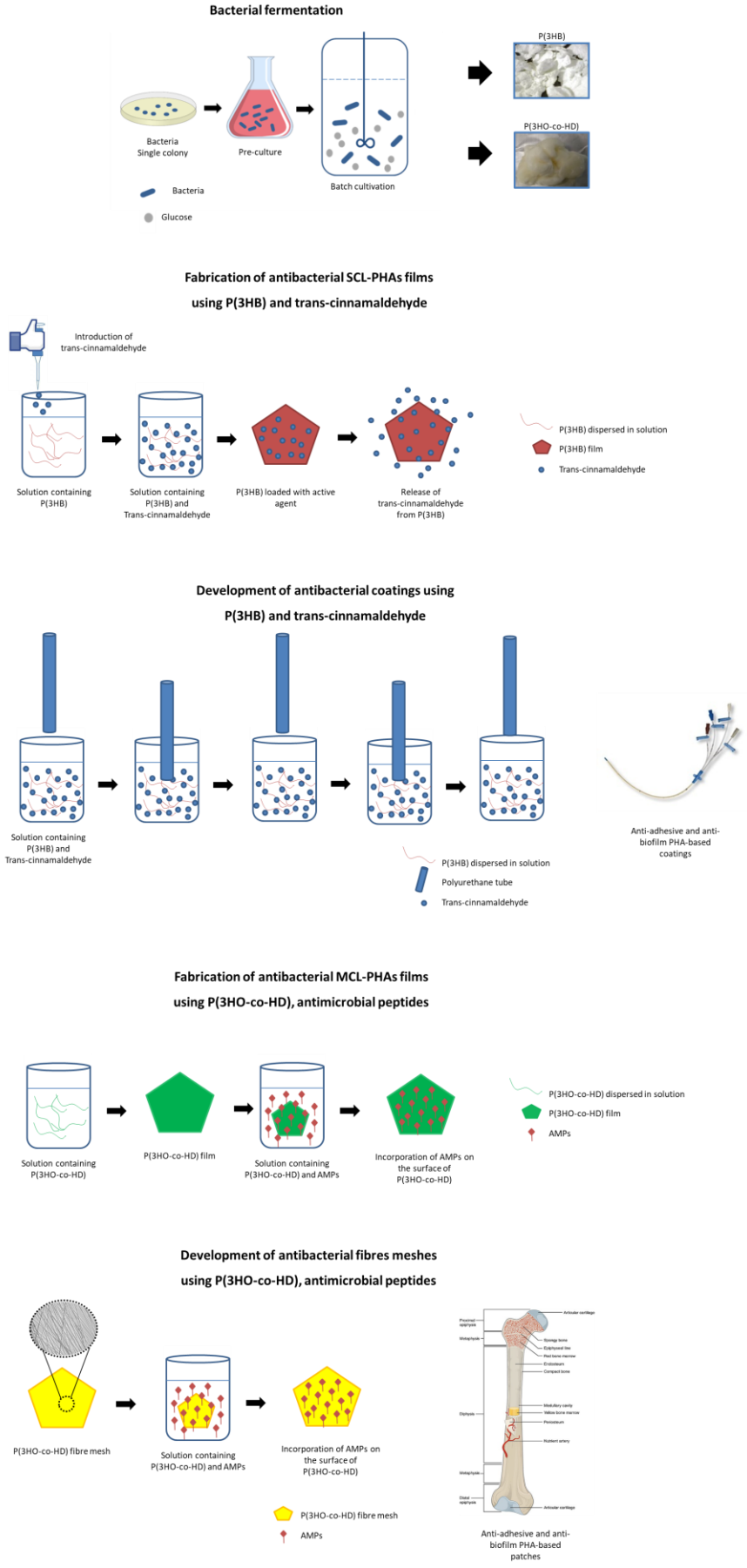

Figure 1: Graphical abstract highlighting the most important tasks of the project.

3HD – 3-hydroxydecanoic acid

3HDD – 3-hydroxydodecanoic acid

3HHx – 3-hydroxyhexanoic acid

3HO – 3-hydroxyoctanoic acid

3HTD – 3-hydroxytetradecanoic acid

3OC12-HSL – 3-oxo-dodecanoyl acyl homoserine lactone

AgNPs – silver nanoparticles

agr – accessory gene regulator

AHLs – N-acyl homoserine lactones

AI-2 – furanosyl borate

AIs – autoinducers

AIPs – autoinducer peptides

AMPs – antimicrobial peptides

ANOVA – one-way analysis of variance

ATR-FTIR – Attenuated Total Reflectance Fourier Transform Infrared Spectroscopy

BCA assay – Bicinchoninic acid assay

BG – bioglass

C4-HSL – N-butanoyl acyl homoserine lactone

CAUTI – catheter-associated urinary tract infections

CC_{50} – 50% cytotoxicity concentration

$CDCl_3$ – deuterated chloroform

CEF – cefamandole nafate

CFU – colony forming units

CH_3 – methyl

CH_2 – methylene

CH-SS – chlorhexidine–silver sulfadiazine

CLABSI – central line associated bloodstream infections

CoNS – Coagulase-negative *Staphylococci*

CRBSI – Catheter-related bloodstream infection

cRPMI – Completed Roswell Park Memorial Institute

CS-NPs – chitosan nanoparticles

CVC – central venous catheters

DB – dispersin B

DCW – dry cell weight

DHPS – dihydropteroate synthase

DMSO – Dimethyl sulfoxide

DNS – Dinitrosalicylic acid

DPBS – Dulbecco's Phosphate-Buffered Saline

DSC – differential scanning calorimetry

E – Elastic modulus

ε_b – Elongation at break

eDNA – extracellular DNA

EDA – ethylenediamine

Eos – essential oils

EPS – extracellular polymeric substances

EthD-III – Ethidium homodimer-III

EUCAST – European Committee on Antimicrobial Susceptibility Testing

FWHM – Full width at half maximum

GC-MS – Gas Chromatography-Mass Spectrometry

HAE – highest antibacterial effect

HAIs – hospital-acquired infections

hBD-3 – human β-defensin-3

HSL – homoserine lactone

IMF – intermolecular forces

ISO – International Organisation for Standardisation

K/R – Kannan and Rehacek

LPS – lipopolysaccharides

MBC – minimum bactericidal concentration

MCL-PHAs – medium-chain-length-PHAs

MHB – Mueller Hinton Broth

MIC – minimum inhibitory concentration

MRSA – methicillin-resistant *Staphylococcus aureus*

MRSE – methicillin-resistant *Staphylococcus epidermidis*

MSM – Mineral salt media

NCO-sP(EO-stat-PO) – amphiphilic six-armed star-shaped poly(ethylene oxide-stat-propylene oxide) containing reactive isocyanate groups at the distal ends of the polymer chains

NIST – National Institute of Standards and Technology

NMR – Nuclear Magnetic Resonance

OECD – Organisation for Economic Co-operation and Development

P(3HB) – Poly(3-hydroxybutyrate)

P(3HB-3HV) – poly(3-hydroxybutyrate-co-3-hydroxyvalerate)

P(3HB-co-3HHx) – poly(3-hydroxybutyrate- co-3-hydroxyhexanoate)

P(3HB-co-3HV-co-3HHx) - poly(3-hydroxybutyrate-co-3-hydroxyvalerate-co-3-hydroxyhexanoate)

P(3HB)/nHA – poly(3-hydroxybutyrate)/nano-hydroxyapatite

P(3HHx) – poly(3- hydroxyhexanoate)

P(3HHx-co-3HO) – poly(3-hydroxyhexanoate-co-3-hydroxyoctanoate)

P(3HO) – poly(3-hydroxyoctanoate)

P(3HO-co-3HD) – poly(3-hydroxyoctanoate-co-3-hydroxydecanoate)

P(3HO-co-12%3HHx) – poly(3-hydroxyoctanoate-co-12%3-hydroxyhexanoate)

P(4HB) – poly(4-hydroxybutyrate)

PE – polyethylene

PEG – poly(ethylene glycol)

PHAs – polyhydroxyalkanoates

PHACOS – poly-3-hydroxy-6-acetylthiohexanoateco-4-acetylthiobutanoate

PJI – prosthetic joint infections

PLA – polylactic acid

PLGA – poly(DL-lactide-co-glycolide)

PMMA – polymethacrylic acid

PMNs – polymorphonuclear leukocytes

PNAG – β-1,6-poly-N-acetylglucosamine

PQS – *Pseudomonas* quinolone signal

PS – polystyrene

PU – polyurethane

QS – quorum sensing

QSI – quorum sensing inhibitors

QQ – quorum quenchers

RPMI – Roswell Park Memorial Institute

RTP – rosa rugosa tea polyphenol

SCL-PHAs – short-chain-length-PHAs

SDS – Sodium dodecyl sulfate

SEM – Scanning Electron Microscopy

T_c – peak crystallisation temperature

T_g – glass transition temperature

T_m – melting temperature

TC – trans-cinnamaldehyde

TCPS – tissue culture polystyrene

TES – Trace elements solution

TMS – tetramethylsilane

UC-MSCs – umbilical cord mesenchymal stem cells

UHV – Ultra-high vacuum system

UVGI – ultraviolet germicidal irradiation

VAP – ventilator-associated pneumonia

vvm – Gas volume flow per unit of liquid volume per minute

WCA – Water Contact Angle

XPS – X-ray photoelectron spectroscopy

ZDEC-PU – zinc diethyldithiocarbamate containing polyurethane

σ – tensile stress

1 Chapter 1 Introduction

1.1 Bacterial infection, major cause of morbidity and mortality

Bacteria are naturally existing microorganisms and one of the first life forms on earth. Besides their role in many biological processes, such as nitrogen fixation, there are numerous species that are pathogenic and cause infection (Hogan, 2014). One of the main concerns of modern medicine is the increasing number of bacteria that are becoming resistant not to one, but to multiple antibiotics (Levy and Marshall, 2004). Also, the extreme resistance of bacterial biofilms to antibiotics is a dangerous development (Lewis, 2001).

Bacteria can spread infection as free cells, also called planktonic cells. Planktonic cells are responsible for several acute infections which, in the past, were effectively eradicated using antibiotics or vaccines. However, with time, bacteria have developed resistance mechanisms and have become more and more tolerant to conventional treatments. In order to give a historical background, the treatment of acute infections started with penicillin, in 1928, initiating the beginning of a new era for the development of modern antibiotics, which prevented millions of deaths. Notwithstanding, whenever a new drug was developed and proven to be effective, bacteria would rapidly develop a form of resistance (Figure 2). Nowadays, this problem is clearly becoming more evident and there are many causes associated with the development of antibiotic resistance. They include the overuse and misuse of antibiotics, inappropriate prescription, excessive use of antibiotics as growth supplements in livestock, lack of new drug development and regulatory barriers. All the listed causes have resulted in the natural selection of the most resistant bacterial strains and consequent failure of the available treatments (Ventola, 2015).

Unfortunately, the problem does not stop there. Apart from the current difficulty in treating acute infections, microbial infections caused by biofilms are also becoming a serious health threat. Besides being able to spread infections as free cells, bacteria can also spread infections as aggregates. Bacterial aggregates, commonly termed as biofilms are not only much more difficult to control with conventional therapies but they are also the source of many recalcitrant infections (Lister *et al*., 2014, Lebeaux *et al*., 2014).

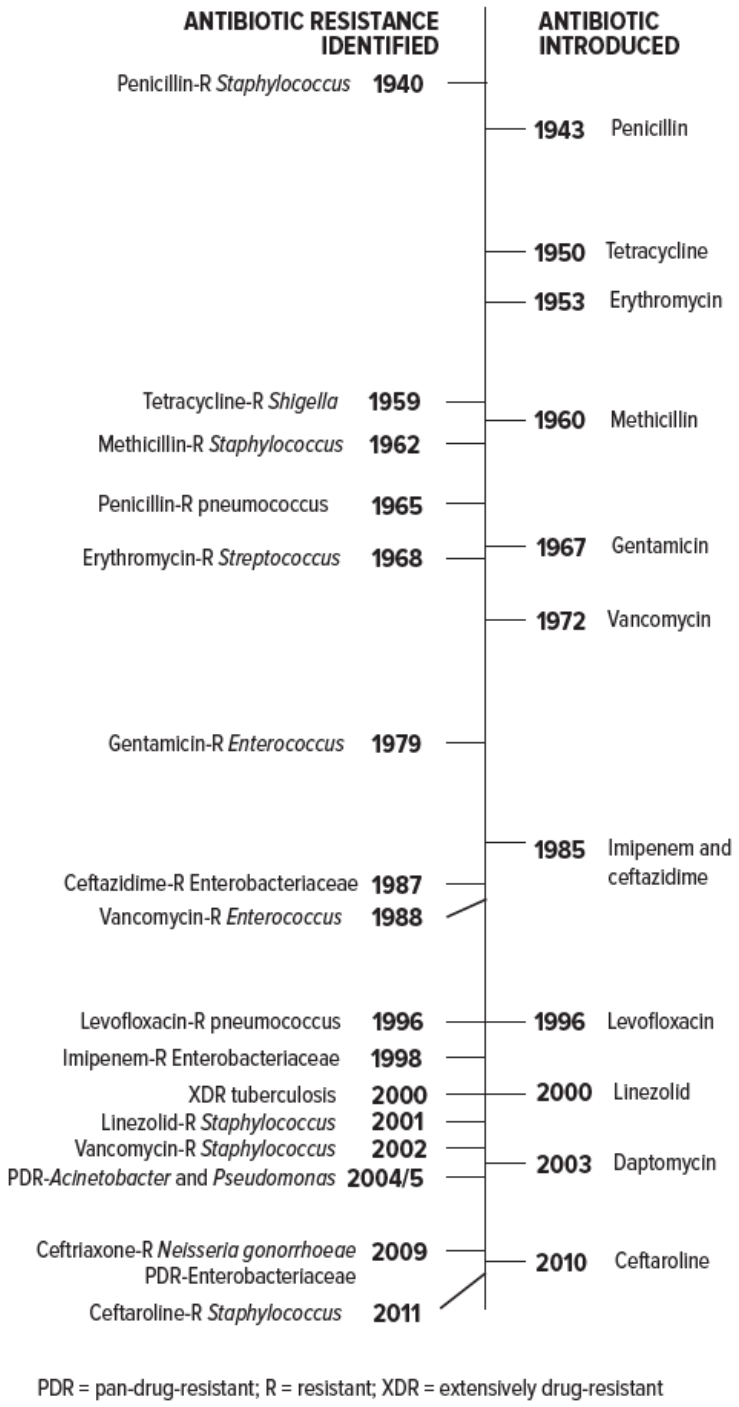

Figure 2: The history of antibiotics and the appearance of bacterial resistance strains (adapted from Ventola, 2015).

The presence of biofilms has been associated with several tissue-related infections such as osteomyelitis and device-related infections derived from central venous catheters that affect millions of people and can cause serious morbidity and mortality (Batoni *et al*., 2015; Brancatisano *et al*., 2014; Segev-Zarco *et al*., 2015). Among the extensive list of pathogens,

Escherichia coli, Staphylococcus epidermidis and *Staphylococcus aureus* are some of the pathogens frequently associated with such type of infections (Table 1) (Costerton *et al*., 1999, Estrela *et al*., 2009, Song *et al*., 2013).

Table 1: Microbes in biofilm associated infections (adapted from Costerton *et al*., 1999).

Infection/disease or source of infection	Common biofilm bacterial species
Periodontitis	Gram-negative anaerobic oral bacteria
Otitis media	*Haemophilus influenza*
Osteomyelitis	Various bacterial and fungal species
Bacterial prostatitis	*E. coli* and other Gram-negative bacteria
Native valve endocarditis	Viridans group *streptococci*
Cystic fibrosis pneumonia	*P. aeruginosa* and *Burkholderia cepacia*
Contact lens	*P. aeruginosa* and Gram-positive cocci
Urinary catheter cystitis	*E. coli* and other Gram-negative rods
Central venous catheters	*S. epidermidis* and others
Mechanical heart valves	*S. epidermidis* and *S. aureus*
Vascular grafts	Gram-positive cocci
Orthopaedic devices	*S. epidermidis* and *S. aureus*

Biofilms are composed of bacterial cells that are attached to a substrate embedded in a self-produced matrix of extracellular polymeric substances (EPS). The development of a biofilm is a complex process which involves different levels of transformation at a genetic and phenotypic level (Figure 3). The development of a mature biofilm involves the initial attachment of planktonic cells onto a surface with the help of type IV pili and flagellum. Microcolony formation begins shortly after the attachment of cells to the surface. Subpopulations interact with each other activating quorum sensing systems that trigger the release of extracellular DNA (eDNA), an important extracellular polymeric substance that allows the binding of motile and non-motile subpopulations of bacteria, leading to the

formation of a mushroom-like biofilm structure. Finally, biofilm dispersion is activated when the biofilm structure is not beneficial for bacterial survival and growth, and pieces of biofilm are liberated and used to colonise new areas and form new biofilms (Costerton *et al*., 1999, Yang *et al*., 2012).

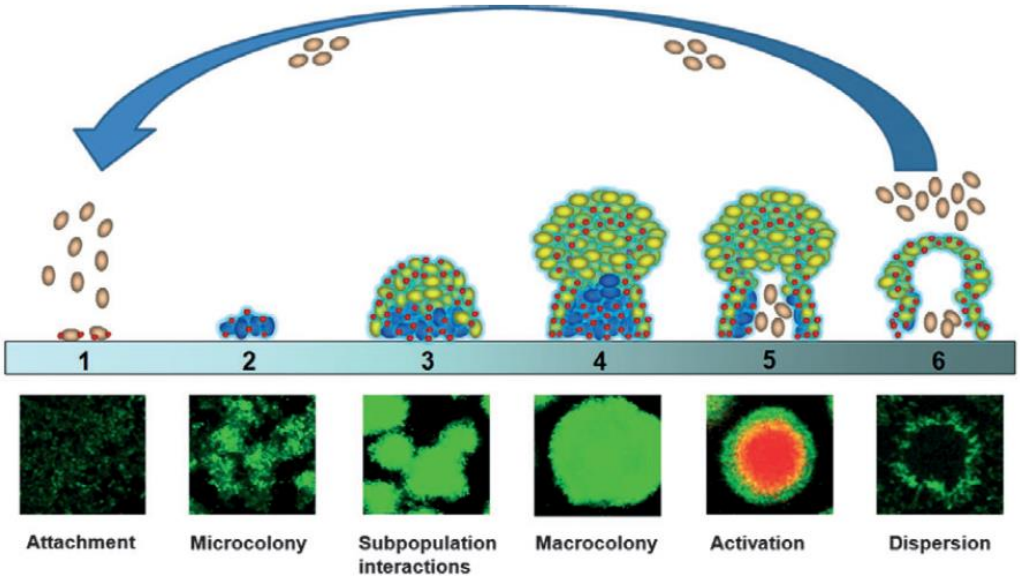

Figure 3: Biofilm development (adapted from Yang *et al*., 2012). 1 – Initial adhesion of planktonic cells to the surface; 2 – Adhered cells initiate microcolony formation; 3 – As the bacterial colony increases, subpopulations begin to interact activating communication systems such as quorum sensing; 4 – The evolution to a macrocolony in a mature biofilm strucutre; 5 – Bacterial cells start to die under stressful conditions and the dispersion of bacterial cells is activated; 6 – Bacterial cells are released from the biofilm and can colonise other areas.

Biofilms are difficult to treat and often are the cause of recurrent infection. For instance, once a biofilm is established, bacteria can tolerate various types of physicochemical treatments including UV light, heavy metals, acidity, changes in hydration or salinity, and phagocytosis. Additionally, biofilms typically resist conventional antibiotics even at high concentrations. Clearly this offers many therapeutic difficulties and most of the times the treatment involves the removal of the infected medical device or surgical excision of the medical tissue (Lebeaux *et al*., 2014). There are some hypotheses that explain the reasons behind why bacterial biofilms are inherently resistant to antibiotic treatments. To begin with, the biofilm structure is complex and different types of exopolysaccharides are involved. Depending on the chemical

structure of the biofilm matrix, the penetration of an antibiotic can be blocked or delayed at different rates. In cases where antibiotics are hindered, deactivation is most likely to occur in the outer layers of the biofilm. When antibiotic diffusion is reduced, even though in most cases the compounds successfully reach bacterial biofilms, they fail to eradicate them. This might be due to metabolic adaptation of bacteria to the antibiotic or secretion of enzymes capable of degrading the antibiotics (Costerton *et al*., 1999, Lebeaux *et al*., 2014). Secondly, the biofilm matrix includes eDNA, polysaccharides, proteins, amyloid fibres and bacteriophages (Figure 4). This extracellular matrix not only offers protection against antibiotics but also helps to establish gradients of nutrients such as oxygen, waste products and signals diffusing outwards, such as nitric oxide. These gradients create areas of nutrient limitation causing bacteria to grow at slower rates. This affects the effect of antibiotics since most of them target metabolically active bacteria (Donlan *et al*., 2002, McDougald *et al*., 2012, Lebeaux *et al*., 2014). Another explanation behind biofilm recalcitrance towards antibiotics is the presence of a subpopulation within biofilms called persisters. They form a very small percentage of the bacterial population and are found in a stationary growth phase. Due to their phenotypic state they become tolerant to the presence of antibiotics and are capable of surviving high concentrations of antibiotics (Lebeaux *et al*., 2014). Bacterial colonization also enables horizontal gene transfer and communication via quorum sensing systems leading to an intra-species and inter-species cooperative behaviour (Segev-Zarko *et al*., 2015).

Currently there are some approaches to try to prevent microbial contamination in medical settings. They include the control of asepsis, sterile procedures, improvement of hygiene, early removal of an unnecessary device and systemic prophylaxis during device insertion (Lebeaux *et al*., 2014). Unfortunately, trying to have bacterial-free environments is hardly possible, therefore, new strategies focusing on the actual source of the problem causing biofilm formation, that is, bacterial adhesion on surfaces such as medical devices or implants, in combination with optimised antibiotic regimens would perhaps reduce the likelihood of biofilm development. This can be achieved by exploring and combining novel antibacterial agents, that in principle will not cause bacterial resistance due to their unusual mechanism of action, with biomedical materials to develop anti-infective, anti-adhesive and anti-biofilm technologies.

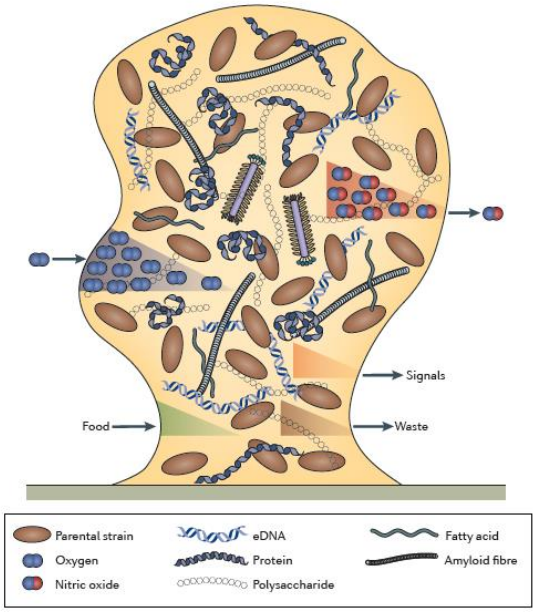

Figure 4: Structure of bacterial biofilms (adapated from McDougald *et al.*, 2012). Mature biofilms are characterised by an extracellular polymeric matrix composed of eDNA, polysaccharides, proteins, amyloid fibres and fatty acids. The biofilm matrix is also characterised by the presence of gradients such as oxygen and nutrients diffusing inwards and nitric oxide and waste diffusing outwards.

1.2 Exploiting novel antibacterial agents

Antibiotics can be classified based on their mechanism of action (Table 2). There are four major categories: (1) interference with the cell wall synthesis, (2) inhibition of protein synthesis, (3) interference with nucleic acid synthesis, and (4) inhibition of a metabolic pathway (Tenover, 2006; Walsh, 2000).

Using this knowledge as a reference, it is much easier to focus on novel antibacterial agents with different mechanisms of action than that of conventional antibiotics that can serve as a potential solution to overcome bacterial resistance and possibly act upon biofilm formation. For example, it is known that biofilm formation can be mediated by a bacterial cell-to-cell communication mechanism, termed quorum sensing, where biofilm associated genes are triggered and expressed as a consequence of a high bacterial cell density. Hence, the study of quorum sensing inhibitors and quorum quenchers would be a possible solution to fight both young and mature biofilms with a minimum risk of inducing resistance as rather than

restricting the cell proliferation, the aim would be to block the expression of genes associated with biofilm formation (Yang *et al*., 2012). Another way to interfere with biofilm formation with a low risk of developing resistance would be by exploring antimicrobial peptides (AMPs). AMPs have been extensively studied against planktonic bacteria and yet recent studies indicate that they are also promising candidates for the treatment of biofilms. As previously mentioned, one of the reasons for conventional antibiotics to fail against biofilms is their inability to target cells with low metabolic activity. Membrane integrity is essential to bacteria regardless of their metabolic state, and since AMPs act by destabilising the bacterial membrane, AMPs do not differentiate between dormant, dividing or mature cells, killing all (Batoni *et al*., 2016). Furthermore, many biofilm degrading enzymes have been identified and could be used as potential anti-biofilm agents (Meireles *et al*., 2016). Since these enzymes act upon biofilm components rather than on biofilm cells, the risk of developing bacterial resistance would also be minimal. The following sections will focus on the above-mentioned classes of agents with a brief introduction to each topic.

Table 2: Mechanism of action of antibiotics and bacterial resistant mechanisms (adapted from Tenover, 2006; Walsh, 2000).

Cell wall			
Antibiotic	**Target**	**Mechanism of action**	**Resistance mechanism**
Beta-lactams (e.g., penicillin)	Transpeptidases/ transglycosylases	Blockade of cross-linking enzymes in the peptidoglycan layer of cell walls	Beta-lactamases, PBP mutants
Glycopeptides (e.g., vancomycin)	D-Ala-D-Ala termini of peptidoglycan and of lipid II	Sequestration of substrate required for crosslinking	Reprogramming of D-Ala-D-Ala to D-Ala-D-Lac or D-Ala-D-Ser
Protein synthesis			
Antibiotic	**Target**	**Mechanism of action**	**Resistance mechanism**

Macrolides of the erythromycin class	Peptidyl transferase, Centre of the ribosome	Blockade of protein synthesis	rRNA methylation, drug efflux
Tetracyclines	Peptidyl transferase	Blockade of protein synthesis	Drug efflux
Aminoglycosides	Peptidyl transferase	Blockade of protein synthesis	Enzymatic modification of drug
Oxazolidinones	Peptidyl transferase	Blockade of protein synthesis	Unknown
DNA replication/repair			
Antibiotic	**Target**	**Mechanism of action**	**Resistance mechanism**
Fluoroquinones	DNA gyrase	Blockade of DNA replication	Gyrase mutations to drug resistance
Metabolic pathway			
Antibiotic	**Target**	**Mechanism of action**	**Resistance mechanism**
Sulfonamides	Dihydropteroate synthase (DHPS)	Blockade of DNA synthesis	DHPS mutants

1.2.1 Quorum sensing

Quorum sensing (QS) is a communication mechanism involved in the formation of differentiated, thick mature biofilm structures. This mechanism was first identified in the 1970's by Hastings and his research group when trying to understand the mechanism behind light production by *Vibrio fischeri*. It was observed that this bacterium had the peculiarity of producing luminescence and that they could be found in open seawater but also in ecological niches. Interestingly, only in the latter case was light produced. Later developments indicated that this phenomenon was related with the presence of high cell densities and QS

mechanisms. The designation of QS is related to the event in which a certain "quorum" must be reached for a particular gene expression (Welch *et al*., 2005). Briefly, bacteria continuously express small signalling molecules. When the cell density increases, the concentration of these molecules reaches a "threshold" value triggering gene transcription for a specific phenotype which can include the formation of biofilms (Welch *et al*., 2005, González *et al*., 2006, Chen *et al*., 2013).

Table 3: Quorum-sensing systems utilized by Gram-positive and Gram-negative bacteria (adapted from LaSarre *et al*., 2013).

Organism	Signal	Synthase	Receptor	Selected phenotypes
P. aeruginosa	C4HSL	RhlI	RhlR	Exoenzymes, virulence, biofilm formation, motility, pyocyanin
	3OC12HSL	LasI	LasR	
	PQS	PqsA	PqsR	
P. stewartii	3OC6HSL	EsaI	EsaR	Adhesion, EPS, plant colonization
B. gluamae	C8HSL	TofI	TofR	Motility, toxoflavin, lipase, virulence
A. tumefaciens	3OC8HSL	TraI	TraR	T_i plasmid conjugation, virulence
C. violaceum	C6HSL	CviI	CviR	Exoenzymes, antibiotics, violacein
S. liquefaciens	C4HSL	SwrI	SwrR	Swarming motility, biofilm formation
V. harveyi	3OHC4HSL	LuxM	LuxN	Bioluminescence, protease and EPS production, virulence
	AI-2	LuxS	LuxP	
	CAI-I	CqsA	CqsS	
V. fischeri	3OC6HSL	LuxI	LuxR	Bioluminescence, host colonization, motility
	C8HSL	AinS	AinR	
	AI-2	LuxS	LuxP	

E. coli	AI-2	LuxS	LsrB	*lsr* operon expression (AI-2 uptake)
S. aureus	AIP	*agrD*	AgrC	Virulence, exotoxins, biofilm dispersal

QS is a communication mechanism employed by several Gram-positive and Gram-negative bacteria. Generally, there is a signal generator, LuxI, responsible for the release of autoinducers (AIs) and a transcriptional receptor, LuxR, involved in the AIs-receptor complex. Once this complex is formed it allows the correct folding and binding to DNA and consequent expression of QS-mediated genes (Ruer *et al*., 2015, Chang *et al*., 2014). The most common AIs are N-acyl homoserine lactones (AHLs). These molecules have a homoserine lactone (HSL) ring connected to an acyl chain that can vary its structure based on the number of carbon atoms (LaSarre *et al*., 2013). Others include oligopeptides, furanosyl borate (AI-2), hydroxyl-palmitic acid methylester, and methyl dodecanoic acid (Kalia *et al*., 2013, González *et al*., 2006, Mohammed Sakr *et al*., 2013). The role of the AIs it to control the expression of genes that regulate a variety of phenotypes such as biofilm formation, bioluminescence, swarming motility, and virulence factor production, all of these are essential to establish pathogenicity (Table 3) (Linthorne *et al*., 2015, Everett *et al*., 2015).

1.2.1.1 Quorum Sensing in Gram-negative bacteria

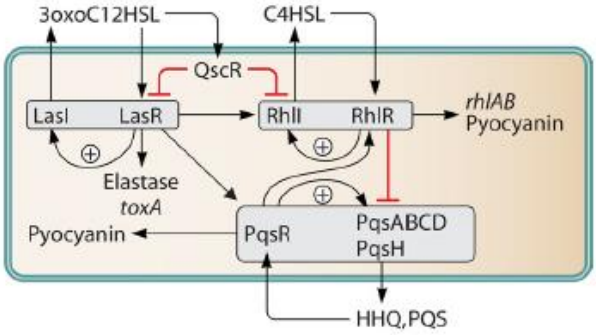

Figure 5: Schematic illustration of quorum-sensing system in *P. aeruginosa* (taken from LaSarre *et al*., 2013). *P. aeruginosa* produces two types of autoinducers, 3oxoC12HSL and C4HSL and signal molecule, PQS which are responsible for activating the three QS systems LasR/I, RhlI/R and PQS, that work hierarchically. Each of the QS system is responsible for the expression of virulent phenotypes (e.g., synthesis of elastase, pyocyanin and toxA).

Pseudomonas aeruginosa produces two types of AHLs, long chain 3-oxo-dodecanoyl acyl homoserine lactone (3OC12-HSL) and small chain N-butanoyl acyl homoserine lactone (C4-HSL). Additionally, it produces 2-heptyl-3-hydroxy-4-quinolone, designated as the *Pseudomonas* quinolone signal (PQS). It has three QS systems, LasR/I, RhlI/R and PQS, that work hierarchically (Allesen-Holm *et al*., 2006). Primarily, LasI starts by producing 3OC12-HSL which triggers the expression of elastase and activates the regulator LasR and subsequently activates the RhlI/R system. The second system is then used to produce C4-HSL and regulate a set of genes, including *phz* operon for pyocyanin synthesis, a toxin that promotes the release of eDNA for biofilm formation. The production of PQS depends on the other two systems and induces the expression of pyocyanin and the activation of RhlI (Figure 5) (Chang *et al*., 2014, Allesen-Holm *et al*., 2006).

1.2.1.2 Quorum Sensing in Gram-positive bacteria

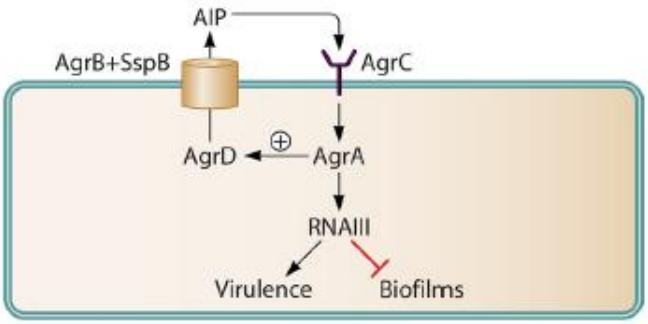

Figure 6: Schematic illustration of the quorum-sensing system in *S. aureus* (taken from LaSarre *et al*., 2013). *S. aureus* produces autoinducer peptides as autoinducers and uses the accessory gene regulator QS system to regulate the expression of virulent factors.

Gram-positive bacteria regulate QS using oligopeptide signals or autoinducer peptides (AIPs), like thiolactone- or lactone-based peptide. For example, *S. aureus* is divided into four specific groups based on the nature of the oligopeptide (AIP-I to AIP-IV) and uses the agr (accessory gene regulator) QS system. Agr possesses two operons, RNAII and RNAIII. The first one contains four genes *agrA*, *agrB*, *agrC* and *agrD*, all of them with specific ordered functions. Firstly, protein AgrD is transformed into an oligopeptide through cleavage by AgrB. The oligopeptide binds to AgrC which autophosphorylates and transfers its phosphate to AgrA.

Phosphorylated AgrA activates the transcription of RNAII and RNAIII that upregulates the expression of virulence factors (Figure 6) (Bhardwaj *et al*., 2013, Chu *et al*., 2013).

1.2.1.3 Quorum sensing in interspecies communication

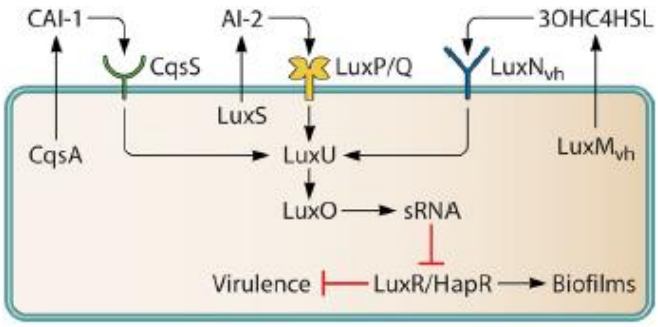

Figure 7: Schematic illustration of quorum-sensing system in *Vibrio harveyi* (taken from LaSarre *et al*., 2013). *Vibrio harveyi* uses AI-2 as an autoinducer and a phosphorelay signalling cascade to activate gene transcription mediated by the LuxQ/P QS system.

Another signalling system makes use of a furanosyl borate diester, also termed AI-2, to establish bacterial communication interspecies (Welch *et al*., 2005). For instance, in *V. harveyi*, AI-2 is detected by a sensor kinase complex that initiates a phosphorelay signalling cascade to activate gene transcription. LuxP acts as a signal receptor and LuxQ has kinase-phosphatase activity depending on its folding. When AI-2 is detected by LuxP it gets phosphorylated by LuxQ and interacts with an intracellular receptor, activating gene transcription for bioluminescence (Figure 7) (Kalia *et al*., 2013). *E. coli* have also developed this AI-2 system to degrade AI-2 signals from other bacteria (Bhardwaj *et al*., 2013, Kalia *et al*., 2013).

1.2.1.4 Finding the ideal quorum quencher as a potential antimicrobial agent

The communication mechanisms discussed above can be disrupted using quorum sensing inhibitors (QSI) or quorum quenchers (QQ). This strategy aims to block the virulence expression, rather than restrict cell proliferation, diminishing the risk of inducing resistance as little or no selective pressure exists (Chu *et al*., 2013, García-Contreras *et al*., 2016). Strategies used to disrupt QS include enzymatic degradation of signalling molecules, interference with

signal receptors using competitive molecules or inhibition of signal synthesis using competitive molecules (Figure 8).

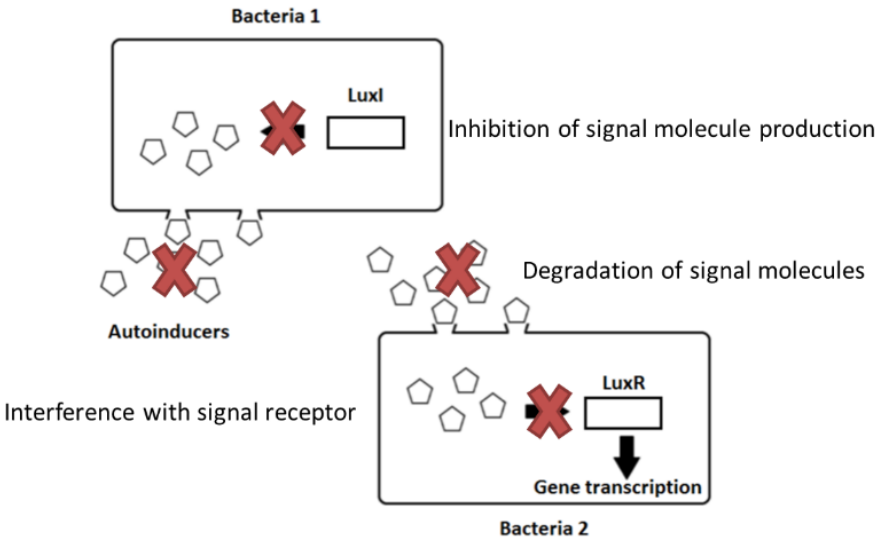

Figure 8: Strategies involved in blocking quorum sensing activity.

Many enzymes with the ability to degrade AHLs have been identified. They belong to three main families, lactonases, acylases and oxidoreductases. Lactonases act by hydrolysing the lactone ring, acylases hydrolyse irreversibly the acyl-amide bond present between the acyl tail and lactone ring of AHLs, and lastly, oxidoreductases do not degrade AHLs but rather alter them into an inactive form by oxidizing or reducing the acyl side chain (LaSarre *et al*., 2013). Since the lactone moiety is conserved in all AHLs, lactonases have broader substrate specificity and are more frequently found in bacteria, whereas in the case of acylases, their specificity varies according to the acyl chain length of the AHLs. Sakr *et al*., was able to isolate and characterise a lactonase with acyl homoserine lactone inhibitory activity, extracted from *Bacillus weihenstephanensis*-isolate P65, against *P. aeruginosa* isolates. Their findings revealed high thermal and high pH stability maintaining over 90% of its maximum catalytic activity within a range of 28-50^{o}C and within pH 6-9. In addition to that, it was verified that this lactonase had a broad spectrum of enzyme activity against both synthetic and natural AHLs, with the highest activity registered for C6-HSL and the lower activity for C8-HSL (Mohammed Sakr *et al*., 2013). Lin *et al*., was able to identify a gene encoding for an acylase in *Ralstonia eutropha*. In this study, the gene *aiiD* was successfully cloned and expressed in *E. coli* and it was able to inactivate three AHLs expressed in *P. aeruginosa*. LC-MS studies indicated that this enzyme hydrolysed the AHL amide, releasing homoserine lactone and the

corresponding fatty acid. Further results confirmed that the presence of this enzyme decreased swarming motility and reduced the production of elastase and pyocyanin (Lin *et al*., 2003).

Other small molecules such as trans-cinnamaldehyde have also been described to have quorum-quenching activities (Estrela *et al*., 2009). In a screening study to find AHL synthase inhibitors, Chang *et al*., identified trans-cinnamaldehyde as a strong AHL synthase inhibitor against *P. aeruginosa* PAO1. Molecular docking revealed that this compound had the ability to bind to LasI by interacting with their substrate binding site. As mentioned before, LasI is responsible for the production of long-chain AHLs which not only trigger the expression of elastase but also activate the RhlI QS system. The study also showed inhibition of AHL production through RhlI, and consequent inhibition of pyocyanin production (Chang *et al*., 2014). In another study ajoene, a sulphur-containing compound found in garlic, exhibited a concentration-dependent attenuation of central QS-controlled genes in *P. aeruginosa*. Two genes significantly downregulated by ajoene were *lasB* and *rhlA*, both regulated by Las and Rhl systems, respectively. The RT-PCR data showed that a concentration of 80 μg/mL ajoene lowered the expression of *rhlA* by almost 12-fold and that of *lasB* almost 5-fold. Due to a more effective down-regulation of *rhlA,* it was suggested that this compound primarily targets the Rhl system, and therefore it is more specific to short chain AHL, C4-HSL. On the other hand, *rhlA* is responsible for rhamnolipid production, a haemolysin responsible to destroy polymorphonuclear leukocytes (PMNs) by lytic necrosis. Besides lysing neutrophils and macrophages, rhamnolipids are also known to impair chemotaxis of neutrophils. As rhamnolipids are associated with bacteria within a biofilm, it is likely to function as a shield towards important cellular components of the host defence. When treated with 20 μg/mL ajoene, the rhamnolipid content was reduced to approximately 1/3 of that for the untreated culture, and there was almost no detectable rhamnolipid present in the sample when the cells were treated with 80 μg/mL ajoene (Jakobsen *et al*., 2012). Cech *et al*., studied the effect of goldenseal (*Hydrastis canadensis*) against Methicillin-Resistant *Staphylococcus aureus* (MRSA). In this study, a reporter strain of *S. aureus* was used. This strain contained a QS controlled promoter that generated bioluminescence in the presence of autoinducer peptides AIPs. However, this strain did not produce its own signalling molecules due to a deletion in the *argBD* genes. Samples containing constant level of autoinducers combined with sub-inhibitory concentrations of goldenseal were exposed to the reporter strain. A dose-dependent

inhibition of bioluminescence was observed with an increase in the concentration of goldenseal (Cech *et al*., 2012). Red algae, *Delisea pulchra* is known to produce halogenated furanones presenting inhibitory activity against quorum sensing systems. In a study conducted by Ren *et al*., this compound was able to repress QS activity in *E. coli* repressing 79% of the genes induced by its system. Additionally, swarming motility and biofilm formation were inhibited with 20 µg/mL and 60 µg/mL, respectively (Ren *et al*., 2001). In a study conducted by Zhang *et al*., Rosa rugosa tea polyphenol (RTP) extract was examined against *Chromobacterium violaceum* CV026, *E. coli* K-12 and *P. aeruginosa* POA1 at sub-inhibitory concentrations to search for QS inhibiting activity. Results showed a minimum inhibitory concentration (MIC) value of 1.8 mg/mL, 1.6 mg/mL and 1.2 mg/mL against *C. violaceum* CV026, *E. coli* K-12 and *P. aeruginosa* PAO1, respectively. Inhibition rates of swarming migration with 640 mg/mL of RTP were 84.90% and 78.03%, for *E. coli* K-12 and *P. aeruginosa* PAO1, respectively, and did not affect their proliferation. Using the same concentration of RTP, biofilm formation decreased by 67.02% and 72.90% for *E. coli* K-12 and *P. aeruginosa* PAO1, respectively (Zhang *et al*., 2014). Aeromonas species have been related with diverse human infections such as wound infections. This bacterium possesses a quorum sensing mechanism similar to that observed in *V. fischeri*. Vanillin, a small molecule has been identified as a potential quorum quencher against this bacterium. In a study conducted by Ponnusamy *et al*., vanillin was added to membrane filters of different compositions and was able to reduce biofilm formation of *A. hydrophila* (Ponnusamy *et al*., 2013).

1.2.2 Antimicrobial peptides

AMPs have been extensively explored as an alternative to conventional antibiotics due to their exceptionally broad spectrum of activity against bacteria, bactericidal efficacy at low concentrations as well as their multiple modes of action (Batoni *et al*., 2015; Onaizi *et al*., 2010, Hancock *et al*., 2006). AMPs are innate immune system molecules that can be isolated from various sources, including plants, bacteria, vertebrates, and insects (Ebbensgaard *et al*., 2015; Steinstraesser *et al*., 2002). AMPs vary by size, net charge, primary and secondary structures, hydrophobicity and amphipathicity. Most of them comprise 10-50 amino-acid residues and most of them have a positive net charge, making them cationic. Because of their positive net charge and amphipathic structure, they are able to interact with the negatively

charged bacterial membrane and integrate into the bacterial membrane by clustering cationic and hydrophobic residues in two distinct faces (Ebbensgaard *et al*., 2015). Because their action is folding mediated, it can be controlled in a dose dependent and reversible manner (Ryan *et al*., 2013). Once in the membranes, the peptides arrange into membrane-disrupting pores or channels that destabilise microbial cells, resulting in cell lysis and death (Powers *et al*., 2003, Brogden *et al*., 2005, Hancock *et al*., 2006).

Based on their structure and amino acid composition they can be classified into three general groups (Figure 9). The first group is composed of β-sheet peptides stabilized by two to four disulphide bridges. This group includes a diverse family of human defensins that can be divided into α- and β-defensins and other defensins derived from insects and plants. The second group includes α-helical peptides which are short and lack cysteine residues. Examples of peptides from this group are cathelicidins, cecropins and magainins. Finally, the third group is composed by extended or loop peptides rich in amino acids such as glycine, proline, tryptophan, arginine and/or histidine. Examples of peptides from this group are bactenicin rich in proline and arginine, and indolicidin, rich in tryptophan residues (Powers *et al*., 2003, Brogden *et al*., 2005, Hancock *et al*., 2006).

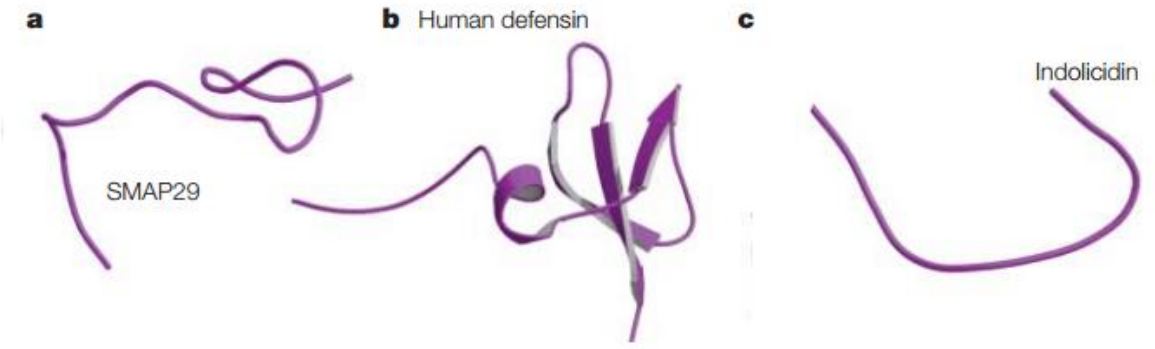

Figure 9: Examples of the three groups of antimicrobial peptides. a: α-helical peptide, SMAP29; b: β-sheet peptide, Human defensins; c: extended peptide, indolicidin (adapted from Brogden *et al*., 2005).

1.2.2.1 Mechanism of action

Although many mechanisms of action have been described for the action of AMPs, the most common and well accepted mechanism relates to the cationic and amphiphilic nature of AMPs with its activity. Firstly, AMPs are attracted to bacterial surfaces via electrostatic interactions between the cationic region of the peptides and the negatively charged surface of bacteria, that is, the anionic phospholipids and phosphate groups on lipopolysaccharides (LPS) of Gram-negative bacteria and the teichoic acids on the surface of Gram-positive bacteria (Bocchinfuso *et al*., 2009). Then AMPs must translocate the LPS present in the membrane of Gram-negative bacteria and capsular polysaccharides in Gram-positive bacteria before they can interact with the cytoplasmic membrane and gain access to the lipid bilayers. Using specific orientations, AMPs can penetrate the lipid bilayers and destabilize their physical integrity (Figure 10).

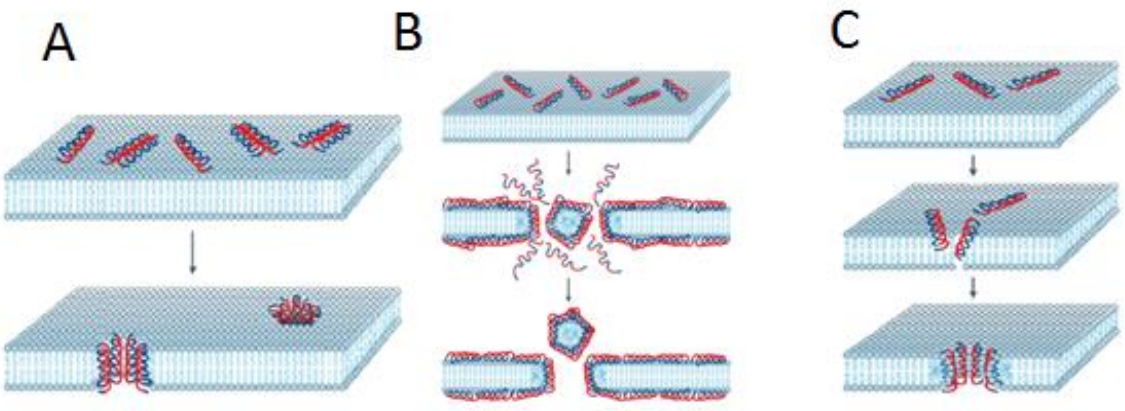

Figure 10: Modes of action of antimicrobial peptides against cytoplasmic membranes. A – barrel-stave model; B – carpet model; C – toroidal model. Red - Hydrophilic regions of the peptide; Blue - hydrophobic regions of the peptide (adapted from Brogden *et al*., 2005).

There are three models that best describe the different orientations these peptides have. In the first model, “barrel-stave model” as the name indicates, helical peptides act as staves in the membrane. The hydrophobic region of the peptide aligns with the lipid core region of the bilayer and the hydrophilic region forms the interior region of the pore. In the second model, “carpet model”, peptides accumulate on the bilayer surface like a carpet covering the surface of the membrane and lead to the formation of micelles, creating holes in the membrane. Finally, in the “toroidal-pore model”, the polar part of the peptides associates with the polar

head groups of the lipids inducing a continuous bending of the head groups through the pore. Ultimately, AMPs cause an interference with the interface of the hydrophilic head groups and the fatty acyl chains of membrane phospholipids leading to the disruption of the membrane or interference with internal targets (Hancock *et al*., 2006, Batoni *et al*., 2015, Ebbensgaard *et al*., 2015, Lee *et al*., 2015, Brogden *et al*., 2005). AMPs can also act as innate immune modulators by recruiting polymorphonuclear cells, lymphocytes or dendritic cells at the site of infection allowing a control of inflammation/sepsis and enhancing bacterial clearance. Moreover, some AMPs can promote wound healing processes by stimulating cell proliferation and angiogenesis, reducing the risk of biofilm formation during the tissue repair process (Steinstraesser *et al*., 2002, Batoni *et al*., 2016). Furthermore, some AMPs are involved in apoptotic events. As an example, in a study conducted by Lee *et al*., magainin 2, isolated from frog skin was related to DNA fragmentation, chromatin condensation and caspase activation events in *E. coli* (Lee *et al*., 2014).

1.2.2.2 AMPs and their therapeutic potential and treatment against biofilms

As mentioned above, AMPs have been extensively explored as an alternative to conventional antibiotics. This so happens because they have a broad-spectrum of activity, reduced resistance rates and immunomodulatory properties. In addition to this, AMPs have demonstrated wound healing properties and several studies have shown that they are up-regulated in all stages of would recovery. This is of special importance as when the skin is wounded, the protective barrier against pathogens becomes open and after wound contamination, the process of wound healing becomes impaired (Pfalzgraff *et al.,* 2018; Carratero *et al*., 2008; Heilborn *et al*., 2003). Together with its wound healing properties, AMPs have shown anti-biofilm activity against many relevant bacteria. Zhu *et al*., studied the effect of human β-defensin-3 (hBD-3) against methicillin-resistant *Staphylococcus epidermidis* (MRSE) and MRSA in medical implant biofilm formation. hBD-3 exhibited a rapid bactericidal effect against multidrug-resistant bacteria (20 minutes), presenting a MIC of 4 μg/mL for *S. epidermidis* and 8 μg/mL for *S. aureus*. Bacterial adhesion was restrained after 6h and biofilm formation after 12h. It was observed that the higher the concentration of hBD-3, the higher the antibacterial effect. Using concentrations above the MIC value revealed potential to eliminate pre-existing biofilms on implants for both strains (Zhu *et al*., 2013). Peptide LL-37, a type of cathelicidin, is one of the most studied peptides. In a study conducted by Overhange

et al., biofilm inhibition activity was evaluated. Results indicated strong biofilm inhibition in *P. aeruginosa* with only 0.5 μg/mL, a value significantly lower compared to its MIC, 64 μg/mL. This peptide also demonstrated downregulation of key components of QS systems present in bacteria (Overhage *et al*., 2008). Synthetic peptide, IDR-1018, derived from bactenecin was found to have anti-biofilm properties against representative bacteria such as *P. aeruginosa*, *E. coli*, and MRSA. At concentrations much lower than the MIC value, IDR-1018 was able to prevent biofilm formation, eradicate mature biofilms and promote biofilm dispersal for the above-mentioned strains. NMR and chromatography studies showed that the peptide caused the bacterial cells to degrade (p)ppGpp, an important signal in biofilm development, accumulated as a response of stress conditions (Zhu and Dai, 2019). Evidence showed that the activity of IDR-1018 was related to this signal by overexpression and blocking the production of (p)ppGpp. In cases where (p)ppGpp was overexpressed, the activity of the peptide was enhanced whereas when blocking the production of (p)ppGpp the effects of the peptide were much lower (de la Fuente-Núñez *et al*., 2014).

Overall AMPs present the characteristics of an ideal antibacterial agent. They possess a rapid killing ability, the capability to act in different microenvironments and target metabolically active and non-active cells and are capable of interfering with bacterial cell machinery. Moreover, they can penetrate the extracellular matrix of biofilms, interfere with its production, whether by destroying mature biofilms or by causing the detachment of bacterial cells from biofilms, and finally to modulate host responses to biofilms (Batoni *et al*., 2016). Despite their activity, naturally occurring AMPs pose some limitations regarding their toxicity to host cells, liability to proteases and high costs of production. Certain physiological conditions may also alter the activity of these peptides such as the presence of divalent anions and extreme non-physiological pH values (Hancock *et al*., 2006). Reduction of cytotoxicity has been attempted to be addressed by developing synthetic AMPs generating minor structural modifications of the peptides (Steinstraesser *et al*., 2002). On the other hand, in order to obtain peptides with the same bioactive properties but with protease resistant characteristics, the development of peptide mimics, called peptidomimetics, has been explored (Avan *et al*., 2014). With regard to production costs, recombinant DNA methods have been used to develop less expensive production methods.

1.2.3 Biofilm degrading enzymes

Another class of proteins that has recently been explored against bacteria, and more specifically against bacterial biofilms are proteins that unlike AMPs, do not target the bacterial membrane but instead degrade and disperse the biofilm matrix. Proteins of this class include enzymes such as proteases, deoxyribonucleases and glycoside hydrolases (Pavlukhina *et al*., 2012). Dispersin B (DB) is a 42 KDa glycoside hydrolase produced by Gram-negative bacteria *Aggregatibacter actinomycetemcomitans,* a human periodontal pathogen. DB is capable of degrading polysaccharides present in the biofilm matrix of many bacterial strains, resulting in the detachment of cells and its release to the environment. More specifically, DB degrades cationic extracellular polysaccharides, namely β-1,6-poly-N-acetylglucosamine (PNAG) that can either be termed as PIA for *Staphylococcus* species and as PGA for *E. coli.* These polysaccharides work as adhesins, mediating the attachment of bacteria to abiotic surfaces and providing bacteria the capability to resist detergent treatment and human phagocytic cells (Kaplan 2009, Wang *et al*., 2004, Kaplan 2010). The initial evidence that DB could promote biofilm dispersal came from studies carried out by Kaplan *et a*l., Itoh *et al*., and Izano *et al*., In the first study it was seen that DB mutant (mutant strain not producing the enzyme) lacked the biofilm dispersal ability as the cells resulting from the mutant produced biofilm colonies that were not released to the medium as opposed to the wild-type strain (Kaplan *et al.,* 2003). The other studies provided further proof that DB was indeed causing biofilm dispersal as the purified enzyme was shown to disperse cells from pre-formed biofilm colonies of PNAG-producing bacteria. The MALDI-TOF mass spectra of PGA after being digested with DB showed a high degree of depolymerization of the polysaccharide (Itoh *et al*., 2005, Izano *et al.*, 2007).

Studies have shown the ability of DB to inhibit biofilm formation of *S. aureus* and *S. epidermidis.* In a study conducted by Izano *et al*., it was shown that the biofilm formation by *S. aureus* and *S. epidermidis* strains was significantly inhibited when the bacterial growth media was supplemented with DB. Furthermore, it was shown that DB was also able to detach pre-formed biofilms by *S. epidermidis* (Izano *et al.,* 2008). Another study demonstrated the ability of DB to prevent *S. epidermidis* biofilm formation on plastic surfaces. Four strains of *S. epidermidis* clinical isolates were obtained from infected intravenous catheters. The strains were allowed to grow under normal conditions in a 96-well treated polystyrene microtiter

plate to stimulate biofilm formation and after a 24-hour period of incubation, DB was added to each well. After only a period of 30 minutes of incubation, no biofilm was shown to remain on the wells, indicating the rapid dispersal effect of the enzyme. *S. epidermidis* biofilms were then allowed to grow on polystyrene rods and treated with 40 µg/mL of DB for 15 minutes. The treated rods showed a 5.8 log reduction in the number of bacteria attached to the surface in comparison with the non-treated rods (Kaplan *et al.*, 2004). Many studies have also evaluated the synergistic effect between DB and other antimicrobial agents. Gawande *et al*., developed a wound gel formulation to target chronic wound infections, based on the combination of DB, antimicrobial peptide KSL-W and gelling agent Pluronic F-127. They observed that by combining DB and the KSL-W, there was a reduction of the MIC and minimum bactericidal concentration (MBC) values by 50% when compared to the peptide solution alone when tested against MRSA, *S. epidermidis*, Coagulase-negative *Staphylococci* (CoNS), and *Acinetobacter baumannii*. They also observed that the presence of DB enhanced significantly the anti-biofilm activity of the peptide as the pre-formed biofilm of *S. epidermidis* and CoNS were completely eradicated when DB and KSL-W were used together at a concentration of 200 µg/mL and 250 µg/mL, respectively (Gawande *et al.,* 2014). In another study, the combination of triclosan and DB was also done to evaluate their synergistic effect so that this combination could be used to coat vascular catheters and prevent bacterial colonisation. They have demonstrated that not only the combination of these two agents led to a significant reduction in bacterial colonisation of *S. aureus*, *S. epidermidis* and *E. coli* when compared to the performance of the agents alone, but that the mixture also provided for a longer and superior antimicrobial activity when compared to chlorhexidine–silver sulfadiazine (CH-SS)-coated vascular catheters. Both (CH-SS)-coated vascular catheters and triclosan + DB-coated catheters showed a significant reduction in bacterial colonization after 1 day of incubation with bacteria, but only triclosan + DB-coated catheters maintained their activity after 4 and 7 days of bacterial incubation (Darouiche *et al.*, 2009). Donelli *et al*., studied the synergistic effect of DB and cefamandole nafate (CEF) in the inhibition of Staphylococcal biofilms grown on polyurethanes. An initial cytotoxicity screening was performed that showed that when Hep-2 cells were exposed to 40 to 400 µg/mL of DB no morphological changes were observed in the cell monolayer as well as in major cytoskeletal components such as F- actin and α- and β-tubulins. Afterwards, three different polyurethane discs with different chemical features were loaded with DB and incubated with bacteria for a period of 24 hours. After this period,

the discs were treated with a CEF solution corresponding to its MBC. The enhancement of the activity of CEF by the presence of DB was evident as a significant reduction in the numbers of colony forming units (CFU) was observed for the loaded polyurethanes versus the non-loaded polyurethanes (Donelli *et al*., 2007). Another study showed the biocompatibility of DB against human foetal osteoblast cell line, hFOB 1.19 (ATCC ® CRL-11372™) as well as its anti-biofilm properties against *S. epidermidis*. The study showed no cytotoxic effects after a period of 4 days of cell cultivation in the presence of a surface coating containing DB loaded poly(allylamine hydrochloride) (PAH) (Pavlukhina *et al.,* 2012).

The fact that DB can inhibit biofilm formation, detach pre-formed biofilms and work synergistically with other antimicrobial compounds gives a new range of possibilities to target biofilm formation. Another aspect which is very important is the fact that this enzyme showed non-cytotoxic effects against mammalian cells and for this reason many studies are focusing on its use in commercial applications such as medical devices, wound care management and biofilm control in medical and industrial settings.

1.3 Combination of technology and knowledge from multiple scientific disciplines

Biomedicine is an interdisciplinary field of research and development which is in constant progress. Areas of speciality found in biomedicine such as biotechnology, microbiology and cell biology are now combining its knowledge in order to develop new strategies and technologies to prevent and treat bacterial infections and biofilm formation in clinical and medical settings. One of the examples is the combination of novel antibacterial agents, such as the ones introduced above, with natural or synthetic polymers to suit a wide range of applications including tissue engineering, development of medical implants and antimicrobial surfaces (Figure 11) (Campoccia *et al*., 2013).

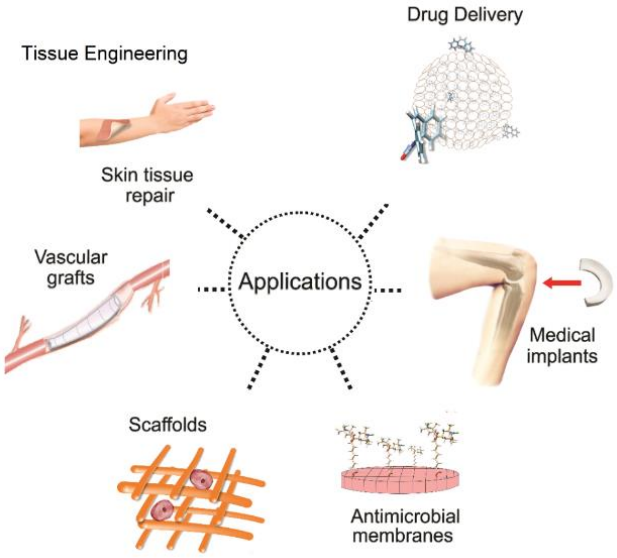

Figure 11: Biomedical applications of polymers and antibacterial agents (adapted from Rojas *et al*., 2015).

1.3.1 Using polymers as antibacterial materials

Anti-bacterial technologies based on antibacterial polymeric materials have progressively become a strategy to prevent tissue-related infections and device-related infections. These materials can be employed as a vehicle for the delivery of antibacterial agents where the mode of action is the prevention, treatment and reduction of infections. The design of such materials can be based on different strategies, including loading antimicrobial molecules in biomaterials, attachment of functional groups that confer bactericidal activity to the polymer, or even the usage of intrinsically active polymers (Campoccia *et al*., 2013, Shah *et al*., 2013). There are many applications for these types of materials. For instance, the earliest step in biofilm formation of foreign-body-related infections is bacterial adhesion. However, if bacteria cannot adhere to a surface it cannot colonise it. Bacteria repelling, and anti-adhesive surfaces can be obtained by working on the surface biomaterial chemistry or by changing the surface morphology/topography. Coatings can be developed with the purpose of achieving anti-infective properties at the biomaterial-tissue interface without creating host responses nor compromising the properties of the biomaterial. They can have non-leachable molecules covalently bound to the biomaterial, granting these materials a long-lasting effect. On the other hand, there are biomaterials capable of releasing antibacterial substances (Campoccia *et al*., 2013).

1.3.1.1 Examples

As it is well known, chitosan is intrinsically active against bacteria. However, there are many studies focusing on improving its activity against bacteria. In one of these studies, chitosan-silver (CS-Ag) nanocomposites were developed by reducing silver nitrate in the presence of chitosan at different reaction temperatures. The final material was tested against a range of Gram-positive and Gram-negative bacteria. The antibacterial tests showed a better performance than the antibiotic streptomycin in the cases where the materials were used against *S. aureus*, *Staphylococcus sp*., *Streptococcus sp*. and *Salmonella sp*. (Arjunan *et al*., 2016). In another study involving silver and another well-known polymer, ε-Poly-L-lysine, Dai *et al*., performed an *in-situ* generation of silver nanoparticles (AgNPs) in order to enhance the material antibacterial activity. The final composite showed an effective synergistic antibacterial activity against *P. aeruginosa* and *S. aureus*. (Dai *et al*., 2016).

Chemical modification is another strategy employed to develop antibacterial polymers. N-halamine groups, i.e. nitrogen-halogen groups are very powerful biocides and have a broad spectrum of activity. In a study conducted by Liu *et al*., methacrylamide (MAM) was chemically grafted to microcrystalline cellulose (MCC). The material was further modified by a chlorination step yielding N-halamine groups which rendered the material active against *S. aureus* and *E. coli* (Liu *et al*., 2015). In another study, amino groups present in chitosan were transformed into chlorinated amines using sodium hypochlorite solution at a specific pH. The final material containing N-halamine structures was capable of killing both Gram-negative and Gram-positive bacteria and to prevent biofilm formation (Cao *et al*., 2007). Quaternary ammonium compounds have been widely used as antimicrobial agents. Kim *et al*., developed alginate–quaternary ammonium complex beads with excellent antimicrobial activity against *E. coli* and *S. aureus* (Kim *et al*., 2007).

Essential oils compose a source of biologically active compounds that are known to possess antimicrobial activity (Prabuseenivasan *et al*., 2006; Inouye *et al*., 2001). Gomes *et al*., developed spherical poly(DL-lactide-co-glycolide) (PLGA) nanoparticles with entrapped eugenol and trans-cinnamaldehyde and studied its inhibiting effect against *Listeria spp.* and *Salmonella spp*. (Gomes *et al*., 2011).

Recent studies included the immobilization of AMPs in many biomaterials. One of the most common methods is the layer-by-layer (LbL) technique. This approach consists in layering

polycations and polyanions on a solid substrate, in an alternate fashion. Etienne *et al*., reported the impregnation of polyelectrolyte multi-layered films with defensin. Films comprising of ten antimicrobial peptide layers were able to inhibit *E. coli* growth up to 98%. The presence of a positively charged outer layer of the film contributed to a close interaction with bacteria, which ultimately allowed AMPs to interact with the bacterial membrane (Etienne *et al*., 2004). In another study, Piras *et al*., performed the encapsulation of frog-skin derived AMP, temporin B (TB) into chitosan nanoparticles (CS-NPs). Antibacterial action was seen against various strains of *S. epidermidis* with a significant reduction of the number of viable bacteria compared to CS-NPs without TB (Piras *et al*., 2015).

Because quorum sensing mechanisms are directly related to the presence of biofilms and because biofilms are directly related to device-related infections, many approaches combining polymers and QSI or QQ are being used as a method to disrupt QS systems and biofilm formation in medical devices. Hume *et al*., studied the use of covalently bound furanones as an antibiofilm coating for biomaterials against *S. epidermidis*. Polystyrene discs with covalently bound furanones were produced and then furanone-coated catheters were developed using a 1-ethyl-3-(dimethylaminopropyl) carbodiimide (EDC) reaction. According to the results, a dose-dependent reduction in bacterial adhesion was observed. Biofilm formation was inhibited by 89% for the discs and by 78% for the catheters. *In vivo* tests using sheep showed that furanone-coated catheters had lower number of bacteria at their implantation site compared to non-treated catheters (Hume *et al*., 2004). Polymers itself can be used as QSI against bacteria as in the case of polyvinyl alcohol. In a study conducted by Lui *et al*., AL-2 concentration was reduced by blocking the signal receptor using competitive molecules. Further work indicated that because AL-2 molecules are borate esters and because polyvinyl alcohol is a polyol, the latter could competitively bind to boric acid, a precursor of AL-2 (Lui *et al*., 2013).

1.4 Polyhydroxyalkanoates (PHAs)

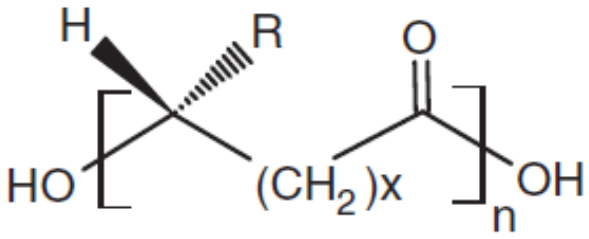

Figure 12: A general chemical structure of PHAs produced within bacteria. (x = number of methylene groups in the backbone; n = number of monomer units; R = alkyl groups, from methyl (C_1) to tridecyl (C_{13}) (taken from Nigmatullin *et al*., 2015).

As seen above, there are a wide range of natural and synthetic polymers being investigated for the development of antibacterial materials. However, a family of biopolymers which gained special attention over the last decade were Polyhydroxyalkanoates (PHAs). PHAs are bacteria derived polyesters which are produced and accumulated within the cytoplasm as energy storing compounds and as a carbon source in the form of granules. PHAs can be obtained by bacterial fermentation processes where the organisms are subjected to metabolic stress conditions (Figure 12). Stress conditions are achieved when one of the growth components, that is, nitrogen, sulphur, magnesium, phosphorus and oxygen is limited, and a suitable carbon source is in excess. Several options can be used as carbon sources for PHA production, such as carbohydrates, lipids, fatty acids, alkanes, alkenes, organic acids, aromatic compounds. Additionally, these polymers can be synthesized using cheap carbon sources and waste material (Nigmatullin *et al*., 2015, Reis *et al*., 2008). Depending on the substrate used for fermentation, a wide variety of PHAs with different monomeric compositions can be obtained and with different physical properties. Usually, PHAs are classified based on the number of carbon atoms present in the side chain of each monomer unit, that is, short-chain-length-PHAs (SCL-PHAs) and medium-chain-length-PHAs (MCL-PHAs). Owing to their biocompatibility and biodegradability, these polymers are good candidates for many biomedical applications (Babinot *et al*., 2012). The following sections contain more detailed information regarding PHAs.

1.4.1 PHA associated proteins

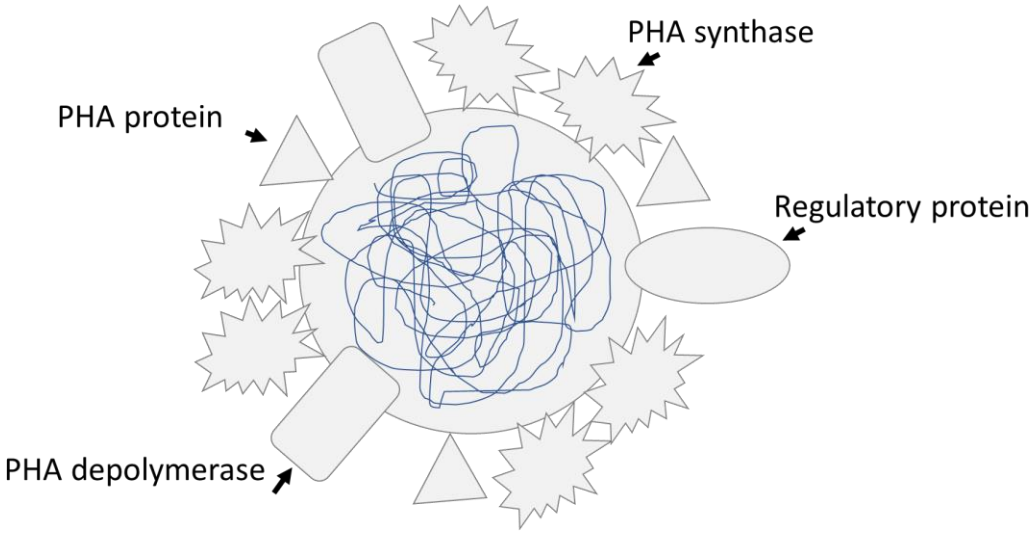

Figure 13: PHAs associated proteins (adapted from Mozejko-Ciesielska *et al*., 2019).

PHAs are stored as insoluble spherical inclusions or as intracellular granules. Early studies demonstrated the polymer core was surrounded by a phospholipid monolayer with proteins attached. These proteins play a major role in the synthesis and degradation of PHAs and they can be identified as PHA synthases, PHA depolymerases, phasins and regulatory proteins (Figure 13). PHA synthases are responsible for the catalysis of the stereoselective conversion of (R)-3-hydroxyacyl CoA to a high molecular weight polymer, with the concomitant release of coenzyme A. PHA depolymerases are enzymes responsible for polymer degradation and they can be divided into two groups, namely, the intracellular depolymerases that degrade PHAs present in the granules, and the extracellular depolymerases that degrade PHAs found in the environment. The PHA granule surface is abundantly covered by phasins, low molecular weight proteins with amphiphilic character (Grage *et al*., 2009). These proteins consist of a hydrophobic domain which is connected to the surface of the PHA granule and a hydrophilic domain which is exposed to the cytoplasm of the bacteria. Although phasins are not needed for PHA production, the amphiphilicity of the protein stabilizes the PHA granules and prevents their coalescence in the cytoplasm (Jurasek *et al*., 2002, Kabilan *et al*., 2012). Regulatory proteins, as the name indicates are connected to the regulation of PHA synthesis and phasin production (Grage *et al*., 2009).

1.4.2 Biosynthesis of PHAs

PHA synthases are the key enzymes in PHA biosynthesis. Depending on the enzyme subunits, they can be classified in to four classes (Figure 14). Class I synthases are composed of two PhaC subunits typically present in *Cupriavidus necator.* In this case only SCL monomers are accepted by the enzyme. Class II synthases are also composed of two PhaC subunits, only in this case the enzymes are mainly from *Pseudomonas* strains and display substrate specificity mostly towards MCL monomers. Class III synthases are composed of two different subunits, namely, PhaC and PhaE which demonstrate high specificity towards SCL monomers but in some cases, they also accept MCL monomers. Finally, Class IV are also composed of two subunits, PhaC and PhaR, commonly found in *Bacillus* strains (Park *et al*., 2012).

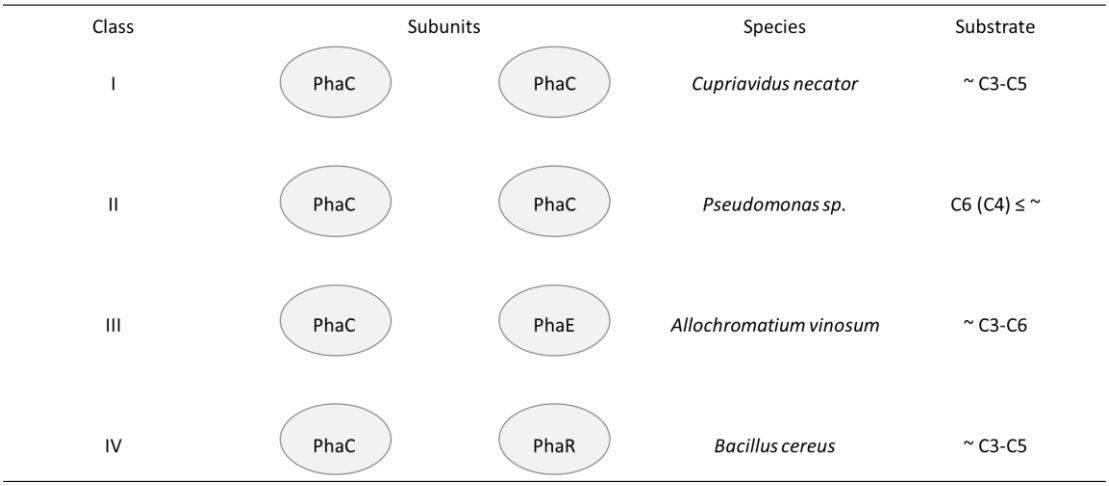

Figure 14: Representative PHA synthases in different classes depending on the subunit composition and substrate specificities (adapted from Park, 2012).

Due to the unusual conditions to which bacteria are subjected, specific metabolic pathways are triggered leading to the production of PHAs. Overall, there are three main pathways for PHA synthesis (Figure 15). The first pathway leads to the direct production of SCL-PHAs. In this case, the carbon source is metabolized via the TCA cycle and two acetyl-CoA molecules are generated. These are then converted to acetoacetyl-CoA by β- ketothiolase which is encoded by the *phaA* gene; acetoacetyl-CoA is then converted to (R)-3-hydroxybutyryl-CoA by acetoacetyl-CoA-reductase which is encoded by the *phaB* gene; finally, (R)-3-hydroxybutyryl-CoA is polymerized into SCL-PHAs by the PHA synthase which is encoded by the *phaC* gene (Chen *et al*., 2015). The second pathway involves the *in situ* fatty acid synthesis cycle resulting

in R-3-hydroxyacyl-ACP for PHA synthesis. The reaction is catalysed by the enzyme (R)-3-hydroxyacyl-CoA-ACP transferase, encoded by the *phaG* gene to generate (R)-3-hydroxyacyl CoA, which is the precursor for MCL-PHA polymerization. (R)-3-hydroxyacyl CoA can then be polymerized into an MCL-PHA by the PHA synthase encoded by the *phaC* gene (Chen *et al*., 2015). Finally, in the third pathway, acyl-CoA is derived from fatty acids and metabolized in the β-oxidation cycle, generating three intermediate products, namely (S)-3-hydroxyacyl-CoA, 2-trans-enoyl-CoA and 3-ketoacyl-CoA. Subsequently, three key enzymes namely, 3-hydroxyacyl-CoA epimerase, enoyl-CoA hydratase and 3-ketoacyl-CoA reductase convert (S)-3-hydroxyacyl-CoA, 2-trans-enoyl-CoA and 3-ketoacyl-CoA, respectively into (R)-3-hydroxyacyl-CoA, which is then polymerized into an MCL-PHA by the PHA synthase encoded by the *phaC* gene (Chen *et al*., 2015).

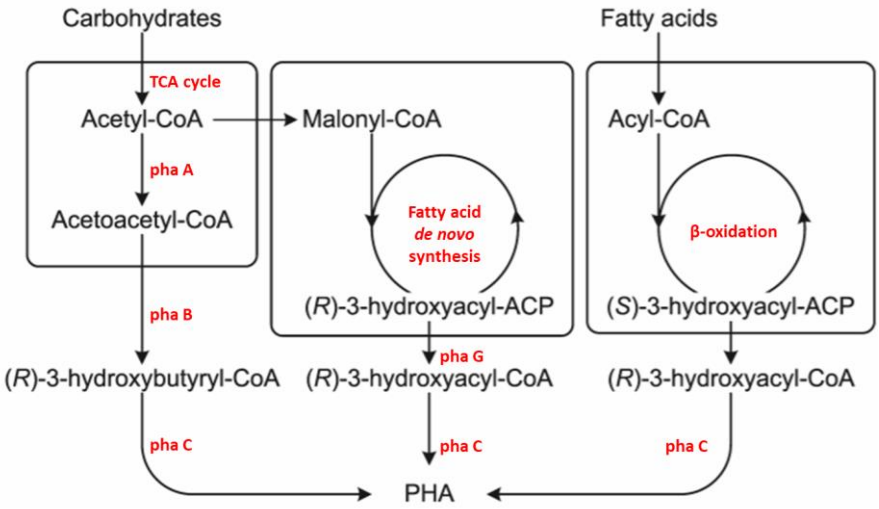

Figure 15: Major pathways related to PHA synthesis (adapted from Tiso *et al*., 2014).

1.4.3 Microbial production of PHAs

PHAs are produced by several Gram-positive and Gram-negative bacteria such as *Pseudomonas, Bacillus, Aeromonas, Rhodobacter* and *Cupriavidus*. They are stored as insoluble granules in the cytoplasm and can reach 80% dry cell weight depending on the growth conditions and the bacteria utilised (Philip *et al*., 2007). *Pseudomonas* spp. have been extensively used to produce MCL-PHAs. These species can grow in structurally related carbon sources like alkanes, alkenes and aldehydes, and unrelated carbon sources which provide precursor substrates that are not similar to its structure (Rai *et al*., 2011). *Cupriavidus necator* is the most widely studied organism to produce PHAs, especially P(3HB). This organism can

produce large amounts of polymer using simple carbon sources such as glucose, lactic acid, acetic acid and several oils such as olive oil and palm oil (Akaraonye, 2010).

1.4.4 Types of PHAs

So far, more than 150 different monomers were identified within the PHA family with a wide range of mechanical and thermal properties (Reis *et al*., 2008). One way to classify PHAs is based on the number of carbon atoms present in the monomer unit. SCL-PHAs have 3-5 carbon atoms present in the monomer unit, whereas MCL-PHAs have 6-14 carbon atoms. PHAs can also be classified as homopolymers or heteropolymers. In the former classification, only one type of hydroxyalkanoate is present in the monomer unit and examples are P(3HB) and poly(3-hydroxyhexanoate), P(3HHx). In the second case more than one kind of hydroxyalkanoate is present in the monomer unit, e.g., P(3HB-co-3HV), poly(3-hydroxyhexanoate-co-3-hydroxyoctanoate), P(3HHx-co-3HO), and poly(3-hydroxybutyrate-co-3-hydroxyhexanoate), P(3HB-co-3HHx) (Rai *et al*., 2011).

Since the monomer composition greatly influences the biopolymer properties, distinct physical properties are expected for both types of PHAs. Poly(3-hydroxybutyrate), P(3HB), and poly(3-hydroxybutyrate-co-3-hydroxyvalerate), P(3HB-3HV), both SCL-PHAs, are brittle, highly crystalline, rigid and have poor mechanical properties, whilst MCL-PHAs, such as poly(3-hydroxyoctanoate), P(3HO), have low crystallinity, low glass transition temperature (T_g), low melting temperature (T_m), low tensile strength and high elongation at break, making them elastomeric polymers (Table 4) (Basnett, 2014, Basnett *et al*., 2013, Roy *et al*., 2014 and Nigmatullin *et al*., 2015).

Table 4: Physical properties of homopolymer SCL-PHAs and homopolymer MCL-PHAs (adapted from Reis *et al*., 2008 and Mozejko-Ciesielska *et al.,* 2019).

	SCL-PHAs	MCL-PHAs
Crystallinity (%)	40-80	20-40
Glass transition temperature (^oC)	-8-9	-60-14
Melting temperature (^oC)	80-180	40-86
Elongation at break (%)	6-10	300-450

1.4.5 Biocompatibility and Biodegradability

One of the most important aspects when considering a material for a biomedical application is its biocompatibility. In 2007, the Food and Drug Administration approved the use of P(4HB) for surgical sutures, which increased the interest of the scientific community to further explore PHAs and its use in biomedical applications (Akaraonye *et* al., 2010, Nigmatullin *et al*., 2015). And so far, there have been many studies, especially the ones exploring tissue engineering applications, showing that PHAs can support the proliferation of several mammalian cell types and are haemocompatible (Nigmatullin *et al*., 2015, Reis *et al*., 2008). Besides biocompatibility, in many cases, the biomaterials used in biomedical applications need to degrade over time, allowing enough time to perform their function and finally be eliminated once their task is completed. Many *in vitro* studies have confirmed a slow hydrolytic degradation of PHAs. One advantage of PHAs is their ability to degrade under both anaerobic and aerobic conditions. As previously mentioned, PHAs can be degraded enzymatically by PHA depolymerases. The rate of biodegradation of a biopolymer is dependent on their physical and chemical properties. Low molecular weight polymers usually degrade faster. Also, microparticles have a higher surface area, thus a higher degradation rate is observed when compared to nanoparticles. Thermal degradation occurs faster if a polymer has a low melting point whereas highly ordered structures have a lower degradation rate (Kalia *et al*., 2016, Phillip *et al*., 2007). The degradation process influences a range of significant events such as cell and host behaviour, tissue regeneration, drug release and naturally the material properties. The degradation products of biomedical biopolymers should not be toxic or immunogenic (Reis *et al*., 2008). PHA degradation products have shown to promote cell proliferation, thereby exhibiting high biocompatibility (Nigmatullin *et al*., 2015).

1.4.6 Applications of PHAs

The fact that PHAs are biocompatible, slowly degrading materials with a wide range of thermal and mechanical properties makes them suitable for several biomedical applications. On one hand, one can have stiff and brittle materials, and on the other hand one can have elastomeric materials. Additionally, the mechanical properties of PHAs can be improved by producing blends, mixing different ratios of the polymers of interest or by producing copolymers using

different fermentation strategies (Kalia *et al*., 2016). A good example is where Escapa *et al*., used a *P. putida* KT2442 mutant and different carbon sources to produce a polymer, poly-3-hydroxy-6-acetylthiohexanoateco-4-acetylthiobutanoate (PHACOS), with high thermal stability up to 200^{o}C, increasing the potential applications due to its processability at higher temperatures (Hazer *et al*., 2012, Escapa *et al*., 2011).

1.4.6.1 Tissue engineering

PHAs are extensively explored in many tissue engineering applications. The principle of tissue engineering is to provide cells that restore, maintain, or improve tissue function. Cells are grown in scaffolds that in principle should be biocompatible and biodegradable. Based on the physical properties of PHAs, hard or soft tissue engineering applications can be targeted. For instance, SCL-PHAs are stiff and brittle so they are often considered for bone tissue engineering. On the other hand, MCL-PHAs and their copolymers are highly elastomeric and flexible materials suitable for applications such as vascular applications and cardiac patches (Rai *et al*., 2011). For instance, in a study conducted by Hayati *et al*., poly(3-hydroxybutyrate)/nano-hydroxyapatite (P(3HB)/nHA) composite scaffolds were fabricated to be used as scaffolds for bone tissue engineering applications. In this case, scaffolds were produced without using organic solvents in order to avoid the presence of traces of substances toxic to cells. The final constructs had interconnected pores, with consistent pore sizes varying from 150 μm to 300 μm and excellent mechanical properties. Finally, the scaffolds seeded with MG-63 cells showed improved cell viability and appropriate cell–scaffold interaction (Hayati *et al*., 2012).

An example of the application of PHAs in the cardiac field is the study done by Kenar *et al*., where the development of a myocardial patch was carried out by blending P(3HB-3HV), poly(L-D,L-lactic acid), (P(L-D,L)LA), and poly(glycerol sebacate), (PGS). In this study, a 3D microfibrous structure was fabricated which allowed the growth of stem cells in an aligned fashion (Kenar *et al*., 2010). In another study, in order to augment the main pulmonary artery in an ovine *in vivo* model, P(4HB) was selected as a biodegradable and absorbable material. Vascular cells isolated from ovine peripheral veins were seeded on bioabsorbable P(4HB) patches. After the procedure was done the seeded patches exhibited a smooth surface with

no dilatation nor signs of stenosis. Macroscopic imaging as well as biochemical assays revealed tissue formation and an increasing cellular and extracellular matrix content. Additionally, the patch showed a near-complete resorption (Stock *et al*., 2000). In terms of cartilage tissue engineering, Zhao *et al*., developed films and scaffolds using P(3HB)/P(3HHx) blends in order to improve the flexibility of the material. The final material showed a higher elongation at break and lower tensile strength as compared with pure P(3HB). Differential scanning calorimetry (DSC) analysis of the blends demonstrated only one glass transition temperature, indicating a good miscibility between the polymers. Further results showed that the scaffolds strongly supported the growth of chondrocytes (Zhao *et al*., 2003).

One of the properties required for cartilage tissue engineering is for the scaffolds to have adequate hydrophilicity since it can affect the biomechanical properties of the engineered cartilage. In order to improve the hydrophilicity of P(3HB-3HV), Bioglass (BG) was used to develop P(3HB-3HV)/BG composite scaffolds. *In vitro* and *in vivo* experiments were conducted to evaluate cartilage regeneration between the cartilage layers grown on P(3HB-3HV) and P(3HB-3HV)/BG scaffolds. The incorporation of BG in the constructs improved its hydrophilicity and consequently its biomechanical properties. Its addition also improved the percentage of adhesion and migration of the cells and resulted in a thicker cartilage-like tissue (Wu *et al*., 2013). P(3HB-3HV) is characterised by its slow degradation, allowing time for tissue regeneration and at the same time giving space for the formation of new tissue. Furthermore, it is known to have controllable drug release profiles, a property suitable for delivering growth factors. Finally, due to its biocompatibility, processes such inflammations are less likely to occur.

In the field of neural tissue engineering, P(3HB-3HV) microspheres were developed to investigate their ability to support the growth of a variety of neuronal cell types such as PC12 cells, cortical neurons (CNs), and neural progenitor cells (NPCs). Overall, the results indicated that P(3HB-3HV) microspheres were good in supporting neuronal growth and proliferation due to an increase in DNA and mitochondrial activity. Additionally, they promoted axon and dendrite segregation, an indication to the support of neuronal maturation (Chen *et al*., 2012).

PHAs have also been explored in liver tissue engineering applications. In a study conducted by Su *et al*., mesenchymal stem cells isolated from umbilical cord (UC-MSCs) were loaded onto poly(3-hydroxybutyrate-co-3-hydroxyvalerate-co-3-hydroxyhexanoate), P(3HB-co-3HV-co-3HHx), scaffolds in order to study the recovery of injured livers. To do so, a liver-injured mouse model was used, and scaffolds loaded with UC-MSC cells were transplanted into them. Compared to a normal liver, a similar liver morphology on scaffolds loaded with UC-MSC cells was obtained. Liver functional assays of animal serum using damaged livers, on which scaffolds loaded with UC-MSCs were used, revealed that the concentration of albumin significantly increased, whereas concentrations of total bilirubin and alanine aminotransferase decreased. A scenario also observed in a normal liver. Finally, liver tissue sections from the scaffolds loaded with UC-MSC cells showed a similar structure, size and shape compared to normal livers and there was almost no cell injury or inflammatory response. Thus, results indicated that P(3HB-3HV-3HHx) and cell therapy approaches can potentially be used in liver tissue engineering applications (Su *et al*., 2014).

One of the most common treatments for bladder cancer is enterocystoplasty (bladder augmentation). This technique consists of bladder reconstruction using natural tissue. However, there are many disadvantages associated with this type of treatment and tissue engineering is gaining more ground in this field. In a recent study, Karahaliloğlu *et al*., performed a surface-modification of P(3HB) with poly(ethylene glycol), (PEG) or ethylenediamine, (EDA), via radio frequency glow discharge method. Because surface modification is known to accelerate tissue regeneration, the selected plasma modification was done to enhance cell attachment and proliferation. The final material showed enhanced uroepithelial cell viability and proliferation. Moreover, an inhibition of calcium oxalate growth was observed, a major constituent of human kidney stones (Karahaliloğlu *et al*., 2016). Also, P(3HB-co-3HV) was chemically modified and used to study the growth of urothelial cells to repair bladder dysfunctions and diseases. In this case, the P(3HB-co-3HV) surface was modified by chemical treatment with EDA and sodium hydroxide (NaOH). This treatment decreased the hydrophobicity of the material, providing functional groups that enabled the grafting of a laminin derived sequence, YIGSR sequence (Tyr-Ile-Gly-Ser-Arg), a pentapeptide known to influence cell differentiation, migration, and adhesion. The modifications made to the material substantially improved cell-scaffold interactions (García-García *et al*., 2012).

1.4.6.2 Medical device development

Medical sutures are important medical devices. They are used for tissue connection, haemostasis and wound healing applications. There are some characteristics required for a good medical suture such as even superficial texture, ease to tie and grip, biocompatibility, tensile strength, ease to sterilize, resistance for bacterial growth and biodegradability. PHAs were explored for the development of medical sutures by making two types of fibres, namely a monofilament made from P(3HB-co-3HHx) and a multi-filament made from P(3HB-3HV) and polylactic acid (PLA) blend. The results obtained were promising as they showed that the fabricated fibres were highly biocompatible and non-toxic. Moreover, after 24 months of implantation in rats, the P(3HB-co-3HHx) fibres maintained more than half of its tensile strength (He *et al*., 2014). Another application exploring PHAs focused on the development of a conduit made of P(3HB) fibres coated with alginate hydrogel containing fibronectin. In this experiment, the fibres were implanted in adult rats after cervical spinal cord injury and in a later stage, the addition of neonatal Schwann cells - known to support regeneration - was carried out. The implants resulted not only on the survival of rubrospinal neurons but also in axon regeneration after addition of neonatal Schwann cells (Novikov *et al*., 2002).

1.4.6.3 Antibacterial PHAs

Many studies have also focused on the development of PHAs with antibacterial features. One of the most common approaches to develop PHAs with antibacterial properties is by loading them with natural agents such as plant-derived compounds or essential oil-derived compounds. Blends containing PHAs and curcumin have been prepared using the solvent casting technique, resulting in films that have shown wound healing properties and antibacterial activity against both Gram-positive and Gram-negative strains (Pramanik *et al*., 2015). Tailoring PHAs to achieve antibacterial properties can also be achieved by chemical functionalisation. Polymer modification can either occur via pre-treatment or via chemical grafting. Pre-treatment methods include ozone, plasma, and alkali treatments that are used to modify the polymer surface so that functional groups such as carboxylic, amine, or hydroxyl groups can be introduced in the side chains of PHAs without affecting their bulk properties and used for covalent immobilization of antibacterial agents (Hoefer *et al*., 2009). P(3HB) and

P(3HB-co-3HV) have been treated with ozone to graft carboxylic groups using acrylic acid. Grafting of chitosan was then carried out by esterification of the carboxylic groups, resulting in a promising antibacterial material (Hu *et al*., 2003). Photografting, a chemical grafting technique, is also widely used due to its green and cost-effective characteristics. This method can be carried out through a one-step grafting process by adding a monomer and a photoinitiator to the polymer, or through preliminary activation of the polymer followed by monomer polymerization. Antibacterial materials based on P(3HB-co-3HV) electrospun fibres have been developed using a ketone-based photoinitiator for UV photografting of polymethacrylic acid (PMMA). Further *in situ* generation of AgNPs complexed by PMMA led to the formation of an active material capable of reducing bacterial adhesion (Versace *et al*., 2013). Chemical grafting has also been employed to produce antibacterial composite membranes based on PHAs and chitosan using radical initiators such as benzoyl peroxide and grafting agents such as maleic anhydride (Wu *et al*., 2015).

By controlling the substrates provided during the fermentation process, it is also possible to produce PHAs with antibacterial properties. For example, using a co-feeding experiment with decanoic acid as an inducer of growth and PHA synthesis and 6-acetylthiohexanoic acid as the PHA precursor, PHAs containing acetylthioester groups in the side chain have been obtained. The final material, also referred to as thio-PHAs, revealed an efficient inhibition of the growth of methicillin-resistant *S. aureus* (MRSA), both *in vitro* and *in vivo* (Dinjaski *et al*., 2014; Escapa *et al*., 2011; Escapa *et al*., 2011).

1.4.7 Limitations of PHAs

One of the major limitations of PHA production is associated with the low yields and productivity, which ultimately leads to high production costs. Over the years, extensive research has been done to optimise PHA production and decrease its associated costs. For instance, studies on the metabolic pathways involved in PHA production have been carried out to optimise PHA production. Firstly, this permitted the development of recombinant strains capable of expressing heterologous PHA biosynthesis genes to produce different types of PHAs; secondly with the use of metabolic engineering, metabolic pathways were created or improved to enhance the production of PHAs; and thirdly by knowing which metabolic pathways were involved in PHA production different fermentation strategies were explored

(Amache *et al*., 2013 and Park *et al*., 2012). Thakor *et al*., used *Comamonas testosterone* and different cheap vegetable oils as sole carbon sources to produce MCL-PHAs. With only one strain, different PHAs with different 3-hydroxyalkanoic acids were produced, namely, 3-hydroxyhexanoic acid, 3HHx; 3-hydroxyoctanoic acid, 3HO; 3-hydroxydecanoic acid, 3HD; 3-hydroxydodecanoic acid, 3HDD; and 3-hydroxytetradecanoic acid, 3HTD. The efficiency of conversion of oils to PHAs varied from 53.1% to 58.3% for different vegetable oils (Thakor *et al*., 2005). In another study, metabolic engineering techniques such as metabolic flux analysis were applied to study P(3HB) production by mixed microbial cultures. Based on a metabolic model, an algorithm was developed to enable an on-line bioprocess monitoring and control of the fermentation process (Dias *et al*., 2009). Another study involved the development of an *in-silico* model to tailor *Pseudomonas putida* for the synthesis of MCL-PHAs using glucose as a carbon source. In this case, elementary flux mode analysis was used to predict genetic targets for strain engineering that would improve polymer accumulation as compared to wild type strains (Poblete-Castro *et al*., 2013). Since the carbon substrate accounts for more than 50% of the overall PHA production costs, the production of PHAs using inexpensive carbon sources has also been explored over the last years. For example, in a study conducted by Allen *et al*., the seed oil of *Jatropha curcas* plant was used as a cheap substrate to produce PHAs by *Pseudomonas oleovorans* (ATCC 29347). The results showed that a yield of 26.06% cell dry weight was achieved after 72 h (Allen *et al*., 2010). In another study conducted by Chaudhry *et al*., corn oil was explored as a potential cheap carbon source for PHA production and in this case, a bacterial strain from *Pseudomonas* spp. was able to accumulate PHAs up to 35.63% (Chaudhry *et al*., 2011). Optimisation of the fermentation strategies are also a way forward to optimise PHA production and accumulation. There are three main fermentation strategies to produce PHAs, that is, batch, fed-batch and continuous cultivation processes. Batch cultivations are based on a constant process in which the substrates (e.g., culture medium and carbon source) are fed in the beginning of the process and the final product (e.g., PHAs) is collected at the end of the process. Additionally, batch cultivations can be done using two different strategies, namely a one-stage cultivation or a two-stage cultivation. A one-stage batch cultivation occurs when the cell proliferation, the synthesis and polymer accumulation take place at the same time, while in a two-stage batch cultivation, the cell proliferation and the synthesis and polymer accumulation are done in separate phases. In the first phase, bacteria are cultivated in ideal conditions to ensure a high cell density, and in the second

phase, nutrient limiting conditions are used to trigger the synthesis and accumulation of PHAs. Fed-batch strategies are characterised by constant supplementation of substrates during the fermentation process and the collection of the final product at the end of the process. This ensures constant supplementation of nutrients and a carbon source contributing to the effective bacterial growth and polymer accumulation. In continuous strategies, the substrates are fed continuously to the bioreactors while the final products are also continuously removed from the bioreactors. If a steady flow of the feed and the effluent are achieved, then a steady state is also reached where the biomass concentration and PHA content are also kept constant. The last two fermentation strategies yield the highest productivity. Fed-batch cultivations are usually more efficient processes because high cell densities and product accumulation can be achieved. On the other hand, continuous cultivations offer higher product consistency and less batch-to-batch variations but if a microbial contamination occurs, it may compromise the entire fermentation process and cause extensive economic loss. Therefore, comprehensive and detailed studies need to be performed to ensure the best method is developed for PHA production in industrial settings (Khanna *et al*., 2005, Mozejko-Ciesielska *et al*., 2019).

1.5 Aims and objectives

The main aim of this project was to develop novel antibacterial, anti-adhesive and anti-biofilm biomaterials based on polyhydroxyalkanoates for biomedical applications.

To achieve this goal, six main objectives were defined as it follows:

1. **Production and characterisation of Polyhydroxyalkanoates**

Gram-positive bacterium *Bacillus subtillis* OK2 and Gram-negative bacterium *Pseudomonas mendocina* CH50 were selected to produce short-chain-length-PHAs, i.e., P(3HB), and medium-chain-length-PHAs, i.e., P(3HO-co-3HD), respectively. Polymer production was carried out by bacterial fermentation using nitrogen limiting conditions and glucose as the carbon source. More specifically, a one-stage batch cultivation was used to grow *Bacillus subtillis* OK2 and a two-stage batch cultivation was used to grow *Pseudomonas mendocina* CH50.

The polymers obtained were characterised using Attenuated Total Reflectance Fourier Transform Infrared Spectroscopy, Gas Chromatography-Mass Spectrometry and Nuclear Magnetic Resonance. The polymers were further characterised using tensile testing and dynamic scanning calorimetry to elucidate the mechanical and thermal properties of the materials, respectively.

2. Selection and antibacterial characterisation of novel antibacterial agents

Potential antibacterial agents belonging to three different classes were selected and characterised with respect to its antibacterial properties against *Staphylococcus aureus* (ATCC® 29213™), *Staphylococcus epidermidis* (ATCC® 35984™) and *Escherichia coli* (ATCC® 35218™). Namely, quorum sensing inhibitor, trans-cinnamaldehyde; three different antimicrobial peptides, i.e., AMP3, Nut2 and LL-37 and a biofilm disrupting enzyme termed Dispersin B were selected.

3. Fabrication of antibacterial SCL-PHAs films using P(3HB) and trans-cinnamaldehyde

Based on the antibacterial screening, three different polymer compositions of P(3HB) and trans-cinnamaldehyde were prepared and films were fabricated using the solvent casting technique. The chemical, mechanical, thermal and surface properties were assessed using Attenuated Total Reflectance Fourier Transform Infrared Spectroscopy, tensile testing, differential scanning calorimetry, scanning electron microscopy and static water contact angle measurements, respectively. Furthermore, the antibacterial properties of the films were evaluated by performing the disc diffusion assay, by evaluating the duration of the antibacterial action of the films over a period of 7-days and by evaluating its anti-biofilm properties against *S. aureus* (ATCC® 29213™), *S. epidermidis* (ATCC® 35984™) and *E. coli* (ATCC® 35218™).

4. Development of antibacterial coatings using P(3HB) and trans-cinnamaldehyde

Based on the antibacterial performance of the films, the best polymer composition of P(3HB) and trans-cinnamaldehyde was selected and used to coat polyurethane tubes in order to develop new antibacterial PHA-based coatings. The surface characterisation of the coated polyurethanes was evaluated by scanning electron microscopy and the antibacterial performance of the coatings was assessed against *Staphylococcus epidermidis* (ATCC® 35984™). The effect against planktonic bacteria and on bacterial adhesion was investigated,

as well as its biofilm inhibiting properties. Finally, cytocompatibility studies were performed to evaluate the cytotoxicity of the materials against L929 murine fibroblasts and haemocompatibility studies were carried out to investigate the reaction of blood cells after direct contact with the materials.

5. **Fabrication of antibacterial MCL-PHAs films using P(3HO-co-3HD), antimicrobial peptides and Dispersin B**

Based on the antibacterial screening, AMP3, Nut2, LL-37 and Dispersin B were physically adsorbed independently to P(3HO-co-3HD) solvent casted films. Surface characterisation of the materials was carried out by X-ray photoelectron spectroscopy, Attenuated Total Reflectance Fourier Transform Infrared Spectroscopy as well as static water contact angle measurements. Cytocompatibility studies were performed to evaluate the cytotoxicity of the materials against L929 murine fibroblasts. The anti-adhesive properties of the materials were evaluated against *S. aureus* (ATCC® 29213™), *S. epidermidis* (ATCC® 35984™) and *E. coli* (ATCC® 35218™).

6. **Development of antibacterial fibre meshes using P(3HO-co-3HD), antimicrobial peptides and Dispersin B**

Beadless and slightly aligned electrospun P(3HO-co-3HD) fibre meshes were fabricated by optimising the electrospinning process. The morphology of the fibre meshes was observed using bright field microscopy and scanning electron microscopy. The same method used in the previous objective was applied to physically adsorb Nut2 and Dispersin B, independently and in combination to electrospun P(3HO-co-3HD) fibre meshes in order to develop new antibacterial PHA-based fibres. In addition, an alternative method was used to covalently couple AMP3 and Dispersin B, independently and in combination with electrospun P(3HO-co-3HD) fibre meshes. Surface changes were evaluated by measuring the water contact angle of the newly developed fibres. Additionally, cytocompatibility studies were performed to evaluate the cytotoxicity of the fibres against L929 murine fibroblasts. Finally, the anti-adhesive and anti-biofilm properties of the fibres were evaluated against *S. epidermidis* (ATCC® 35984™).

2 Chapter 2 Materials and Methods

2.1 Chemicals, reagents and materials

Chemicals, reagents and materials were obtained from Sigma-Aldrich Company Ltd (UK and Germany), Thermo Fisher Scientific (UK and Germany), VWR International (UK) and Carl Roth GmbH + Co. KG (Germany). Antibiotic discs were obtained from Oxoid Germany GmbH and Mast Diagnostica Labortechnik (Germany). Polyurethane tubes were purchased from Amazon.de (supplier: GreitaPigu, Lithuania). Teleflex medical ARROWg+ard Blue PLUS Central Venous Catheters were provided by Operative Intensive Care Unit, University Medical Centre Knappschaftskrankenhaus Bochum, Hospital of the Ruhr-University Bochum, Germany.

2.2 Cell lines and cell culture materials

L929 murine fibroblasts were obtained from DSMZ (Collection of Microorganisms and Cell Cultures GmbH). Roswell Park Memorial Institute (RPMI) medium, L-glutamine, 10% foetal bovine serum and 1% Penicillin-Streptomycin (10.000 U/mL Penicillin, 10 mg/mL Streptomycin) were obtained from PAN Biotech (Germany), as well as trypsin 0.25%/1 mM EDTA and Dulbecco's Phosphate-Buffered Saline (DPBS) without calcium and magnesium. Triton® X-100 lysis solution and CellTiter-Blue® Cell Viability Assay Kit were purchased from Promega. Live/dead Cell Staining Kit II was purchased from PromoKine. Cytocompatible control material polyethylene (PE), and cytotoxic control material zinc diethyldithiocarbamate containing polyurethane (ZDEC-PU) were obtained from Goodfellow and Hatano Research Institute, respectively.

2.3 Bacterial strains

Polyhydroxyalkanoate production: *Bacillus subtilis* OK2 and *Pseudomonas mendocina* CH50 were obtained from the culture collection of the University of Westminster to produce SCL-PHAs and MCL-PHAs, respectively.

Antibacterial testing: *Staphylococcus aureus* (ATCC® 29213™), *Staphylococcus epidermidis* (ATCC® 35984™) and *Escherichia coli* (ATCC® 35218™) were purchased from the American Type Culture Collection (ATCC). Bacteria were kept in a glycerol stock in the freezer, at -20°C for routine usage or at -80°C for longer storage duration.

2.4 Polymers and antibacterial agents

Trans-cinnamaldehyde (TC) was obtained from Sigma-Aldrich Company Ltd. (UK and Germany) and used without further modifications. DB was provided by Kane Biotech, Inc (Canada) in a buffer solution consisting of 50 mM phosphate buffer (pH 5.8) with 100 mM sodium chloride and 50% glycerol. AMPs here called LL-37, Nut2 and AMP3 were synthesised by the National Physical Laboratory (UK) and were provided in the form of lyophilised powder. The peptides were kept in the freezer, at -20°C for routine usage.

An amphiphilic six-armed star-shaped poly(ethylene oxide-stat-propylene oxide) containing reactive isocyanate groups at the distal ends of the polymer chains, NCO-sP(EO-stat-PO), was provided by Dr. Jürgen Groll, Department for Functional Materials in Medicine and Dentistry and Bavarian Polymer Institute, University of Würzburg, Würzburg, Germany.

2.5 Production of polyhydroxyalkanoates (PHAs)

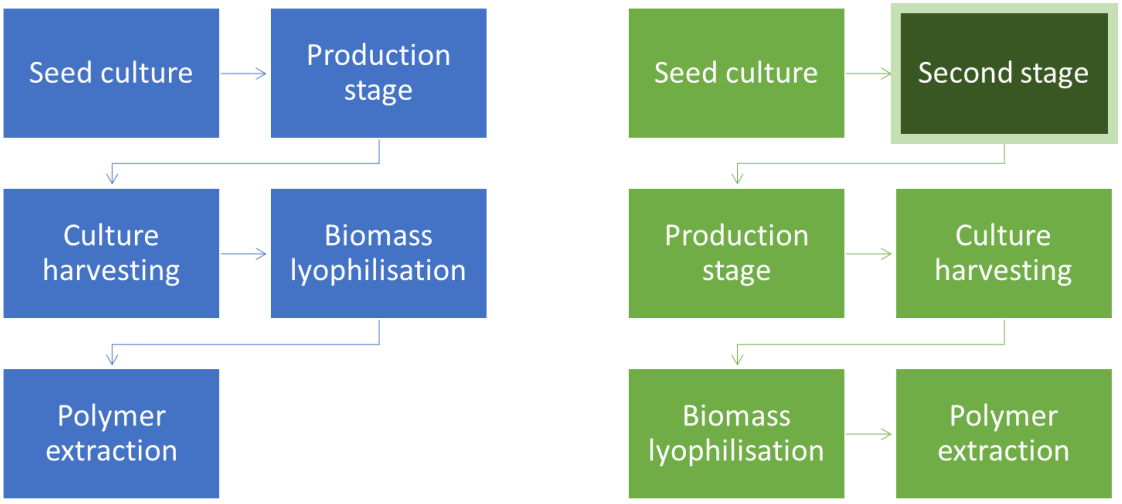

Figure 16: Schematic representation of the steps involved in the production of SCL-PHAs (left) and MCL-PHAs (right).

The production of PHAs was carried out in a batch cultivation mode using two different strategies. Briefly, the seed culture was obtained by growing a single bacterial colony in a nutritious media to ensure that bacteria entered the exponential phase (log phase). In the case of SCL-PHA production, the seed culture was then transferred to the production stage media with a nutrient deficient media to induce the synthesis of PHAs. On the other hand, in

the case of MCL-PHA production, the seed culture was firstly transferred to the second stage media as an acclimatisation step and then transferred to the production stage media to induce the synthesis of PHAs. After the production stage, the culture was harvested, and the biomass lyophilised. Once the biomass was dried, the polymer was extracted and further characterised (Figure 16).

2.5.1 Media composition

The following tables contain the different media compositions used to produce SCL and MCL-PHAs.

Table 5: Seed culture medium (Nutrient Broth No2).

	Concentration (g/L)
Meat peptone	4.30
Casein peptone	4.30
Sodium chloride	6.40

Table 6: Mineral Salt Media, MSM (Rai *et al.,* 2011b and Tian *et al.,* 2000).

	Second Stage Concentration (g/L)	**Production Stage Concentration (g/L)**
Potassium dihydrogen phosphate	2.38	2.65
Ammonium sulphate	0.45	0.50
Sodium hydrogen phosphate	3.42	3.80
Magnesium sulphate	0.80	0.80
Glucose	20.00	20.00
Trace elements solution	1 mL/L	1 mL/L

Table 7: Kannan and Rehacek medium, K/R (Kannan and Rehacek, 1970).

	Concentration (g/L)
Ammonium sulphate	5.00
Potassium chloride	3.00
Yeast extract	2.50
Glucose	35.0

Table 8: Trace elements solution, TES (Rai et al., 2011b).

	Concentration (g/L)
$CoCl_2$	0.22
$CaCl_2$	7.80
$FeCl_3$	9.70
$NiCl_3$	0.12
$CrCl_3 \cdot 6H_20$	0.11
$CuSO_4 \cdot 5H_20$	0.16

2.5.2 Production of MCL-PHAs by *Pseudomonas mendocina* CH50

The production of MCL-PHAs by *P. mendocina* CH50 was carried out in a 14L glass bioreactor (Electrolab Biotech Ltd) with a working volume of 10L as previously described by Basnett *et al.,* 2017 with minor modifications. After media preparation, the pH of the media was adjusted to 7 before sterilisation. All media components were then sterilised at 121°C for 15 minutes, except glucose which was sterilised at 110°C for 10 minutes. The inoculum was obtained by growing a single colony of *P. mendocina* CH50 in the seed culture medium (Table 5) for 16 hours at 30°C, 130 rpm. 10% (v/v) of the inoculum was grown in the second stage MSM (Table 6) and incubated for 24 hours at 30°C, 130 rpm. 10% (v/v) of the inoculum was used to inoculate the production stage MSM (Table 6) and the culture was incubated for 48 hours at

30°C, 200 rpm. The fermentation process ran with an air flow of 1 gas volume flow per unit of liquid volume per minute (vvm).

2.5.3 Production of SCL-PHAs by *B. subtilis* OK2

The production of SCL-PHAs by *B. subtilis* OK2 was carried out in a 20L stirred stainless steel tank bioreactor (Electrolab Biotech Ltd) with a working volume of 14L as previously described by Valappil *et al.,* 2007 with minor modifications. After media preparation, the pH of the media was adjusted to 6.8 before sterilisation. All media components were then sterilised at 121°C for 15 minutes, except glucose which was sterilised at 110°C for 10 minutes. The inoculum was obtained by growing a single colony of *B. subtilis* OK2 in the seed culture medium (Table 5) for 16 hours at 30°C, 130 rpm. 10% (v/v) of the inoculum was grown in the production stage of K/R medium (Table 7) and incubated for 48 hours at 30°C, 200 rpm. The fermentation process ran with an air flow of 1 vvm.

2.5.4 Culture harvesting, biomass lyophilisation and polymer extraction

After the fermentation process, the culture was harvested, and the biomass was obtained by centrifuging the cultures at 4600 rpm for 30 minutes. The biomass was lyophilised and once dried, the polymer was extracted via a Soxhlet extraction method. Briefly, the biomass was crushed into a fine powder and placed into an extraction thimble. The Soxhlet extraction apparatus was assembled to perform a two-stage extraction. On a first stage methanol was used to remove any impurities present in the biomass, and the solvent was refluxed at 90°C for 16 hours. On a second stage, chloroform was used to extract the polymer from the biomass, and the solvent was refluxed at 80°C for 24 hours. The polymer was concentrated using a rotary vacuum evaporator until a viscous solution was observed and precipitated in ice-cold methanol under stirring conditions. The polymer was left to dry at ambient conditions for a period of 7 days inside a continuously running fume hood.

2.5.5 Temporal profiling of polyhydroxyalkanoate production

A temporal profiling of the batch cultivation was carried out to monitor and control the fermentation process. Briefly, 1 mL samples were taken, in triplicate, from the culture at specific time points to monitor the pH, biomass content, optical density, glucose and nitrogen concentration over time. For each sample taken, the optical density was measured either at

450 nm for *P. mendocina* CH50 or at 600 nm for *B. subtillis* OK2, using a spectrophotometer (Single Beam Spectrophotometer, SB038 Cadex Inc) and using the seed culture media as a blank. If needed, the culture was diluted with sterile seed culture media. The samples were transferred into pre-weighed eppendorfs and centrifuged at 13.200 rpm for 10 minutes (Heraeus Pico 17 Centrifuge, Thermofisher Scientific, MA, US). The supernatant was used to measure the pH (Mettler Toledo Ltd., Leicester) and the pellet was freeze dried to obtain the biomass in dry cell weight (DCW).

Glucose concentration was estimated according to Miller, with minor modifications (Miller, 1959). Briefly, 1 mL of Dinitrosalicylic acid (DNS) assay reagent was mixed with 1 mL of diluted supernatant and incubated in a water bath for 10 minutes at 90°C. After the incubation period, 330 µL of 40% sodium potassium tartrate solution were added to the mixture to maintain the colour intensity. The absorbance was read at 575 nm and a glucose standard curve was used to determine the glucose concentration of each profiling sample supernatant.

The amount of nitrogen was estimated in the form of ammonia ions using the phenol hypochlorite method. 250 µL of diluted supernatant were mixed with 100 µL of phenol nitroprusside buffer and mixed gently. To this mixture, 150 µL of hypochlorite reagent containing 4% active chlorine and 40 mL of 1M sodium hydroxide solution were added and the samples were incubated for 45 minutes, protected against light. The absorbance was read at 635 nm and nitrogen was estimated using a calibration curve prepared with ammonium sulphate.

2.6 Characterisation of polyhydroxyalkanoates

2.6.1 Attenuated Total Reflectance Fourier Transform Infrared Spectroscopy (ATR-FTIR)

The functional groups of PHAs were identified by ATR-FTIR using the Perkin-Elmer Spectrum Two Spectrometer equipped with a Universal ATR accessory (Perkin-Elmer, USA). Polymer samples were placed in a diamond/ZnSe crystal with a depth of penetration between 2 and 4 µm. A spectral range between 4000 to 400 cm^{-1} with a spectral resolution of 8 cm^{-1} was considered. Each spectrum was generated with 4 scans. The analysis was carried out at the University of Westminster, London, UK.

2.6.2 Gas Chromatography-Mass Spectrometry (GC-MS)

The monomeric composition of PHAs was identified by GC-MS using a Chrompack CP-3800 gas chromatograph and a Saturn 200 MS/MS block (Varian Inc, California, USA). Prior to the analysis, PHAs were converted into monomeric volatile esters via methanolysis. Briefly, 30 mg of polymer were placed inside a reflux tube and dissolved in 3 mL of chloroform. 20 µl of methyl benzoate (internal standard) were added to the mixture followed by the addition of 3 mL of 15% sulphuric acid solution in methanol. The reaction mixture was refluxed for 16h in the case of MCL-PHAs and for 4h in the case of SCL-PHAs. Afterwards, the tubes were cooled down on ice for 5 minutes. 2 mL of HPLC water was added to the sample and vortexed for 1 minute. A layer separation was observed and the bottom layer containing the polymer was dried using a mixture of sodium bicarbonate (10 mg) and sodium sulphate (10 mg), and vortexed for 5 min. Finally, the mixture was filtered using a Whatman No 1 filter paper and transferred to a clean vial to be further analysed. The analysis was carried out at the University of Westminster, London, UK.

2.6.3 Nuclear Magnetic Resonance (NMR)

Structural characterisation of the polymer was done by ^{13}C and ^{1}H NMR spectroscopy using an Avance III 600 equipped with an inverse TXI $^{1}H/^{13}C/^{15}N$ probe (Bruker, Coventry UK). For this analysis, 20 mg of polymer were dissolved in 1 mL of deuterated chloroform ($CDCl_3$) and transferred into an NMR tube. Data acquisition and processing were performed using standard Bruker TopSpin (version 2.1) software. ^{1}H and ^{13}C chemical shifts were calibrated using residual solvent peak (^{1}H 7.26 ppm, ^{13}C 77.15 ppm for chloroform) and all NMR spectra were measured at 298 K. The samples were sent to the Department of Chemistry, University College London, UK for NMR analysis.

2.6.4 Mechanical analysis: Tensile testing

Tensile testing was performed using a 5942 Instron Testing system equipped with a 500 N load cell (Buckinghamshire, UK), in ambient conditions. SCL and MCL-PHA films were prepared by the solvent casting technique where PHAs were dissolved in chloroform at 5 w/v%. The solution was mixed overnight and then poured onto a glass petri dish. The glass petri dish was covered to prevent any contamination from the environment and kept inside a continuously

running fume hood for 7 days at ambient conditions to allow the solvent evaporation. Once the films were dry, film strips were cut into a pre-defined size of 5-mm wide and 35-mm long. Their thickness was measured with a micrometer caliper. The specimens were placed in the tensile machine and clamped with a hydraulic grip and the length between the upper clamping jaw and lower clamping jaw was set to 23 mm. The samples were stretched at 5 mm/minute in the case of SCL-PHAs and 10 mm/minute in the case of MCL-PHAs, until break. The extension and load were recorded throughout the stretching process and used to calculate the elastic modulus (E), tensile stress (σ) and elongation at break (ε_b) for each sample. The data obtained was processed using the BlueHill 3 software. The analysis was carried out at the University of Westminster, London, UK. The experiments were performed in three independent experiments, in quintuplicates (N= 3, n=5).

2.6.5 Thermal analysis: Differential Scanning Calorimetry (DSC)

The thermal properties of PHAs were analysed using a DSC 214 Polyma equipped with an Intracooler IC70 cooling system (Netzsch, Germany). Polymer samples were placed in standard aluminium pans and transferred to the autosampler. Initially, polymer samples were cooled down to -70^{o}C. The first heating ramp was set to +200^{o}C for SCL-PHAs or +130^{o}C for MCL-PHAs with a heating rate of 10^{o}C/minute. After the first heating ramp, the samples were maintained for 2 minutes at either +200^{o}C for SCL-PHAs or +130^{o}C for MCL-PHAs to allow the melting of the sample and eradicate its thermal history. The samples were then cooled to -70^{o}C with a heat flow of 20^{o}C/minute and stabilised at that temperature for 15 minutes. A second heating ramp was performed to +210^{o}C for SCL-PHAs or +130^{o}C for MCL-PHAs with a heating rate of 10^{o}C/minute and then the samples were cooled down to 25^{o}C. This analysis allowed the calculation of the melting temperature (T_m), glass transition temperature (T_g) and peak crystallisation temperature (T_c). Thermograms were analysed using Netzsch - Proteus 7.0 software. The analysis was carried out at the University of Westminster, London, UK.

2.7 *In vitro* antibacterial characterisation of TC

2.7.1 Minimum inhibitory concentration and minimum bactericidal concentration

The MIC and MBC of TC was determined against *E. coli* (ATCC® 35218™), *S. epidermidis* (ATCC® 35984™) and *S. aureus* (ATCC® 29213™), according to the ISO 20776-1:2006 guidelines in a 96 tissue-culture polystyrene (TCPS) microplate (ISO 20776-1:2006(E)).

The preparation of the inoculum was done by culturing bacteria overnight on blood agar plates at 37°C for 16 hours. Using a sterile loop, a single colony was re-suspended in a glass tube containing 2 mL of 0.9% NaCl and using a densitometer, the bacterial suspension was adjusted to McFarland 0.5 (10^8 CFU/mL). The bacterial suspension was further diluted 1:200 in Mueller-Hinton-Broth (MHB) to obtain the recommended inoculum of $5x10^5$ CFU/mL.

TC was prepared by making a stock solution of 4M in 100% dimethyl sulfoxide (DMSO). The stock solution was further diluted in MHB to obtain a concentration of 40 mM in 1% DMSO.

Serial two-fold dilutions of TC were prepared by incubating 50 µL of the bacterial suspension with 50 µL of the TC solution to provide a range of TC testing concentrations from 20 mM to 0 mM. The plates were incubated at 37°C for 24 hours and the MIC was determined as the lowest concentration of TC that completely inhibited bacterial growth by observing the turbidity of the wells by naked eye. The experiments were performed in three independent experiments, in triplicates (N=3, n=3).

The MBC was determined directly after identifying the MIC. For that, the supernatant of the wells corresponding to the MIC and of three concentrations above the MIC (when possible) were removed and spread homogeneously onto blood agar plates with the help of a sterile loop. The plates were incubated at 37°C for 24 hours. After the incubation period, the number of colonies were counted and compared to the number of colonies obtained in the growth controls at the beginning of the experiment. The MBC was determined as the lowest concentration of the compound that killed 99.9% or more of the bacteria, relative to that in the initial inoculum. The experiments were performed in three independent experiments, in duplicates (N=3, n=2).

Wells containing 100 µL of MHB without bacteria were considered as negative controls and wells containing 100 µL of MHB with bacteria were considered as the growth controls.

2.7.2 Anti-biofilm properties: Inhibition of biofilm formation

The ability of TC to inhibit biofilm formation was evaluated by quantifying the biofilm biomass formed after a 24-hour incubation of bacteria with increasing concentrations of TC by adapting the protocol described by Kiran *et al*. (Kiran *et al.,* 2008). The preparation of the inoculum, the preparation of the TC stock solution as well as the incubation of bacteria with increasing

concentrations of TC was performed as described in section 2.7.1. After the 24-hour incubation period, the supernatant was entirely removed from the wells and the wells were carefully washed twice with 100 µL of DPBS and dried at room temperature. To fix the biofilms, 100 µL of 100% ethanol were added to each well and the plate was incubated for 15 minutes at room temperature. The ethanol was removed, and the biofilms were stained with 100 µL of a 0.1% safranin-O solution and incubated for 5 minutes at room temperature followed by a washing step with 100 µL of DPBS. Finally, the stained biofilms were re-suspended in 100 µL of 1% sodium dodecyl sulfate (SDS) and the amount of biofilm was quantified by measuring the optical density of the dissolved safranin-O at 495nm (OD_{495}). The experiments were performed in three independent experiments, in triplicates (N=3, n=3).

2.8 Fabrication of P(3HB) films loaded with TC

2.8.1 Film development

P(3HB) was dissolved in chloroform at 5 w/v% and the solution was mixed overnight. After this period, TC was added to the polymer solution at different weight percentages and the mixture was stirred overnight until a homogenous solution was obtained. Finally, the mixture was poured onto a glass petri dish covered with a lid to prevent any contamination from the environment. The glass petri dishes were kept inside a continuously running fume hood at ambient conditions and allowed to dry for a period of 7 days. The resulting P(3HB)/TC films are here described as P(3HB) films with 11.5 wt% TC, P(3HB) films with 13 wt% TC and P(3HB) films with 16.7 wt% TC. The films samples were stored in glass petri dish sealed with parafilm for further use.

2.8.2 Entrapment efficiency

The amount of TC entrapped in the different P(3HB) films was measured by GC-MS (Agilent Technologies 5975C Series GC/MSD, Loading system CTC-Pal system, Agilent Technologies, USA). Briefly, a TC stock solution of 1 mg/mL was prepared in chloroform and TC standards were prepared by making serial dilutions from the stock solution in chloroform. A TC calibration curve was made from the peak areas of TC at different concentrations. The samples were prepared by cutting 1 cm diameter discs from the original film using a puncher and were weighed and dissolved in chloroform with the help of a sonication bath. The solutions were analysed by GC-MS and the different peak areas recorded. Using the calibration curve, the

concentration of TC present in each sample was calculated. The entrapment efficiency was calculated as follows:

$$EE\% = \left(\frac{A - B}{A}\right) * 100$$

Where A is the expected amount of TC present in the disc if the entrapment efficiency was 100%, and B is the observed amount of TC present in the disc. The measurements were performed at Lucideon, Stoke-on-Trent, UK, in duplicates (n=2).

2.9 Characterisation of P(3HB) films loaded with TC

2.9.1 Attenuated Total Reflectance Fourier Transform Infrared Spectroscopy (ATR-FTIR)

The surface of P(3HB) films with 11.5 wt% TC, P(3HB) films with 13 wt% TC and P(3HB) films with 16.7 wt% TC was analysed by ATR-FTIR as described in section 2.6.1.

2.9.2 Mechanical analysis: Tensile testing

The mechanical properties of P(3HB) films with 11.5 wt% TC, P(3HB) films with 13 wt% TC and P(3HB) films with 16.7 wt% TC were analysed by the tensile testing as described in section 2.6.5 as per the conditions described for SCL-PHAs. The experiments were performed in three independent experiments, in triplicates (N=3, n=3).

2.9.3 Thermal analysis: Differential Scanning Calorimetry (DSC)

The thermal properties of P(3HB) films with 11.5 wt% TC, P(3HB) films with 13 wt% TC and P(3HB) films with 16.7 wt% TC were analysed as described in section 2.6.4 as per the conditions described for SCL-PHAs.

2.9.4 Surface analysis: Scanning Electron Microscopy (SEM)

The surface morphology of P(3HB) films with 11.5 wt% TC, P(3HB) films with 13 wt% TC and P(3HB) films with 16.7 wt% TC was analysed by SEM. Polymer discs of 1 cm diameter, cut from the original films, were placed on aluminium stubs and the samples were sputter-coated with a gold layer of approximately 15-20 nm for 15 minutes. The samples were imaged using a JOEL 5610LV-SEM (Jeol, Welwyn UK). The images were taken with an acceleration voltage of 5kV at

a 10 mm working distance. The analysis was carried out at the Eastman Dental Institute, University College London.

2.9.5 Surface analysis: Water Contact Angle (WCA)

The wettability of P(3HB) films with 11.5 wt% TC, P(3HB) films with 13 wt% TC and P(3HB) films with 16.7 wt% TC was evaluated by the static sessile drop method using a custom-built contact angle goniometer. On an average, 30 µL of deionised water was dropped onto the surface of 1 cm diameter discs, cut from the original films, with the help of a syringe. The contact angle was measured using a custom-built software. Analysis was carried out by the Analytical Chemistry – Biointerfaces groups located at the Ruhr-University Bochum, Germany. The measurements were performed in triplicates (n=3).

2.9.6 Antibacterial characterisation of P(3HB) films loaded with TC

All the antibacterial tests described below were done using 1 cm diameter discs cut from the original solvent cast film. P(3HB) discs without TC were used as negative controls. Before each experiment, all samples were sterilised under the UV light - ultraviolet germicidal irradiation (UVGI) at short-wavelength ultraviolet (UV-C, mercury-based lamp emitting UV light at the 253.7 nm line) for 15 minutes on each side.

2.9.6.1 Disc diffusion assay

As a preliminary test, the antibacterial activity of P(3HB)/TC materials was evaluated by performing the disc diffusion assay against *E. coli* (ATCC® 25922™), *S. aureus* (ATCC® 29213™) and *S. epidermidis* (ATCC® 35984™) according to Matuschek *et al*., with minor modifications (Matuschek *et al*, 2014). Bacterial strains were cultured overnight on blood agar plates and incubated at 37°C for 16 hours. Using a sterile loop, a single colony was re-suspended in a glass tube containing 2 mL of 0.9% NaCl and with the help of a densitometer the turbidity was adjusted to McFarland 0.5 (10^8 CFU/mL). A sterile cotton swab was immersed in the bacterial suspension. For Gram-negative bacteria, the cotton swab was pressed against the tube to remove the excess fluid and to avoid over-inoculation. The cotton swab was used to spread the inoculum evenly on the entire surface of the agar plates. The plates were left to dry for 15 minutes at room temperature. The discs were placed on Mueller-Hinton agar plates and incubated at 37°C for 24 hours. After the incubation period, the zones of inhibition were

measured. Antibiotic standard discs containing streptomycin (300 µg/disc) or oxacillin (1 µg/disc) were used as a positive control. The experiments were performed in three independent experiments, in triplicates (N=3, n=3).

2.9.6.2 Biocidal and anti-biofilm properties

A more comprehensive evaluation of the antibacterial properties of P(3HB)/TC materials was performed by incubating P(3HB) discs loaded with TC with bacteria for a consecutive period of 7-days to assess the biocidal and anti-biofilm properties of the materials. The preparation of the inoculum was done as described in section 2.7.1.

Assessment of the biocidal properties: P(3HB) discs loaded with TC were placed on a 24 TCPS microplate containing 2 mL of the bacterial suspension and incubated at 37°C for 24 hours. At day 1, 3 and 7, 100 µL of the supernatant were transferred to a 96 TCPS microplate and the bacterial growth was quantified by measuring the optical density at 600nm (OD_{600}) using a microplate spectrophotometer (Thermo Scientific Multiskan GO - Thermo Fisher Scientific).

Assessment of the anti-biofilm properties: After the 7-day incubation period, the supernatant was removed from the wells and the wells were carefully washed twice with 1 mL of DPBS and dried at room temperature. To fix the bacterial biofilms formed on the bottom of the wells, 1 mL of 100% ethanol was added to each well and the plate was incubated for 15 minutes at room temperature. The ethanol was removed, and the biofilms were stained with 1 mL of 0.1% safranin-O solution and incubated for 5 minutes at room temperature, followed by a washing step with DPBS. Finally, the stained biofilms were re-suspended in 1 mL of 1% SDS. A volume of 100 µL of the supernatant was transferred to a 96 TCPS microplate and the amount of biofilm was quantified by measuring the optical density of the dissolved safranin-O at 495nm (OD_{495}) using a microplate spectrophotometer (Thermo Scientific Multiskan GO - Thermo Fisher Scientific). For both experiments, a bacterial growth control composed of wells containing 2 mL of bacterial suspension were considered as well as a sterility control composed of wells containing 2 mL of MHB. The experiments were performed in two independent experiments, in duplicates (N=2, n=2) against *E. coli* (ATCC® 25922™), *S. aureus* (ATCC® 29213™) and *S. epidermidis* (ATCC® 35984™).

2.10 Development and characterisation of antibacterial P(3HB)/TC based coatings

In order to be able to explore the combination of P(3HB)/TC for coating medical devices such as central venous catheters (CVC), neat polyurethane (PU) tubes with an outer-diameter of 4 mm and an inner-diameter of 2.5 mm were selected as the materials to be coated with different P(3HB)/TC solutions. Commercially available polyurethane-based catheters impregnated with chlorhexidine and silver sulfadiazine (ARROWg+ard Blue PLUS Central Venous Catheters) here termed as ARROW were used as controls for the biological experiments.

2.10.1 Dip coating of polyurethanes using P(3HB)/TC solutions

Two different P(3HB)/TC solutions were prepared to coat PU tubes. Both solutions were prepared in chloroform being the first solution composed of P(3HB) at a concentration of 5 w/v% and TC at a concentration of 13 wt% and the second solution composed of P(3HB) at a concentration of 10 w/v% and TC at a concentration of 13 wt%. Briefly, P(3HB) was dissolved in chloroform either at 5 w/v% or 10 w/v% and mixed overnight. TC was added to each polymer solution at 13 wt% and the solution was mixed overnight. Different length sizes of PU tubes, namely 1 cm and 1.5 cm length tubes, were dip coated manually into the P(3HB)/TC solutions. A dwelling time of 3 seconds was used, and a drying time of 30 seconds was used between coating cycles. The number of coating cycles varied from 3 to 5. Coated PU tubes were left to dry vertically for 3 days at room temperature, in covered sample holders to prevent environmental contaminations. The dip coating procedure resulted in the fabrication of two different types of PU coated materials. Depending on the P(3HB) concentration and the amount of TC, the resulted materials were termed here as $PU_{5,13}$ and $PU_{10,13}$.

2.10.2 Surface analysis: Scanning Electron Microscopy (SEM)

The surface of 1 cm length uncoated and coated $PU_{5,13}$ and $PU_{10,13}$ tubes and its cross-sections were analysed using SEM as described in section 2.9.4.

2.10.3 Biocidal, anti-adhesion and anti-biofilm properties

The antibacterial performance of the coated $PU_{5,13}$ and $PU_{10,13}$ was analysed against *S. epidermidis* (ATCC® 35984™) in a 24 TCPS microplate according to Darouiche *et al*., 2009,

with some modifications. The experiment was divided into three parts to assess the biocidal properties of the materials, the effect on bacterial adhesion and the prevention of biofilm formation on surrounding areas.

Sterile 1 cm length PU coated tubes, 1 cm length uncoated tubes and 1 cm length tubes derived from the ARROW CVC were placed in a 24 TCPS microplate. The preparation of the inoculum was done by culturing bacteria overnight on blood agar plates at 37°C for 16 hours. Using a sterile loop, a single colony was re-suspended in a glass tube containing 2 mL of 0.9% NaCl and using a densitometer, the bacterial suspension was adjusted to McFarland 0.5 (10^8 CFU/mL). The bacterial suspension was further diluted 1:10 in MHB to obtain an inoculum of 10^7 CFU/mL. Then 2 mL of the bacterial suspension were added per well and incubated for 24 hours at 37^{o}C, with a shaking speed of 100 rpm.

Biocidal effect: After the incubation period, the supernatant of each well was serially diluted in 0.9% NaCl (six 10-fold dilutions were prepared) and 100 µL of each dilution were plated onto blood agar plates. After an 18-hour incubation at 37°C, the colonies were counted and expressed as CFU/ml.

Anti-adhesion properties: After the incubation period, each tube was carefully washed twice with DPBS to remove loosely adhered cells and was placed in sterile tubes containing 10 mL of 0.9% NaCl and sonicated in a sonication bath at 40 kHz (Branson 2510 Ultrasonic Cleaner) for 5 minutes followed by vortex mixing for 10 seconds to detach the bacterial cells. The procedure was repeated three times. The sonicates were serially diluted in 0.9% NaCl (five 10-fold dilutions were prepared) and 100 µL of each dilution were plated onto blood agar plates. After an 18-hour incubation at 37°C, the colonies were counted and expressed as CFU/ml.

Anti-biofilm properties: After the incubation period and after the supernatant had been removed from the wells to evaluate the biocidal effect of the materials, the wells were washed with DPBS and the bacterial biofilms formed in the wells were fixed using 1 mL of 100% ethanol and incubated for 15 minutes at room temperature. The ethanol was removed, and the biofilms were stained with 1 mL of 0.1% safranin-O solution and incubated for 5 minutes at room temperature, followed by a washing step with DPBS. Finally, the stained biofilms were re-suspended with 1 mL of 1% SDS. 100 µL of the content of each well was transferred to a 96 TCPS microplate and the bacterial biomass was quantified by measuring the optical density of the dissolved safranin-O at 495nm (OD_{495}) using a microplate spectrophotometer (Thermo

Scientific Multiskan GO - Thermo Fisher Scientific). The experiments were performed in triplicates (n=3).

2.10.4 *In vitro* indirect cytotoxicity studies

The cytotoxicity of the TC extracts released from the PU coatings were evaluated by performing an indirect cytotoxicity study and by calculating the cell viability using the CellTiter-Blue® Cell Viability Assay. The experiment was performed following the ISO 10993-5 guidelines (ISO 10993-5:2009(E)) in 24 TCPS microplates. According to the ISO 10993-5, L929 murine fibroblasts are a recommended cell line to be tested as an indicator of *in vitro* cytotoxicity, hence the biological evaluation of the materials and agents described in the next sections was evaluated using this cell line.

2.10.4.1 Cell proliferation and maintenance

L929 murine fibroblasts were cultured in 75 cm^2 tissue culture flasks in complete Roswell Park Memorial Institute medium, containing L-glutamine, 10% foetal bovine serum and 1% Penicillin-Streptomycin (10.000 U/mL Penicillin, 10 mg/mL Streptomycin) (cRPMI) and maintained in a humidified atmosphere at 5% CO_2 in air at 37°C. To sub-culture the cells, when cells reached a 70% cell confluency, cRPMI medium was removed from the tissue culture flasks and the cells were washed with 10 mL of DPBS. Then, 5 mL of Trypsin 0.25 %/1 mM EDTA were added to the flasks and incubated at 5% CO_2 at 37^oC for 2 minutes to promote the detachment of the adhered cells from the surface of the tissue culture flasks. To inactivate the trypsin, 5 mL of cRPMI were added to the flasks (trypsinisation step). Cell splitting was then done by transferring the required volumes of the cell suspension into new 75 cm^2 tissue culture flasks and the cells were incubated at 5% CO_2 at 37^oC until a 70% cell confluency was reached. The media was changed to fresh media when necessary. Note: Each sub-culturing of the cells is equivalent to a passage number. In order to avoid variations in cell viability tests, the cells used in this study were between passage 4 and 10.

2.10.4.2 Cell counting and seeding

To seed the cells, the cells were washed and trypsinised as described above. The cell suspension was transferred into a sterile 15 mL centrifuge tube and centrifuged at 1100 rpm for 5 minutes. The supernatant was discarded, and the resulting pellet was re-suspended in 1

mL of cRPMI. A 1:1 dilution of the cell suspension in 0.4% Trypan blue to selectively colour dead cells or cells with damaged membranes was done. Using a haemocytometer, viable cells were counted, and the desired cell number suspended in cRPMI.

2.10.4.3 CellTiter-Blue® Cell Viability Assay

The CellTiter-Blue® Cell Viability Assay was used to estimate the number of viable cells. This fluorescent method is composed of a highly purified solution of resazurin. The assay is based on the capability of metabolically active cells, that is, living cells to convert the redox dye resazurin into a fluorescent resorufin which is analysed using a plate-reading fluorometer. Briefly, on a 24 TCPS microplate, 2 mL of a cell suspension containing $5x10^4$ cells was seeded per well and incubated in a humidified atmosphere at 5% CO_2 in air at 37°C for 24 hours, to promote cell attachment. On the next day, the cell media was discarded from each well and replaced by 24-hour extracts, in cRPMI, deriving either from the $PU_{5,13}$, $PU_{10,13}$, uncoated PU or from the ARROW tube samples. The cells were incubated in a humidified atmosphere at 5% CO_2 in air at 37°C for another 24 hours. TCPS was used as negative control and the positive control was composed of lysed cells after being treated with 5 µL of 9% Triton® X-100 (Promega) for 5 minutes after the 24-hour incubation period. After the incubation period, the cell supernatant was removed from the wells and 250 µL of the assay reagent (CellTiter-Blue diluted with cRMPI) was added to each well and incubated in a humidified atmosphere at 5% CO_2 in air at 37°C, for 2 hours. After the incubation period, 120 µL of each well were transferred to a black 96 TCPS microplate and the fluorescence was read at 560 nm. The experiments were performed in triplicates (n=3).

2.10.4.4 Live/Dead measurements

In order to correlate the data obtained by the CellTiter-Blue® Cell Viability Assay, a fluorescent cell staining was performed using a two-colour fluorescent staining. Calcein-AM was used to stain live cells in green and Ethidium homodimer-III (EthD-III) was used to stain dead cells in red. Living cells are characterised by the presence of intracellular esterase activity which can convert non-fluorescent Calcein-AM to green fluorescent Calcein. On the other hand, EthD-III can enter the cells that have a damaged membrane and upon binding to nucleic acids can produce red fluorescence.

After culturing the cells in the presence of 24-hour extracts, in cRPMI, deriving either from the $PU_{5,13}$, $PU_{10,13}$, uncoated PU and from the ARROW tube samples for 24 hours in a humidified atmosphere at 5% CO_2 in air at 37°C, the culture medium was removed, and each well was washed with DPBS. A staining solution of 2 µM Calcein-AM/4 µM EthD-III was prepared in DPBS and 480 µL of the staining solution were added directly to each well. The cells were imaged using an inverted fluorescence microscope (Olympus IX51, Hamburg, Germany). The experiments were performed in triplicates (n=3).

2.10.5 Haemocompatibility studies

In order to see whether the PU coated tubes would cause the rupture of red blood cells, a haemolysis test was performed according to Wang *et al*., 2013. Fresh human blood was collected in heparinised tubes according to legal and ethical guidelines with informed consent of the donor and was used within 12h after donation. PU tubes of 1.5 cm length coated with the different P(3HB)/TC solutions were placed into the wells of a 24 polystyrene (PS) microplate and sterilised under the UV light - UVGI at short-wavelength ultraviolet (UV-C, mercury-based lamp emitting UV light at the 253.7 nm line) for 30 minutes. The samples were washed three times using 1 mL of 0.9% NaCl for 1 minute at 300 rpm. Then, the samples were equilibrated by giving 980 µL of 0.9% NaCl to each sample and incubating them for 30 minutes at 37°C. To each pre-equilibrated sample, 20 µL of pre-diluted blood (4:5 with 0.9% NaCl) was added. The PS plate was shaken for 1 minute at 300 rpm and then incubated for 1 hour at 37°C at 200 rpm. The release of haemoglobin was assessed by centrifugation and spectrophotometric determination of the absorbance of the supernatant. Briefly, the solutions of each well were transferred to sterile centrifuge tubes and centrifuged at 700 rcf for 10 minutes. The supernatant was transferred into a 96 TCPS microplate (200 µL per well) and the absorption was measured at 542 nm to assess the haemoglobin content in a cell-free solution.

The negative control was composed of wells with 1 mL of 0.9% NaCl and the positive control was composed of wells with 1 mL of distilled water. PU tubes of 1.5 cm length were used as negative control materials and 1.5 cm length ARROW tubes were used as positive control materials. The experiments were performed in sextuplicates (n=6).

2.11 *In vitro* antibacterial characterisation of antimicrobial peptides (AMPs)

2.11.1 Minimum inhibitory concentration and minimum bactericidal concentration

The MIC and MBC of three different AMPs, here termed, AMP3, Nut2 and LL-37 were determined against *E. coli* (ATCC® 35218™), *S. epidermidis* (ATCC® 35984™) and *S. aureus* (ATCC® 29213™), according to the ISO 20776-1:2006 guidelines in 96 TCPS microplates as described in section 2.7.1. The AMP solutions were prepared by making a stock solution of 1 mg/mL in sterile Milli Q water. The stock solution was further diluted in MHB to a concentration of 200 µg/mL. The MIC determination was performed in three independent experiments, in triplicates (N=3, n=3) and the MBC determination was performed in three independent experiments, in duplicates (N=3, n=2).

2.11.2 Anti-biofilm properties: Inhibition of biofilm formation

The ability of AMP3, Nut2 and LL-37 to inhibit biofilm formation was evaluated by quantifying the biofilm biomass produced after a 24-hour incubation of the bacterial strains with increasing concentrations of AMPs as described in section 2.7.2. The AMPs stock solution were prepared as described in section 2.11.1. The experiments were performed in three independent experiments, in triplicates (N=3, n=3).

2.12 *In vitro* antibacterial characterisation of Dispersin B (DB)

2.12.1 Anti-biofilm properties: Dispersion of pre-established biofilms

The ability of DB to disperse 24-hour pre-formed biofilms was tested against *S. aureus* (ATCC® 29213™), *S. epidermidis* (ATCC® 35984™) and *E. coli* (ATCC® 35218™) in a 96 TCPS microplate according to Marcano *et al.* (Marcano *et al*., 2015). The preparation of the inoculum was done as described in section 2.7.1. Each well was loaded with 100 µL of the bacterial suspension and incubated at 37^{o}C for 24 hours. After this period, the supernatant was carefully removed and filled with 100 µL of serial two-fold dilutions of DB in MHB (from 400−0 µg/mL) and incubated at 37^{o}C for 24 hours. After the incubation period, the supernatant was removed, and the quantification of the biofilm biomass was performed as described in section 2.7.2. The experiments were performed in three independent experiments, in triplicates (N=3, n=3).

2.13 *In vitro* direct cytotoxicity evaluation of AMPs and DB

The cytotoxicity of AMP3, Nut2, LL-37 and DB were evaluated by performing a direct cytotoxicity study and by calculating the cell viability using the CellTiter-Blue® Cell Viability Assay. The experiment was performed following the ISO 10993-5 guidelines (ISO 10993-5:2009(E)) in 96 TCPS microplates.

The cell proliferation and maintenance as well as the cell counting and seeding were performed as described in section 2.10.4.1 and 2.10.4.2, respectively.

The CellTiter-Blue® Cell Viability Assay was used to estimate the number of viable cells after their exposure to increasing concentrations of AMPs and DB for a period of 24 hours. Briefly, on a 96 TCPS microplate, 100 µL of a cell suspension containing 10^4 cells was seeded per well and incubated in a humidified atmosphere at 5% CO_2 in air at 37°C for 24 hours, to promote cell attachment. On the next day, the cell media was discarded from each well and 100 µL of increasing concentrations of each agent (from 0 to 400 µg/mL), in cRPMI, were added to each well. The cells were incubated in a humidified atmosphere at 5% CO_2 in air at 37°C for another 24 hours. TCPS was used as negative control and the positive control was composed of lysed cells after being treated with 2 µL of 9% Triton® X-100 (Promega) for 5 minutes after the 24-hour incubation period. After the incubation period, the cell supernatant was removed from the wells and 120 µL of the assay reagent (CellTiter-Blue diluted with cRMPI) was added to each well and incubated in a humidified atmosphere at 5% CO_2 in air at 37°C, for 2 hours. After the incubation period, the supernatant was transferred to a black 96 TCPS microplate and the fluorescence was read at 560 nm. The experiments were performed in two independent experiments, in quadruplicate (N=2, n=4).

2.14 Fabrication of P(3HO-co-3HD) films incorporated with AMPs and DB

2.14.1 Film development

P(3HO-co-3HD) films were prepared by the solvent casting technique. PHAs were dissolved in chloroform at 5 w/v%. After mixing overnight, the solution was poured onto a glass petri dish and covered to prevent any contamination from the environment and kept inside a continuously running fume hood for 7 days at ambient conditions to allow the solvent evaporation. Polymer discs of 1 cm diameter were cut from the original solvent casted film with the help of a puncher and the discs were sterilised under the UV light - UVGI at short-wavelength ultraviolet (UV-C, mercury-based lamp emitting UV light at the 253.7 nm line) for

30 minutes. The fabrication of modified antibacterial P(3HO-co-3HD) discs with AMP3, Nut2, LL-37 and DB was performed by immersing the discs in an AMP or a DB solution at a concentration of 200 μg/mL for 24 hours at 37^{o}C. Following the incubation period, the discs were incubated with DPBS for 2 hours and then dried overnight inside a biological safety cabinet, in ambient conditions. The films samples were stored in glass petri dish sealed with parafilm for further use.

2.14.2 Adsorption quantification

The quantification of the adsorbed DB and AMPs to the surface of the discs was done by calculating the difference between the initial amount of agent in solution and the amount that remained in the solution after the incubation step. The Bradford assay was used to quantify the presence of DB and LL-37 and the Bicinchoninic acid (BCA) assay was used to quantify the presence of AMP3 and Nut2 (Thermofisher Scientific). Different assays were used due to the difference in the molecular weight of the agents. The Bradford assay is recommended for high molecular weight proteins and the BCA assay is recommended for lower molecular weight proteins. The obtained modified discs are here termed as P(3HO-co-3HD)/AMP3, P(3HO-co-3HD)/Nut2, P(3HO-co-3HD)/LL-37 and P(3HO-co-3HD)/DB. The experiments were performed in three independent experiments, in triplicates (N=3, n=3).

2.15 Characterisation of P(3HO-co-3HD) films incorporated with AMPs and DB

2.15.1 X-ray photoelectron spectroscopy (XPS)

XPS was performed on 1 cm diameter P(3HO-co-3HD) discs modified with DB to detect the presence of amino groups deriving from the agent. The experiment was done using an ultra-high vacuum system (UHV) with a fast entry specimen assembly, sample preparation and an analysis chamber. XPS measurements were performed using an X-ray source of un-monochromatized AlKα line with a characteristic energy of 1486.6 eV and an electron analyser at constant pass energy of 97 eV resulting in a full width at half maximum (FWHM) of 1.7 eV for the Ag $3d_{5/2}$ peak. A Shirley background subtraction was done, and the spectra was analysed using a fitting routine which decomposed each spectrum into individual mixed Gaussian-Lorentzian peaks. The calibration of the kinetic energy scale was done according to the ASTM-E 902-88. Samples were analysed at the Institute of Chemical Engineering Sciences, Patras, Greece.

2.15.2 Attenuated Total Reflectance Fourier Transform Infrared Spectroscopy (ATR-FTIR)

The surface of 1 cm diameter P(3HO-co-3HD) discs modified with AMP3, Nut2 and LL-37 were analysed by ATR-FTIR as described in section 2.6.1. Lyophilised AMP powders as well as the surface of unmodified P(3HO-co-3HD) discs were also analysed via ATR-FTIR.

2.15.3 Surface analysis: Water Contact Angle (WCA)

The wettability of 1 cm diameter P(3HO-co-3HD) discs modified with AMP3, Nut2, LL-37 and DB was evaluated by the static sessile drop method as described in section 2.9.5. The experiments were performed in triplicates (n=3).

2.15.4 Antibacterial characterisation

The antibacterial test described below was done using 1 cm diameter discs cut from the original solvent cast film with the help of a puncher. Unmodified P(3HO-co-3HD) discs with the same size were used as negative controls.

2.15.4.1 Anti-adhesion properties

The anti-adhesion properties of the modified discs were evaluated against *S. aureus* (ATCC® 29213™), *S. epidermidis* (ATCC® 35984™) and *E. coli* (ATCC® 35218™) in a 24 TCPS microplate. The preparation of the inoculum was done as described in section 2.10.3. The discs were placed in a 24 TCPS microplate and each well was inoculated with 2 mL of the bacterial suspension. The plate was incubated at 37°C for 24 hours in static conditions. After the incubation period, the samples were washed twice with DPBS to remove loosely adhered cells. Each disc was placed in a sterile tube containing 10 mL of 0.9% NaCl and sonicated in a sonication bath at 40 kHz (Branson 2510 Ultrasonic Cleaner) for 5 minutes followed by vortex mixing for 10 seconds to detach the bacterial cells. The procedure was repeated three times. The sonicates were serially diluted in 0.9% NaCl (five 10-fold dilutions were prepared) and 100 µL of each dilution were plated onto blood agar plates. After an 18-hour incubation at 37°C, the colonies were counted and expressed as CFU/mL. The experiments were performed in two independent experiments, in duplicates (N=2, n=2).

2.15.5 *In vitro* direct cytotoxicity studies

The cytotoxicity of the modified materials was evaluated by performing a direct cytotoxicity study and by calculating the cell viability using the CellTiter-Blue® Cell Viability Assay. The experiment was performed following the ISO 10993-5 guidelines (ISO 10993-5:2009(E)) in 24 TCPS microplates.

The cell growth and maintenance and the cell counting, and seeding were performed as described in section 2.10.4.1 and 2.10.4.2, respectively.

Briefly, 1 cm diameter discs modified with either AMP3, Nut2, LL-37 or DB were placed on a 24 TCPS microplate and a cell suspension of $5x10^4$ cells was seeded per well and incubated in a humidified atmosphere at 5% CO_2 in air at 37°C for 24 hours. Following the incubation period, the cell supernatant was removed and 250 µL of assay reagent (CellTiter-Blue diluted with cRMPI) were added to each well and incubated in a humidified atmosphere at 5% CO_2 in air at 37°C, for 2 hours. After the incubation period, 120 µL of the supernatant was transferred to a black 96 TCPS microplate and the fluorescence was read at 560 nm. TCPS, unmodified 1 cm diameter P(3HO-co-3HD) discs and PE discs were used as negative controls. The positive controls were composed of lysed cells after being treated with 5 µL of 9% Triton® X-100 (Promega) for 5 minutes after the 24-hour incubation period and ZDEC-PU discs. The experiments were performed in two independent experiments in triplicates (N=2, n=3).

2.16 Fabrication of P(3HO-co-3HD) fibres incorporated with AMPs and DB

2.16.1 Electrospinning process

The production of P(3HO-co-3HD) fibres was carried out using a custom-build electrospinning setting composed of a high voltage power supply, a syringe pump and a rotating steel cylindrical collector. A 2 mL polypropylene syringe (BD Discardit™ II) equipped with a 23-gauge steel needle was used to fabricate the fibres. The polymer solutions were fed air bubble-free to the 2 mL syringe and the fibres were electrospun at a flow rate of 5 mL/h, with a 14kV voltage, a needle-to-collector distance of either 14 cm or 18 cm and a rotator speed of either 400 rpm or 1000 rpm. All fibres were electrospun to 1 cm diameter glass coverslips. After the electrospinning process, a drying period of at least 24 hours was used to allow the complete evaporation of any remaining solvent from the fibres inside a biological safety cabinet, in ambient conditions. Subsequently, the fibres were sterilised under the UV light - UVGI at short-wavelength ultraviolet (UV-C, mercury-based lamp emitting UV light at the 253.7 nm

line) for 30 minutes. P(3HO-co-3HD) was dissolved in a 60:40 chloroform/acetone solution at 25 w/v% and the fibres were electrospun directly from this solution. The fibre samples were stored in 24 TCPS microplates sealed with parafilm for further use.

2.16.2 Surface analysis: Bright field Imaging and Scanning Electron Microscopy (SEM)

The surface morphology of P(3HO-co-3HD) fibres was analysed by bright field microscopy (Olympus IX51, Hamburg, Germany) and by SEM. For the SEM analysis, glass coverslips covered by fibres were placed on aluminium stubs and the samples were sputter-coated with a gold layer. The images were taken with an acceleration voltage of 5kV at a 10 mm working distance. The analysis was carried out at Analytical Chemistry Department at the Ruhr-Universität-Bochum, Germany.

2.16.3 Physical adsorption of active agents to P(3HO-co-3HD) fibres

Sterile 1 cm diameter glass coverslips containing P(3HO-co-3HD) fibres were immersed in a Nut2, DB or a Nut2+DB solution containing 200 µg/mL of each agent for 24 hours at 37°C. Following the adsorption process, the fibres were washed with DPBS for 2 hours and dried overnight at room temperature inside a biological safety cabinet, in ambient conditions. The resulted modified fibres are here termed as P(3HO-co-3HD)/Nut2 fibres, P(3HO-co-3HD)/DB fibres and P(3HO-co-3HD)/Nut2+DB fibres. The fibre samples were stored in 24 TCPS microplates sealed with parafilm for further use.

2.17 Characterisation of P(3HO-co-3HD) fibres incorporated with AMPs and DB

2.17.1 Surface analysis: Water Contact Angle (WCA)

The wettability of the modified fibres was evaluated by the static sessile drop method as described in section 2.9.5. The experiments were performed in triplicates (n=3).

2.17.2 *In vitro* direct cytotoxicity studies

The cytotoxicity of the modified fibres was evaluated by performing a direct cytotoxicity study and by calculating the cell viability using the CellTiter-Blue® Cell Viability Assay. The experiment was performed following the ISO 10993-5 guidelines (ISO 10993-5:2009(E)) in 24 TCPS microplates as described in section 2.15.5.

In order to correlate the data obtained by the CellTiter-Blue® Cell Viability Assay, a fluorescent cell staining was performed using a two-colour fluorescent staining based on Calcein-AM and EthD-III. Briefly, 1 cm diameter glass coverslips containing the modified fibres were placed on a 24 TCPS microplate and a L929 cell suspension of $5x10^4$ cells was seeded per well and incubated in a humidified atmosphere at 5% CO_2 in air at 37°C for 24 hours. Following the incubation period, the supernatant was removed, and each well was washed with DPBS. A staining solution of 2 µM Calcein-AM/4 µM EthD-III was prepared in DPBS and 480 µL of the staining solution were added directly to each well. The cells were imaged using an inverted fluorescence microscope (Olympus IX51, Hamburg, Germany). The experiments were performed in two independent experiments, in triplicates (N=2, n=3).

2.17.3 Anti-adhesion and anti-biofilm properties

The anti-adhesion and anti-biofilm properties of the modified fibres were evaluated against *S. epidermidis* (ATCC® 35984™) in a 24 TCPS as described in section 2.15.4.1. To complement the test, after the sonication procedure the glass coverslips were immersed in an 100% ethanol solution for 15 minutes, then stained with a 0.1% safranin-O solution and incubated for 5 minutes at room temperature, followed by two-washing steps with DPBS. The stained-glass coverslips were dried overnight and imaged using a Panasonic DMC-FZ100. The experiments were performed in two independent experiments, in triplicates (N=2, n=3).

2.18 Alternative development of P(3HO-co-3HD) fibres incorporated with AMPs and DB

2.18.1 Covalent attachment of active agents to P(3HO-co-3HD) fibres

An alternative approach to develop antibacterial P(3HO-co-3HD) fibres was carried out using an amphiphilic six-armed star-shaped poly(ethylene oxide-stat-propylene oxide) containing reactive isocyanate groups at the distal ends of the polymer chains, NCO-sP(EO-stat-PO), to promote the covalent coupling of active agents. For that, P(3HO-co-3HD) was dissolved in a 60:40 chloroform/acetone solution at 20 w/v% and NCO-sP(EO-stat-PO) was dissolved in acetone at 5 w/v%. Once each solution was homogeneous, both solutions were mixed and vortexed vigorously. P(3HO-co-3HD)-NCO-sP(EO-stat-PO) fibres were electrospun directly from this solution. Bioactivated fibres were produced by coupling either AMP3 or AMP3+DB to P(3HO-co-3HD)-NCO-sP(EO-stat-PO) fibres. Briefly, 1:10 AMP3:NCO-sP(EO-stat-PO) was prepared by directly adding AMP3 in the form of lyophilised powder into the P(3HO-co-3HD)-

NCO-sP(EO-stat-PO) polymer solution. The solution was mixed and vortexed vigorously and fibres were electrospun directly from this solution. To bioactivate the fibres with both AMP3 and DB, the same amount of peptide was firstly dissolved in a solution containing 50 µg/mL of DB in a buffer solution consisting of 50 mM phosphate buffer (pH 5.8) with 100 mM sodium chloride and 50% glycerol. The active agents containing solution was then added to the P(3HO-co-3HD)-NCO-sP(EO-stat-PO) polymer solution, mixed and vortexed vigorously and fibres were electrospun directly from this solution. The polymer solutions were fed to a 2 mL syringe and fibres were electrospun at a flow rate of 5 mL/h, with a 14kV voltage, a needle-to-collector distance of 14 cm and a rotator speed of 1000 rpm. All fibres were electrospun to 1 cm diameter glass coverslips. After the electrospinning process, a drying period of at least 24 hours was used to allow the complete evaporation of any remaining solvent from the fibres, inside a biological safety cabinet, in ambient conditions. Subsequently, the fibres were sterilised under the UV light - UVGI at short-wavelength ultraviolet (UV-C, mercury-based lamp emitting UV light at the 253.7 nm line) for 30 minutes. The resulted modified fibres are here termed as P(3HO-co-3HD)-NCO-sP(EO-stat-PO), P(3HO-co-3HD)-NCO-sP(EO-stat-PO)+AMP3 and P(3HO-co-3HD)-NCO-sP(EO-stat-PO)+AMP3+DB. The fibre samples were stored in 24 TCPS microplates sealed with parafilm for further use.

The water contact angle, anti-adhesion properties and *in vitro* direct cytotoxicity studies of the functionalised fibres were evaluated as described in sections 2.9.5, 2.15.4.1 and 2.16.5, respectively.

2.19 Statistical analysis

Experiments were performed on freshly prepared samples and the results were reported as averages and standard deviations of these measurements. The statistical analysis was done using GraphPad Prism 5 version 5.00. Data were compared using unpaired t-test or a one-way analysis of variance (ANOVA) Turkey and Dunnett's test. Differences were considered significant for p-values lower than 0.05 ($p<0.05$).

3 Chapter 3 Production and characterisation of MCL-PHAs and SCL-PHAs for biomedical applications

3.1 Introduction

Polymers are a highly diverse class of materials, explored in many fields that go from aircraft and aerospace, to food packaging to regenerative medicine (Landel and Nielsen, 1993). Regenerative medicine cares to replace or as the name indicates, regenerate damaged or diseased tissues and organs to re-establish its normal function. The re-establishment of tissue and organ functions can be done by tissue engineering strategies or by using medical devices such as implants, and for that, polymer-based biomaterials play a fundamental role (Hacker *et al*., 2019). However, one limitation of its use is the ease with which they get contaminated by bacteria during implantation procedures. Such events happen frequently because bacteria are present almost everywhere and therefore, there are many opportunities for bacteria to contaminate the surface of a biomaterial. For instance, the surface of a biomaterial can be inoculated by airborne bacteria even before the implantation occurs, they can be pushed from the skin of the patient towards the surface of the biomaterial during implantation, or they can reach the biomaterial haematogenously at any time after implantation (Gottenbos, *et al*., 2002). When the surface of a biomaterial gets contaminated by bacteria, bacteria rapidly starts colonising it and developing complex structures called biofilms (Gristina, 1987). Biofilms are extremely resistant to antibiotics and other physicochemical treatments, and in most of the times, when biofilms are formed, the solution involves the removal of the infected medical device or surgical excision of the infected tissue (Ciofu *et al*., 2017). Therefore, due to the ineffectiveness of conventional treatments to target biofilms, the medical community is striving to develop complementary or alternative strategies to prevent biofilm formation on implantable materials by developing biomaterials with added antibacterial features. Ideally, biomaterials should have a combination of antibacterial, that is, bacteriostatic or bactericidal, anti-adhesive and anti-biofilm properties so that both planktonic bacteria and bacteria in the form of biofilms can be targeted.

Using this as a motivation we proposed to develop new bioactive materials based on natural polymers as they offer some advantages over the synthetic ones as they can be highly biocompatible, biodegradable and bioresorbable (Rahmati *et al*., 2018).

PHAs are highly biocompatible and naturally occurring bacteria-derived polyesters and can be produced by bacterial fermentation (Panchal *et al.,* 2013 and Li *et al.,* 2016). By controlling the fermentation process (e.g., bacterial strain, carbon source and operational conditions),

different types of PHAs can be obtained which either belong to the class of SCL-PHAs or MCL-PHAs. SCL-PHAs have 3-5 carbon atoms in the monomer unit and up to two carbon atoms in the side chain, and MCL-PHAs have 6-14 carbon atoms in the monomer unit and 3-11 carbon atoms in the side chain. Depending on its monomer composition different physical properties can be obtained. For instance, the Young's Modulus can vary from 0.2 GPa-149 GPa, the tensile strength from 10 MPa-104 MPa and the elongation at break from 5%-1080%. Moreover, their melting point can vary from 39^{o}C-180^{o}C, and their glass transition temperature can range from -43^{o}C-9^{o}C. Besides having a wide range of physical properties, PHAs can be processed using several techniques such as solvent casting, dip moulding, 3D printing and electrospinning, making them versatile materials for a variety of medical applications (Reis *et al.,* 2008, Roy *et al.,* 2014). For instance, PHA microporous scaffolds have been prepared by solvent casting and salt leaching for bone tissue engineering (Köse *et al*., 2003). They have also been processed in the form of sheets consisting of compressed PHA fibres to fabricate conduits for nerve regeneration (Mohanna *et al*., 2003). Moreover, PHAs have been processed into the form of nanoparticles by a precipitation/solvent evaporation technique to serve as drug carriers (Chen *et al.*, 2006).

Considering its biocompatibility, wide range of physical properties and processability, the main objective of this section was to produce an SCL-PHA using Gram-positive bacteria *Bacillus subtilis* OK2 and an MCL-PHA using Gram-negative bacteria *Pseudomonas mendocina* CH50 and to perform its chemical and physical characterisation so that they could be further modified with antibacterial features.

3.2 Results

3.2.1 Temporal profiling of polyhydroxyalkanoate production

B. subtilis OK2 and *P. mendocina* CH50 were used for the synthesis of SCL-PHAs and MCL-PHAs, respectively. To better understand how PHA accumulation was triggered during the fermentation process with an excess carbon source and in nutrient-limiting conditions, a temporal profiling was done. Parameters such as the optical density, biomass, nitrogen, glucose and pH were monitored from samples taken throughout the fermentation process. The results are shown in Figure 17.

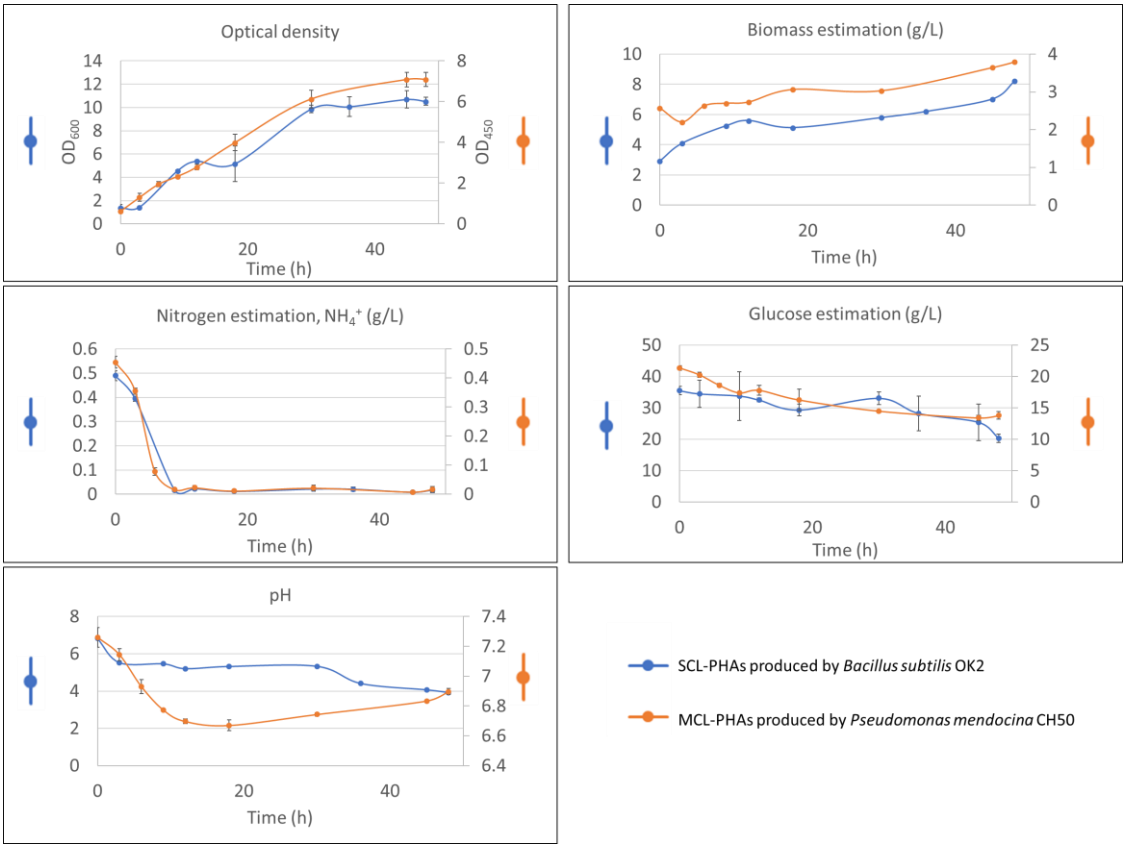

Figure 17: Fermentation profile of *B. subtilis* OK2 (blue) and *P. mendocina* CH50 (orange) using glucose as the carbon source and nitrogen as limiting factor. Variation of the optical density, biomass, nitrogen and glucose consumption, and pH throughout a 48-hour fermentation process.

The optical density chart showed that *B. subtilis* OK2 had a lag phase in the initial three hours, while *P. mendocina* CH50 did not show any. Nonetheless, both bacteria showed a constant increase in the optical density throughout the fermentation process, resulting in final values of OD_{600} of 10.5 for *B. subtilis* OK2 and OD_{450} of 7.1 for *P. mendocina* CH50. In terms of the biomass concentration, at 0 hours, high values of biomass were recorded in both fermentation profiles. A constant increase in the biomass concentration was observed for the two strains, reaching a value of 8.2 g/L for *B. subtilis* OK2 and 3.8 g/L for *P. mendocina* CH50 at 48h. Bacteria accumulate PHAs under metabolic stress conditions such as nitrogen limiting conditions coupled with an excess carbon source. Within 9h, nitrogen was practically depleted from the media for both fermentation processes, while glucose was slowly consumed. In the case of *B. subtilis* OK2, the glucose concentration decreased from 35.5 g/L to 20.3 g/L and in

the case of *P. mendocina* CH50, from 21.4 g/L to 13.4 g/L, remaining in excess throughout the fermentation process. In both cases, the pH dropped over time, reaching a value of 3.9 for *B. subtilis* OK2 and 6.9 for *P. mendocina* CH50. The polymer yield was calculated from the biomass recovered after the fermentation process. A polymer yield of 28.5% DCW and of 41.6% DCW was obtained for *B. subtilis* OK2 and *P. mendocina* CH50, respectively.

3.2.2 Characterisation of polyhydroxyalkanoates

The PHAs obtained by the two fermentation processes described above were chemically characterised by firstly identifying the type of PHAs produced by ATR-FTIR, secondly by determining the monomeric composition of the polymers by GC-MS, and finally by determining the polymer structure by NMR. Tensile testing and DSC were used to determine the mechanical and thermal properties of the materials, respectively.

3.2.2.1 Attenuated Total Reflectance Fourier Transform Infrared Spectroscopy (ATR-FTIR)

Quick molecule or compound identification can be done by ATR-FTIR analysis. PHAs are generally identified by the presence of peaks corresponding to the ester carbonyl group C=O with absorbance bands located between 1720 – 1740 cm^{-1}, the C-O-C stretching vibrations with absorbance bands located between 1160 – 1300 cm^{-1} and the stretching vibration of C-H bonds of methyl (CH_3), and methylene (CH_2) groups with absorbance bands located between 3000 – 4000 cm^{-1} (Shamala *et al*., 2009, Renard *et al*., 2015). The results obtained by ATR-FTIR analysis are presented in Figure 18 and Figure 19 for MCL-PHAs and SCL-PHAs, respectively.

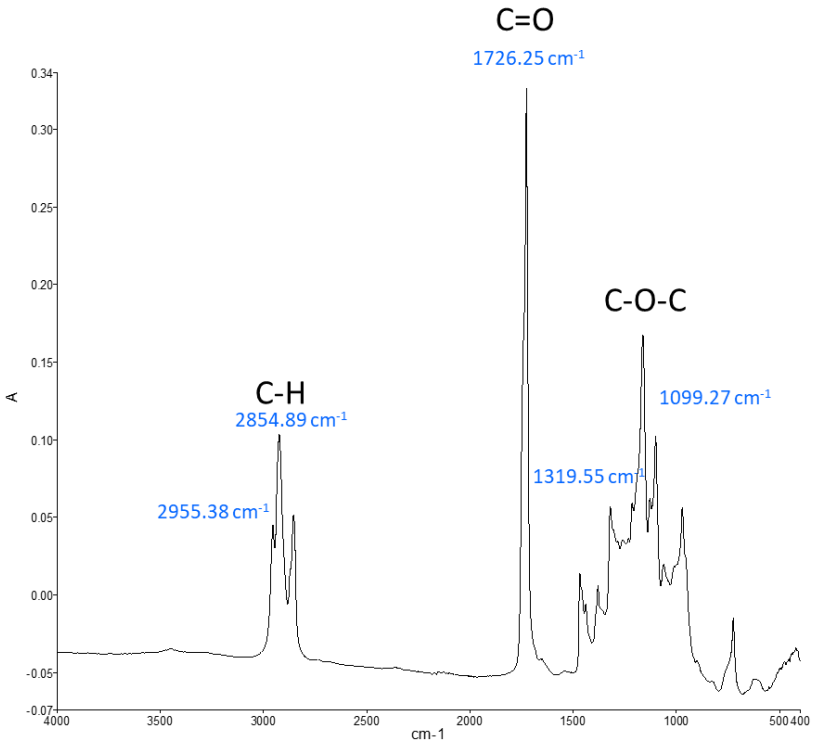

Figure 18: ATR-FTIR spectrum of the polymer produced by *P. mendocina* CH50 using glucose as the carbon source.

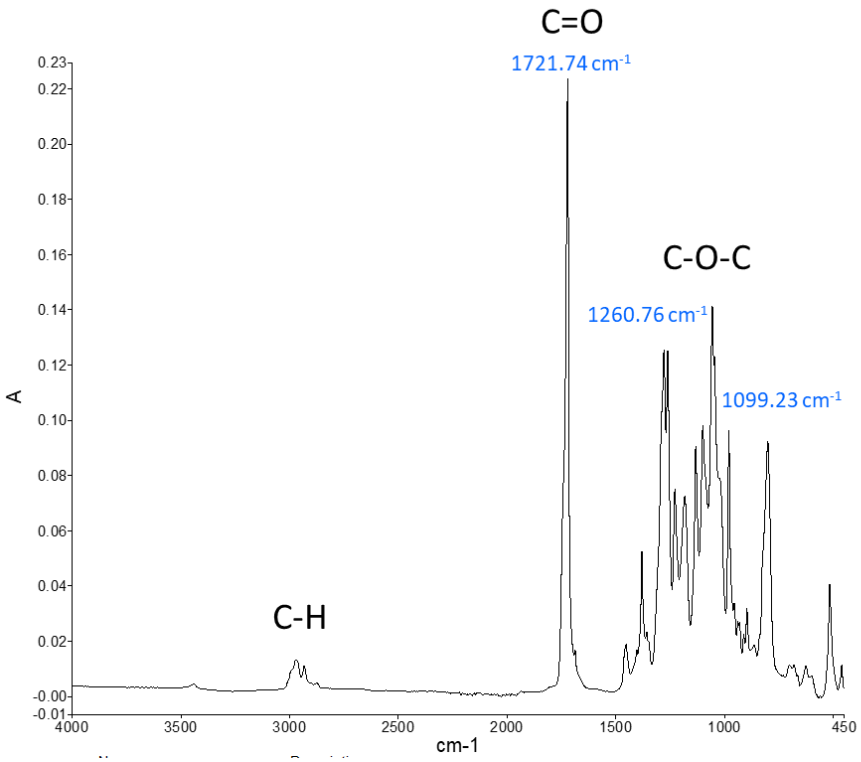

Figure 19: ATR-FTIR spectrum of the polymer produced by *B. subtilis* OK2 using glucose as the carbon source.

The results showed that, in both spectra, it was possible to identify the characteristic peaks of PHAs. In the case of the PHAs produced by *P. mendocina* CH50, the peak corresponding to the ester carbonyl group appeared at 1726.25 cm^{-1}, while in the case of the polymer produced by *B. subtilis* OK2 the peak appeared at 1721.74 cm^{-1}. In both cases, the peaks located at around 1300 cm^{-1} corresponded to C-O-C bonds and the peaks located around 1100 cm^{-1} corresponded to C-O and C-C stretching vibrations. Finally, in both spectra, the peaks recorded between 2855 cm^{-1} and 2955 cm^{-1} corresponded to the CH_3 group and the CH_2 groups present in the side chains of the monomeric units with the difference being that in the case of the spectrum of the polymer produced by *P. mendocina* CH50, more intense peaks were recorded closer to 3000 cm^{-1}.

3.2.2.2 Gas chromatography-Mass Spectrometry (GC-MS)

The identification of the monomer units was carried out using GC-MS and by referring to the National Institute of Standards and Technology (NIST) library. The results are shown in Figure 20 and Figure 21 for MCL-PHAs and SCL-PHAs, respectively.

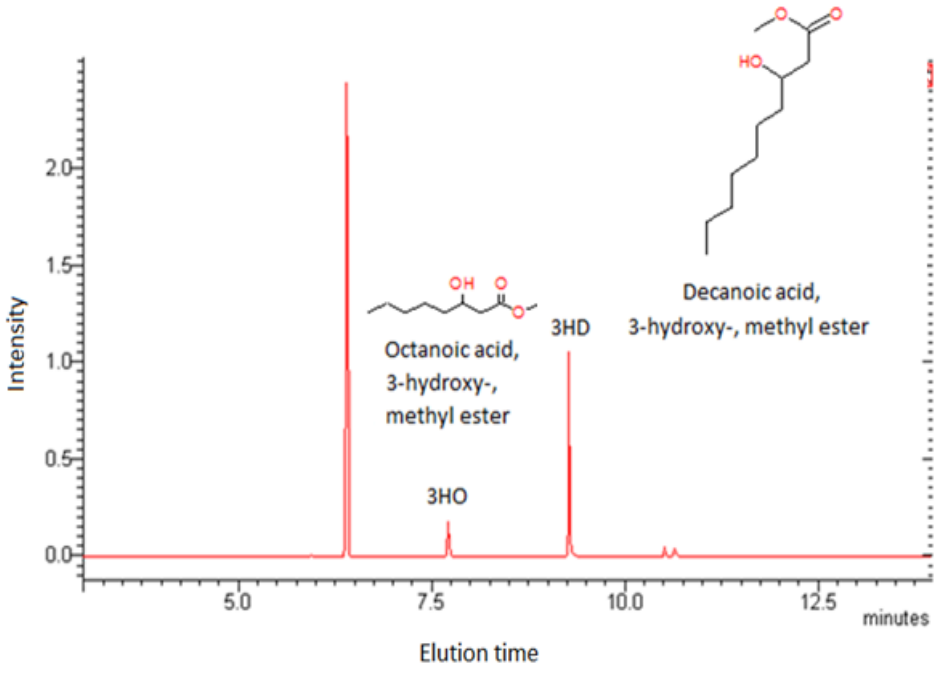

Figure 20: GC-MS analysis of the polymer produced by *P. mendocina* CH50 using glucose as the carbon source.

In the case of MCL-PHAs, two peaks were observed and identified by MS. The peak observed at a retention time of 7.74 min was identified as the methyl ester of 3-hydroxyoctanoic acid (3HO) and the peak observed at a retention time of 9.32 min was identified as the methyl ester of 3-hydroxydecanoic acid (3HD), showing that the polymer produced was poly(3-hydroxyoctanoate-co-3-hydroxydecanoate), P(3HO-co-3HD).

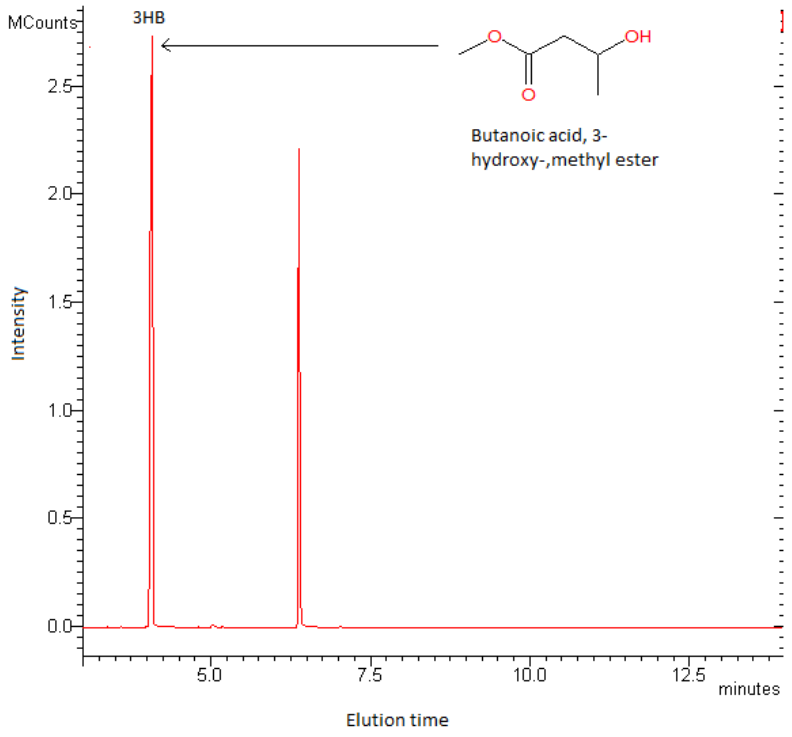

Figure 21: GC-MS analysis of the polymer produced by *B. subtilis* OK2 using glucose as the carbon source.

In the case of SCL-PHAs, the revealed peak located at 6.5 min was attributed to the methyl ester of 3-hydroxybutyric acid, indicating that the SCL-PHA produced was poly(3-hydroxybutyrate), P(3HB). In both chromatograms the peak corresponding to methyl benzoate, the internal standard used, was visible with a retention time at around 6.4 minutes.

3.2.2.3 Nuclear Magnetic Resonance (NMR)

To further confirm the molecular structure of the PHAs, ^{1}H and ^{13}C NMR spectroscopy was carried out. The ^{1}H and ^{13}C NMR spectra of P(3HO-co-3HD) are shown in Figure 22 and 23, respectively, and the ^{1}H and ^{13}C NMR spectra of P(3HB) are shown in Figure 24 and 25, respectively.

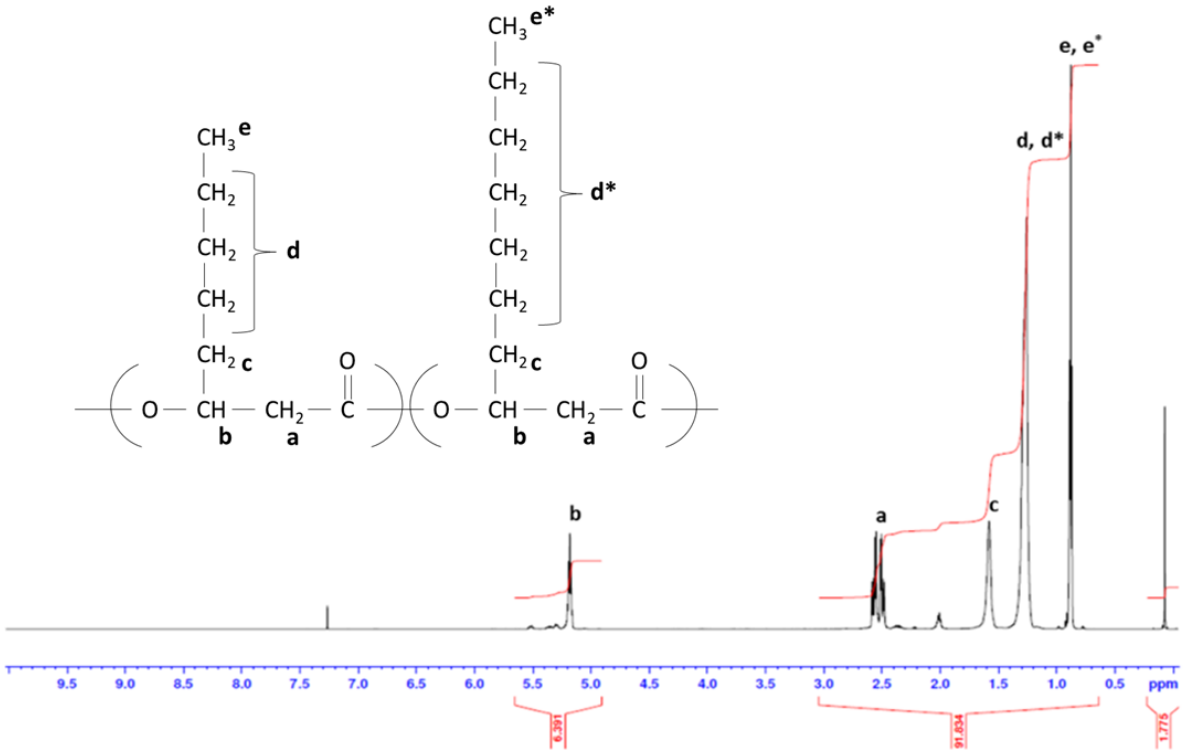

Figure 22: ^{1}H NMR spectrum of P(3HO-*co*-3HD) produced by *P. mendocina* CH50 using glucose as the carbon source.

Five different ^{1}H NMR peaks were identified and assigned to P(3HO-co-3HD). The chemical shifts at 2.5 ppm (a) and 5.2 ppm (b) corresponded to the hydrogen atoms present in the polymer backbone, namely -CH_2 and -CH. The chemical shift observed at 1.5 ppm (c) originated from the hydrogen atoms bonded to the first carbon atom of the alkyl side chain. The chemical shift at 1.3 ppm (d, d*) was assigned to the hydrogen atoms of the alkyl chain and the peak at 1 ppm (e, e*) corresponded to the hydrogen atoms of the terminal methyl group of the side chain. The peak at 0 ppm corresponded to the internal standard tetramethylsilane (TMS) and

the peak at 7.2 ppm corresponded to the proton of the $CDCl_3$ used to dissolve the sample (Figure 22).

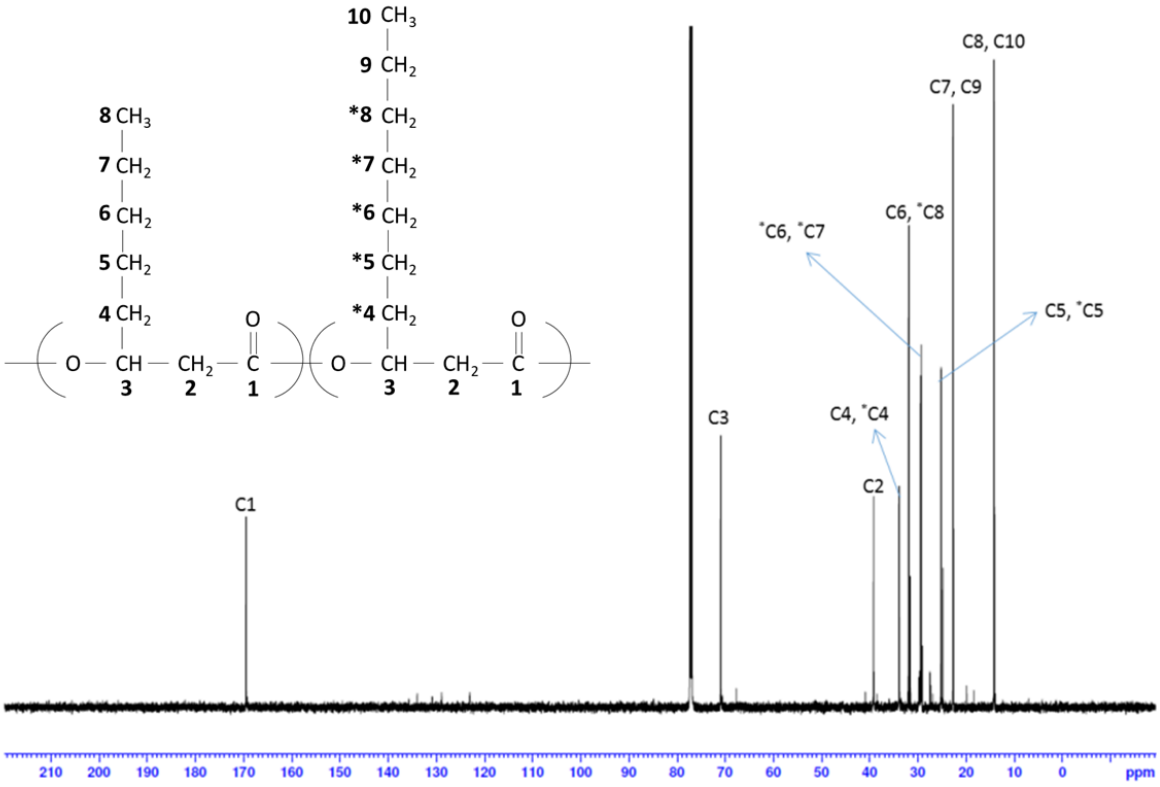

Figure 23: ^{13}C NMR spectrum of P(3HO-*co*-3HD) produced by *P. mendocina* CH50 using glucose as the carbon source.

Nine different peaks were identified in the ^{13}C NMR spectrum of P(3HO-co-3HD). The chemical shift at 170 ppm (C1) corresponded to the carbon of the carbonyl group, the peak at 40 ppm (C2) and 70 ppm (C3) corresponded to the $-CH_2$ and -CH groups present in the polymer backbone, respectively. The chemical shifts at 34 ppm (C4, C4*) and 24 ppm (C5, C5*) corresponded to the first two carbon atoms of the side chains. Finally, the chemical shifts at 32 ppm (C6, C8*), 30 ppm (C6*, C7*) and 23 ppm (C7, C9*) corresponded to the carbons present on the side chains of the monomer unit and the carbon of the terminal methyl group of the side chain showed a peak at 14 ppm for both monomer units (C8, C10). The peak at 77 ppm corresponded to $CDCl_3$ used to dissolve the sample (Figure 23).

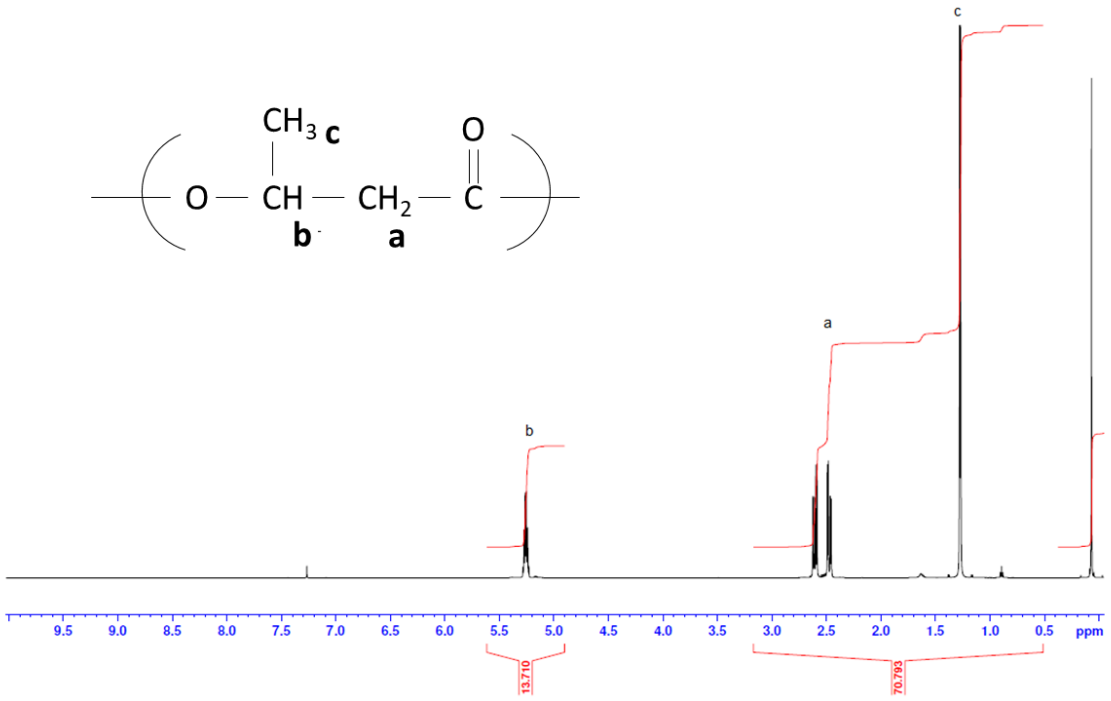

Figure 24: ^{1}H NMR spectrum of P(3HB) produced by *B. subtilis* OK2 using glucose as the carbon source.

In the case of P(3HB), the ^{1}H NMR spectrum showed three different ^{1}H NMR peaks which were assigned using the letters a, b, and c. Similarly, as observed in the P(3HO-co-3HD) spectra, the chemical shifts at δ=2.5 ppm and δ=5.2 ppm corresponded to the hydrogen atoms present in the polymer backbone and the chemical shift at δ=1.4 ppm corresponded to the -CH_3 group present in the side chain. Once again, the peak at 0 ppm corresponded to the internal standard TMS and the peak at 7.2 ppm corresponded to $CDCl_3$ used to dissolve the sample (Figure 24).

In the ^{13}C NMR spectrum of P(3HB), four peaks were observed. Similarly, to P(3HO-co-3HD), the chemical shifts corresponding to the carbons present in the polymer backbone showed peaks at 170 ppm (C1), 41 ppm (C2) and 68 ppm (C3). The carbon of the terminal methyl group of the side chain showed a peak at 20 ppm (C4). The peak at 77 ppm corresponded to the $CDCl_3$ used to dissolve the sample and the peak at 0 ppm corresponded to the internal standard TMS (Figure 25).

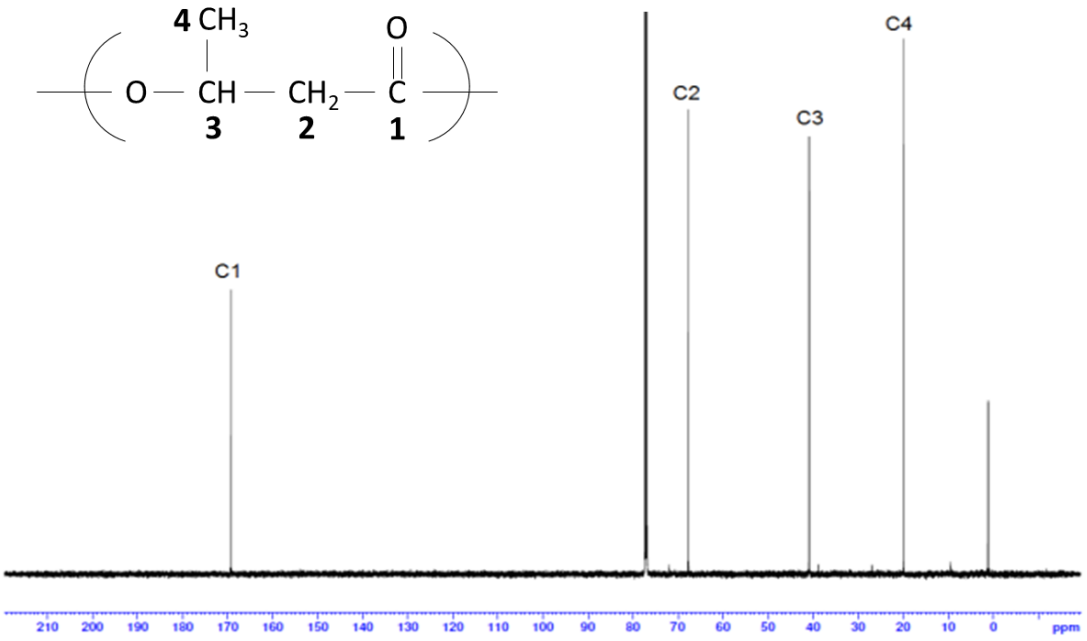

Figure 25: ^{13}C NMR spectrum of P(3HB) produced by *B. subtilis* OK2 using glucose as the carbon source.

3.2.2.4 Mechanical analysis: Tensile testing of P(3HB) and P(3HO-co-3HD)

Tensile tests were performed to evaluate the Young's modulus (E), tensile strength (σ) and elongation at break (ε_b) of P(3HO-co-3HD) and P(3HB) and the results are shown in Figure 26 and Table 9.

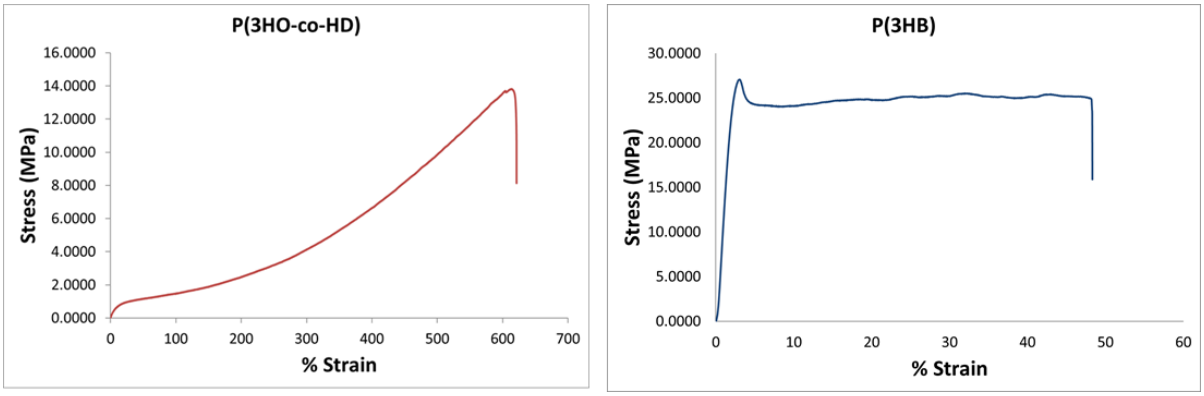

Figure 26: Example of a stress-strain curve of P(3HO-co-3HD) produced by *P. mendocina* CH50 and P(3HB) produced by *B. subtilis* OK2 using glucose as the sole carbon source.

Figure 26 shows an example of the stress-strain curve obtained for P(3HO-co-3HD) and P(3HB). By looking at the mechanical profiles of each material, it was shown that the tensile strength, which can be identified as the maximum stress value present in the curve, was higher for P(3HB) than for P(3HO-co-3HD) with values of 27MPa and 14MPa, respectively. Secondly, by observing the values of the failure strain, it was observed that they were much higher for P(3HO-co-3HD) than for P(3HB) with values of 615% and 3%, respectively. Finally, an idea of the Young's Modulus values was taken by observing the linearity of the stress-strain relationship. The higher the linearity behaviour, the higher the Young's Modulus. Many materials show a linear behaviour at the beginning of the curve, often translated to the elastic deformation region, in which the original shape is kept when the force or stress is removed. When the curve starts showing a non-linear behaviour it means that the deformations become plastic and that the deformations of the material will be permanent and non-reversible when the stress is removed (Ward and Hadley, 1993, Meyers and Chawla, 2008). In the case of P(3HO-co-3HD), a non-linear stress-strain relationship was observed, while in the case of P(3HB), a linear stress-strain relationship was observed.

Table 9: Mechanical properties of P(3HO-*co*-3HD) produced by *P. mendocina* CH50 and P(3HB) produced by *B. subtilis* OK2 using glucose as the sole carbon source.

	P(3HO-co-3HD)	P(3HB)
Young's Modulus (MPa)	8.7±2.1	1205.5±12.7
Elongation at break (%)	609.5±6.4	3.22±0.1
Tensile strength (MPa)	14.3±0.7	24.9±0.1

During the tensile test, it was observed that given an uniaxial extensive stress, P(3HB) retained its original shape and broke quite easily, while P(3HO-co-3HD) suffered a continuous change in length when stress was applied until it broke. P(3HO-co-3HD) exhibited a Young's Modulus of 8.7±2.1 MPa and P(3HB) exhibited a Young's Modulus of 1205.5±12.7 MPa. The values calculated for the elongation at break were 609.5±6.4 % for P(3HO-co-3HD) and 3.2±0.1 % for P(3HB). Finally, the values obtained for the tensile strength were 24.9±0.1 MPa for P(3HB) and 14.3±0.7 MPa for P(3HO-co-3HD).

3.2.2.5 Thermal analysis: Differential Scanning Calorimetry (DSC) of P(3HB) and P(3HO-co-3HD)

Thermal characterisation was carried out by DSC analysis where phase changes were observed allowing for the determination of the glass transition temperature (T_g), melting temperature (T_m) and peak crystallisation temperature (T_c). The results obtained are shown in Table 10.

Table 10: Thermal properties of P(3HO-co-3HD) produced by *P. mendocina* CH50 and P(3HB) produced by *B. subtilis* OK2 using glucose as the sole carbon source.

	P(3HO-co-3HD)	P(3HB)
Glass transition temperature (T_g)	-42.1	-0.4
Melting temperature (T_m)	52.8	165.4
Peak crystallisation temperature (Tc)	-	54

P(3HO-co-3HD) exhibited a glass transition temperature of -42.1^oC and P(3HB) exhibited a glass transition temperature of -0.4^oC. In terms of their melting temperature, P(3HO-co-3HD) exhibited a melting temperature of 52.8^oC while P(3HB) exhibited a melting temperature of 165.4^oC. Furthermore, P(3HB) showed a peak crystallisation temperature of 54^oC.

3.3 Discussion

Much attention has been given to PHAs over the past years. Not only do they present similar properties to that of conventional synthetic plastics such as polypropylene, but in contrast to these plastics they can be obtained from renewable carbon sources and are therefore considered as environmentally friendly materials (Albuquerque *et al.,* 2007, Anjum *et al*., 2016). Furthermore, as described in the introductory section, they are highly biocompatible and present a wide range of physical properties (Mathuriya, A.S. and Yakhmi, J.V., 2017, Junyu *et al*, 2018, Koller 2018). For this reason, PHAs are widely explored in the biomedical field as drug delivery systems, wound management and healing products, surgical implant devices and tissue engineering scaffolds (Zhang *et al*., 2018). Since one of the major drawbacks in

biomedical materials has to do with its early contamination by bacteria during implantation procedures, the idea was to improve the properties of PHAs by adding antibacterial features to further increase their success in clinical and medical settings. Hence, two types of PHAs were produced and characterised in this chapter. SCL-PHA, P(3HB) was produced using Gram-positive bacteria *B. subtilis* OK2 and MCL-PHA, P(3HO-co-3HD) was produced using Gram-negative bacteria *P. mendocina* CH50.

The production of MCL-PHAs and SCL-PHAs was achieved by bacterial fermentation using nitrogen-limiting conditions and glucose as an excess carbon source. The fermentation profile of both bacterial strains gave an elucidation of how bacteria behaved towards the culture media that was provided and towards the specific operational conditions. The results showed that *B. subtilis* OK2 exhibited a lag phase in the beginning of the fermentation process while *P. mendocina* CH50 did not. The lag phase is characterised by the period in which bacteria adjust to the environment that they are in and no cell division occurs. The cultivation of *P. mendocina* CH50 included a second stage of cultivation where the bacteria was able to adapt to the limited growth conditions. While, on the other hand, the cultivation of *B. subtilis* OK2 was performed without this second stage, where the seed culture or inoculum was directly transferred from a media containing optimal growth conditions to a production media containing nitrogen-limiting conditions. Considering that *B. subtilis* OK2 was transferred from normal cultivation conditions directly to metabolically challenging condition, the presence of a lag phase was expected. In terms of the biomass concentration, values higher than zero were recorded at the beginning of both fermentation profiles. Such values could either derive from insoluble impurities present in the biomass or from an incomplete drying of the sample, thus contributing for higher readings. In terms of the pH for both fermentation processes, it was observed that the pH dropped from its initial value. Studies have reported the ability of *Pseudomonas* species to produce alginic acid when in nutrient-limiting conditions and glucose as the carbon source (Hacking *et* al., 1983, Sengha *et al*., 1989). Others have reported the ability of *Bacillus* species to produce lactic acid as a by-product during the fermentation process. (Ramos *et al*., 2000). The biosynthesis of PHAs using glucose as the carbon source is characterised firstly by the conversion of glucose to pyruvate during glycolysis and secondly by the conversion of pyruvate to acetyl-CoA. However, when the levels of oxygen are insufficient, pyruvate undergoes lactic acid formation. This is usually what happens during the

log phase, or exponential phase of the fermentation process. Since in such a phase, the percentage of dissolved oxygen is very low, the conversion of pyruvate to lactic acid might be triggered, thus lowering the pH of the media. Since in comparison to *P. mendocina* CH50, the consumption of glucose was higher for *B. subtilis* OK2, it could be that more pyruvate was produced via glycolysis leading to a higher accumulation of lactic acid, and therefore, a sharper decrease in the pH. The glucose and nitrogen estimation during the fermentation process of both bacteria showed that the conditions to trigger PHA accumulation were reached and maintained during the fermentation process as nitrogen was almost depleted from the media in the beginning of the process and glucose remained in excess. The fermentation profiles also showed that although during the fermentation process of *B. subtilis* OK2, higher optical densities and higher amounts of biomass were recorded in comparison to that of *P. mendocina* CH50, the latter produced PHAs more efficiently than *B. subtilis* OK2. More specifically, at the end of the fermentation process, the biomass produced by *B. subtilis* OK2 was 8.2 g/L with a polymer accumulation of 28.5% DCW and the biomass produced by *P. mendocina* CH50 was 3.8 g/L with a polymer accumulation of 41.6% DCW. A similar scenario was observed in a study conducted by Lukasiewicz *et al.,* in which *B. subtilis* OK2 and *P. mendocina* CH50 were grown with glucose and waste frying oil as carbon sources, respectively. In this case, although the amount of biomass produced by *B. subtilis* OK2 was higher than the amount of biomass produced by *P. mendocina* CH50, higher PHA content was obtained for the latter bacterial strain than the one obtained for *B. subtilis* OK2. More specifically, the biomass produced by *B. subtilis* OK2 was 4.8 g/L with a polymer accumulation of 30.8% DCW and the biomass produced by *P. mendocina* CH50 was 4.3 g/L with a polymer accumulation of 40% DCW (Lukasiewicz *et al*., 2018). The polymer yield obtained in both fermentation processes was reasonable and comparable to what is described in literature. Although optimisation strategies could be implemented to improve the PHA productivity, the scope of this study did not cover this aspect and the fermentation strategies described in this chapter yielded enough material to be further modified with antibacterial properties. The focus of this chapter was to briefly describe the production of different types of PHAs and their characterisation with respect to their chemical, mechanical and thermal properties. These properties are important since they reveal the most relevant properties of a polymer and aid in determining its

application. Furthermore, chemical characterisation techniques can also aid in the detection of impurities that can in a later stage affect the biocompatibility of the materials.

There are numerous tests that can be done to chemically characterise a material, including spectrometry and spectroscopy methods. Herein, ATR-FTIR, GC-MS and NMR techniques were employed to provide the chemical characterisation of the materials and identify the polymers produced. The ATR-FTIR analysis confirmed that the polymers produced were PHAs by revealing the typical peaks of PHAs. The peaks around 3000 cm^{-1} correspond to the methylene groups of the side chains of PHAs. The fact that more intense peaks were recorded in this region when analysing the polymer produced by *P. mendocina* CH50 than for the polymer produced by *B. subtilis* OK2 suggested that the first polymer had longer side chains, and thus suggested that the polymer produced by *P. mendocina* CH50 was an MCL-PHA and that the polymer produced by *B. subtilis* OK2 was an SCL-PHA. Considering the substrate specificity of the PHA synthases present in the *Bacillus* species and *Pseudomonas* species, this outcome was expected. The PHA synthase of *Bacillus* species can polymerise 3-hydroxyalkanoates consisting of 3-5 carbon atoms, whereas the PHA synthase of *Pseudomonas* species can polymerise 3-hydroxyalkanoates consisting of 6-14 carbon atoms (Lee, 1996). GC-MS identified the monomeric composition of the polymers produced leading to the further confirmation that the polymer produced by *B. subtilis* OK2 was an SCL-PHA, namely P(3HB), and that the polymer produced by *P. mendocina* CH50 was an MCL-PHA, namely, P(3HO-co-3HD). Furthermore, it was possible to see that P(3HO-co-3HD) was composed by two different monomer units. The first monomer unit was HO with five carbon atoms in the side chain and three carbon atoms in the backbone and the second monomer unit was HD with seven carbon atoms in the side chain and three carbon atoms in the backbone. On the other hand, the GC-MS results showed that P(3HB) had one monomer unit with three carbon atoms in the backbone and one carbon atom in the side chain. NMR analysis was used to finalise the structure of the polymers produced. None of the methods showed the presence of impurities as no extra or unexpected peaks were detected.

The mechanical profiles of P(3HB) and of P(3HO-co-3HD) showed very distinct mechanical properties of the materials. Firstly, the mechanical profiles of the materials showed that the

tensile strength was higher for P(3HB) than for P(3HO-co-3HD), indicating that P(3HB) was a stronger material than P(3HO-co-3HD). The mechanical profile also showed that the values of the failure strain were much higher for P(3HO-co-3HD) than for P(3HB) suggesting that the former was more ductile, and the latter was more brittle. Finally, by observing the stress-strain relationship, a non-linear behaviour was observed for P(3HO-co-3HD) suggesting that this material was a soft material and a linear behaviour was observed for P(3HB) suggesting that this material was a stiff material. The calculated mechanical parameters further confirmed that P(3HB) was a strong, stiff and brittle material with a high Young's modulus, high tensile strength and low elongation at break and that P(3HO-co-3HD) was a weak, soft and ductile material with a low Young's modulus, low tensile strength and high elongation at break. The high Young's modulus recorded for P(3HB) indicated that P(3HB) could better resist changes in strain/deformation when a stress/force would be applied while P(3HO-co-3HD) would not. Furthermore, the higher tensile strength of P(3HB), compared to the lower tensile strength of P(3HO-co-3HD) indicated that the former material could resist higher stress/force values before breaking as compared to the latter. The parameters obtained for P(3HB) seem to be in accordance with the literature (Van de Velde *et al*., 2002). However, since P(3HO-co-3HD) is a novel MCL-PHA, the only way to compare its mechanical properties is by comparing it to some of the most well described MCL-PHAs, such as P(3HO) and P(3HO-co-12%3HHx). P(3HO) has a Young's modulus of 11.4 MPa, a tensile strength of 6.6 MPa and an elongation at break of 40% (Rai *et al.,* 2011c). Similarly, P(3HO-co-12%3HHx) has a Young's modulus of 8 MPa, a tensile strength of 9 MPa and an elongation at break of 380% (Valappil *et al*., 2006). Comparing both polymers with P(3HO-co-3HD), they all show similar Young's modulus and tensile strength values, i.e. they have similar strength and stiffness. However, the difference in properties is evident when observing the elongation at break values where P(3HO-co-3HD) shows the highest flexibility (value) and P(3HO) the lowest flexibility. This suggests that the presence of a second monomer unit makes the material more pliable as the extension at break increases with the addition of a longer second monomer unit P(3HO)<P(3HO-co-12%3HHx)<P(3HO-co-3HD).

DSC analyses are based on the collection of the thermal events that a material experiences when heat is applied. Initially the materials are cooled down and then gradually, the temperature starts increasing. With increasing temperatures, the structure of the material,

which was initially ordered, starts becoming more mobile as the vibrations of the atomic bonds increase. The increase in vibrations result in phase transitions (e.g., glass transition temperature and melting temperature). Glass transition events are recorded when the amorphous domain of a polymer transits from a glassy state into a rubbery state while the temperature increases. On the other hand, melting events are recorded when a solid polymer becomes liquid. Not all materials have a glass transition temperature or a melting temperature. For instance, crystalline materials (ordered structures) do not have a glass transition temperature, but instead, when increasing temperatures are applied, they exhibit a distinct melting event. Amorphous materials (non-ordered structures), on the other hand, do not have a melting point, but instead, they have a glass transition temperature, where the polymer transitions from rigid or solid structure to soft and pliable structures. Semi-crystalline materials (composed of a crystalline domain and an amorphous domain) have both a glass transition temperature and a melting temperature (Leng, 2009). In this case both polymers showed a glass transition temperature and a melting temperature indicating that they are both semi-crystalline polymers.

The polymer properties are influenced by their structure, the length of the side chains being one of the factors that influences the physical properties of a material. The longer the side chains, the higher the amorphous domains of a polymer (Muangwong *et al.,* 2016). Given that P(3HO-co-3HD) is an MCL-PHA, it has longer side chains than P(3HB), hence P(3HB) is more crystalline than P(3HO-co-3HD). This explains the lower glass transition temperature and melting temperature observed for P(3HO-co-3HD). If a polymer is dominated by amorphous regions, less energy or lower temperatures are needed to go from a glassy state to a rubbery state, and consequently less energy is needed to melt a polymer.

Besides the glass transition and melting point peaks, P(3HB) also showed a crystallisation peak. Heating of a polymer, results in a mobile polymer structure. Hence, beyond the glass transition peak, as the temperature increases, the polymer structure re-arranges itself into a crystalline form, which is more stable than the amorphous state. And in this case, excess energy is released which results in an exothermic event. The process of crystallisation depends on many factors, one of them being the molecular structure. Since P(3HO-co-3HD) is sterically more hindered, the process of crystallisation is less likely to occur as it is more difficult for the molecules to re-arrange in a close stacked manner. Crystallinity relates to the mechanical

properties of a polymer, the higher the crystallinity of a polymer, the higher the stiffness, hence, higher the Young's modulus and the lower the elongation at break (Lu *et* al., 2001, Meyers and Chawla, 2008, Sharma *et al*., 2017). Both mechanical and thermal analyses confirmed this correlation as P(3HB) showed a higher crystallinity, higher Young's modulus and lower elongation at break when compared to P(3HO-co-3HD).

The characterisation of the materials confirmed that both polymers produced had very distinct thermal and mechanical properties, and hence a wide range of applications could be targeted. In this study, the idea was to use one of the materials for applications in the area of tissue engineering and the other material for the development or improvement of medical devices.

Tissue engineering scaffolds should of course be biocompatible and biodegradable, but their architecture and surface topography are also highly relevant for the proliferation of cells. For this reason, polymer fibres are gaining a lot of attention for tissue engineering applications. Usually, PHA-based fibres are made from blends of SCL-PHAs and MCL-PHAs or blends of PHAs and other polymers (Volova *et* al., 2014, Basnett *et al*., 2016, Hufenos *et al*., Li and Loh., 2016). Since the fabrication of MCL-PHA-based fibres is not widely explored we have proposed to develop antibacterial P(3HO-co-3HD)-based fibres for tissue engineering applications. On the other hand, antibacterial coatings could be a way forward to mitigate the problem of bacterial infections caused by medical devices. In this sense, while the main bulk material of which the medical device is made maintains its mechanical behaviour, the bioactivity can be associated with the surface, and hence P(3HB) was selected to be used as an antibacterial coating.

The strategies that will be described in the following chapters will focus on the development of antibacterial PHA films and the further development of an antibacterial PHA-based demonstrator for the applications mentioned above.

4 Chapter 4 Development of antibacterial P(3HB) materials: From 2D films to 3D surface coatings

4.1 Introduction

Medical devices are instruments used for the diagnosis, treatment or prevention of diseases found in patients. Examples of medical devices include prosthetic joints, pacemakers, intraocular lenses and vascular catheters. Usually, medical devices function as intended, however if they get in contact with pathogens, such as bacteria, there can be serious complications such as the development of device-related infections (Zhang and Wagner, 2017). It is estimated that device-related infections contribute over 60% to hospital-acquired infections (HAIs) which are one of the leading causes of morbidity and mortality. Some of the most frequent and serious device-related infections are catheter-associated urinary tract infections (CAUTI), central line associated bloodstream infections (CLABSI), ventilator-associated pneumonia (VAP) and prosthetic joint infections (PJI). Such infections are intimately related to device colonisation by bacteria and biofilm formation and some of the most frequent bacteria recovered from contaminated medical devices are coagulase-negative staphylococci (e.g., *S. epidermidis*), *S. aureus* and *E. coli* (Maathuis *et* al., 2007, Subbiahdoss *et al*., 2011). Not only are these types of infections major causes of death, they also contribute to a significant financial burden (Wang *et al.,* 2017). For this reason, many researchers and medical device companies are trying to develop antibacterial technologies specifically targeting the prevention and treatment of biofilms on medical devices. One of the most explored approaches focuses on the development of polymer-based antimicrobial coatings for medical implants. Polymer-based antimicrobial coatings can be developed by immobilising bioactive molecules on its surface which are not released to the environment and act either as a barrier for bacterial adhesion or kill bacteria on contact; they can have a designed topography conferring the surface with anti-fouling properties; or they can have loaded bioactive molecules on its surface which are released to the environment when implanted. Focusing on the latter strategy, bioactive releasing coatings can be easily developed by incorporating bioactive molecules in the bulk of a polymer by mixing both the components during the processing phase (e.g., solvent casting) (Campoccia *et al*., 2013). When it comes to select the bioactive molecule, it is important to consider that when a device gets contaminated by bacteria, adjacent tissues can also become susceptible of being infected by planktonic bacteria, therefore bioactive releasing coatings containing molecules that could

target planktonic bacteria, but also prevent bacterial adhesion and biofilm formation of the surface of medical devices would be highly desirable in this context.

A class of agents capable of doing so derive from essential oils (EOs). EOs compose a vast source of bioactive compounds and many of them have been studied against pathogenic bacteria (Dal Pozzo *et al*., 2012, Nieto-Bobadilla *et al*., 2015). One example of such an essential oil and its bioactive component is cinnamon bark oil and trans-cinnamaldehyde (TC). TC is known to be active against many bacterial strains and many studies have reported different mechanisms of action for TC. For instance, it has been showed that TC can alter the bacterial membrane permeability leading to the loss of cellular and enzymatic functions and, consequently to cell death, it has been shown that TC can interfere with bacterial cell division by targeting a cell division protein, filamentation temperature sensitive protein Z, and many other studies describe the ability of TC to act as a quorum sensing inhibitor in quorum sensing systems found in *P. aeruginosa* and *E. coli* (Bouhdid *et al*., 2010, Domadia *et al.,* 2007, Niu *et al*., 2006; Chang *et al*., 2014). This last aspect is of special importance as many pathogenic bacterial phenotypes are controlled by the process of quorum-sensing, especially in terms of biofilm formation (Chang *et al*., 2014). Therefore, the development of coatings based on PHAs loaded with TC seemed like a promising strategy to target the problem of biofilm formation. In addition to its antibacterial properties, there are many studies reporting the plasticising effect of essential oils and components of EOs, including TC. Typically, a plasticiser reduces the intermolecular forces (IMF) of polymer chains and consequently improves the flexibility and extensibility of the polymer. The role of plasticisers is to improve the mechanical properties of a material by reducing the tension-dependent structural deformation, hardness (resistance to localized plastic deformation), density and viscosity, as well as to increase the polymer chain flexibility and resistance to fracture, thereby decreasing the material stiffness (Lee *et al*., 2005). Hence, by combining P(3HB) which is a stiff and brittle material with TC would not only lead to development of an antibacterial material but also a material with improved mechanical properties suitable for coatings and perhaps other biomedical applications in which P(3HB) is usually not explored.

Since the process of solvent casting is a straightforward, fast and cheap method to produce films, and since such materials are easy to characterise, the development of P(3HB)/TC films was carried out, and it is described in this section. The films were characterised in order to

assess their chemical, thermal, mechanical and surface properties as well as their antibacterial properties. Based on the results obtained, the knowledge was translated into P(3HB)/TC coatings and a preliminary surface and biological characterisation was performed.

4.2 Results

4.2.1 *In vitro* antibacterial characterisation of TC

4.2.1.1 Minimum inhibitory concentration and minimum bactericidal concentration

As a starting point, the antibacterial properties, namely, the bacteriostatic and bactericidal properties of TC, were tested against *E. coli* (ATCC® 35218™), *S. epidermidis* (ATCC® 35984™) and *S. aureus* (ATCC® 29213™) by determining the MIC and MBC, respectively. The selected bacterial strains were cultured in the presence of increasing concentrations of TC for a period of 24 hours and the TC concentration that completely inhibited visible bacterial growth was determined as the MIC while the TC concentration that resulted in a reduction of 99.9% of CFUs relative to that in the initial inoculum was determined as the MBC. The results are summarised in Table 11.

Table 11: MIC and MBC of TC against *E. coli* (ATCC® 35218™), *S. epidermidis* (ATCC® 35984™) and *S. aureus* (ATCC® 29213™).

Bacterial strain	MIC	MBC
E. coli (ATCC® 35218™)	5 mM	10 mM
S. epidermidis (ATCC® 359842™)	0.63 mM	-
S. aureus (ATCC® 29213™)	1.25 mM	-

TC showed a MIC of 5 mM, 0.63 mM and 1.25 mM against *E. coli* (ATCC® 35218™), *S. epidermidis* (ATCC® 35984) and *S. aureus* (ATCC® 29213™), respectively. Furthermore, in the range of concentrations tested (20 mM – 0 mM), TC showed an MBC of 10 mM against *E. coli* (ATCC® 35218™) and in the case of *S. epidermidis* (ATCC® 35984) and *S. aureus* (ATCC® 29213™), no MBC was detected.

4.2.1.2 Anti-biofilm properties: Inhibition of biofilm formation

Furthermore, the anti-biofilm properties of TC were determined by quantifying the biofilm biomass that was produced after a 24-hour bacterial exposure to increasing concentrations of TC. The biofilm biomass was quantified using a safranin staining method and the results were expressed as percentage of biofilm inhibition compared to a typical biofilm growth control. The results are shown in Figure 27.

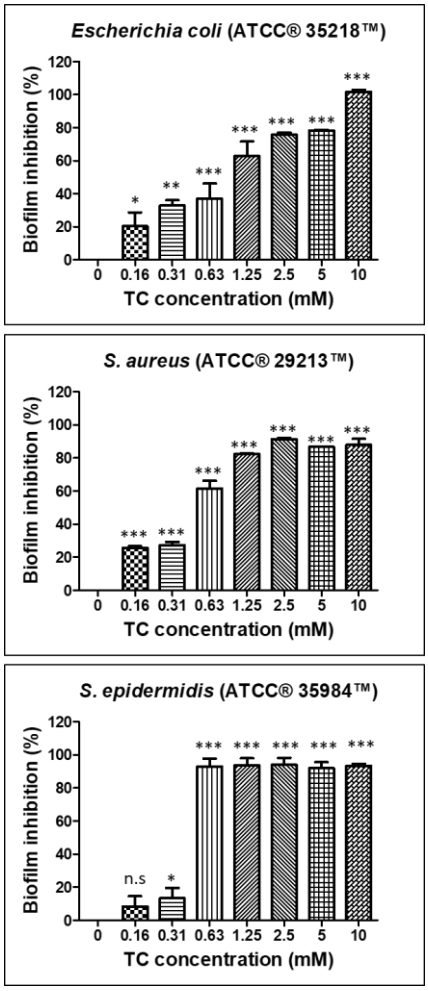

Figure 27: Percentage of biofilm inhibition of TC against *E. coli* (ATCC® 35218™); *S. aureus* (ATCC® 29213™) and *S. epidermidis* (ATCC® 35984™) after bacterial exposure to increasing concentrations of TC for a period of 24 hours. The biofilm growth control is represented by the column in which no TC was added. The experiments were performed in three independent experiments, in triplicates (N=3, n=3). * indicates p<0.05, ** indicates p<0.001, * indicates p<0.0001 and n.s indicates no statistical difference when compared with biofilm growth control.**

Biofilms can be obtained by culturing bacteria on microplates. As they proliferate, they form a layer of bacterial cells on the surface of the microplates. The detection and quantification of biofilms can be done by staining this layer of bacterial cells using safranin-O, a stain capable of detecting extracellular substances present in biofilm matrices (Bueno, J., 2014). The safranin-O-stained substances of the biofilm are dispersed in an aqueous SDS solution and thus the biofilm is indirectly quantified by measuring the absorbance at 495nm.

Each graph shows the percentage of biofilm inhibition compared to that obtained with the biofilm growth control when the selected bacterial strains were cultured in the presence of increasing concentrations of TC for a period of 24 hours. The growth control is represented by the column in which no TC was added.

The results showed that, in the case of *E. coli* (ATCC® 35218™), the higher the TC concentration, the higher the biofilm inhibitory effect. More specifically, with concentrations of 0.16 mM, 0.31 mM, 0.63 mM, 1.25 mM and 2.5 mM, the biofilm formation was inhibited by 20%, 33%, 37%, 63% and 76%, respectively. With concentrations higher than the MIC, that is, 5 mM, the biofilm formation was inhibited by more than 75%. On the other hand, in the case of *S. aureus* (ATCC® 29213™) and *S. epidermidis* (ATCC® 35984™), a different effect of TC was observed towards the inhibition of biofilm formation as very similar inhibitory effects were obtained by using the highest TC concentration or the concentration equivalent to the MIC. More precisely, in the case of *S. aureus* (ATCC® 29213™), with a concentration of 10 mM, the biofilm formation was inhibited by 88% and with the concentration equivalent to the MIC, that is 1.25 mM, the biofilm formation was inhibited by 82%. In the case of *S. epidermidis* (ATCC® 35984™), with a concentration of 10 mM and with the concentration equivalent to the MIC, that is 0.63 mM, the biofilm formation was inhibited by 93%.

4.2.2 Fabrication of P(3HB) films loaded with TC

4.2.2.1 Film development

Having done the antibacterial screening of TC it was possible to formulate three different types of P(3HB)/TC films by the solvent casting technique. Three different TC weight percentages were considered, corresponding to an addition of 3.5x, 4x and 5x more than highest antibacterial concentration (HAC) determined, that is the MBC calculated for *E. coli* (ATCC® 35218™) in order to have materials that would target all three bacterial strains. The

three different P(3HB)/TC films were formulated by the solvent casting technique and are described as P(3HB) films with 11.5 wt% TC, P(3HB) films with 13 wt% TC and P(3HB) films with 16.7 wt% TC.

4.2.2.2 Entrapment efficiency

Table 12: Entrapment efficiency of TC into the P(3HB) polymer matrix.

Film	TC in relation to the HAC*	TC EE%	TC in relation to the HAC
P(3HB), 11.5 wt% TC	3.5x	47.08±1.63	1.65x
P(3HB), 13 wt% TC	4x	47.93±2.14	1.92x
P(3HB), 16.7 wt% TC	5x	29.73±0.72	1.49x

* considering 100% TC EE

Considering the volatility of TC and of the solvent where the polymer was dissolved (chloroform), it was necessary to measure the amount of TC that remained entrapped in the P(3HB) films after the drying process of the films to ensure that the amount that remained entrapped would be sufficient to cause an antibacterial effect against bacteria. For that, pre-weight samples were dissolved in a defined volume of chloroform and the solutions analysed via GC-MS. Using a calibration curve, the peak areas recorded for each sample were used to calculate the concentration of TC present in each sample and the entrapment efficiency was calculated using the formula indicated in the Materials and Methods section 2.8.2. The results are summarised in Table 12.

The results showed that the entrapment of TC into the polymer films varied according to the initial loadings. With the lowest loading, 11.5 wt% TC, an entrapment efficiency of 47% was obtained which corresponded to a TC concentration of 1.65x higher than the HAC. With a loading of 13 wt% TC, an entrapment efficiency of 48% was obtained which corresponded to a TC concentration of 1.92x higher than the HAC. Finally, with a loading of 16.7 wt% TC, an

entrapment efficiency of 30% was obtained which corresponded to a TC concentration of 1.49x higher than the HAC.

4.2.3 Characterisation of P(3HB) films loaded with TC

4.2.3.1 Attenuated Total Reflectance Fourier Transform Infrared Spectroscopy (ATR-FTIR)

ATR-FTIR was carried out to see the chemical changes on the surface of P(3HB) films after the incorporation of TC and the results are shown in Figure 28.

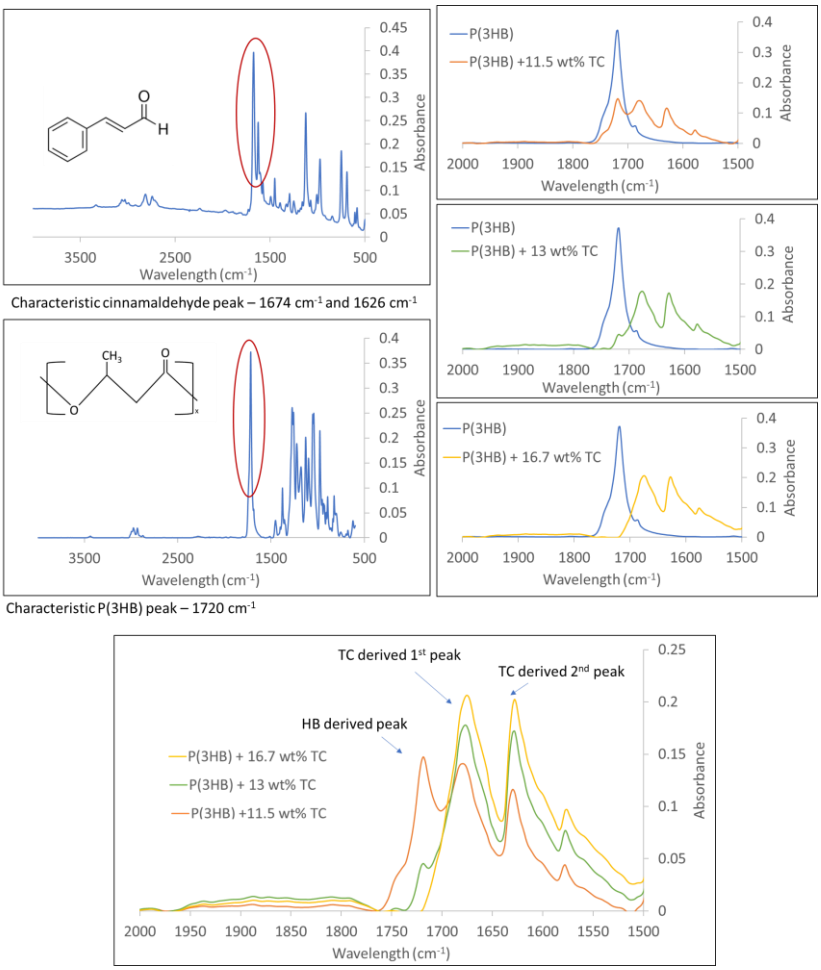

Figure 28: ATR-FTIR spectra of P(3HB) and TC and their respective characteristic peaks. ATR-FTIR spectra of P(3HB) loaded with 11.5 wt% TC, 13 wt% TC and 16.7 wt% TC and its comparison with the P(3HB) spectrum.

Since P(3HB) and TC characteristic peaks are located in the same region, it is easy to identify the surface changes on the surface of P(3HB) films after the incorporation of TC. P(3HB) has a characteristic peak located at 1720 cm^{-1} that corresponds to the ester carbonyl group. And on the other hand, TC has two characteristic peaks located at 1674 cm^{-1} and 1626 cm^{-1} that

correspond to the C=O and C=C stretching vibrations (Hanai *et al.*, 2001). By overlapping the P(3HB) spectrum with the different P(3HB)/TC spectra and by selecting the wavelength range correspondent to the area of the characteristic peaks of both P(3HB) and of TC it was possible to confirm if P(3HB) films contained TC on its surface and also to correlate the intensity of the peaks with the TC content.

The spectrum correspondent to the surface of the films loaded with 11.5 wt% TC showed the presence of three peaks, more specifically at 1718.4 cm^{-1}, 1679.9 cm^{-1} and 1629.7 cm^{-1}. In the case of the P(3HB) films loaded with 13 wt% TC, three peaks were also identified at 1718.4 cm-1, 1677.9 cm^{-1} and 1627.8 cm^{-1}. In the case of P(3HB) films loaded with 16.7 wt% TC, only two peaks were detected at 1676.0 cm^{-1} and 1627.8 cm^{-1}.

4.2.3.2 Mechanical analysis: Tensile testing

Tensile tests were performed to evaluate the differences in the mechanical behaviour of P(3HB) films loaded with TC. The Young's Modulus (E), tensile strength (σ) and elongation at break (ε_b) were measured and the results are shown in Figure 29.

The tensile test showed that the addition of TC caused significant changes on the mechanical properties of P(3HB), i.e., with increasing weight percentages of TC, a decrease in the tensile strength and Young's modulus and an increase in the elongation at break was observed.

More specifically, P(3HB), P(3HB) loaded with 11.5 wt% TC, P(3HB) loaded with 13 wt% TC and P(3HB) loaded with 16.7 wt% TC, showed a tensile strength of 24 MPa, 14 MPa, 10 MPa and 10 MPa, respectively. In terms of the Young's Modulus, P(3HB), P(3HB) loaded with 11.5 wt% TC, P(3HB) loaded with 13 wt% TC and P(3HB) loaded with 16.7 wt% TC showed values of 1156 MPa, 802 MPa, 625 MPa and 357 MPa, respectively. Finally, regarding the elongation at break, P(3HB), P(3HB) loaded with 11.5 wt% TC, P(3HB) loaded with 13 wt% TC and P(3HB) loaded with 16.7 wt% TC showed values of 3%, 54%, 104% and of 116%, respectively.

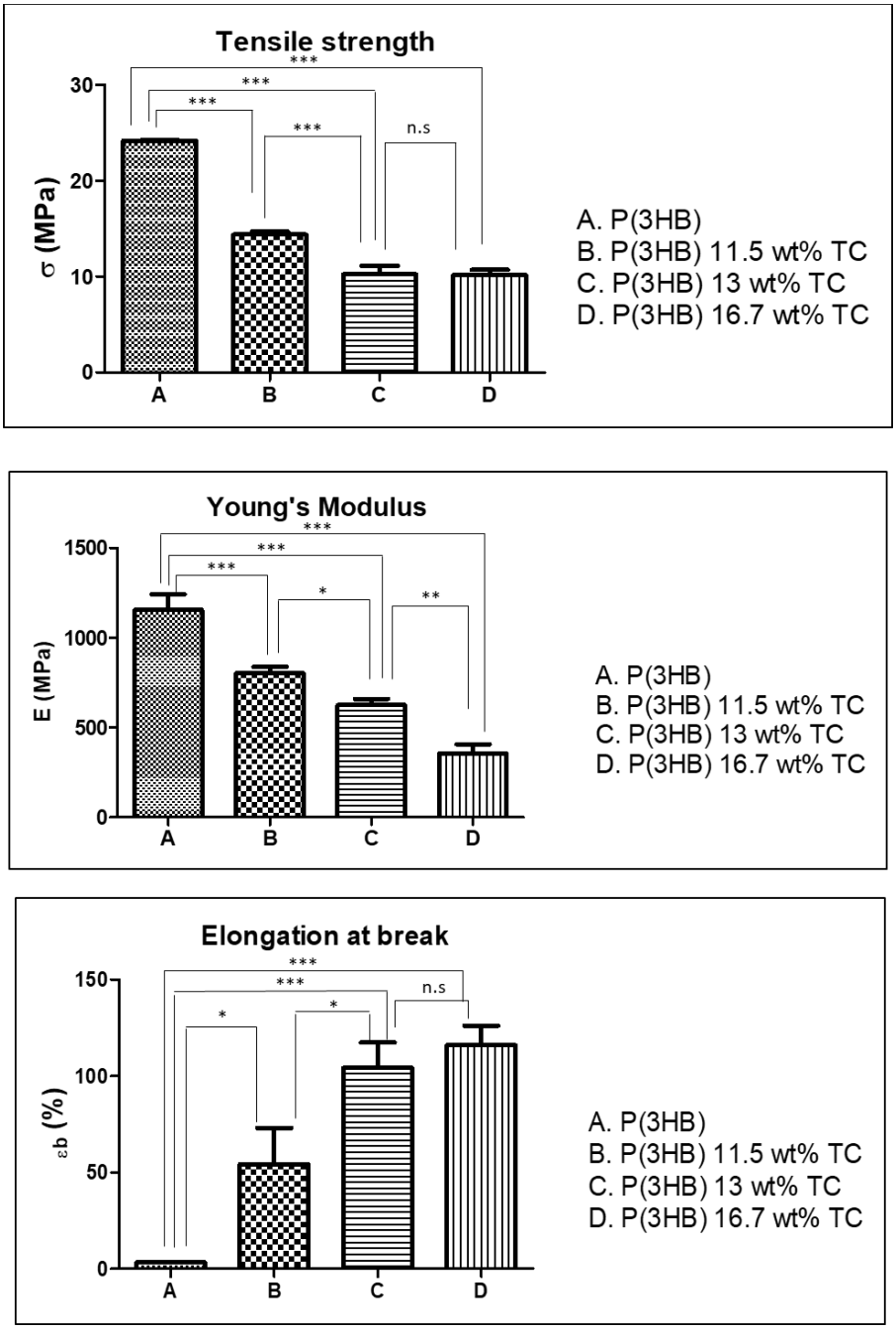

Figure 29: Mechanical evaluation of P(3HB) loaded and non-loaded with TC. Evaluation of the tensile strength, Young's Modulus and elongation at break. The experiments were performed in three independent experiments, in triplicates (N=3, n=3). All pairs of columns were compared. * indicates p<0.05, ** indicates p<0.001 and * indicates p<0.0001.**

4.2.3.3 Thermal analysis: Differential Scanning Calorimetry (DSC)

A thermal characterisation was carried out by DSC where phase changes were observed during heating and cooling steps, allowing for the determination of the glass transition temperature

(T_g), melting temperature (T_m) and peak crystallisation temperature (T_c) of the different P(3HB)/TC materials. The results obtained are shown in Figure 30 and Table 13.

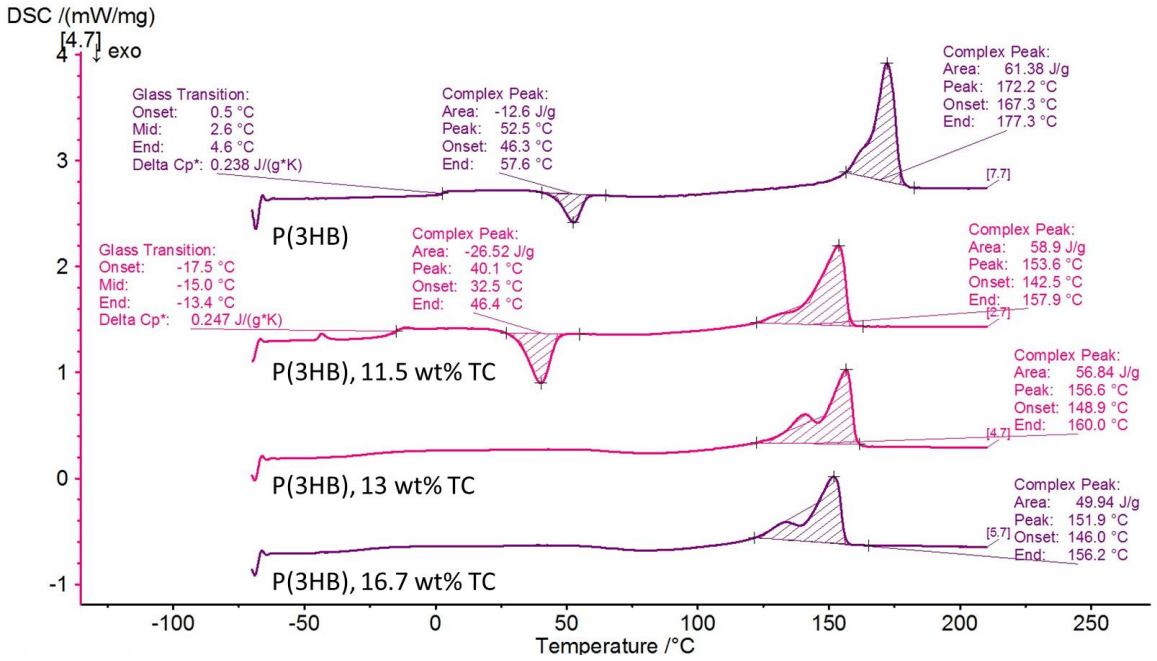

Figure 30: DSC thermograms of P(3HB), P(3HB) loaded with 11.5 wt% TC, P(3HB) loaded with 13 wt% TC and P(3HB) loaded with 16.7 wt% TC.

From the DSC thermograms it was possible to visualise that P(3HB) presented the typical phase changes, more specifically, a glass transition temperature, a peak crystallisation temperature and a melting temperature. The same thermal events were also observed for P(3HB) loaded with 11.5 wt% TC. In the case where P(3HB) was loaded with 13 wt% TC and with 16.7 wt% TC, only the peak corresponding to the melting temperature was observed.

P(3HB) showed a melting temperature of 172.2°C, a glass transition temperature of 2.6°C and a crystallisation peak temperature of 52.5°C. The addition of 11.5 wt% TC caused a decrease in all determined temperatures. More specifically, a melting temperature of 153.6°C, a glass transition temperature of -15°C and a crystallisation peak temperature of 40.1°C was observed. The materials with the highest addition of TC, that is, P(3HB) loaded with 13 wt% TC and P(3HB) loaded with 16.7 wt% TC, exhibited a melting temperature of 156.6°C and of 151.9°C, respectively.

Table 13: Thermal properties of P(3HB) loaded with TC

	P(3HB)	P(3HB), 11.5 wt%	P(3HB), 13 wt%	P(3HB), 16.7 wt%
T_m (°C)	172.2	153.6	156.6	151.9
T_g (°C)	2.6	-15	n.d	n.d
Tc (°C)	52.5	40.1	n.d	n.d

n.d. – non-detected

4.2.3.4 Surface analysis: Scanning Electron Microscopy (SEM)

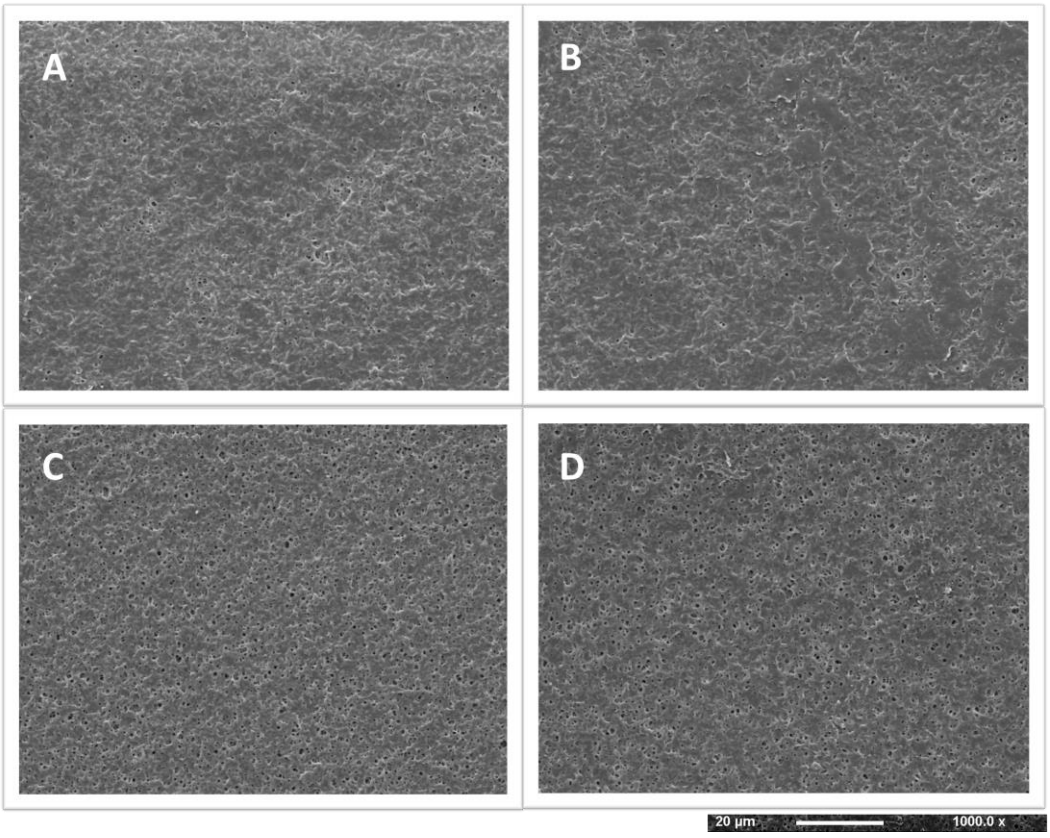

Figure 31: SEM micrographs of the surface morphology of P(3HB) films non-loaded and loaded with TC. A – P(3HB); B – P(3HB), 11.5 wt% TC; C – P(3HB), 13 wt% TC; D – P(3HB), 16.7 wt% TC. Magnification of micrographs, 1000x and scale bar of 20 µm.

The surface morphology of the different P(3HB)/TC materials was studied by SEM and compared to the surface morphology of P(3HB) films. The results are shown in Figure 31.

The results showed that with the addition of TC the surface of the materials became more porous as the pore content increased with increasing loadings of TC.

4.2.3.5 Surface analysis: Water Contact Angle (WCA)

To evaluate the surface wettability of P(3HB) films loaded with TC, static water contact angle studies were performed, and the results are shown in Figure 32.

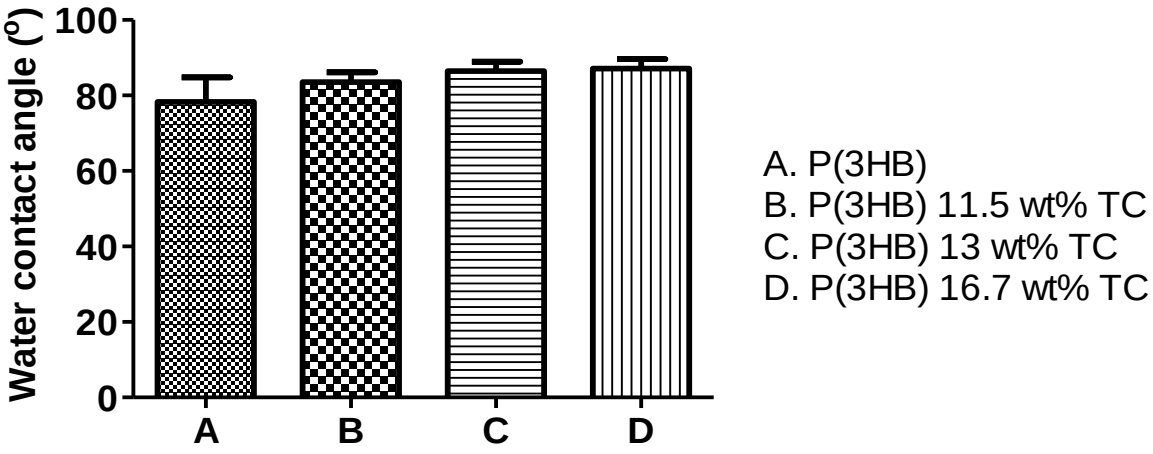

Figure 32: Static water contact angle measurements of P(3HB) non-loaded and loaded with TC. A – P(3HB), B – P(3HB), 11.5 wt% TC, C – P(3HB), 13 wt% TC and D – P(3HB), 16.7 wt% TC.

The results showed that P(3HB) had a water contact angle of 78.3°, P(3HB) films loaded with 11.5 wt% TC had a water contact angle of 83.5°, P(3HB) films loaded with 13 wt% TC had a water contact angle of 86.5° and P(3HB) films loaded with 16.7 wt% TC had a water contact angle of 87.2°. The values obtained were not statistically different.

4.2.4 Antibacterial characterisation of P(3HB) films loaded with TC

4.2.4.1 Disc diffusion assay

As a first screening, the antibacterial activity of the different P(3HB)/TC materials was evaluated by the disc diffusion assay against *E. coli* (ATCC® 35218™), *S. epidermidis* (ATCC® 35984™) and *S. aureus* (ATCC® 29213™) and the results are shown in Figure 33.

Figure 33 shows the zones of inhibition that resulted from the incubation of different 1 cm diameter P(3HB) discs loaded and non-loaded with TC for a period of 24 hours when in contact with a layer of bacteria. Antibiotic discs were used as the positive control.

The results showed that *S. epidermidis* (ATCC® 35984™) was more susceptible to the antibacterial action of the films, followed by *S. aureus* (ATCC® 29213™), and *E. coli* (ATCC® 35218™). In all cases, P(3HB) discs non-loaded with TC did not exhibit any inhibition zone.

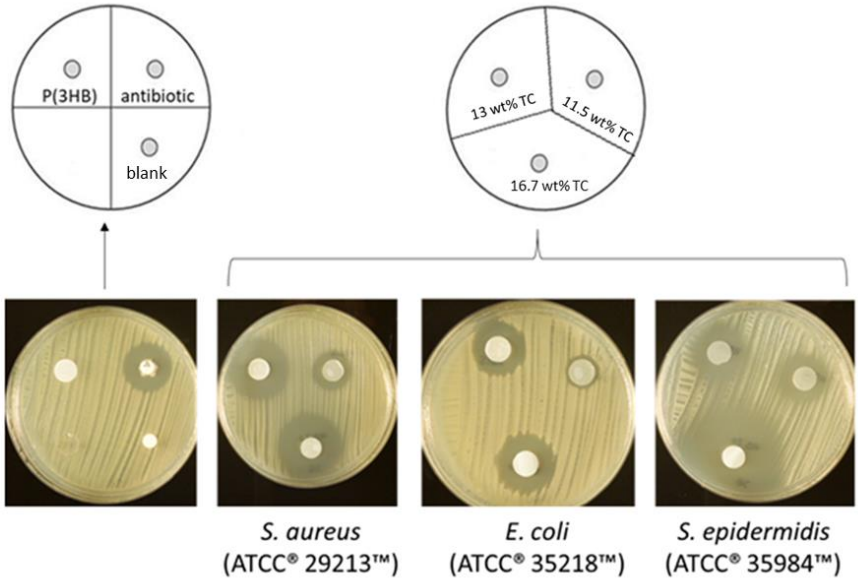

Figure 33: Disc diffusion assay using 1 cm diameter P(3HB) discs loaded and non-loaded with TC. Inhibition zones of each material after a 24-hour incubation with *S. aureus* (ATCC® 29213™), *E. coli* (ATCC® 35218™) and *S. epidermidis* (ATCC® 35984™).

More specifically, in the case of *S. aureus* (ATCC® 29213™), the loadings of 11.5 wt% TC, 13 wt% TC and 16.7 wt% TC, resulted in inhibition zones of 0.75±0.07 cm, 1.75±0.07 cm and 2.1±0.14 cm, respectively. In the case of *E. coli* (ATCC® 35218™), the 11.5 wt% TC loading and the 13 wt% TC loading resulted in inhibition zones of 0.45±0.07 cm and 1.45±0.07 cm, respectively. Increasing the loading to 16.7 wt% TC resulted in an inhibition zone of 1.55±0.07 cm. Finally, in the case of *S. epidermidis* (ATCC® 35984™), the highest loading resulted in an inhibition zone of 3.15±0.07 cm, whereas the lower loadings, that is 11.5 wt% TC loading and with a 13 wt% TC loading, the inhibition zones obtained were of 1.25±0.35 cm and 1.55±0.07 cm, respectively.

4.2.4.2 Biocidal and anti-biofilm properties

The encouraging results led to a more in-depth evaluation of the antibacterial activity of the materials, more specifically its biocidal and anti-biofilm properties. To do so, 1 cm diameter P(3HB) discs loaded and non-loaded with TC were incubated in liquid bacterial cultures for a period of 7 consecutive days and the results are shown in Figure 34 and Figure 35.

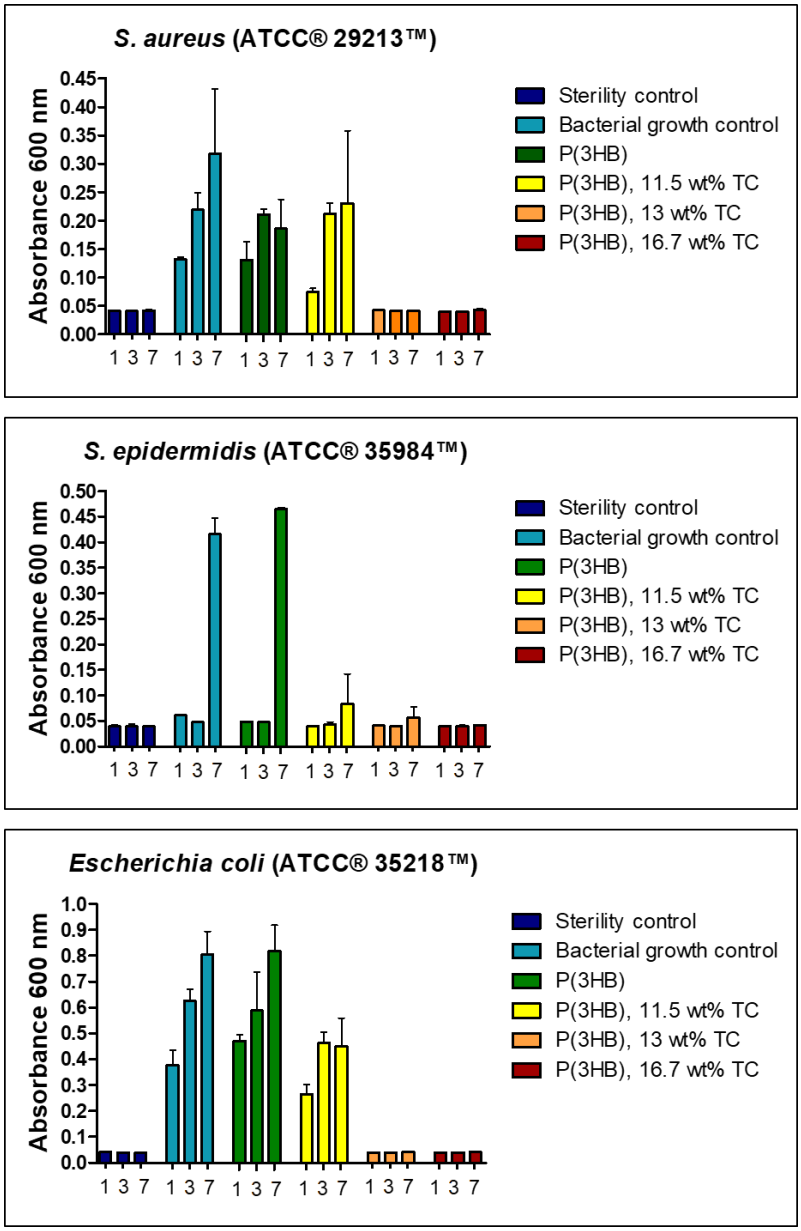

Figure 34: Biocidal effect of P(3HB) discs loaded and non-loaded with TC against *S. aureus* (ATCC® 29213™), *S. epidermidis* (ATCC® 359842™) and *Escherichia coli* (ATCC® 25922™). Optical density of bacterial cultures during the exposure of the materials for 1, 3 and 7 days of incubation. A typical bacterial growth control and a sterility control were used.

Each graph shows the result of the monitoring of the optical density of the bacterial cultures for day 1, 3 and 7 by measuring the absorbance at 600 nm when bacteria were in the presence of non-loaded and TC loaded P(3HB) discs. A typical bacterial growth control and a sterility control were considered in order to have a term of comparison.

The results showed that the sterility growth controls exhibited a constant absorbance and a value close to zero throughout the 7-day incubation period. In addition, the results showed that for each bacterium, the bacterial growth control showed an increase in the absorbance values as the incubation period augmented and the same effect was observed for the cases where bacteria were incubated with P(3HB) discs non-loaded with TC.

Focusing on the results obtained for *S. aureus* (ATCC® 29213™), it was observed that the discs loaded with 13 wt% TC and the discs loaded with 16.7 wt% TC showed a similar trend to the one observed for the sterility growth control in which the absorbance values remained constant and close to zero throughout the 7-day incubation period, while the discs loaded with 11.5 wt% TC, showed an increase in the absorbance values as the incubation period increased.

In the case of *S. epidermidis* (ATCC® 35984™), the discs loaded with 11.5 wt% TC, showed a slight increase in the absorbance values only on the 7th day of incubation, while on the 1st and 3rd day of incubation, the absorbance values remained similar to the ones obtained in the sterility growth control. In terms of the discs loaded with 13 wt% TC and the discs loaded with 16.7 wt% TC, the absorbance values also remained constant and close to zero throughout the 7-day incubation period

Finally, regarding *E. coli* (ATCC® 35218™), a similar scenario to the one observed for *S. aureus* (ATCC® 29213™) was obtained where the discs loaded with 13 wt% TC and the discs loaded with 16.7 wt% TC showed a similar trend to the one observed for the sterility growth control, while with the discs loaded with 11.5 wt% TC, showed an increase in the absorbance values, similar to the ones observed for the bacterial growth control and the discs non-loaded with TC.

After performing the liquid culture test for a period of 7 days, the amount of biofilm formed at the bottom of a 24 TCPS microplate was quantified using the safranin staining method and the results are shown in Figure 35.

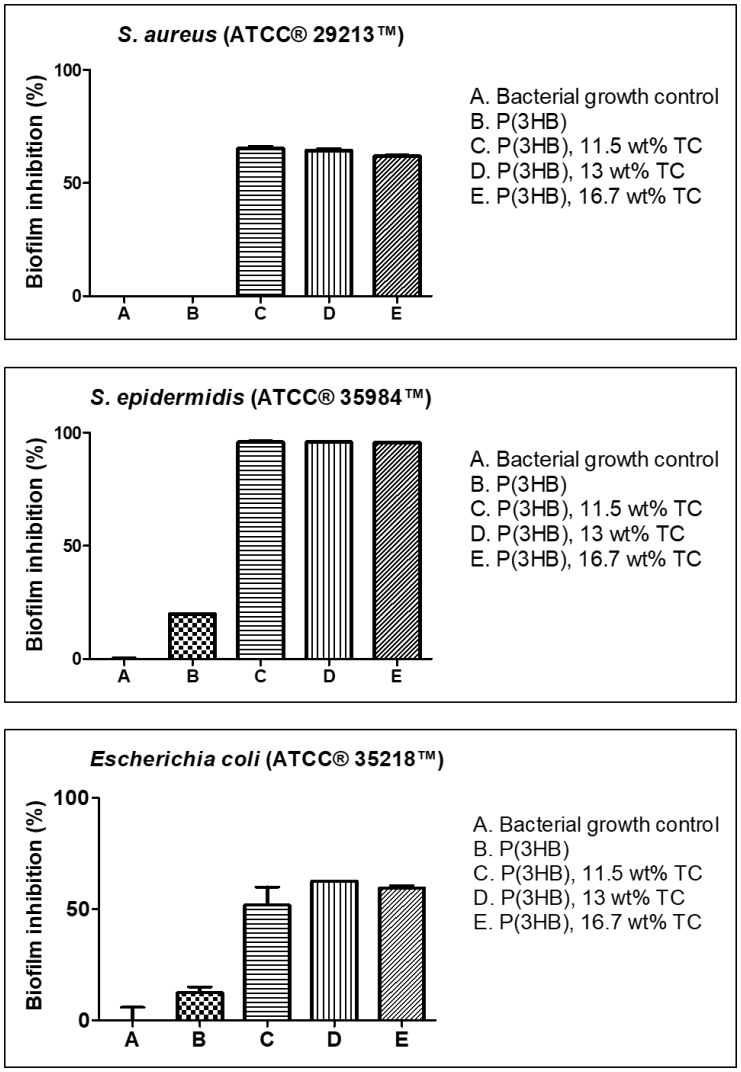

Figure 35: Percentage of biofilm inhibition on a 24 TCPS microplate after the incubation of P(3HB) discs non-loaded and loaded with TC for a period of 7 days with *S. aureus* (ATCC® 29213™), *S. epidermidis* (ATCC® 35984™) and *E. coli* (ATCC® 35218™). A typical bacterial growth control was considered in order to have a term of comparison.

Each graph shows the percentage of biofilm formation that was inhibited on a 24 TCPS microplate after the exposure of P(3HB) discs non-loaded and loaded with TC for a period of 7 days with *S. aureus* (ATCC® 29213™), *S. epidermidis* (ATCC® 35984™) and *E. coli* (ATCC® 35218™). A typical bacterial growth control was considered in order to have a term of comparison.

The results showed that, in all cases, the P(3HB) discs loaded with TC were able to prevent biofilm formation to an extent. Particularly, in the case of *S. aureus* (ATCC® 29213™), the materials were able to prevent biofilm formation over 60%. In the case of *S. epidermidis* (ATCC® 35984™), a higher percentage of inhibition was obtained as the materials prevented biofilm formation over 95%. Lastly, in the case of *E. coli* (ATCC® 35218™), the materials were able to prevent biofilm formation over 50%.

4.2.5 Development and characterisation of antibacterial P(3HB)/TC based coatings

4.2.5.1 Dip coating of polyurethanes using P(3HB)/TC solutions

The characterisation steps provided an idea of the performance and properties of the different materials. Besides the chemical, mechanical, thermal and surface analysis, it was clear that the materials loaded with 13 wt% TC and the materials loaded with 16.7 wt% TC yielded better antibacterial results than the materials loaded with 11.5 wt% TC. Since the antibacterial performance of the two highest loadings was not significantly different and in order to minimise the chances of cytotoxicity, the 13 wt% TC loading was selected to further develop P(3HB)-based coatings. Biomedical catheters are mainly made using polyurethane (PU), therefore PU tubes were selected to be coated with P(3HB)/TC solutions. Two different P(3HB)/TC solutions were prepared. The first solution consisted of a less concentrated P(3HB) solution defined at 5 w/v% and the second solution consisted of a more concentrated solution of P(3HB) defined at 10 w/v%. Both solutions were loaded with the same concentration of TC, that is 13 wt% TC. Depending on the P(3HB) concentration and the amount of TC loaded, the final PU coated tubes were termed here as $PU_{5,13}$ and $PU_{10,13}$.

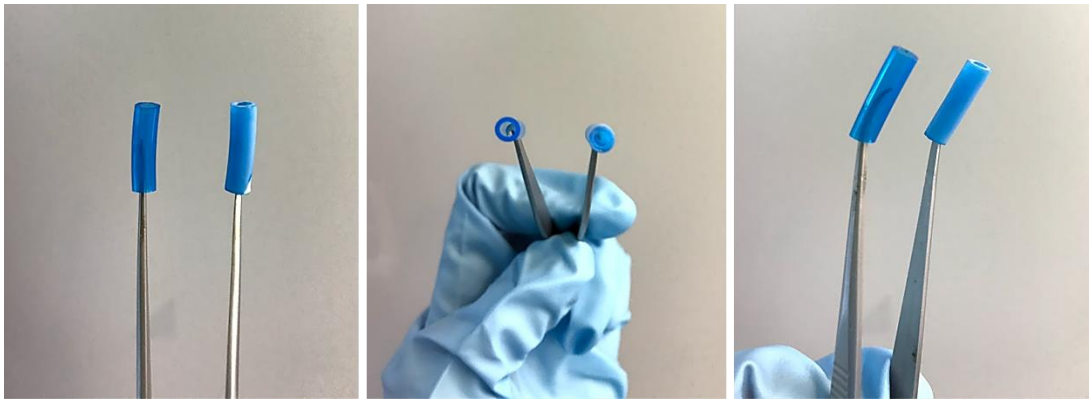

Figure 36: Differences between a non-coated PU tube (left) and a PU tube coated with a P(3HB) solution at 5 w/v% with a TC loading of 13 wt% (right).

4.2.5.2 Surface analysis: Scanning Electron Microscopy (SEM)

In order to visualise the differences of the surface of the PU tubes after the coating procedure, SEM micrographs of the cross-section, inner and outer surface of the P(3HB)/TC coated PU and non-coated PU tubes were taken. The results are shown in Figure 37.

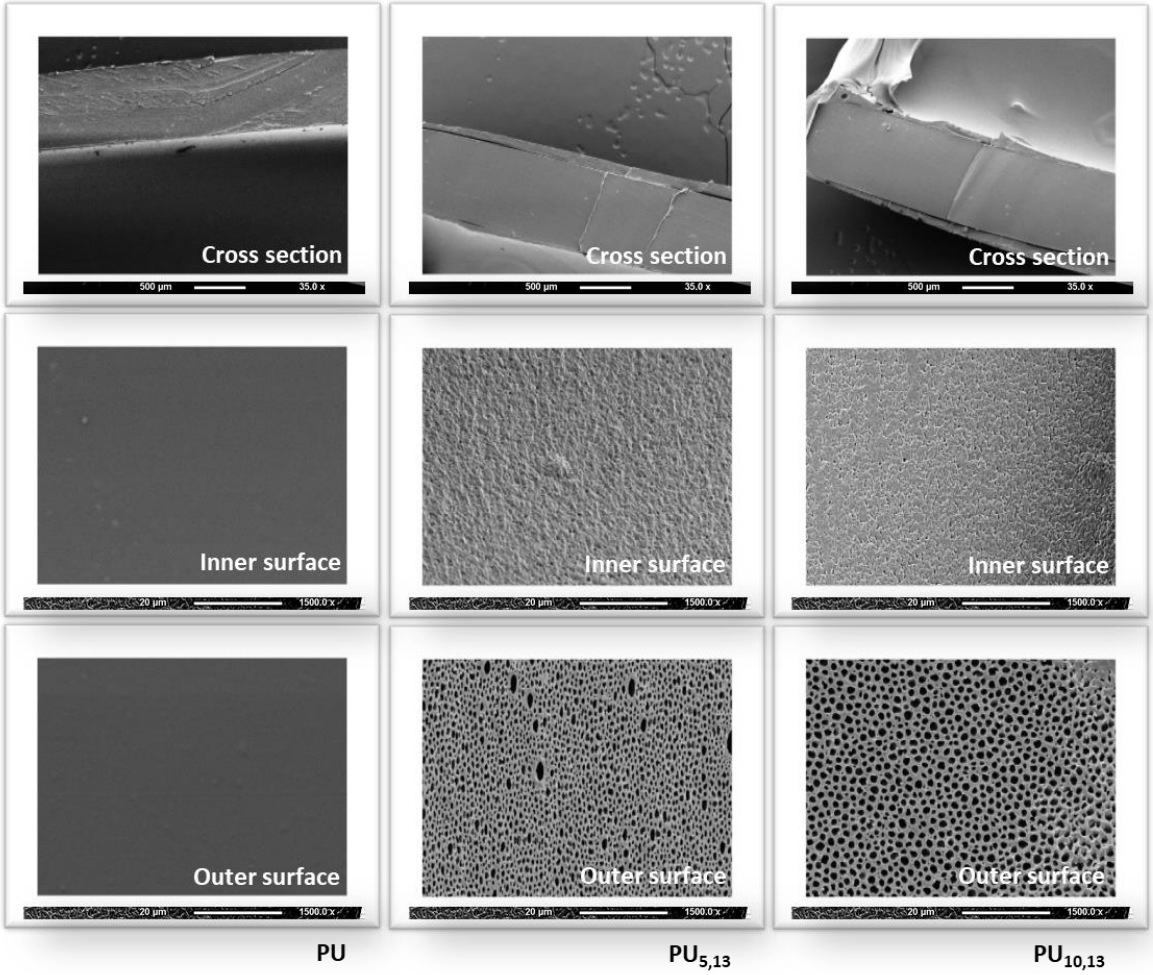

Figure 37: SEM sectional micrographs of P(3HB)/TC coated PU and non-coated PU. Magnification of cross-sectional micrographs, 35x and scale bar of 500 µm; magnification of inner and outer surface micrographs of 1500x and scale bar of 20 µm.

The results show the surface morphologies of the different sections of the coated and non-coated PU tubes.

The cross-sectional micrographs showed that contrary to the uncoated PU, $PU_{5,13}$ and $PU_{10,13}$ presented a film layer covering the intraluminal and extraluminal surfaces of the PU tubes. In terms of the inner surface, the uncoated PU showed a smooth intraluminal surface while on

the other hand, $PU_{5,13}$ and $PU_{10,13}$ showed an irregular intraluminal surface. The PU extraluminal surface, in contrast, exhibited a smooth morphology. In addition, the extraluminal surface of $PU_{5,13}$ and $PU_{10,13}$ became porous, with larger pores shown on the extraluminal surface of $PU_{10,13}$ tubes.

4.2.5.3 Biocidal, anti-adhesion and anti-biofilm properties

In order to evaluate the antibacterial performance of the PU coated tubes, an antibacterial test composed of three parts was performed to assess the biocidal, anti-adhesion and anti-biofilm properties of the materials against *S. epidermidis* (ATCC® 35984™).

After incubating the samples with bacteria for a period of 24 hours, the biocidal effect was investigated by quantifying the number of planktonic bacteria that were able to grow when exposed to the different samples and compared to the concentration of the initial inoculum used to incubate the samples and the results are shown in Figure 38. Furthermore, the adhesion of bacteria to the samples was also quantified by a sonication procedure allowing the determination of the number of bacteria that were able to adhere to the samples and the results are shown in Figure 39. Finally, in order to evaluate if the content released from each sample was able to prevent biofilm formation on the surrounding surfaces, an anti-biofilm test was performed by quantifying the biofilm biomass that was produced using the safranin staining method and the results are shown in Figure 40. As a positive control, commercially available polyurethane-based catheters impregnated with chlorhexidine and silver sulfadiazine (ARROWg+ard Blue PLUS Central Venous Catheters) here termed as ARROW were used.

Figure 38 shows the number of planktonic bacteria recovered from coated and non-coated PU tubes after the incubation with *S. epidermidis* (ATCC® 35984™) for 24 hours and in relation to the bacteria present in the initial inoculum and with ARROW tubes used as the positive control.

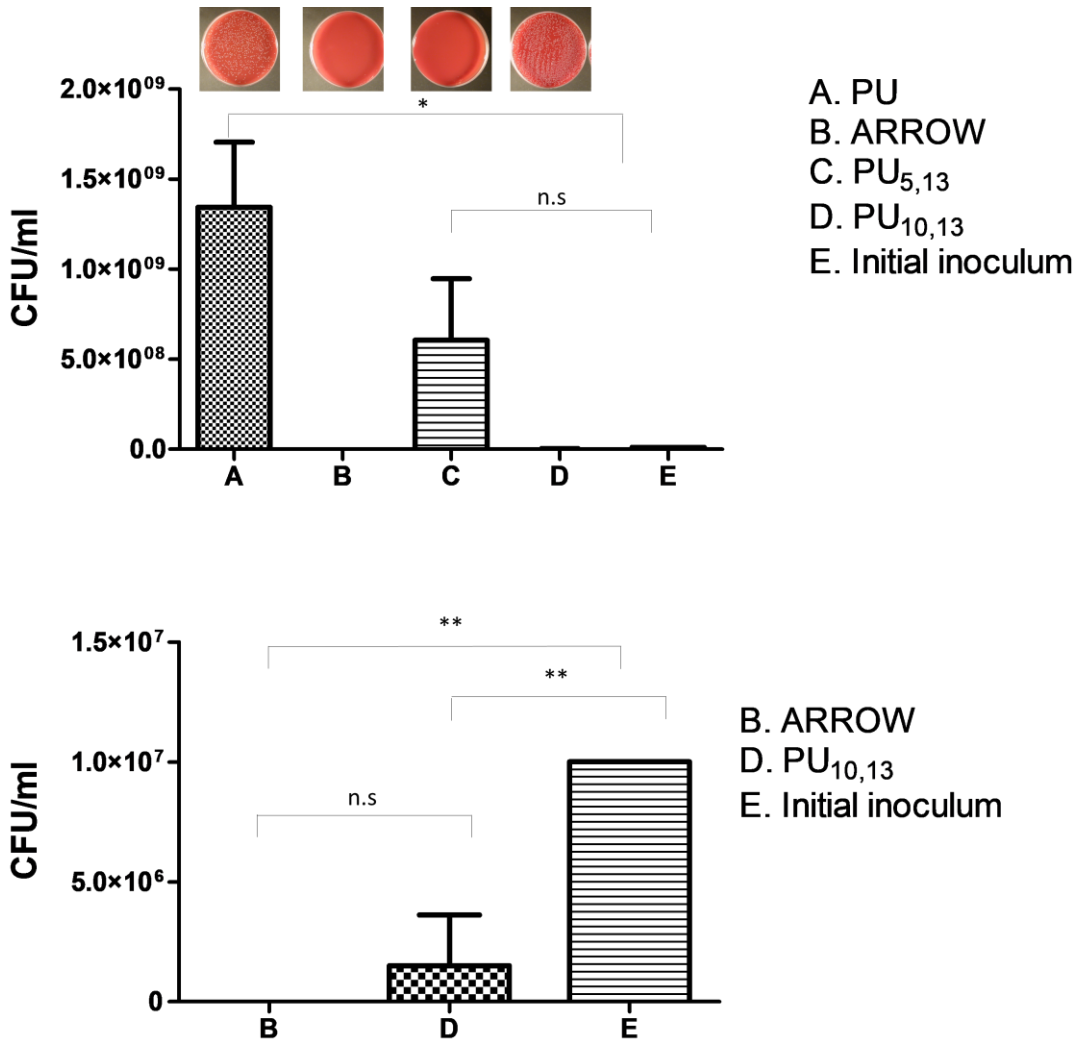

Figure 38: Planktonic bacteria recovered from coated and non-coated PU tubes after the incubation with *S. epidermidis* (ATCC® 35984™) for 24 hours and in relation to the bacteria present in the initial inoculum. ARROW tubes were used as the positive control. The experiments were performed in triplicates (n=3). All pairs of columns were compared. ** indicates p<0.001 and n.s indicates no statistical difference.

From the results obtained it was possible to see that the number of bacteria recovered from the PU tubes and from the $PU_{5,13}$ tubes were higher than that of the initial inoculum, however there was no significant difference between the number of bacteria recovered from the $PU_{5,13}$ tubes and the bacteria present in the initial inoculum. On the other hand, the ARROW tubes and the $PU_{10,13}$ tubes showed a significant decrease in the number of bacteria recovered after the incubation period and in relation to that of the initial inoculum. More specifically, the number of bacteria recovered from the PU tubes and the $PU_{5,13}$ tubes was $1.3x10^9$ CFU/mL and

6.0x10^{8} CFU/mL, respectively, while the number of bacteria recovered from the ARROW tubes and the $PU_{10,13}$ tubes were 0 CFU/mL and 1.5x10^{6} CFU/mL, respectively.

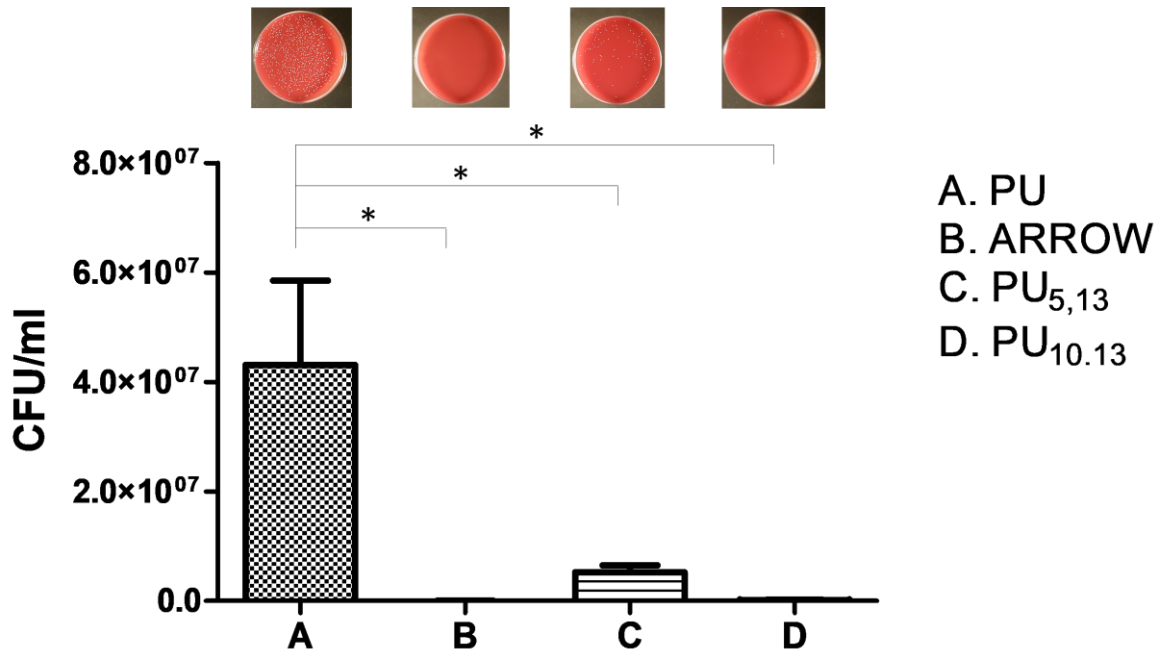

Figure 39: Bacterial sonicates recovered from coated and non-coated PU tubes after the incubation with *S. epidermidis* (ATCC® 35984™) for 24 hours, here expressed as CFU/mL. ARROW tubes were used as the positive control. The experiments were performed in triplicates (n=3) and for statistical purposes compared to non-coated PU tubes. * indicates p<0.05.

Figure 39 shows the bacterial sonicates recovered from coated and non-coated PU tubes after the incubation with *S. epidermidis* (ATCC® 35984™) for 24 hours, here expressed as CFU/mL. ARROW tubes were used as the positive control.

The sonication procedure applied to the samples after the incubation period allowed for the quantification of the number of bacteria that adhered to the samples during the experiment. The results showed that in comparison to the number of bacteria recovered from the PU tubes, the number of bacteria recovered from either the ARROW tubes or the $PU_{5,13}$ and $PU_{10,13}$ tubes were much lower. More precisely, the number of bacteria recovered from the PU tubes was 4.3x10^{7} CFU/mL, while the number of bacteria recovered from the ARROW

tubes, the $PU_{5,13}$ and $PU_{10,13}$ tubes were $5.0x10^4$ CFU/mL, $5.2x10^6$ CFU/mL and $15x10^4$ CFU/mL, respectively.

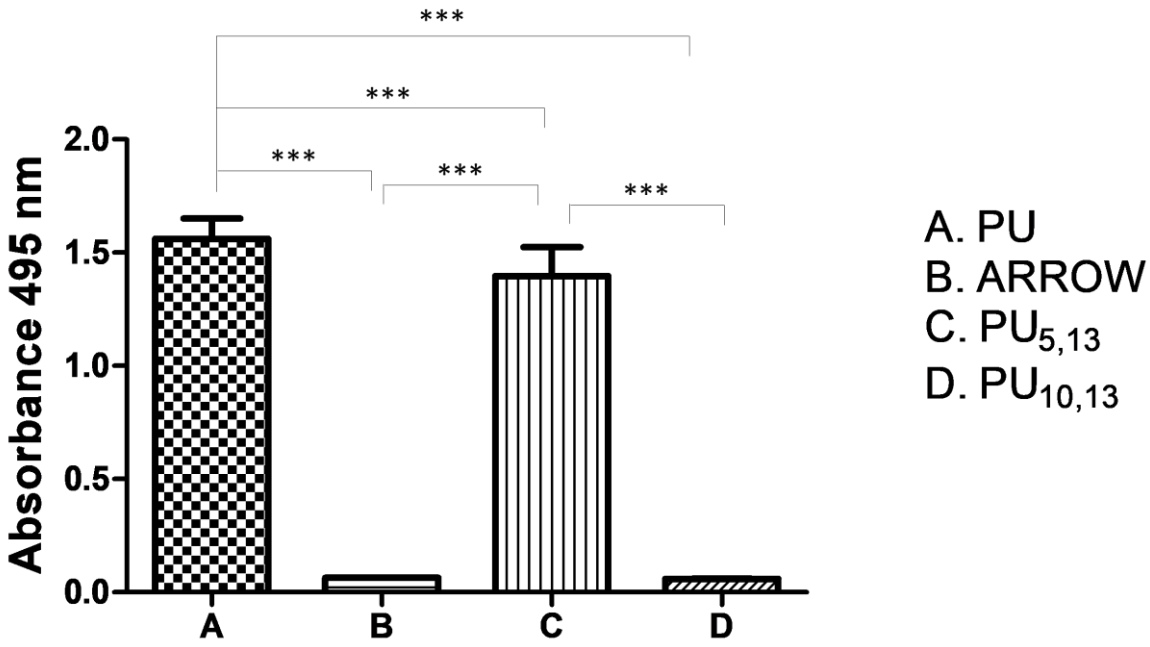

Figure 40: Biofilm formation on a 24 TCPS microplate by *S. epidermidis* (ATCC® 35984™) after incubation with coated and non-coated PU tubes for 24 hours. ARROW tubes were used as the positive control. The experiments were performed in triplicates (n=3). All pairs of columns were compared. * indicates p<0.0001.**

Figure 40 shows the amount of biofilm that was formed on a 24 TCPS microplate by *S. epidermidis* (ATCC® 35984™) after incubation with coated and non-coated PU tubes for 24 hours. The biofilm biomass formed on the 24 TCPS microplates was rinsed, fixed, and stained with safranin and the absorbance was measured at 495 nm. ARROW tubes were used as the positive control.

The results showed high absorbance values for the PU tubes and the $PU_{5,13}$ tubes, while low to almost non-existent absorbance values were obtained for the ARROW tubes and the $PU_{10,13}$ tubes. The absorbance values measured for the PU tubes and the $PU_{5,13}$ tubes were 1.56 and 1.40, respectively, while the absorbance values measured for the ARROW tubes and the $PU_{10,13}$ tubes were, in both cases, 0.06.

4.2.5.4 In vitro indirect cytotoxicity studies and Live/Dead measurements

In order to evaluate the compatibility of the materials with mammalian cells, the cytotoxicity of the TC extracts released from the PU coated tubes was evaluated by performing an indirect cytotoxicity study and by assessing the cell viability and the results are shown in Figure 41.

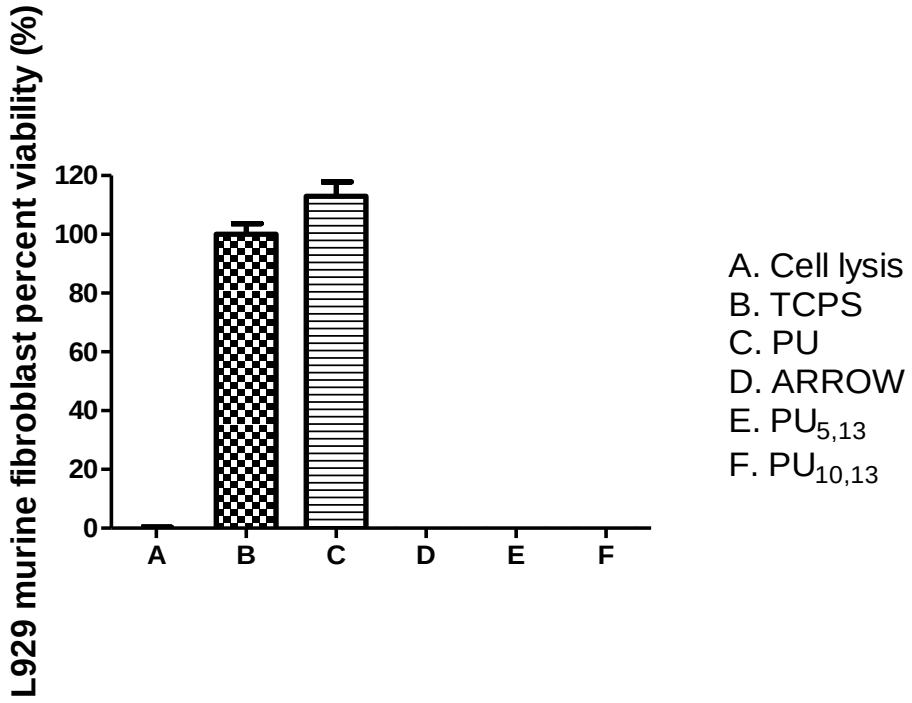

Figure 41: Percentage of cell viability of L929 murine fibroblasts after a 24-hour incubation in cRPMI media containing extracts from coated and non-coated PU for a period of 24 hours. TCPS was used as negative control and the positive control was composed of lysed cells after being treated with 5 µL of 9% Triton® X-100 (Promega) for 5 minutes after the 24-hour incubation period as well as the extracts derived from the ARROW tubes.

The graph shows the percentage of cell viability of L929 murine fibroblasts after a 24-hour incubation period of the cells with extracts from coated and non-coated PU tubes and ARROW tubes eluted for a period of 24 hours in cRPMI media.

The results showed that both the extracts eluted from the ARROW tubes and the coated PU tubes had a cytotoxic effect against the mammalian cell line as the percentage of cell viability was similar of that of the cell lysis control. On the contrary, the extracts coming from the PU tubes showed no cytotoxic effect as the cell viability was higher than 70%.

In order to correlate the data obtained with the cytotoxic study, a fluorescent cell staining was performed using a two-colour fluorescent staining and the results are shown in Figure 42.

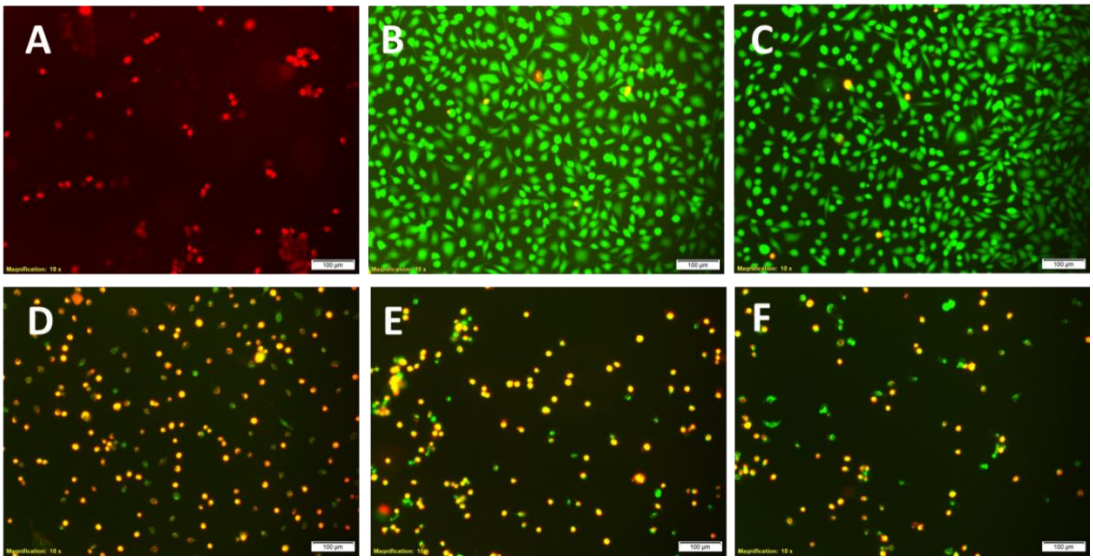

Figure 42: Fluorescence micrographs of L929 murine fibroblasts stained with the Live/Dead staining kit (Calcein-AM and EthD-III) after a 24-hour incubation in cRPMI media containing extracts from coated and non-coated PU tubes and ARROW tubes eluted for a period of 24 hours. TCPS was used as negative control and the positive control was composed of lysed cells after being treated with 5 µL of 9% Triton® X-100 (Promega) for 5 minutes after the 24-hour incubation period. A – Cell lysis; B – TCPS; C – PU; D – ARROW; E – $PU_{5,13}$; F – $PU_{10,13}$. The dead cells are represented in red and live cells are represented in green. Scale bar = 100 µm.

The micrographs show the presence of live and dead L929 murine fibroblasts after being stained with a Live/Dead staining kit (Calcein-AM and EthD-III). The cells were stained after a 24-hour incubation in cRPMI media containing extracts from coated and non-coated PU tubes and ARROW tubes eluted for a period of 24 hours. TCPS was used as negative control and the positive control was composed of lysed cells after being treated with 5 µL of 9% Triton® X-100 (Promega) for 5 minutes after the 24-hour incubation period.

The qualitative fluorescent micrographs showed that the cells exposed to the PU extracts were above all, live green cells with an elongated morphology. On the other hand, the cells exposed to the ARROW extracts and the extracts deriving from the $PU_{5,13}$ tubes and $PU_{10,13}$ tubes showed mainly red dead cells with a round morphology.

4.2.5.5 Haemocompatibility studies

In order to test if the PU coated tubes induced the lysis of red blood cells, a haemolysis test was performed. The materials were incubated with fresh pre-diluted blood and the amount of released haemoglobin determined by measuring the absorbance at 542 nm. The results are shown in Figure 43 and are expressed as haemolysis ratios.

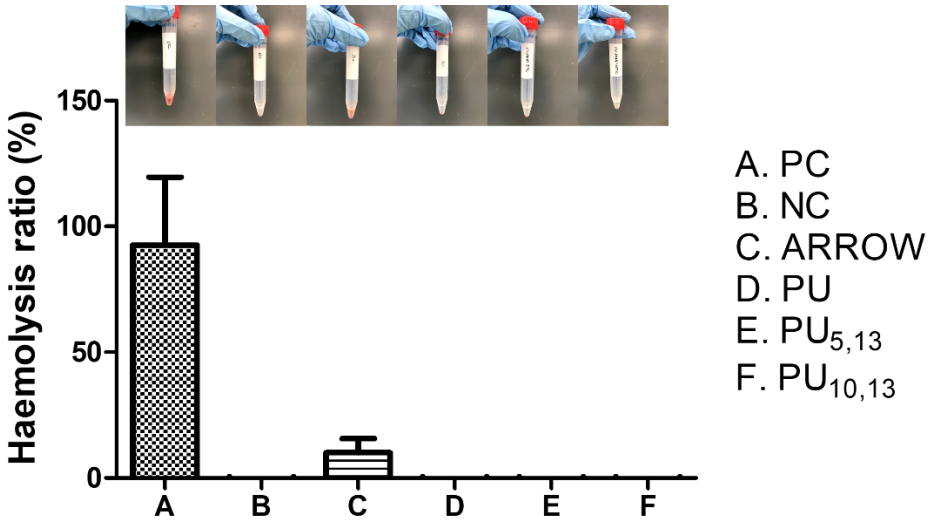

Figure 43: Haemolysis testing performed on coated and non-coated PU tubes and ARROW tubes, using fresh human pre-diluted blood and polystyrene as negative control. The positive control was composed of lysed cells induced by incubation with distilled water instead of 0.9% NaCl.

Figure 43 shows the results from the haemolysis test performed on coated and non-coated PU tubes and ARROW tubes, using fresh human pre-diluted blood. PS was used as the negative control and the positive control was composed of lysed cells induced by incubation with distilled water instead of 0.9% NaCl.

The haemolysis ratio obtained for the positive control was of 93% while for the ARROW tubes was of 10%. PU tubes, as well as $PU_{5,13}$ tubes and $PU_{10,13}$ tubes did not show any haemolysis effect.

4.3 Discussion

Despite the increasing use of biomaterials in regenerative medicine applications, the problem of early bacterial contamination of biomaterials persists. Besides having to consider that the implantation procedure itself is a gate for bacteria to enter, grow and proliferate inside the human body, it is also important to acknowledge that once bacteria enter in contact with the surface of a biomaterial they can adhere and colonise its surface, initiating the process of biofilm formation and device-associated infections. Therefore, designing technologies for both coatings and improved biomaterial structures that not only prevent bacterial growth, but also bacterial adhesion and biofilm formation are of utmost importance. The development of antibacterial, anti-adhesive and anti-biofilm P(3HB) materials was achieved by combining TC with P(3HB), resulting in a bioactive releasing polymer against some of the most frequent bacterial strains associated with device-associated infections (Chessa *et al*., 2016, Magana *et al*., 2018, Stefani *et al*., 2017, Hogan *et al*., 2017).

Though TC has been evaluated in many studies regarding its antibacterial properties, the concentrations in which TC acts often vary from study to study and of course depend on the bacterial strain used and the methodology applied (Balouiri *et al*., 2016). The bioactive nature of TC against *E. coli* (ATCC® 35218™), *S. epidermidis* (ATCC® 35984™) and *S. aureus* (ATCC® 29213™) was confirmed with a preliminary antibacterial testing. With the range of concentrations tested, a bacteriostatic, bactericidal and anti-biofilm effect was shown against Gram-negative bacteria, *E. coli* (ATCC® 35218™), while only a bacteriostatic and anti-biofilm effect was shown against Gram-positive bacteria, *S. epidermidis* (ATCC® 35984™) and *S. aureus* (ATCC® 29213™). Although different activities were observed for both types of bacteria, that is Gram-positive and Gram-negative bacteria, it is not safe to assume that TC will not have a bactericidal effect against Gram-positive bacteria as the classification of an agent can be influenced by the growth conditions and experimental set up (e.g., bacterial density and test duration). Moreover, by comparing the MIC values obtained, a higher susceptibility of Gram-positive bacteria towards TC was observed in relation to Gram-negative bacteria as their MICs were considerably lower than the one determined for the latter type of bacteria. One of the major differences between Gram-positive bacteria and Gram-negative bacteria is the constitution of their membrane. Gram-positive bacteria and Gram-negative bacteria are

protected by an inner cell membrane. However, Gram-negative bacteria possess an outer membrane which grants them an extra protection against external factors. In certain cases, this membrane can exclude antibiotics or other agents from penetrating the cell (Nikaido, 1988 and Delcour, 2009). It is, therefore, not surprising that the ESKAPE pathogens, that is, the six bacterial pathogens most commonly associated with antimicrobial resistance, namely *Enterococcus faecium, Staphylococcus aureus, Klebsiella pneumoniae, Acinetobacter baumannii, Pseudomonas aeruginosa* and *Enterobacter* spp., are composed mainly of Gram-negative species. Therefore, this could be a possible explanation as to why, in this case, Gram-positive bacteria were more susceptible to TC than Gram-negative bacteria. As mentioned above, the results also showed the ability of TC to inhibit biofilm formation, confirming what has already been described in literature. For instance, Albano *et al*., showed the anti-biofilm properties of TC against *S. epidermidis* (Albano *et al*., 2019). While in another study conducted by Kim *et al*., the anti-biofilm properties of TC were shown against *P. aeruginosa* and *E. coli* (Kim *et al*., 2015). While the mechanism of action of TC is not well-established, many describe TC as a quorum-sensing inhibitor, or in other words an inhibitor of a bacterial communication process that mediates the expression of many virulent phenotypes including biofilm formation and bacterial adherence. More specifically, studies have reported the ability of TC to interfere with signal receptors present in quorum sensing systems of Gram-negative bacteria or that TC can interfere with the metabolic pathways involved in the production of autoinducers, signal molecules, present in Gram-negative bacteria (Niu *et* al., 2006, Chang *et al*., 2014). Others described that due to the hydrophobic nature of TC, it can more easily disturb the lipid bilayer and alter the bacterial membrane permeability, causing cell membrane lysis, interference with the cytoplasmatic content and damage to the cell morphology (Zhang *et al*., 2014, Shen *et al*., 2015). Since the mechanism of action of TC was outside the scope of this thesis, this question still remains open.

The initial antibacterial screening of TC was a step forward for the preparation of P(3HB) films loaded with TC. According to the antibacterial screening, the HAC, that is, 10 mM of TC, was the one that resulted in the killing of *E. coli* (ATCC® 35218™). Apart from this concentration, the volatility of TC and of chloroform were considered, and therefore, in order to ensure that enough amount of TC would be entrapped in P(3HB) films and enough would be present to exert an antibacterial effect against all three selected bacterial strains, higher loadings than

the HAC were used to produce P(3HB)/TC films, resulting in three different films, P(3HB) films loaded with 11.5 wt% TC, P(3HB) films loaded with 13 wt% TC and P(3HB) films loaded with 16.7 wt% TC.

The investigation of how much TC remained in the film form after the solvent casting procedure was evaluated by calculating the entrapment efficiency. Overall, the entrapment efficiency results showed that less than half of the TC that was loaded into the polymer solution remained in the polymer in the film form. Given the volatile nature of TC and of chloroform, it was expected that a partial evaporation of TC would occur during the drying process of the films. The results showed that an entrapment efficiency close to 50% was obtained for films loaded with either 11.5 wt% TC and 13 wt% TC, a satisfactory result considering that the concentration of TC that was entrapped in P(3HB) was still higher than the HAC. The results also showed that the amount of TC entrapped in the P(3HB) films loaded with 16.7 wt% TC was also higher than the HAC, however, the entrapment efficiency was only 30%.

The considerably lower entrapment efficiency of TC loaded at 16.7 wt% might be associated to the polymer-compound compatibility, or in other words, the P(3HB)-TC compatibility. Three types of polymer solutions were prepared to fabricate the films, all with the same polymer concentration. The difference between the three solutions was related to the TC content, which increased. During the solvent casting process, as chloroform evaporated, the polymer solubility decreased, resulting in a more concentrated P(3HB)-TC solution. In every solution TC occupied the intermolecular spaces between the polymer chains. However, when the TC content was too high, such as in the case where a 16.7 wt% TC loading was used, it could be that an interference with the thermodynamic equilibrium of the system might have occurred, decreasing the polymer-TC compatibility. This might have caused a surface segregation of TC from the bulk to the surface of the polymer by diffusion methods which possibly influenced the amount of TC that evaporated. Due to the volatile nature, TC would have easily evaporated from the surface as it became nearer to the liquid-air interphase (Dowben et al., 1987, Affrossman et al., 2000). Nonetheless, the encapsulation efficiency results showed that, in all cases, the amount of TC loaded in all films was superior to the HAC, indicating the potential bioactive effect against all three bacterial strains.

The ATR-FTIR results confirmed the presence of TC on the surface of P(3HB) films. The characteristic peaks of P(3HB) and of TC were targeted in order to be able to observe the chemical changes on the surface of P(3HB)/TC materials. The fact that these peaks were at very close wavelengths, allowed for an easy identification of the peaks shifts. The films loaded with 11.5 wt% TC and the films loaded with 13 wt% TC showed the characteristic peaks of both P(3HB) and TC, the films loaded with 16.7 wt% TC showed only the presence of the characteristic peaks of TC. This suggested that the P(3HB) films loaded with 16.7 wt% TC had a higher TC content on the surface, possibly due to the surface segregation mechanism described earlier, and hence only the peaks associated with the characteristic peaks of TC were shown. The amount of TC present on the surface of P(3HB) films was also correlated with the intensity of the peaks showed in the ATR-FTIR spectra. It was observed that the higher the TC loading, the higher the intensity of the peaks. Since the peak intensities of an IR spectra are proportional to the concentration of a molecule, it was only expected that, with increasing TC loadings, the intensity of the peaks corresponding to the TC characteristic peaks would increase, and this was indeed observed with the ATR-FTIR results (Smith, 1998). Overall all the TC loaded films showed the characteristic peaks of TC showing that the surface of the P(3HB) films had been modified.

The evidence that TC was present on the surface of P(3HB) polymer films had been given by the ATR-FTIR results, however when loading compounds to the polymer matrix, compound-polymer interactions are expected to occur, which in turn cause structural changes within the material that are reflected in the mechanical and thermal properties of a material (Bazaka *et al*., 2015). Indeed, the combination of TC with P(3HB) caused structural changes at a mechanical and thermal level confirming the presence of TC in the polymer matrix.

Firstly, it was shown that P(3HB) became less stiff and less strong, as the Young's Modulus and tensile strength decreased with increasing loadings of TC. The results also showed that with increasing loadings of TC, the materials became less brittle as the elongation at break increased. Secondly, it was observed that the films loaded with 13 wt% TC and the films loaded with 16.7 wt% TC had very similar mechanical properties. It was shown that in all parameters except for the Young's Modulus, there were no statistical differences between the values obtained. Thirdly, it was shown that in comparison to P(3HB), although the materials loaded with 11.5 wt% TC exhibited the same thermal events, all the observed temperatures were

lower than the original material. Fourthly, it was not possible to detect any glass transition temperature nor peak crystallisation temperature for the materials loaded with 13 wt% TC and 16.7 wt% TC. And finally, it was observed that with increasing TC loadings, single-melting peaks became double-melting peaks.

The explanation for the first part of observations can be clarified by the plasticising effect created by TC. TC is a small molecule with a very low molecular weight, and for this reason it is able to occupy the intermolecular spaces between the polymer chains, thereby reducing secondary forces between them. Such effect causes an improvement of flexibility and extensibility of the films, and hence the mechanical properties of P(3HB) were enhanced by the presence of TC. Similar effects were reported in other studies. For instance, in a study conducted by Qin *et al*., poly(lactic acid)/poly(trimethylene carbonate) (PLA/PTMC) films were incorporated with TC. It was seen that after the addition of the compound, the films had better flexibility and extensibility (Qin *et al*., 2015). In another study, the addition of TC into polyethylene-co-vinylacetate (EVA) films also changed the mechanical properties of the material by decreasing the elastic modulus and tensile strength and by increasing the elongation at break (Nostro *et al*., 2012). Additionally, the SEM micrographs showed that the materials became more porous as the pore content increased with increasing loadings of TC. Hence, another explanation to the changes of the mechanical properties observed in the materials could be related to the porosity of the materials. The second observation suggests that the amount of TC present in the films loaded with 13 wt% TC and in films loaded with 16.7 wt% TC was very similar. The entrapment efficiency results showed that the films loaded with 11.5 wt% TC and 13 wt% TC had a similar entrapment efficiency, so logically, the films loaded with 13 wt% TC would have more TC and hence its mechanical properties would be improved compared to the material with the lowest loading of TC. However, the entrapment efficiency results also showed that while the films loaded with 13 wt% had an entrapment efficiency of almost 50%, the materials with the highest loading had only a 30% entrapment efficiency which indicates that a lower amount of TC was present in materials with the highest loading of TC. This immediately implies that the solvent casting procedure is prone to variations. These variations might be associated due to the absence of control of parameters such as humidity and temperature during the solvent casting procedure, therefore influencing the amount of TC that remains present in the films. Since the films used for the entrapment

efficiency analysis were from a different batch than the films used to evaluate the mechanical properties, different entrapments of TC must have occurred. The explanation for the third observation is also related to the plasticising effect created by TC. As the IMF of the polymer chains are reduced, so is the energy required for molecular motion, therefore it is expected that less energy is needed to alter the material from a crystalline phase to an amorphous phase and this is supported by the decrease in the melting temperature, glass transition temperature and peak crystallisation temperature of films loaded with 11.5 wt% TC. Since the degree of crystallinity decreases, the polymer becomes more flexible and resistant to fracture and this is also supported by the results obtained with the mechanical test (Vieira *et al*., 2011). To explain the fourth observation, where no glass transition temperature nor a crystallisation peak were recorded for the materials loaded with 13 wt% TC and 16.7 wt% TC, it is also necessary to refer again to the plasticising effect created by TC. The addition of TC increases the segmental mobility of the P(3HB) amorphous chain due to plasticisation, and as mentioned above, less energy is needed to alter the material from a crystalline phase to an amorphous phase. Hence, one of the reasons why no glass transition temperature was recorded could be associated with the fact that the range of cooling temperature was not low enough to detect these peaks. Additionally, since the amorphous domains of the polymer become so mobile it is less likely that they will re-arrange into a crystalline form, and thus no crystallisation occurs. Lastly, to explain the fifth observation, the presence of double-melting peaks deriving from the increase in the TC loadings might be associated with the relatively high cooling rate used in the DSC experiments (20^{o}C/min). In the protocol used, after the samples are heated and melted, a cooling step is applied. If the cooling rate is too fast, the crystallisation of the material will not occur necessarily in a uniform manner producing two crystal populations, one deriving from P(3HB) and the other deriving from TC. Once the sample is re-heated, the crystallites melt separately, causing an appearance of a shoulder, or a double-melting peak due to the recrystallisation and re-organisation of the crystals initially formed, and thus indicate that a phase separation occurred (Cho *et al*., 1999).

The surface morphology and wettability are also important properties of materials. It is known that porosity has a great influence on the water contact angle of a material, and that hydrophobic materials, when fabricated into highly porous substrates, become even more hydrophobic (Szewczyk *et al*., 2019, Law 2014, Yuan and Lee, 2013). The surface analysis

showed that P(3HB) films loaded with TC had a higher pore content than P(3HB) films non-loaded with TC. This result can be explained by the partial evaporation of certain amounts of the TC during the drying period of the films owing to its volatile nature, but it can also be related to the surface segregation process described before which leads to a phase separation. Frequently reported in literature, is the production of porous membranes by phase separation techniques such as air-casting of a polymer solution. Here, a polymer is dissolved in a mixture containing a volatile solvent, i.e., chloroform and a less volatile non-solvent, i.e. TC. As the solvent evaporates, the polymer solubility decreases, leading to a process of phase separation where pores are formed on the surface of the membrane or film and hence the pore content increases with the presence of TC (Van de Witte *et al*., 1996, Matsuyama *et al*., 2002). As mentioned before, a higher pore content is related to a higher hydrophobicity. P(3HB) showed a water contact angle of 78.3^{o} which correlated with the studies described in literature (Basnett *et al*., 2017, Bagdadi *et al*., 2018). As for the remaining materials, the hydrophobicity of the material increased, though not in a significant way, which might be related to the increase in the pore content on the surface of all the TC-loaded films.

The disc diffusion assay results served as a first indicator of the antibacterial properties of the newly developed materials. Promising results were obtained as for all the bacteria tested, clear halos were formed around the polymer discs. This not only indicated that the agent was being released from the polymer films, but also that the amount loaded was enough to cause an antibacterial effect, which in this case was translated to the inhibition of bacterial growth. The results showed that *S. epidermidis* (ATCC® 35984™) was more susceptible to the antibacterial action of the films, followed by *S. aureus* (ATCC® 29213™), and *E. coli* (ATCC® 35218™), showing a correlation with the MIC determinations as the same susceptibility tendencies were observed. Furthermore, an increase in the inhibition zones with increasing TC loadings were observed, reinforcing once again that the solvent casting procedure might be prone to variations and that in this case, higher TC loadings, resulted in a higher TC entrapment, which in turn led to higher zones of inhibition.

The assessment of the bioactivity of the P(3HB) films loaded with TC for a consecutive period of 7 days showed promising results as some of the loadings were enough to maintain an antibacterial effect for at least 7 days. On one hand, the measurements of the optical density showed an increase in the absorbance values when the three bacterial strains were incubated

with the materials loaded with 11.5 wt% TC demonstrating that the TC loading was not enough to maintain an antibacterial effect for the desired period of time. On the other hand, the materials loaded with 13 wt% TC and with 16.7 wt% TC, showed much more effective results. The fact that the absorbance values were similar to the ones obtained with the sterility control, where no bacteria was inoculated, showed that the materials had a biocidal effect towards bacteria. Additionally, it was shown that the activity of the films remained constant for the entire duration of the experiment, demonstrating that the materials were able to maintain a biocidal effect for a period of 7 days. Contrary to the antibacterial screening of TC, where it was shown that TC was not capable of killing *S. aureus* (ATCC® 29213™) and *S. epidermidis* (ATCC® 35984™), here it was shown that the TC concentration present in the films loaded with 13 wt% TC and in the films loaded with 16.7 wt% TC were enough to cause a killing effect against these strains. Important to refer is the fact that *S. epidermidis* spp. grows slower than *S. aureus* spp. and Gram-negative bacteria in general, hence the absorbance values observed were so low compared to the other bacterial strains (Zhou and Li, 2015). Nonetheless, between the third and seventh day there was a substantial increase in the absorbance for the bacterial growth control and wells containing discs of P(3HB) non-loaded with TC, thus giving a clearer idea of how effective the materials were in inhibiting the growth of *S. epidermidis* (ATCC® 35984™) after a 7-day incubation time. The assessment of the bioactivity of the films also showed that the release of TC was also able to prevent biofilm formation in surrounding areas after a 7-day incubation period of the materials with bacteria, and in this case, all materials exhibited a similar anti-biofilm effect against the respective bacterial strain. Biofilms only form if enough bacteria are present. Although the materials loaded with 11.5 wt% TC did not have a biocidal effect, they appeared to have slowed down the growth of bacteria, since despite observing an increase in the absorbance values, they were still lower than the ones obtained for the growth control. Therefore, the low bacterial population was perhaps insufficient to form complex biofilm structures and therefore, a similar anti-biofilm effect was observed for the materials that had a higher loading of TC. The results also showed better anti-biofilm properties against *S. epidermidis* (ATCC® 35984™) followed by *S. aureus* (ATCC® 29213™) and *Escherichia coli* (ATCC® 25922™) showing once again, an accordance with the MIC determinations as the same susceptibility was observed.

With all the characterisation information, the idea was of course to find a suitable application for the P(3HB)/TC materials. Available facts indicate that CRBSI and CAUTIs are some of the most common device associated infections; short-term catheters stay inside the patient for a period less than 10 days; *S. epidermidis* strains account for 50 to 70% of catheter related infections; and flexibility is usually a requirement for some type of coatings to prevent cracking and loosing adhesion (O'grady *et al.*, 2011, Schaeffer *et al*., 2015, Koleske, 2006). Considering the above-mentioned facts, it seemed promising that a catheter coating composed of a P(3HB)/TC solution could be developed. PU are some of the most used materials for catheter development, therefore as a starting point, PU tubes were selected to be coated with the P(3HB)/TC solution. Since mechanical, thermal, surface and antibacterial properties of the films loaded with 13 wt% TC and the films loaded with 16.7 wt% TC was very similar and to prevent any cytotoxic effect against mammalian cells, the materials composed of a loading of 13 wt% TC were selected and applied as coatings. Depending on the P(3HB) concentration and the amount of TC loaded, the final PU coated tubes were termed here as $PU_{5,13}$ and $PU_{10,13}$.

The SEM analysis of the different cross-sections of the PU tubes showed that the intraluminal and extraluminal layers of the materials were coated as polymer films surrounding the PU tubes were visible. Such observations indicated that the coating procedure had been successful. In addition, the SEM analysis showed a difference between the intraluminal and extraluminal layers of the PU tubes. The intraluminal layer became irregular and less smooth and the extraluminal layer became highly porous. Since the extraluminal area is more exposed to air, TC would have more easily evaporated from the surface, therefore explaining the differences in the morphology of the intraluminal and extraluminal layers of the PU tubes. However, the presence of pores in the extraluminal layer also suggest that a de-wetting process occurred. De-wetting occurs when a polymer solution coats another surface which is non-wettable or hydrophobic to an extent, using for instance, dip coating techniques. When the film coating becomes unstable, the coating or polymer film breaks down. This process is mediated by nucleation and growth of randomly formed holes which in a later stage coalesce to form a network of polygons. In this case, the network of polygons is possibly responsible for the network of pores observed in the P(3HB)/TC coating. This means that, a coating that before the drying process was composed of a homogeneous film, transforms into a network of pores as the drying process occurs (Stange *et al*., 1997). Though the formation of pores

might lead to an increase in hydrophobicity and although bacteria prefer hydrophobic surfaces, in this case, the high pore content appears to have limited the surface adhesion points. As explained before, the process of quorum sensing mediates the formation of biofilms. To do so, it is necessary that a certain bacterial "quorum" must be reached for a particular gene expression. Because of the gaps created by the pores, and consequently the small number of adhesion points, this "quorum" would perhaps never form, thus blocking or hindering the process of quorum sensing. Allied to this would be the potential antibacterial effect of TC present in the coatings towards bacteria, thereby contributing to an additional decrease in the bacterial concentration. However, bacteria could also aggregate in clusters and increase in thickness, thus altering the typical biofilm morphology.

In terms of the effect of the coatings against planktonic bacteria, it was observed that the amount of TC released from the $PU_{5,13}$ coatings was sufficient to exert a bacteriostatic effect as the number of bacteria recovered was not statistically different from the number of bacteria present in the initial inoculum. On the other hand, the amount of TC released from the $PU_{10,13}$ coatings showed a biocidal effect as the number of bacteria recovered was much lower than the one present in the initial inoculum. Additionally, both coatings showed anti-adhesive effects as the number of bacteria recovered from the coated tubes was significantly lower than the one recovered from the PU tubes. Furthermore, the anti-biofilm experiment showed that same coatings were able to prevent biofilm formation, however the $PU_{10,13}$ coatings could prevent in a better extent formation of biofilms than the $PU_{5,13}$ coatings. Overall, the experiment confirmed that the $PU_{5,13}$ coatings had bacteriostatic, anti-adhesive and anti-biofilm properties whilst the $PU_{10,13}$ coatings had bactericidal, anti-adhesive and anti-biofilm properties. Comparable bioactive results of that of the $PU_{10,13}$ coatings were obtained with the ARROW catheter. The differences in the antibacterial properties might be related to polymer concentration of each coating. Since the $PU_{10,13}$ coatings were composed of a more concentrated polymer solution, a more viscous solution was expected to be formed, which when applied as a coating would result in a thicker coating layer and as a result a higher amount of TC.

Considering that this material could be used as a biomedical coating, it was necessary to evaluate the cytotoxicity of the eluates released from the coatings. According to the ISO 10993-5, L929 murine fibroblasts are a recommended cell line to be tested as an indicator of

in vitro cytotoxicity. The cytotoxic assay showed interesting results as both the eluates derived from the $PU_{5,13}$ and $PU_{10,13}$ coatings, as well as the eluate derived from the ARROW tube caused no cell viability suggesting a high cytotoxic effect of the materials towards the cell line tested. The results were confirmed with fluorescence micrographs of the cells, where again the presence of no live cells was observed. To further complement the results, a haemolysis test was performed where the materials were directly incubated with fresh pre-diluted blood. Surprisingly, the $PU_{5,13}$ and $PU_{10,13}$ coatings showed no haemolysis effect while the ARROW catheter showed a haemolysis ratio of 10%. As described by Van Oeveren, haemolysis ratios below 2% correspond to non-haemolytic materials (Van Oeveren, 2013). Therefore, this test suggested that the PU coated materials were non-haemolytic. A possible explanation for the haemolysis ratio obtained for the ARROW materials could be associated with the fact that they contain silver sulfadiazine which has been shown to cause the rupture of red blood cells (Fuller, 2009).

5 Chapter 5 Development of antibacterial P(3HO-co-3HD) materials: From 2D films to 3D fibrous scaffolds

5.1 Introduction

Tissue engineering (TE) has become an extremely valuable tool in the regenerative medicine field offering an alternative to conventional therapies for the repair and regeneration of tissues. The basic principle in TE, is to combine specific cells with a temporary supporting structure (i.e., scaffold), which is able to support the growth, proliferation, migration and differentiation of mammalian cells, leading to tissue formation (Murugan and Ramakrishna, 2007). However, with any material being implanted inside the human body, as in the case of TE scaffolds, one of the conundrums that remains is the ease with which these materials can get contaminated by bacteria as they offer bacteria another platform to adhere (Busscher *et al*., 2012). Bacterial adhesion leads to the formation of mature and complex biofilm structures, further infection of surrounding tissues and consequent development of complicated chronic infections (Katsikogianni and Missirlis, 2004). Since chronic infections are associated to biofilms, and since biofilms do not respond to most conventional therapies, novel TE scaffolds delivering biofilm-targeted therapies are highly relevant (Sánchez *et al*., 2013). This can be achieved by designing TE scaffolds with surface activated properties that allow tissue formation but at the same time impede bacterial adhesion because following the concept of the "race for the surface" introduced by Anthony G. Gristina, a TE scaffold that could effectively promote tissue formation would leave less surface available for bacterial cells to adhere, and on the other hand, the anti-adhesive properties of the TE scaffold would impede bacterial colonisation and biofilm formation, because if bacteria are unable to adhere to a surface, they are unable to colonise it and form a biofilm (Gristina *et al*., 1988).

Tissue formation can be prompted by using TE scaffolds with specific characteristics. For instance, fibrous scaffolds are extremely attractive for TE applications due to their topographical similarities with the fibrillae of the extracellular matrix (ECM) and can be produced via a simple, cost-effective, and versatile approach such as electrospinning (Repanas *et al*., 2016). On the other hand, bacterial adhesion can be impeded by exploring anti-biofilm molecules. More specifically, since the interference of bacterial adhesion is one of the mechanisms of action of many anti-biofilm molecules, bacterial adhesion could be prevented or inhibited by incorporating antibacterial agents with unique anti-biofilm properties to the surface of biocompatible fibrous TE scaffolds. Two strong candidates are antimicrobial

peptides (AMPs) and Dispersin B (DB). One of the reasons for conventional antibiotics to fail against biofilms is their inability to target cells with low metabolic activity. However, membrane integrity is essential to bacteria regardless of their metabolic state, and AMPs, known to act at a bacterial membrane level, do not differentiate between dormant, dividing or mature cells, killing all (Ryan *et al*., 2013). On the other hand, DB is a glycoside hydrolase capable of degrading polysaccharides present in the biofilm matrix of many bacterial strains, resulting in the dispersion of pre-established biofilms (Kaplan, 2009, Kaplan, 2010).

Many techniques have been used to surface-modify fibre meshes with bioactive molecules for biomedical applications. Within the list, physical adsorption is the simplest method for modifying the surface of fibres, in which the driving force for surface adsorption can be driven by electrostatic interactions, hydrogen bonding, hydrophobic interactions and van der Waals interactions (Agarwal *et al*., 2008, Yoo *et al*., 2009). Chemical immobilisation is another method used to attach bioactive molecules on the surface of the fibres, however, covalent attachment usually involves several activation steps and includes the use of chemical cross-linkers. An alternative approach was reported by Grafahrend *et al*., as they used an amphiphilic six-armed star-shaped poly(ethylene oxide-stat-propylene oxide) containing reactive isocyanate groups at the distal ends of the polymer chains, NCO-sP(EO-stat-PO), as an additive to the poly(lactic-co-glycolic acid) (PLGA) spinning solution. The presence of the isocyanate groups facilitated the coupling of cell adhesion peptides by addition of these peptides to the spinning solution, thus resulting in the production of surface-activated fibres in a single step (Grafahrend *et al*., 2011).

As described in the previous chapter, since the process of solvent casting technique is a straightforward, fast and cheap method to produce films, and since such materials are easy to characterise, the development of anti-adhesive films composed of P(3HO-co-3HD) with physically adsorbed AMPs or DB, is described in this section. The films were characterised in order to assess their chemical and surface properties. A biological evaluation was also performed to evaluate the antibacterial and cytotoxic properties of the films. Based on the results obtained, the knowledge was translated into the development of anti-adhesive P(3HO-co-3HD)-based fibres either including an AMP or DB as single functionalisation or using the agents in combination and a preliminary surface and biological characterisation was performed. Furthermore, an alternative approach was studied in which the knowledge

described by Grafahrend *et a*l., was transferred to PHAs to develop P(3HO-co-3HD)-NCO-sP(EO-stat-PO)-based blend fibres, functionalised with an AMP as a single functionalisation, as well as in combination with DB and a preliminary surface and biological characterisation was also performed.

5.2 Results

5.2.1 *In vitro* antibacterial characterisation of antimicrobial peptides (AMPs)

5.2.1.1 Minimum inhibitory concentration and minimum bactericidal concentration

As a starting point, the antibacterial properties of AMP3, Nut2 and LL37, namely, bacteriostatic and bactericidal properties, were tested against *E. coli* (ATCC® 35218™), *S. epidermidis* (ATCC® 35984™) and *S. aureus* (ATCC® 29213™) by determining the MIC and MBC, respectively. The selected bacterial strains were cultured in the presence of increasing concentrations of AMPs for a period of 24 hours. The peptide concentration that completely inhibited visible bacterial growth was determined as the MIC, while the peptide concentration that resulted in a reduction of 99.9% of CFUs relative to that in the initial inoculum was determined as the MBC. The results are summarised in Table 14.

Table 14: MIC and MBC of AMPs against *S. epidermidis* (ATCC® 35984™) and *E. coli* (ATCC® 35218™).

AMP3	**MIC**	**MBC**
S. epidermidis (ATCC® 35984™)	6.3 µg/mL	6.3 µg/mL
Nut2	**MIC**	**MBC**
S. epidermidis (ATCC® 35984™)	12.5 µg/mL	12.5 µg/mL
LL-37	**MIC**	**MBC**
E. coli (ATCC® 35218™)	25 µg/mL	50 µg/mL

Note: None of the selected AMPs was active against *S. aureus* (ATCC® 29213™). LL-37 did not show activity against *S. epidermidis* (ATCC® 35984™) and AMP3 and Nut2 did not show activity against *E. coli* (ATCC® 35218™).

Different antibacterial activities were revealed for each peptide. Firstly, it was observed that each peptide was only active against one of the three bacterial strains tested, more specifically, AMP3 and Nut2 were active against *S. epidermidis* (ATCC® 35984™) while LL-37 was active against *E. coli* (ATCC® 35218™). Secondly, it was observed that none of the peptides was active against *S. aureus* (ATCC® 29213™) and thirdly all the peptides showed bacteriostatic and bactericidal properties against the respective bacteria. AMP3 showed a MIC and an MBC of 6.3 µg/mL, while Nut2 showed a MIC and MBC of 12.5 µg/mL and finally, LL-37, showed a MIC of 25 µg/mL and an MBC of 50 µg/mL.

5.2.1.2 Anti-biofilm properties: Inhibition of biofilm formation

Furthermore, the anti-biofilm properties of AMP3, Nut2 and LL-37 were evaluated against the bacterial strain to which they have shown antibacterial activity by quantifying the biofilm biomass that was produced after a 24-hour bacterial exposure to increasing concentrations of AMPs. The biofilm biomass was quantified using a safranin staining method and the results were expressed as percentage of biofilm inhibition compared to a typical biofilm growth control. The results are shown in Figure 44.

Each graph shows the percentage of biofilm inhibition compared to that obtained with the biofilm growth control. The results showed that, in the case of Nut2, biofilm formation of *S. epidermidis* (ATCC® 35984™) was not inhibited with a peptide concentration of 1.6 µg/mL. With a peptide concentration of 3.1 µg/mL and 6.3 µg/mL, biofilm formation was inhibited by 20% and 34%, respectively. With concentrations equal or higher to the MBC, that is 12.5 µg/mL, biofilm formation was inhibited by more than 90%. In the case of AMP3, with the lowest peptide concentration, that is 1.6 µg/mL, biofilm formation of *S. epidermidis* (ATCC® 35984™) was inhibited by only 3%. A 50% biofilm formation inhibition effect was observed with a peptide concentration of 3.1 µg/mL. With concentrations equal or higher to the MBC, that is 6.3 µg/mL, biofilm formation was inhibited by more than 90%. Finally, in the case of LL-37, the development of biofilms by *E. coli* (ATCC® 35218™) was inhibited by 28% with a peptide concentration of 1.6 µg/mL. Concentrations between 3.1 µg/mL and 25 µg/mL resulted in the inhibition of biofilm formation by more than 60%. With concentrations equal or higher than the MBC, that is 50 µg/mL, biofilm formation was inhibited by more than 80%.

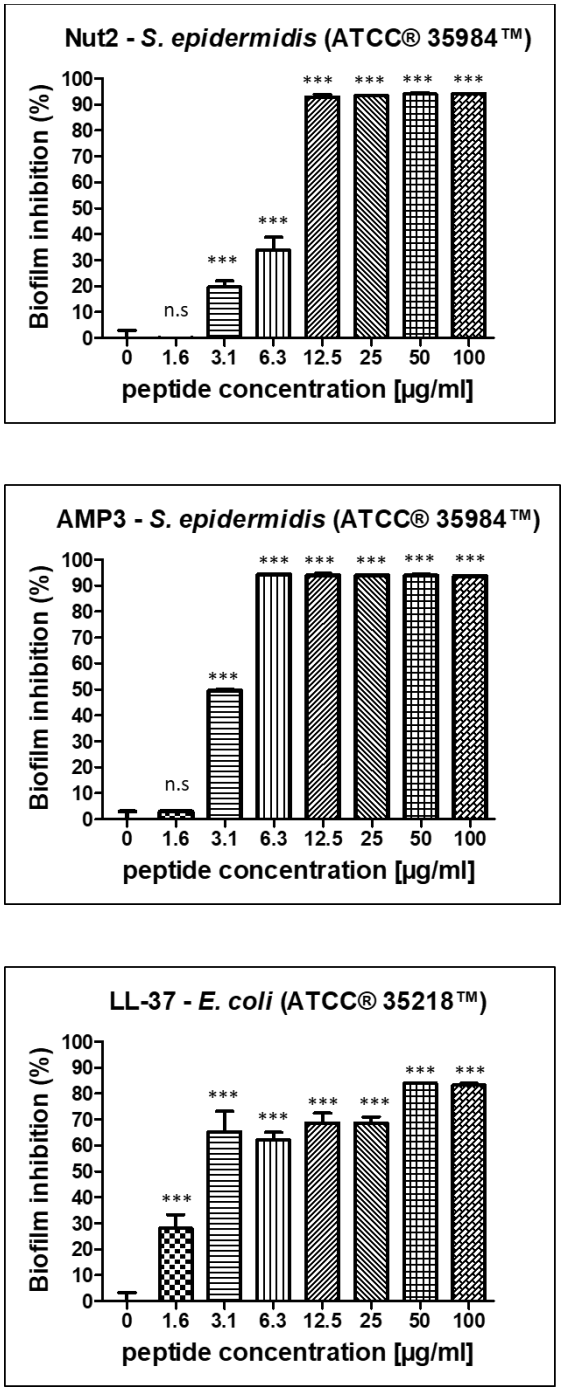

Figure 44: Percentage of inhibition of biofilm formation by AMPs against selected bacterial strains. *S. epidermidis* (ATCC® 35984™) was exposed to increasing concentrations of either AMP3 and Nut2 and *E. coli* (ATCC® 35218™) was exposed to increasing concentrations of LL-37 for a period of 24 hours. The biofilm growth control is represented by the column in which no AMP was added. The experiments were performed in three independent experiments, in triplicates (N=3, n=3). * indicates p<0.0001 and n.s indicates no statistical difference when compared with biofilm growth control.**

5.2.2 *In vitro* antibacterial characterisation of Dispersin B (DB)

5.2.2.1 Anti-biofilm properties: Dispersion of pre-established biofilms

The ability of DB to disperse pre-formed biofilms was tested against *S. aureus* (ATCC® 29213™), *S. epidermidis* (ATCC® 35984™) and *E. coli* (ATCC® 35218™) by incubating 24-hour pre-established biofilms with increasing concentrations of DB for a period of 24-hours and by quantifying the biofilm biomass that remained intact after the incubation period, using a safranin staining method. The results were expressed as a percentage of biofilm dispersal comparatively to a typical biofilm growth control and the results are shown in Figure 45.

Each graph shows the percentage of biofilm that was dispersed as a result of the incubation of 24-hour pre-established biofilms of *S. aureus* (ATCC® 29213™), *S. epidermidis* (ATCC® 35984™) and *E. coli* (ATCC® 35218™) with increasing concentrations DB for 24 hours.

In the case of *E. coli* (ATCC® 35218™), the results showed that with concentrations up until 100 μg/mL almost 20% of the pre-formed biofilms were dispersed and that with a concentration of 200 μg/mL and 400 μg/mL, pre-formed biofilms were dispersed by 25% and 41%. In the case of *S. aureus* (ATCC® 29213™), a gradual dispersal effect was observed. More specifically, with a concentration of 3.1 μg/mL, 6.3 μg/mL, 12.5 μg/mL and 25 μg/mL, pre-established biofilms were dispersed by 2%, 8%, 16% and 20%, respectively. With concentrations of 50 μg/mL, 100 μg/mL, 200 μg/mL and 400 μg/mL, pre-established biofilms were dispersed by 22%, 34%, 44% and 52%. Finally, in the case of *S. epidermidis* (ATCC® 35984™), a similar dispersal activity was observed for all the testing DB concentrations. With concentrations up until 50 μg/mL, 70% of pre-established biofilms were dispersed. By increasing the DB concentrations to 100 μg/mL, 200 μg/mL and 400 μg/mL, pre-established biofilms were dispersed by 76%, 73% and 78% respectively.

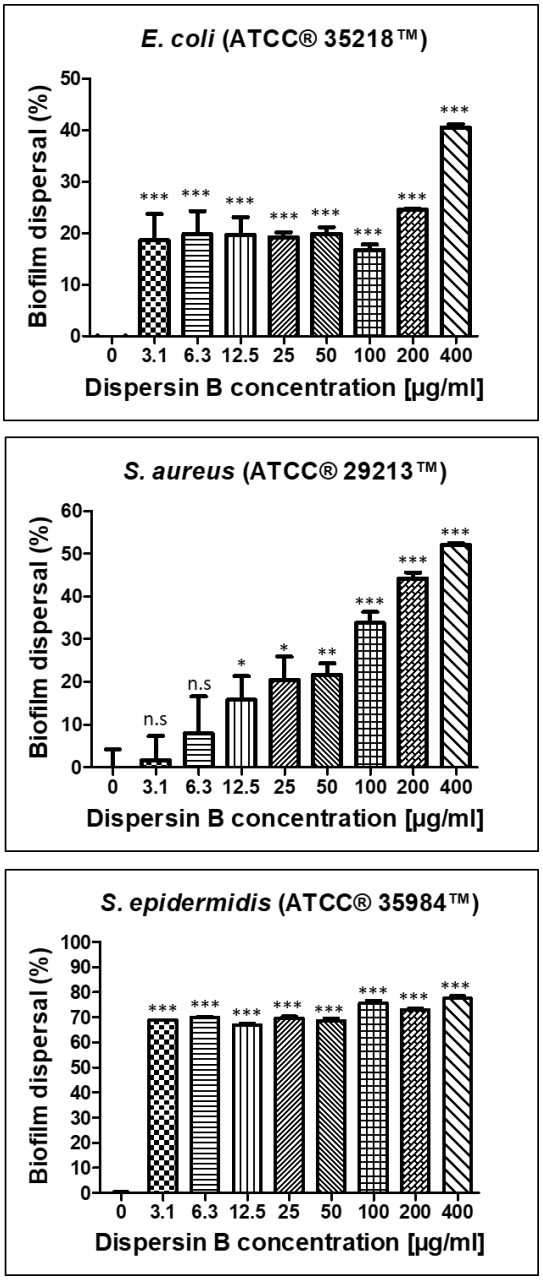

Figure 45: Percentage of biofilm dispersal as a result of the incubation of 24-hour pre-established biofilms of *E. coli* (ATCC® 35218™), *S. aureus* (ATCC® 29213™) and *S. epidermidis* (ATCC® 35984™) with increasing concentrations DB for 24 hours. The biofilm growth control is represented by the column in which no DB was added. The experiments were performed in three independent experiments, in triplicates (N=3, n=3). * indicates p<0.05, ** indicates p<0.001, * indicates p<0.0001 and n.s indicates no statistical difference when compared with biofilm growth control.**

5.2.3 *In vitro* direct cytotoxicity evaluation of AMPs and DB

In order to evaluate the cytotoxicity of each of the active agents, cytocompatibility studies were performed by incubating pre-adhered L929 murine fibroblasts with increasing concentrations of AMP3, Nut2, LL-37 and DB for a period of 24 hours and by evaluating the percentage of cell viability after the incubation period. The results are shown in Figure 46.

Each graph shows the percentage of viable L929 murine fibroblasts after being exposed to increasing concentrations of AMP3, Nut2, LL-37 and DB for 24 hours in comparison to a cell growth control.

With the results obtained, it was possible to determine the 50% cytotoxicity concentration (CC_{50}), that is, the concentration resulting in a 50% viability of L929 murine fibroblasts of each agent. AMP3 and Nut2, showed a CC_{50} of 143 µg/mL and 123 µg/mL, respectively, while LL-37 showed a CC_{50} of 83 µg/mL and DB showed a CC_{50} of 134 µg/mL.

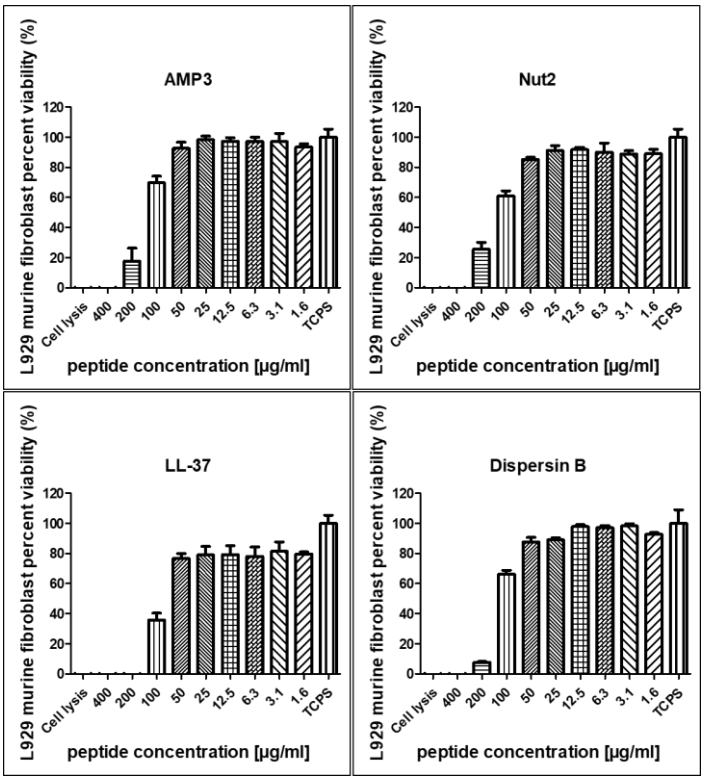

Figure 46: Percentage of cell viability of L929 murine fibroblasts after growing in the presence of increasing concentrations of AMP3, Nut2, LL-37 and DB for a period of 24 hours. A typical cell growth control and a positive control were considered and are represented as TCPS and cell lysis, respectively.

5.2.4 Film development

The antibacterial and cytocompatibility screening of the agents provided an idea of the concentration of agent that should be adsorbed to the surface of P(3HO-co-3HD) discs that would confer to them antibacterial properties without causing a cytotoxic effect on mammalian cells. Firstly, 1 cm diameter P(3HO-co-3HD) discs were obtained from solvent cast P(3HO-co-3HD) films. Based on the assumption that not all of the initial loading would be adsorbed to the surface of the films and that the amount adsorbed should also not be higher than the CC_{50} estimated for the AMPs and DB, an experimental trial using an initial loading of 200 µg/mL of the agents was used.

5.2.4.1 Adsorption quantification

The measurement of the adsorbed agents to the surface of P(3HO-co-3HD) discs was done by calculating the difference between the concentration of agent in solution before and after the adsorption process. The Bradford assay was used to measure the concentration of DB and LL-37 in solution and the BCA assay was used to measure the concentration of AMP3 and Nut2 in solution and the results are shown in Table 15. Four different types of modified P(3HO-co-3HD) discs were developed, namely, P(3HO-co-3HD)/AMP3, P(3HO-co-3HD)/Nut2, P(3HO-co-3HD)/LL-37 and P(3HO-co-3HD)/DB.

Table 15: Concentration of the active agents adsorbed on the surface of P(3HO-co-3HD) discs.

Concentration of the incubation solution	
200 µg/mL	
Concentration of agent adsorbed to the surface of P(3HO-co-3HD) discs (µg/mL)	
DB	56.29±3.79
LL-37	47.74±0.34
Nut2	38.06±0.54
AMP3	32.43±5.60

The Bradford assay measurements showed that 57 μg/mL of DB and 48 μg/mL of LL-37 were adsorbed, on an average, to the surface of P(3HO-co-3HD) discs. The BCA assay measurements showed that 38 μg/mL of Nut2 and that 32 μg/mL of AMP3 were adsorbed, on an average, to the surface of P(3HO-co-3HD) discs.

5.2.5 Characterisation of P(3HO-co-3HD) films adsorbed with AMPs and DB

In order to evaluate the surface changes of the modified discs with the active agents, XPS analysis, ATR-FTIR measurements and WCA studies were performed and compared to unmodified P(3HO-co-3HD) discs.

5.2.5.1 X-ray photoelectron spectroscopy (XPS) and Attenuated Total Reflectance Fourier Transform Infrared Spectroscopy (ATR-FTIR)

XPS analysis was performed to detect chemical changes on the surface of modified P(3HO-co-3HD) discs with DB. More specifically, since DB is an enzyme, or in other words, a nitrogen-containing macromolecule, the XPS analysis was performed to see whether the presence of nitrogen could be detected on the surface of modified P(3HO-co-3HD) discs and the results are shown in Figure 47.

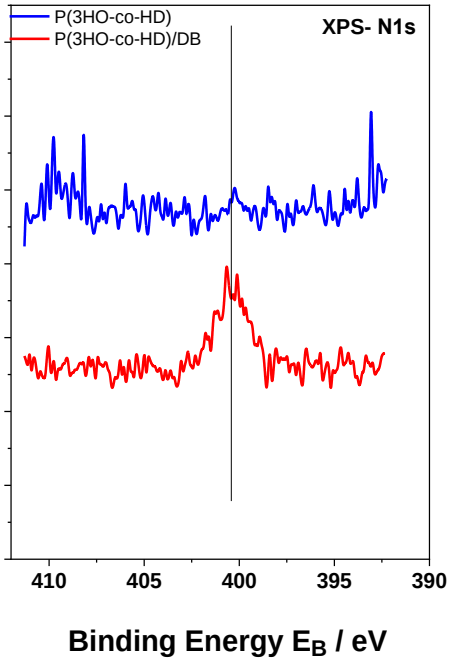

Figure 47: N1s XPS peaks of modified and unmodified P(3HO-co-3HD) discs with DB. The peak is centred at 400.5eV and assigned to amide bonds.

Figure 47 shows the N1s spectrum of unmodified and modified P(3HO-co-3HD) discs with DB. The spectrum is assigned to amide bonds with the main peak centred at 400.5eV. The results showed that contrary to the surface of unmodified P(3HO-co-3HD) discs, modified P(3HO-co-3HD) discs with DB contained nitrogen on its surface.

The presence of AMPs on the surface of P(3HO-co-3HD) discs was evaluated by ATR-FTIR and the results are shown in Figure 48.

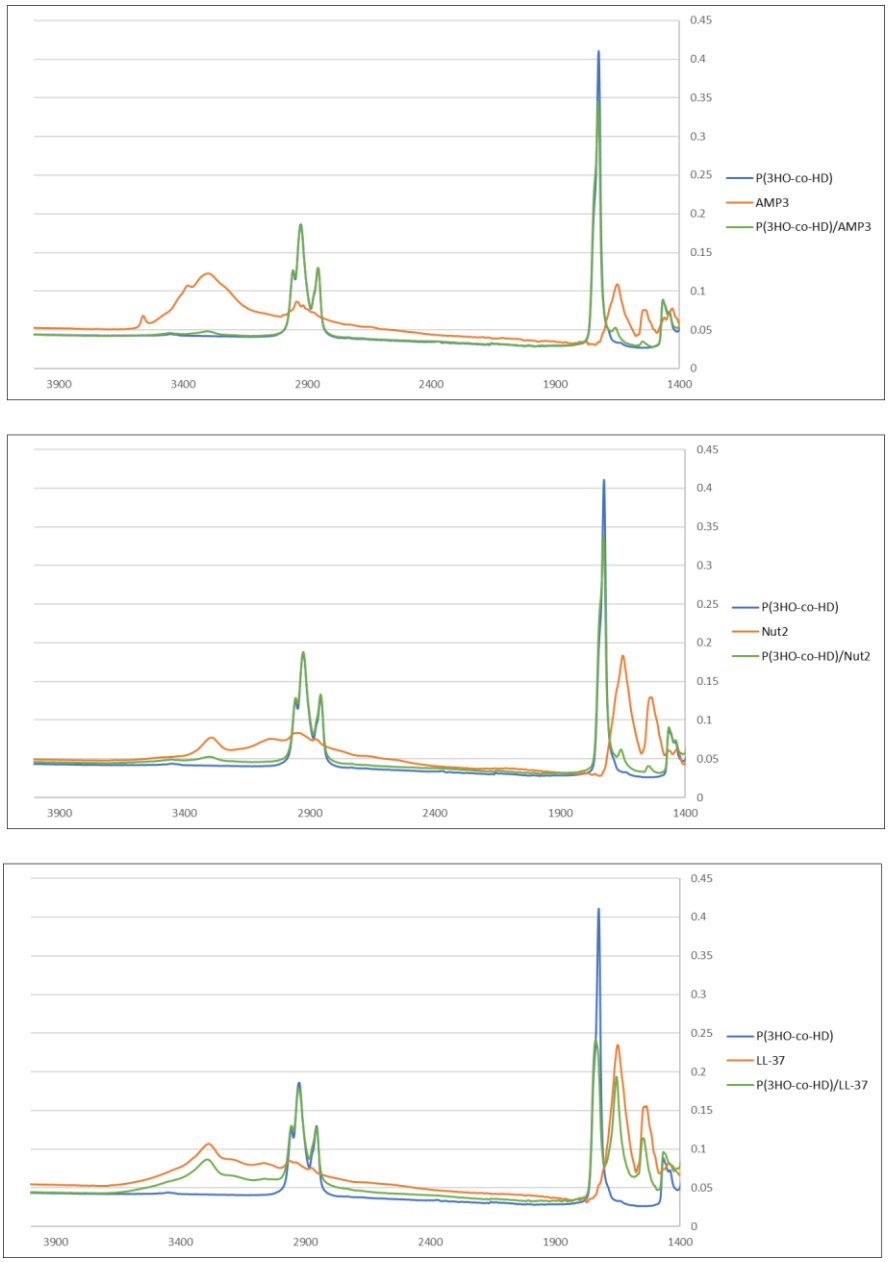

Figure 48: Comparison of the ATR-FTIR spectrum of the surface of unmodified P(3HO-co-3HD) discs with the ATR-FTIR spectrum of the surface of modified P(3HO-co-3HD) discs with AMP3, Nut2 and LL-37 and with the spectrum of AMP3, Nut2 and LL-37.

There are nine characteristic IR absorption bands of peptides and proteins and some of the major bands of the protein infrared spectrum can be associated with the so-called amide I, amide II, and amide A bands. Amide I bands are located between 1600-1690 cm^{-1} and correspond to C=0 stretching and amide II bands are located between 1480-1575 cm^{-1} and correspond to C-N stretching and N-H bending. The amide A band is located between 3225 cm^{-1} and 3280 cm^{-1} (Adochitei and Drochioiu, 2011, Krimm and Bandekar, 1986). By observing the ATR-FTIR spectra of the peptides it was possible to visualise peaks in the region of the three above-mentioned characteristic bands, which were not visible in the unmodified P(3HO-co-3HD) spectrum. More specifically, AMP3 showed peaks at 1656 cm^{-1}, 1548 cm^{-1} and 3284 cm^{-1}, Nut2 showed peaks at 1652 cm^{-1}, 1546 cm^{-1} and 3282 cm^{-1} and LL-37 showed peaks at 1646 cm^{-1}, 1538 cm^{-1} and 3282 cm^{-1}. Although with less intensity, the surface of the modified P(3HO-co-3HD) discs with AMPs showed in all cases, the presence of the characteristic IR absorption peaks of the peptides apart from the characteristic peaks of MCL-PHAs. More specifically, P(3HO-co-3HD)/AMP3 discs showed peaks at 1646 cm^{-1}, 1534 cm^{-1} and 3282 cm^{-1}, P(3HO-co-3HD)/Nut2 discs showed peaks at 1648 cm^{-1}, 1534 cm^{-1} and 3282 cm^{-1}, and P(3HO-co-3HD)/LL-37 discs showed peaks at 1650 cm^{-1}, 1544 cm^{-1} and 3272 cm^{-1}.

5.2.5.2 Surface analysis: Water Contact Angle (WCA)

To evaluate the wettability changes after the incorporation of active agents, wettability studies were conducted by measuring the water contact angle on the surface of unmodified and modified P(3HO-co-3HD) discs. The results are shown in Figure 49.

PHA discs exhibited a water contact angle of 88° confirming the hydrophobic nature of the material. The adsorption of AMP3 and Nut2 did not cause significant changes on the surface wettability of the discs, resulting in materials with contact angles of 82° and 84°, respectively. However, when adsorbing DB or LL-37 to the surface of P(3HO-co-3HD) discs, the wettability decreased to 53° and 51°, respectively, rendering the material with hydrophilic properties.

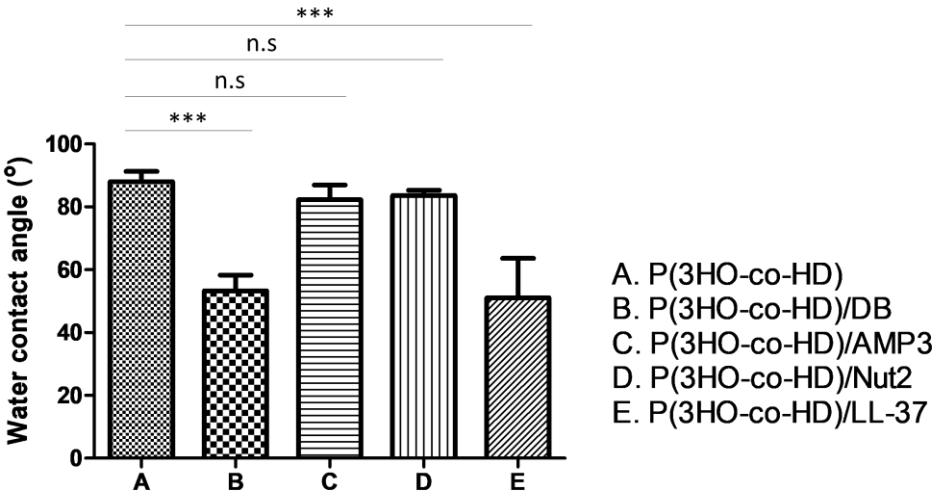

Figure 49: Water contact angle of unmodified P(3HO-co-3HD) discs and P(3HO-co-3HD) discs modified with DB, AMP3, Nut2 and LL-37. The experiments were performed in triplicates (n=3). * indicates p<0.0001 and n.s indicates no statistical difference when compared with unmodified P(3HO-co-3HD) discs.**

5.2.6 Antibacterial characterisation

5.2.6.1 Anti-adhesion properties

To evaluate the anti-adhesive properties of the modified materials, unmodified P(3HO-co-3HD) discs and modified P(3HO-co-3HD) discs were incubated with bacteria for a period of 24 hours. The bacteria that adhered to the surface of the materials were removed by sonication and quantitated by plating on blood agar plates. The ability of the modified materials to prevent bacterial adhesion was expressed as a percentage by comparing the number of bacteria that adhered to the surface of unmodified materials with the number of bacteria that adhered to the surface of modified materials. Based on the previous antibacterial screenings (broth dilution method and anti-biofilm activity of AMPs and dispersal biofilm activity of DB) each type of material was incubated with the bacterial strain to which they exhibited antibacterial activity. Therefore, modified discs with DB were tested against *S. aureus* (ATCC® 29213™),

S. epidermidis (ATCC® 35984™) and *E. coli* (ATCC® 35218™), modified discs with AMP3 and Nut2 were tested against *S. epidermidis* (ATCC® 35984™) and modified discs with LL-37 were tested against *E. coli* (ATCC® 35218™). The results are shown in Figure 50.

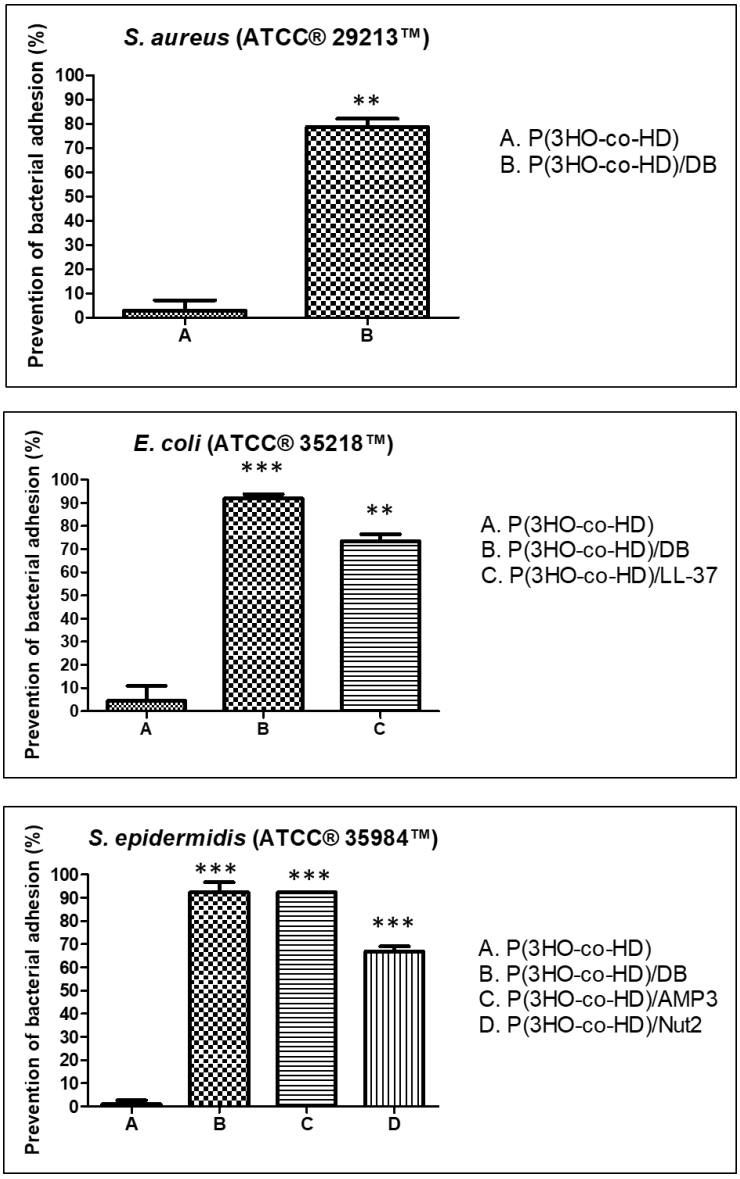

Figure 50: Percentage of prevention of bacterial adhesion of modified P(3HO-co-3HD) discs with DB compared to unmodified P(3HO-co-3HD) discs after their incubation with *S. aureus* (ATCC® 29213™) for a period of 24 hours; percentage of prevention of bacterial adhesion of modified P(3HO-co-3HD) discs with DB and LL-37 compared to unmodified P(3HO-co-3HD) discs after their incubation with *E. coli* (ATCC® 35218™) for a period of 24 hours; percentage of prevention of bacterial adhesion of modified P(3HO-co-3HD) discs with DB, AMP3 and Nut2 compared to unmodified P(3HO-co-3HD) discs after their incubation with *S. epidermidis* (ATCC® 35984™) for a period of 24 hours. The experiments were performed in two independent experiments, in duplicates (N=2, n=2). ** indicates p<0.001 and * indicates p<0.0001 when compared with unmodified P(3HO-co-3HD) discs.**

Each graph shows the percentage of prevention of bacterial adhesion by modified materials in comparison to unmodified materials.

The results showed that P(3HO-co-3HD) discs modified with DB were able to prevent the adhesion of *S. aureus* (ATCC® 29213™) by 79% compared to unmodified P(3HO-co-3HD) discs and that the adhesion of *S. epidermidis* (ATCC® 35984™) and *E. coli* (ATCC® 35218™) was prevented by 92%. Modified P(3HO-co-3HD) discs with LL-37 were able to prevent the bacterial adhesion of *E. coli* (ATCC® 35218™) by 74% in comparison with unmodified P(3HO-co-3HD) discs. Materials modified with AMP3 and Nut2 resulted in the prevention of bacterial adhesion of *S. epidermidis* (ATCC® 35984™) by 92% and 67%, respectively.

5.2.7 *In vitro* direct cytotoxicity studies

In order to evaluate the cytotoxicity of the modified materials against mammalian cells, L929 murine fibroblasts were seeded on the surface of unmodified and modified P(3HO-co-3HD) discs with AMP3, Nut2, LL-37 and DB for a period of 24 hours and the cytotoxicity of each material was evaluated by calculating the percentage of cell viability after the incubation period in comparison to the growth control. The results are shown on Figure 51.

The graph shows the percentage of viable L929 murine fibroblasts in comparison to the cell growth control, TCPS, after its seeding on unmodified and modified discs with AMP3, Nut2, LL-37 and DB for a period of 24 hours.

Quantitative CTB assays revealed that when cells were grown on the negative cytotoxic control PE, 84% cell viability was obtained. When cells grew on the P(3HO-co-3HD) discs modified with AMP3, Nut2, LL-37 and DB, a signal of 76%, 67%, 51% and 47%, respectively were obtained. Cells cultured on the P(3HO-co-3HD) discs resulted in 66% cell viability.

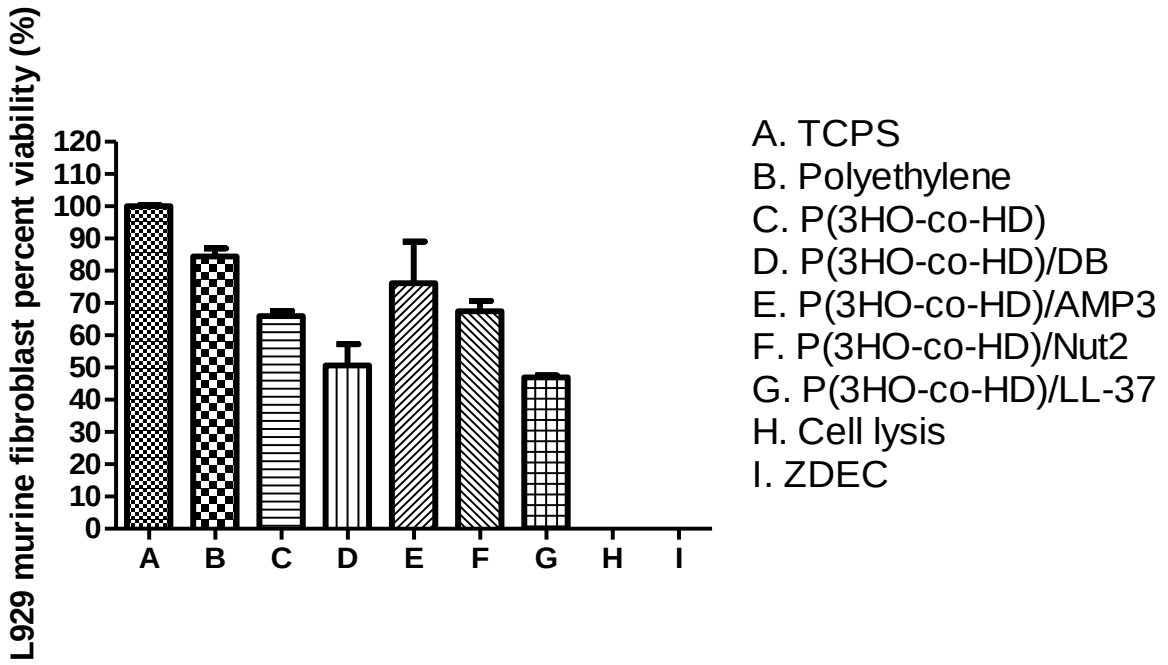

Figure 51: Percentage of cell viability of L929 murine fibroblasts after its seeding on the surface of unmodified P(3HO-co-3HD) discs and on the surface of P(3HO-co-3HD) discs modified with DB, AMP3, Nut2 and LL-37 for a period of 24 hours. A typical cell growth control and a positive control were considered and are represented as TCPS and cell lysis, respectively. Additionally, PE and ZDEC-PU were considered as negative and positive cytotoxic control materials, respectively.

5.2.8 Fabrication of P(3HO-co-3HD) fibres adsorbed with AMPs and DB

5.2.8.1 Electrospinning process

The development of anti-adhesive P(3HO-co-3HD) discs by physically adsorbing AMPs and DB to its surface led to the further development of antibacterial P(3HO-co-3HD)-based fibres. Prior to the activation of P(3HO-co-3HD) fibres, an optimisation of the electrospinning process was carried out in order to obtain well spread fibres without bead formation. Parameters such as the polymer concentration, applied voltage and flow rate were kept constant. Two different rotation speeds (400 and 1000 rpm) as well as two different needle-to-collector distances (14 and 18 cm) were studied. The fibres were electrospun on glass coverslips and the electrospinning conditions are summarised in Table 16.

Table 16: Summary of the electrospinning conditions used to electrospin P(3HO-co-3HD) fibres on glass coverslips.

Condition	% Polymer (w/v%)	Voltage (kV)	Flow rate (ml/h)	Rotator speed (rpm)	Distance (cm)
1	25	14	5	400	14
2	25	14	5	400	18
3	25	14	5	1000	18
4	25	14	5	1000	14

5.2.9 Surface analysis: Bright field Imaging and Scanning Electron Microscopy (SEM)

The electrospun fibres were evaluated by bright field microscopy where it was possible to identify the best electrospinning condition and the results are shown in Figure 52.

The bright field micrographs showed that when using a slow rotation speed (condition 1 and 2), the formation of polymer beads was prompted whereas when using higher rotation speeds (condition 3 and 4), the formation of beads was much less or almost non-existent. Furthermore, a shorter needle-to-collector distance resulted in more aligned fibres with no bead formation (condition 4) as compared to a longer needle-to-collector distance (condition 3). Overall, the micrographs showed that the most suitable condition was condition 4.

Further SEM imaging was carried out for the fibres obtained with the 4th condition and the results are shown in Figure 53.

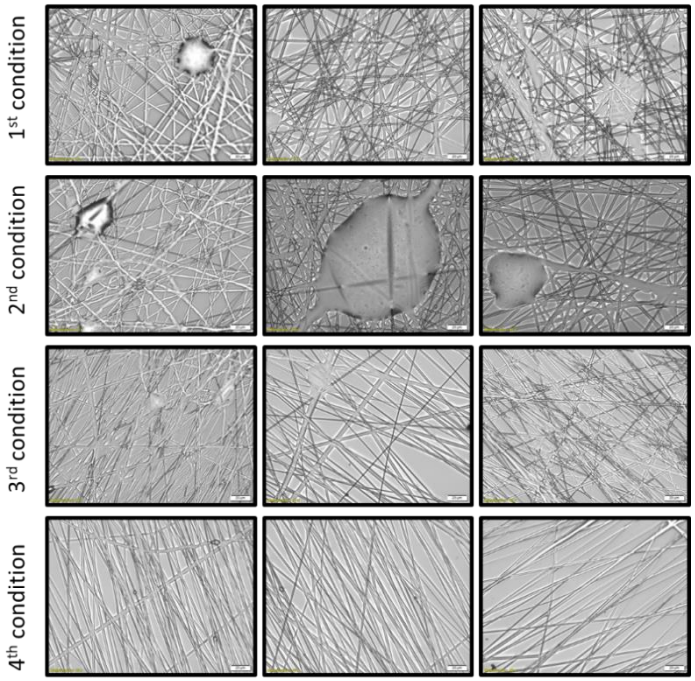

Figure 52: Bright field imaging of electrospun fibres using 25 w/v% of P(3HO-co-3HD) in a 60:40 chloroform/acetone solution. 1st condition: Electrospun fibres obtained using 14 kV, flow rate of 5 mL/h, 400 rpm and a needle-to-collector distance of 14 cm; 2nd condition: Electrospun fibres obtained using 14 kV, flow rate of 5 mL/h, 400 rpm and a needle-to-collector distance of 18 cm; 3rd condition: Electrospun fibres obtained using 14 kV, flow rate of 5 mL/h, 1000 rpm and a needle-to-collector distance of 18 cm; 4th condition: Electrospun fibres obtained using 14 kV, flow rate of 5 mL/h, 1000 rpm and a needle-to-collector distance of 14 cm. Magnification 40x and scale bar = 20 µm.

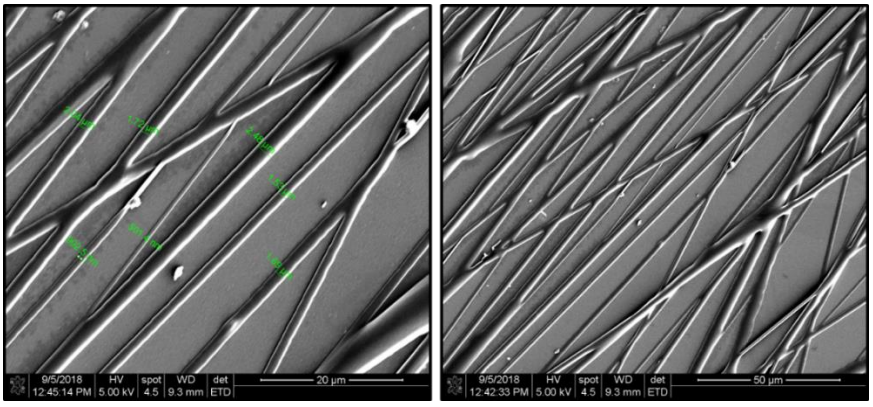

Figure 53: SEM micrographs of P(3HO-co-3HD) fibres using a 25 w/v% polymer concentration in a 60/40, chloroform/acetone solution, 14 kV, 5mL/h flow rate, needle-to-collector

distance of 14 cm and 1000 rpm. Magnification of micrographs on the left-side of 1500x and scale bar of 20 µm. Magnification of micrographs on the right-side of 500x and scale bar of 50 µm. Low fibre density samples were used for imaging purposes.

The electrospinning process resulted in slightly aligned fibres with different diameters, ranging from 500 nm to 2.5 micron.

5.2.10 Physical adsorption of active agents to P(3HO-co-3HD) fibres

The activation of P(3HO-co-3HD) fibres was done by physically adsorbing the active agents to the surface of the fibres. Following the same principle applied for the physical adsorption process of the active agents to P(3HO-co-3HD) discs, an initial concentration of the incubation solution of 200 µg/mL of the agents was used. The fibres were modified by adsorbing Nut2 and DB on their own, as well as in combination to evaluate if the anti-adhesive properties of the fibres would be enhanced. Three different modified fibres were obtained, namely, P(3HO-co-3HD)/Nut2 fibres, P(3HO-co-3HD)/DB fibres and P(3HO-co-3HD)/Nut2+DB fibres.

5.2.11 Characterisation of P(3HO-co-3HD) fibres adsorbed with AMPs and DB

5.2.11.1 Surface analysis: Water Contact Angle (WCA)

Since the wettability properties play an important role in cell and bacterial adhesion, the wettability changes after fibre formation and after the incorporation of active agents to the fibres were evaluated by measuring the water contact angle of unmodified and modified fibres and compared to the water contact angle of the P(3HO-co-3HD) discs and the results are shown in Figure 54.

P(3HO-co-3HD) discs exhibited a water contact angle of 89.7^{o} confirming the hydrophobic nature of the material. P(3HO-co-3HD) fibres showed a significant increase in hydrophobicity, rendering the material an almost superhydrophobic character since the water contact angle measured was 120.9^{o}. P(3HO-co-3HD)/Nut2 fibres exhibited a water contact angle of 97.2^{o}, while P(3HO-co-3HD)/DB fibres and P(3HO-co-3HD)/Nut2+DB fibres showed a water contact angle of 79.9^{o} and 69.9^{o}, respectively.

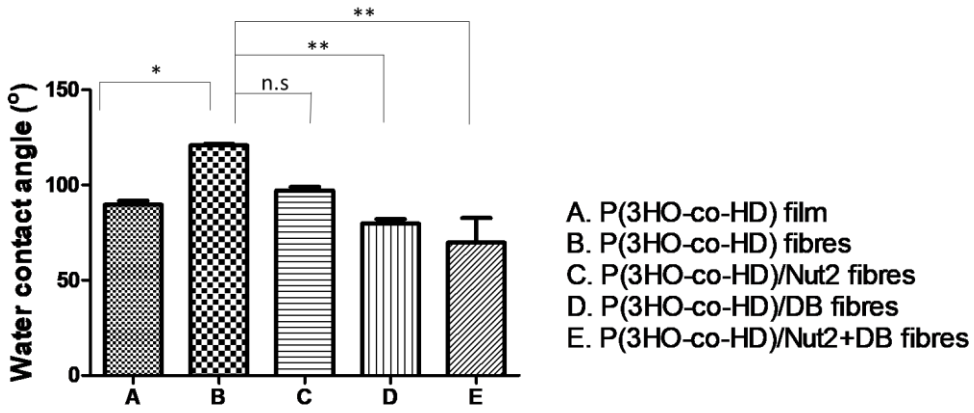

Figure 54: Water contact angle of P(3HO-co-3HD) films, unmodified P(3HO-co-3HD) fibres, and modified P(3HO-co-3HD) fibres with Nut2, DB and Nut2+DB. The experiments were performed in triplicates (n=3). P(3HO-co-3HD) films were compared to unmodified P(3HO-co-3HD) fibres and unmodified P(3HO-co-3HD) fibres were compared to all the remaining materials. * indicates p<0.05, ** indicates p<0.001 and n.s indicates no statistical difference.

5.2.11.2 In vitro direct cytotoxicity studies

In order to evaluate the cytotoxicity of the modified fibres against mammalian cells, L929 murine fibroblasts were seeded on the surface of unmodified P(3HO-co-3HD) fibres and modified P(3HO-co-3HD) fibres with Nut2, DB and Nut2+DB for a period of 24 hours and the cytotoxicity of each material was evaluated by calculating the percentage of cell viability after the incubation period in comparison to the growth control. The results are shown in Figure 55. Additionally, a fluorescent cell staining was carried out to observe the presence of live and dead cells on the fibres and the results are shown in Figure 56.

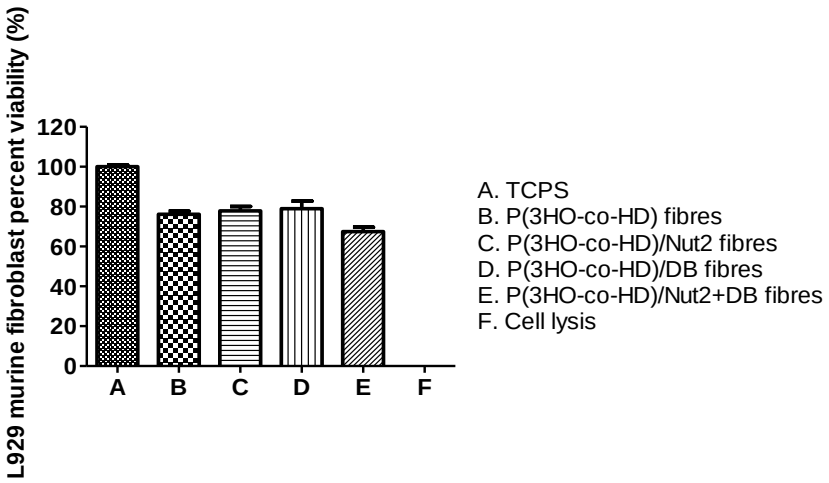

Figure 55: Percentage of cell viability of L929 murine fibroblasts after its seeding on the surface of unmodified P(3HO-co-3HD) fibres and on the surface of P(3HO-co-3HD) fibres modified with Nut2, DB and Nut2+DB for a period of 24 hours. A typical cell growth control and a positive control were considered and are represented by TCPS and cell lysis, respectively.

The graph shows the percentage of viable L929 murine fibroblasts in comparison to the cell growth control, TCPS, after its seeding on unmodified and modified fibres with Nut2, DB and Nut2+DB for a period of 24 hours.

Quantitative CTB assays revealed that a cell viability of 76% was obtained for unmodified P(3HO-co-3HD) fibres, while the fibres modified with Nut2, DB and Nut2+DB exhibited a cell viability of 78%, 79% and 67%, respectively.

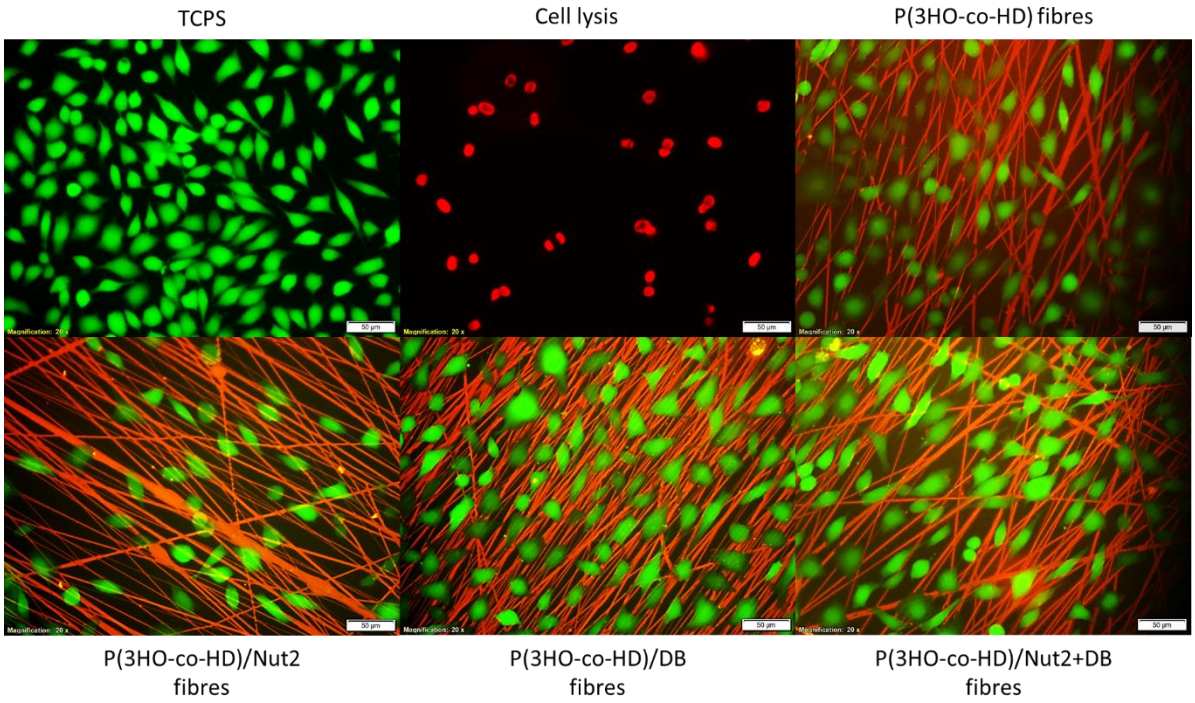

Figure 56: Fluorescence micrographs of L929 murine fibroblasts grown on top of unmodified P(3HO-co-3HD) fibres and on top of modified P(3HO-co-3HD) fibres with Nut2, DB and Nut2+DB after a 24-hour incubation period. The dead cells are represented in red and live cells are represented in green. Magnification of micrographs of 20x and scale bar of 50 µm. Negative and positive controls represented by TCPS and cell lysis, respectively.

The fluorescent micrographs showed the presence of live cells (green) on unmodified P(3HO-co-3HD) fibres and on modified P(3HO-co-3HD) fibres with Nut2, DB and Nut2+DB. Furthermore, the morphology of the cells grown on the four different types of fibres was similar to the morphology of cells grown on TCPS. P(3HO-co-3HD) fibres and fibres modified with Nut2 showed a lower cell density as compared to the remaining types of fibres.

5.2.11.3 Anti-adhesion and anti-biofilm properties

To evaluate the anti-adhesive properties of the modified fibres, unmodified P(3HO-co-3HD) fibres and P(3HO-co-3HD) fibres modified with Nut2, DB and Nut2+DB were incubated with *S. epidermidis* (ATCC® 35984™) for a period of 24 hours. The bacteria that adhered to the surface of the fibres were removed by sonication and quantified by plating on blood agar plates. The ability of the modified fibres to prevent bacterial adhesion was expressed as percentage by comparing the number of bacteria that adhered to the surface of unmodified

fibres with the number of bacteria that adhered to the surface of modified fibres. The results are shown in Figure 57. Additionally, after the incubation period, the biofilm biomass that was formed on the surface of the fibres as a result of bacterial adhesion was stained using safranin and the results are shown in Figure 58.

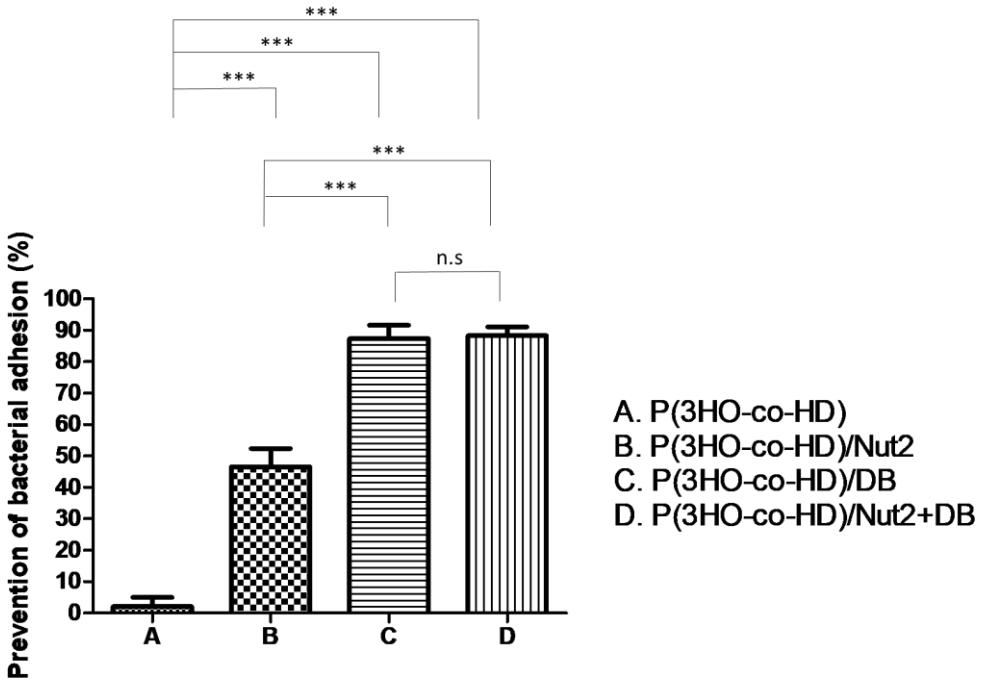

Figure 57: Percentage of prevention of bacterial adhesion on P(3HO-co-3HD) fibres modified with Nut2, DB and Nut2+DB compared to unmodified P(3HO-co-3HD) fibres after their incubation with *S. epidermidis* (ATCC® 35984™) for a period of 24 hours. The experiments were performed in two independent experiments, in triplicates (N=2, n=3). All pair of columns were compared. * indicates p<0.0001 and n.s indicates no statistical difference.**

The graph shows the percentage of prevention of bacterial adhesion by the modified fibres in comparison to the unmodified fibres. Fibre meshes modified with Nut2 exhibited a 47% prevention in bacterial adhesion when compared to unmodified P(3HO-co-3HD) fibres. Furthermore, fibre meshes modified with DB exhibited an 87% prevention in bacterial adhesion when compared to unmodified P(3HO-co-3HD) fibres. Although the combination of Nut2+DB showed a prevention in bacterial adhesion of 88%, there was no significant difference in the preventive effect between fibres modified with DB and fibres modified with DB+Nut2.

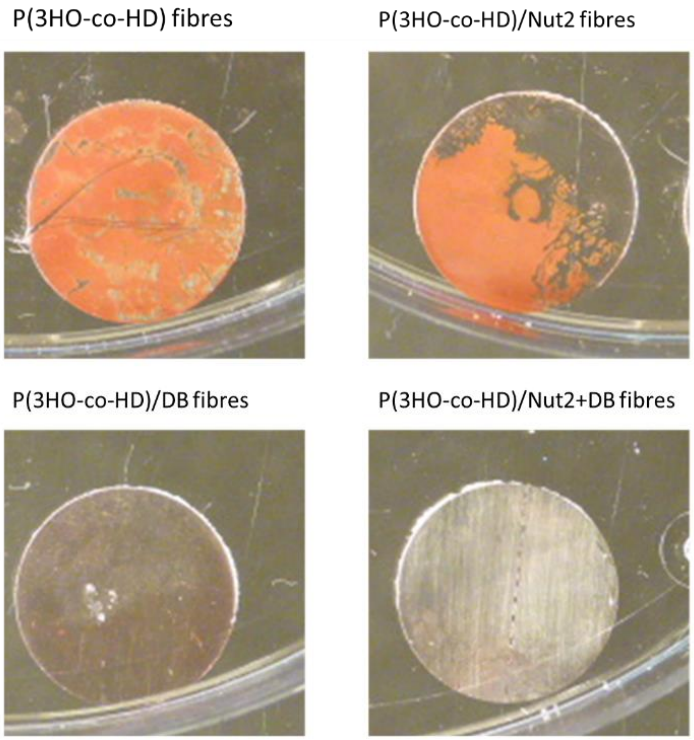

Figure 58: Safranin staining of bacterial biofilms formed on the unmodified P(3HO-co-3HD) fibres and on the P(3HO-co-3HD) fibres modified with Nut2, DB and Nut2+DB after a 24-hour bacterial incubation.

The biofilm biomass that was formed on the surface of the fibres after the 24-hour incubation period was stained with safranin and the results showed that the unmodified P(3HO-co-3HD) fibres were covered by a biofilm layer, whereas the fibres modified with Nut2 showed a slightly less covered area by *S. epidermidis* (ATCC® 35984™) biofilms. The fibres modified with DB and Nut2+DB showed the absence of *S. epidermidis* (ATCC® 35984™) biofilms on their surface.

5.2.12 Alternative development of P(3HO-co-3HD) fibres adsorbed with AMPs and DB

5.2.12.1 Covalent attachment of active agents on P(3HO-co-3HD) fibres

An alternative approach to develop antibacterial P(3HO-co-3HD)-based fibres was carried out using an amphiphilic six-armed star-shaped poly(ethylene oxide-stat-propylene oxide) containing reactive isocyanate groups at the distal ends of the polymer chains, NCO-sP(EO-stat-PO), as an additive to the P(3HO-co-3HD) spinning solution in order to promote the covalent coupling of active agents, thus resulting in the production of surface-activated fibres

in a single step. The fibres were electrospun on glass coverslips and the fibres produced were P(3HO-co-3HD) fibres coupled with NCO-sP(EO-stat-PO), P(3HO-co-3HD) fibres coupled with NCO-sP(EO-stat-PO) and AMP3 and fibres coupled with NCO-sP(EO-stat-PO), AMP3 and DB.

5.2.13 Characterisation of P(3HO-co-3HD) fibres adsorbed with AMPs and DB

5.2.13.1 Surface analysis: Water Contact Angle (WCA)

To evaluate the wettability changes after the functionalisation process, wettability studies were conducted by measuring the water contact angle of P(3HO-co-3HD)-NCO-sP(EO-stat-PO) fibres, P(3HO-co-3HD)-NCO-sP(EO-stat-PO)+AMP3 fibres and of P(3HO-co-3HD)-NCO-sP(EO-stat-PO)+AMP3+DB fibres and compared to the water contact angle of P(3HO-co-3HD) discs and P(3HO-co-3HD) fibres and the results are shown in Figure 59.

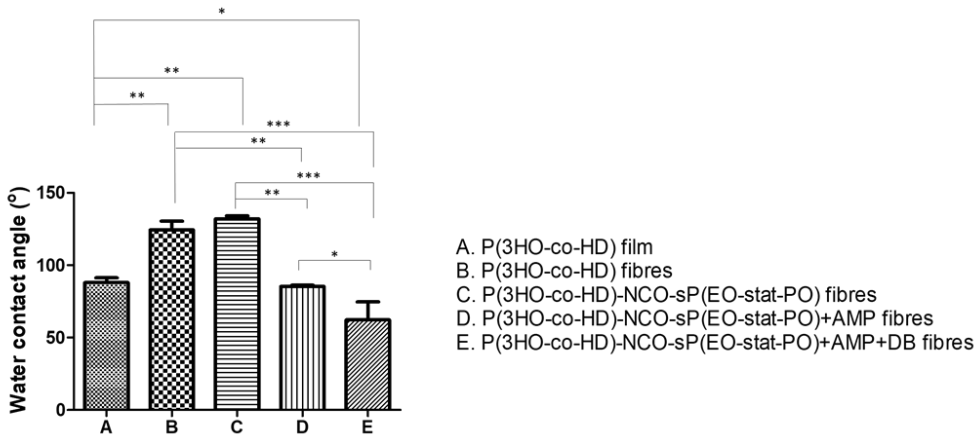

Figure 59: Water contact angle of P(3HO-co-3HD) discs, P(3HO-co-3HD) fibres, P(3HO-co-3HD)-NCO-sP(EO-stat-PO) fibres, P(3HO-co-3HD)-NCO-sP(EO-stat-PO)+AMP3 fibres and P(3HO-co-3HD)-NCO-sP(EO-stat-PO)+AMP3+DB fibres. The experiments were performed in triplicates (n=3). All pair of columns were compared. * indicates p<0.05, ** indicates p<0.001 and * indicates p<0.0001.**

P(3HO-co-3HD) discs exhibited a water contact angle of 88^{o} confirming once again the hydrophobic nature of the material. As observed before, P(3HO-co-3HD) fibres showed a significant increase in hydrophobicity, with a water contact angle of 124.4^{o}. A further increase in hydrophobicity was observed for P(3HO-co-3HD)-NCO-sP(EO-stat-PO) fibres which showed a water contact angle of 132^{o}. P(3HO-co-3HD)-NCO-sP(EO-stat-PO)+AMP3 fibres showed a

water contact angle of 85.3º and P(3HO-co-3HD)-NCO-sP(EO-stat-PO)+AMP3+DB fibres showed a water contact angle of 62.3º.

5.2.13.2 In vitro direct cytotoxicity studies

In order to evaluate the cytotoxicity of the functionalised fibres against mammalian cells, L929 murine fibroblasts were seeded on the surface of unmodified P(3HO-co-3HD) fibres and on functionalised P(3HO-co-3HD) fibres for a period of 24 hours. The cytotoxicity of each material was evaluated by calculating the percentage of cell viability after the incubation period in comparison to the growth control. The results are shown on Figure 60. Additionally, a fluorescent cell staining was carried out to observe the presence of live and dead cells on the fibres and the results are shown in Figure 61.

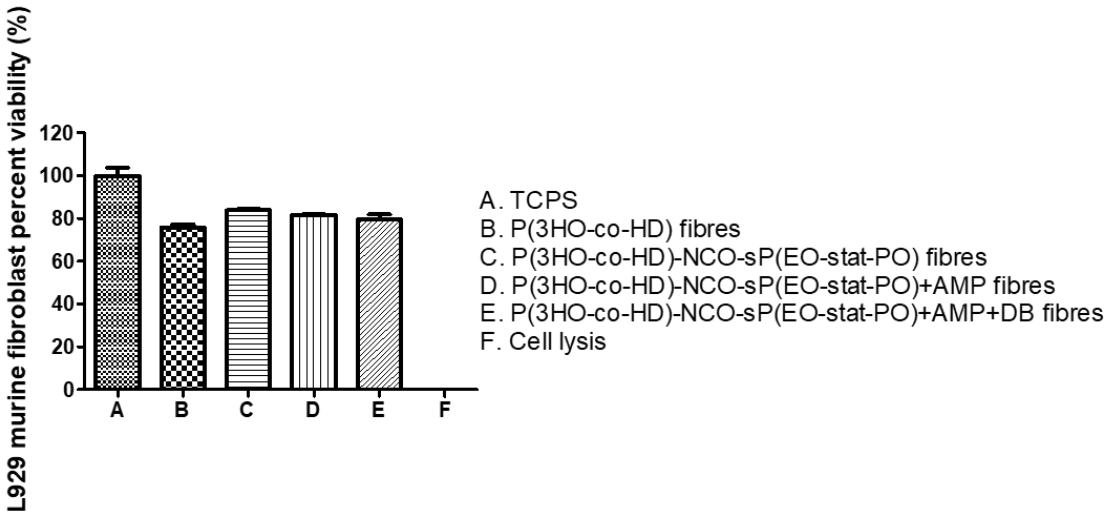

Figure 60: Percentage of cell viability of L929 murine fibroblasts after its seeding on the surface of P(3HO-co-3HD) fibres, P(3HO-co-3HD)-NCO-sP(EO-stat-PO) fibres, P(3HO-co-3HD)-NCO-sP(EO-stat-PO)+AMP3 fibres and P(3HO-co-3HD)-NCO-sP(EO-stat-PO)+AMP3+DB fibres for a period of 24 hours. A typical cell growth control and a positive control were considered and are represented by TCPS and cell lysis, respectively.

The graph shows the percentage of viable L929 murine fibroblasts in comparison to the cell growth control, TCPS, after its seeding on P(3HO-co-3HD) fibres, P(3HO-co-3HD)-NCO-sP(EO-stat-PO) fibres, as well as P(3HO-co-3HD)-NCO-sP(EO-stat-PO)+AMP3 fibres and P(3HO-co-3HD)-NCO-sP(EO-stat-PO)+AMP3+DB fibres for a period of 24 hours.

A cell viability of 76% and 84% was observed for P(3HO-co-3HD) fibres and P(3HO-co-3HD)-NCO-sP(EO-stat-PO) fibres, respectively. P(3HO-co-3HD)-NCO-sP(EO-stat-PO)+AMP3 fibres and P(3HO-co-3HD)-NCO-sP(EO-stat-PO)+AMP3+DB fibres exhibited a cell viability of 82% and 80%, respectively.

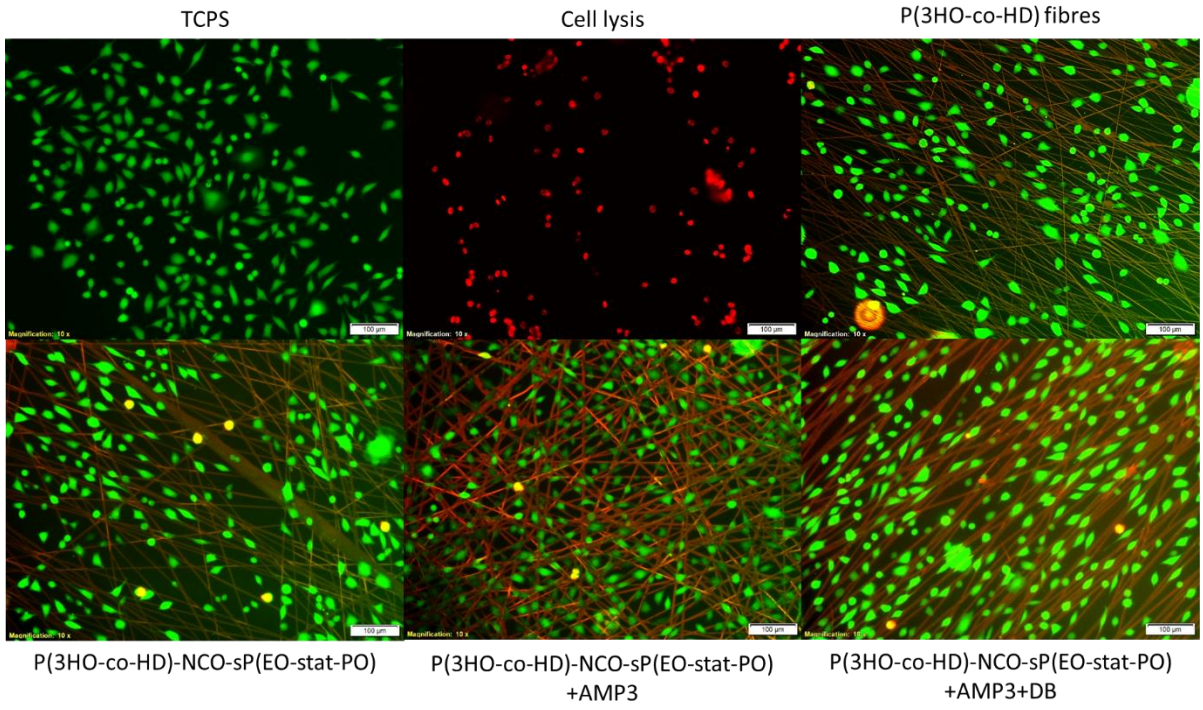

Figure 61: Fluorescence micrographs of L929 murine fibroblasts grown on top of P(3HO-co-3HD) fibres, P(3HO-co-3HD)-NCO-sP(EO-stat-PO) fibres, P(3HO-co-3HD)-NCO-sP(EO-stat-PO)+AMP3 fibres and P(3HO-co-3HD)-NCO-sP(EO-stat-PO)+AMP3+DB fibres. The dead cells are represented in red and live cells are represented in green. Magnification of micrographs of 10x and scale bar of 100 µm. Negative and positive controls are represented by TCPS and cell lysis, respectively.

The fluorescent micrographs showed the presence of live cells (green) on the four different types of fibres. Furthermore, the morphology of the cells grown on the four different types of fibres was similar to the morphology of cells grown on TCPS. P(3HO-co-3HD)-NCO-sP(EO-stat-PO) fibres showed a slightly lower cell density as compared to the remaining types of fibres.

5.2.13.3 Anti-adhesion and anti-biofilm properties

To evaluate the anti-adhesive properties of the functionalised fibres, unmodified P(3HO-co-3HD) fibres, and functionalised fibres were incubated with *S. epidermidis* (ATCC® 35984™) for a period of 24 hours. The bacteria that adhered to the surface of the fibres was removed by sonication and quantitated by plating on blood agar plates. The ability of the functionalised fibres to prevent bacterial adhesion was expressed as a percentage by comparing the number of bacteria that adhered to the surface of unmodified fibres with the number of bacteria that adhered to the surface of functionalised fibres. The results are shown in Figure 62. Additionally, after the incubation period, the biofilm biomass that was formed on the surface of the fibres as a result of bacterial adhesion, which was stained using safranin and the results are shown in Figure 63.

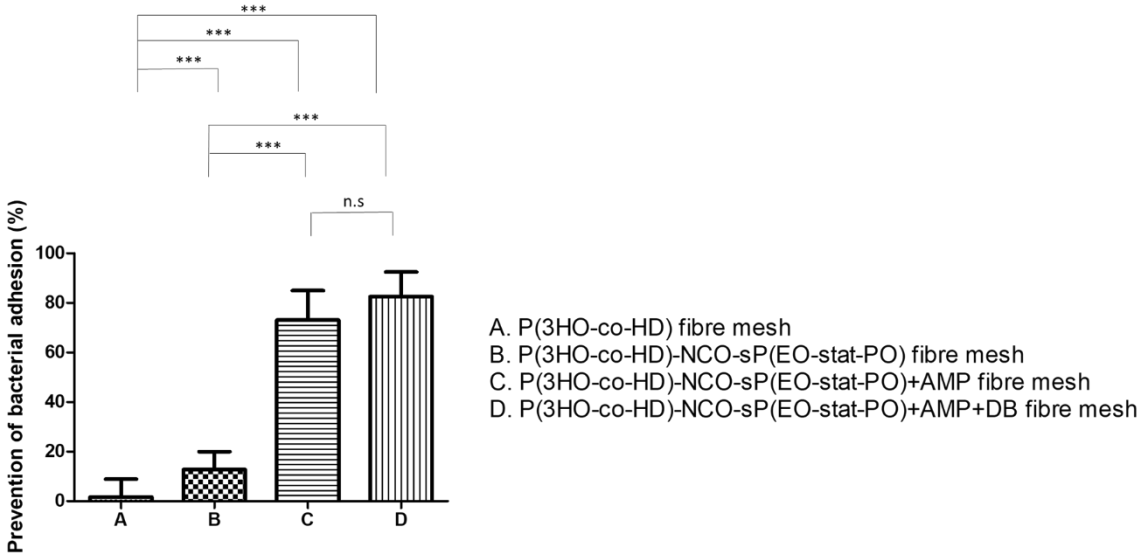

Figure 62: Percentage of prevention of bacterial adhesion of functionalised P(3HO-co-3HD)-NCO-sP(EO-stat-PO) fibres and P(3HO-co-3HD)-NCO-sP(EO-stat-PO) fibres functionalised with AMP3 and AMP3+DB comparatively to unmodified P(3HO-co-3HD) fibres after their incubation with *S. epidermidis* (ATCC® 35984™) for a period of 24 hours. The experiments were performed in two independent experiments, in triplicates (N=2, n=3). All pair of columns were compared. * indicates p<0.0001 and n.s indicates no statistical difference.**

The graph shows the percentage of prevention of bacterial adhesion by functionalised fibres in comparison to unmodified fibres. P(3HO-co-3HD)-NCO-sP(EO-stat-PO)+AMP3 fibres exhibited a 73% prevention of bacterial adhesion when compared to unmodified P(3HO-co-3HD) fibres. Furthermore, P(3HO-co-3HD)-NCO-sP(EO-stat-PO)+AMP3+DB fibres exhibited an 83% prevention of bacterial adhesion when compared to unmodified P(3HO-co-3HD) fibres. The fibres containing NCO-sP(EO-stat-PO) showed similar bacterial adhesion to that of the P(3HO-co-3HD) fibres.

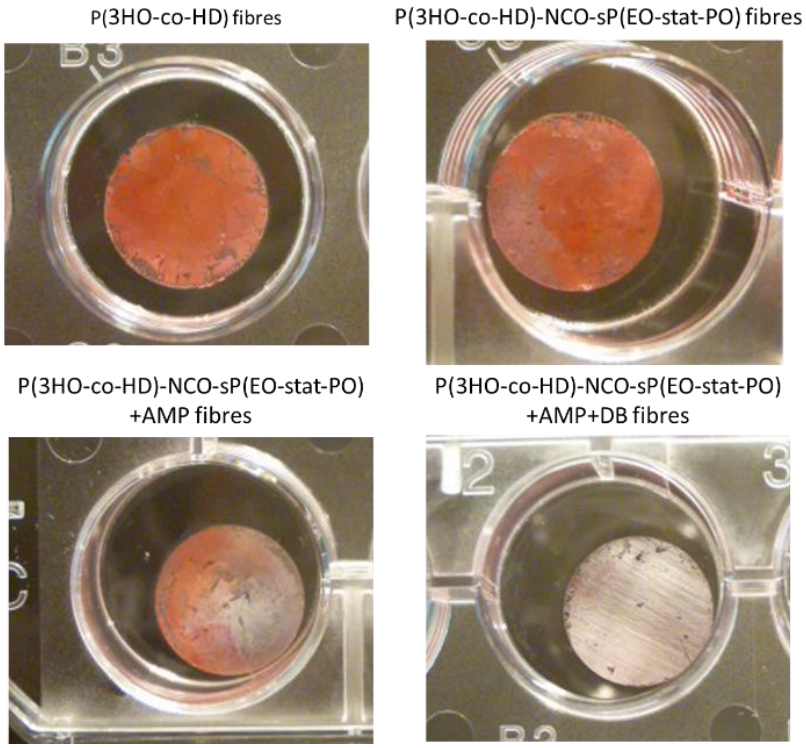

Figure 63: Safranin staining of bacterial biofilms formed on top of unmodified P(3HO-co-3HD) fibres, functionalised P(3HO-co-3HD)-NCO-sP(EO-stat-PO) fibres and P(3HO-co-3HD)-NCO-sP(EO-stat-PO) fibres functionalised with AMP3 and AMP3+DB after a 24-hour bacterial incubation.

The biofilm biomass that was formed on the surface of the fibres after the 24-hour incubation period was stained with safranin and the results showed that the unmodified P(3HO-co-3HD) fibres and P(3HO-co-3HD)-NCO-sP(EO-stat-PO) fibres were covered by a biofilm biomass layer. The fibres functionalised with AMP3 were slightly less covered by *S. epidermidis* (ATCC®

35984™) biofilms and the fibres functionalised with AMP3+DB showed the absence of *S. epidermidis* (ATCC® 35984™) biofilms on its surface.

5.3 Discussion

Despite the success of many regenerative medicine strategies such as TE, the problem of contamination of implantable biomaterials by bacteria persists. Bacteria can rapidly recognise a foreign material and start its adhesion process. As the implants get more and more colonised by bacteria, they start forming a protective layer which becomes much harder to treat than usual planktonic bacteria. Thus, there is a strong need to mitigate bacterial adhesion on implants such as TE scaffolds with features such as surface activated properties that are unfavourable for bacterial adhesion but favourable for tissue cell adhesion. The development of non-cytotoxic and anti-adhesive TE scaffolds was achieved by surface modifying P(3HO-co-3HD) films and fibres with bacterial membrane targeting AMPs, and the biofilm disrupting enzyme DB, to prevent bacterial colonisation without creating host responses.

The antibacterial screening of three synthetic AMPs, AMP3, Nut2 and LL-37 was evaluated against *E. coli* (ATCC® 35218™), *S. epidermidis* (ATCC® 35984™) and *S. aureus* (ATCC® 29213™), confirming the bacteriostatic and bactericidal nature of the AMPs. According to the European Committee on Antimicrobial Susceptibility Testing (EUCAST) MIC Breakpoints, the most commonly used antibiotics such as vancomycin, gentamycin and rifampicin have a MIC of 4 mg/mL, 1 mg/mL and 60 µg/mL, respectively, against some of the most relevant pathogenic bacteria (The European Committee on Antimicrobial Susceptibility Testing, 2019). Herein, the obtained MIC and MBC values showed concentrations ranging from 6.3 µg/mL to 50 µg/mL, suggesting an extremely good efficacy at low concentrations.

An interesting outcome of the antibacterial screening was the different bacterial susceptibilities towards the AMPs. Firstly, an immediate observation was that, with the range of concentrations tested, none of the peptides was active against *S. aureus* (ATCC® 29213™) and secondly, it was observed that each peptide was only active against one bacterial strain, either *E. coli* (ATCC® 35218™) or *S. epidermidis* (ATCC® 35984™). Since AMPs act at a bacterial membrane level, the different activities could be a consequence of the different membrane organisations and compositions observed in Gram-positive and Gram-negative bacteria. One

of the major differences between Gram-negative and Gram-positive bacteria is that Gram-negative bacteria possess an outer membrane composed of proteins, phospholipids, and LPS while Gram-positive bacteria do not (Beveridge, 1999). Another major difference is the constitution of the peptidoglycan membrane of both types of bacteria. Gram-positive bacteria contain many surface proteins anchored to the peptidoglycan membrane such as protein A, fibrinonectin-binding proteins and collagen adhesin, while in Gram-negative bacteria the only protein anchored to the peptidoglycan membrane is the Braun's lipoprotein (Vollmer *et al*., 2008). Furthermore, the peptidoglycan membrane of Gram-positive bacteria contains teichoic acids, and teichuronic acids while the peptidoglycan membrane of Gram-negative bacteria does not (Navarre *et al*., 1999). Hence, it is possible that such differences result in different bacterial susceptibilities towards the AMP action. In addition, there are differences between species belonging to the group of Gram-positive bacteria as it is the case of *S. aureus* (ATCC® 29213™) and *S. epidermidis* (ATCC® 35984™). For instance, *S. aureus* species express much more virulent factors, such as proteins and polysaccharides than *S. epidermidis* species (Foster, 1996). If these factors are membrane associated, then it is also expected that their susceptibility against AMPs will also be different.

Besides the confirmation of the bacteriostatic and bactericidal nature of the peptides, promising results were obtained regarding the anti-biofilm action of the AMPs. The antibacterial screening showed that with concentrations equivalent to the MBC, biofilm formation was inhibited between 80 and 90% compared to the biofilm growth control. Although the mechanism of action behind the killing effect of AMPs has been described in literature, its mechanism of action against biofilms is still not entirely understood. Literature suggests that they interfere with cell communication systems such as quorum sensing, bind to polysaccharides present in the biofilm matrix, downregulate genes responsible for biofilm formation or disrupt and depolarise the membrane potential of biofilm embedded cells (Yasir *et al*., 2018). Since the mechanism of action of the AMPs at a biofilm level was not the main focus of this thesis, this question still remains open.

The antibacterial screening of DB against *E. coli* (ATCC® 35218™), *S. aureus* (ATCC® 29213™) and *S. epidermidis* (ATCC® 35984™) confirmed the ability of DB to disperse pre-formed biofilms. Different dispersal activities were observed for each bacterial strain. In the case of *E. coli* (ATCC® 35218™), despite testing increasing concentrations of DB, the dispersal activity

remained stable as with the lowest DB concentration, the biofilms were dispersed by 20% and with one of the highest DB concentrations, the biofilms were dispersed by 25%. On the other hand, in the case of *S. aureus* (ATCC® 29213™), a much more gradual dispersal effect was observed. It was noted that with the lowest DB concentration, the biofilms were dispersed by only 2% and with the highest DB concentration, the biofilms were dispersed by 52%. These results suggested that, in the first case, the dispersal activity against *E. coli* (ATCC® 35218™) might not have been dose-dependent whereas in the second case, the dispersal activity was dependent on the DB concentration. In the case of *S. epidermidis* (ATCC® 35984™) with the lowest DB concentration, the biofilms were dispersed by 70% and with the highest DB concentration, the biofilm were dispersed by 90%. Although in this case, the dispersal activity of DB also seemed to be non-dose-dependent, the effect of DB against pre-established biofilms produced by *S. epidermidis* (ATCC® 35984™) was much more effective compared to the other bacterial strains.

Biofilms are enclosed in a self-produced extracellular matrix composed primarily by EPS whose major components are polysaccharides, proteins and eDNA (Donlan, 2002). DB is known to hydrolyse glycoside linkages of a type of polysaccharides present in the EPS of some bacterial species termed β-1,6-poly-N-acetylglucosamine (PNAG) (Ramasubbu *et* al., 2005, Itoh *et al*., 2005, Otto, 2009). PNAG synthesis has been described to occur in organisms including *S. epidermidis*, *S. aureus* and *E. coli* (Lin *et al*., 2015, Cerca and Jefferson, 2008). However, its synthesis varies from species to species. For instance, in a study conducted by Donelli *et al*., it was observed that the level of polysaccharide production by *S. epidermidis* (ATCC® 35984™) was more than 2-fold higher than the level of polysaccharide production by *S. aureus* strains (Donelli *et al*., 2007). Assuming that each bacterial strain produces different levels of PNAG and different types of polysaccharides, it might be that the different DB activities are a consequence of such differences.

The cytocompatibility evaluation of the different AMPs and DB demonstrated a higher selectivity for bacteria over mammalian cells, as the estimated MICs and MBCs were considerably lower than the CC_{50} calculated when L929 murine fibroblasts were exposed to increasing concentrations of the agents for a period of 24 hours. The fact of having such a safe therapeutic window in which the agents could be used was extremely convenient if the aim was to prevent bacterial adherence to the maximum without interfering with the adherence

of tissue cells. Therefore, modified P(3HO-co-3HD) discs were produced by physically adsorbing high concentrations of the active agents to the surface of the polymer.

The amount of adsorbed agents was quantified using the BCA and Bradford protein assays. The Bradford assay was used to determine the concentration of agents with high molecular, namely, DB (42 kDa) and LL-37 (45 kDa) and the BCA protein assay was used for the agents with low molecular weight, namely, AMP3 (24 kDa) and Nut2 (23 kDa). The assays showed that the adsorption of DB and LL-37 was much higher than the adsorption of Nut2 and AMP3, despite using the same starting concentration. Protein or peptide adsorption on solid surfaces occurs as a result of various intermolecular interactions, such as Coulombic forces, van der Waals forces, Lewis acid-base forces and hydrophobic interactions, and intramolecular forces, that derive from within the molecules and cause conformational changes (Hlady and Buijs, 1996). One of the common features of all four active agents is their amphiphilicity, meaning that they are composed of hydrophobic and hydrophilic domains. Although the mechanism by which hydrophobic interactions occur is not quite well deciphered, it is possible that during the physical adsorption process, a conformational re-arrangement of the molecules occurs in such way that the hydrophobic content gets adsorbed to the surface of the hydrophobic polymer, P(3HO-co-3HD), leaving the hydrophilic content exposed to the environment. Additionally, it might be that molecules with a higher hydrophobic content will more easily adsorb to the surface of hydrophobic materials as a consequence of stronger hydrophobic interactions. The four agents are composed not only by different hydrophobic amino acids but different contents of hydrophobic amino acids being DB the agent with the highest hydrophobic content, followed by LL-37, Nut2 and AMP3, thus explaining the same trend in the adsorption process. Apart from this, the BCA and Bradford protein assays revealed that the concentrations of adsorbed agents were enough to exert an efficient antibacterial and anti-biofilm effect against bacteria without compromising the viability of the mammalian cells as the amount adsorbed was higher than the MBC and considerably lower than the CC_{50}.

XPS and ATR-FITR are very useful techniques to the determine the near surface chemical composition of a material. Because XPS is a very expensive technique with a slow processing time, only samples modified with DB were analysed by this technique, whereas samples modified with AMPs were analysed by much simpler and faster technique, ATR-FTIR.

XPS allows for the elemental characterisation of a material by targeting specific binding energies as each binding energy correlates with different elements at a surface level (Brundle *et* al., 1992, Leng, 2009). Since one of the major differences between P(3HO-co-3HD) and DB is that the latter contains nitrogen atoms present in its structure, the binding energy correspondent to nitrogen, N1s, was targeted. Indeed, the results showed that P(3HO-co-3HD) discs modified with DB contained nitrogen and samples without DB did not, thus confirming the presence of DB on the surface of P(3HO-co-3HD) films. On the other hand, the ATR-FTIR results confirmed the presence of each AMP on the surface of P(3HO-co-3HD) discs. This confirmation was obtained by targeting three characteristic IR absorption bands of peptides and proteins, namely, the amide I band, the amide II band and the amide A band, so ideally P(3HO-co-3HD) films modified with AMPs should have presented peaks in these particular bands and indeed these peaks were identified in all P(3HO-co-3HD) discs modified with AMPs. Furthermore, higher peak intensities in the regions corresponding to the adsorption band of the peptides were observed for P(3HO-co-3HD) discs modified with LL-37 unlike what was observed for P(3HO-co-3HD) discs modified with either Nut2 and AMP3, supporting the results obtained with the BCA and Bradford protein assays, where it was observed that a higher concentration of LL-37 were adsorbed relatively to Nut2 and AMP3.

Another way to evaluate the changes of a material at a surface level is by evaluating the WCA. As described by Absolum *et al*., one of the consequences of protein or peptide adsorption on hydrophobic surfaces is its change in wettability (Absolom *et al*., 1981, Absolom and Neumann, 1987). Typically, hydrophobic surfaces will display higher hydrophilicity after protein or peptide adsorption. As hypothesised before, one of the mechanisms by which amphiphilic proteins or peptides adsorb to the surface of hydrophobic materials might involve its conformational re-arrangement, leaving the hydrophobic domains in contact with the hydrophobic surfaces of the materials and the hydrophilic domains exposed to the exterior. This means that a material that was once hydrophobic will suffer changes in terms of its wettability properties if a significant hydrophilic content gets exposed to the environment. The data obtained by the BCA and Bradford protein assay and the ATR-FTIR results showed that a higher DB and LL-37 content was adsorbed to the surface of P(3HO-co-3HD) films compared to Nut2 and AMP3. Since the number of hydrophilic amino acids present in DB and LL-37 is much higher than that present in Nut2 and AMP3, it would be expected that a sharper

decrease in wettability would be observed for P(3HO-co-3HD) films incorporated with DB and LL-37 rather than with Nut2 and AMP3, and indeed the results showed such expected results.

The cytocompatibility studies revealed different cytotoxic effects when L929 murine fibroblasts were seeded on the modified samples. The surface properties of the materials such as porosity, surface charge, topography and wettability are known to play a critical role in the process of cell adhesion, proliferation and differentiation. For instance, many studies acknowledge that cells prefer hydrophilic surfaces, rather than hydrophobic surfaces (Lampin *et al*., 1997). However, the recommended negative control of the ISO 10993-5 to perform the biological evaluation of medical devices is high density PE (ISO 10993-5:2009(E)). Interestingly, PE is hydrophobic with contact angles close to 100^{o}, and despite its wettability properties, cells become adherent, spread on the materials with a normal phenotypic shape and proliferate well (PeŠŠková *et al*., 2007, De Geyter *et al*., 2008). Another example is the case of PHAs which despite their hydrophobicity, have shown to support cell growth extremely well and are heamocompatible (Nigmatullin *et al*., 2015, Sanhueza *et al*., 2018, Lukasiewicz *et al*., 2018). Certainly, the process of cell adhesion and proliferation will not solely be dependent on the wettability properties of a material, but it will depend on the combination of all parameters indicated above. In this study, however, the information gathered from the surface characterisation allowed only for the correlation between the surface wettability of the materials with its cytotoxicity. Fibroblasts have shown very good cell adhesion for materials with contact angles ranging between 70^{o} to 80^{o} (Tamada and Ikada, 1993, Bumgardner *et al.,* 2003). Discs modified with AMP3 and Nut2 resulted in WCA close to 80^{o}, hence higher cell viabilities were recorded. On the other hand, the adsorption of DB and LL-37 resulted in materials with considerably lower WCA, and therefore, in this case, the high hydrophilicity of the materials might not have been beneficial for the process of cell adhesion and growth, thus contributing to lower cell viabilities.

The anti-adhesive tests showed that less bacteria adhered to the modified materials in comparison to the unmodified materials. More specifically, modified P(3HO-co-3HD) with AMP3, LL-37, and Nut2 resulted in the prevention of bacterial adhesion by 92%, 74%, and 67%, respectively, when compared to unmodified controls. Such results were encouraging as their anti-adhesive performance was similar or even better to the performance of other anti-adhesive materials described in literature. For instance, in a study conducted by Humbolt *et*

al., gold surfaces grafted with AMP magainin I, reduced by more than 50% the adhesion of different Gram-positive bacteria (Humblot *et al*., 2009). In another study, it was observed that when adsorbing lysozyme to hydrophobic surfaces the number of *B. subtilis* 168 colonies present in the surface of the materials was reduced by 30% as compared to unmodified materials (Muszanska *et al*., 2011).

Regarding the anti-adhesive performance of P(3HO-co-3HD) modified with DB, the Bradford assay revealed that approximately 60 µg/mL of DB was adsorbed to the surface of P(3HO-co-3HD) discs, which correlated with its dispersive activity should lead to the dispersion of *S. aureus* (ATCC® 29213™), *S. epidermidis* (ATCC® 35984™) and *E. coli* (ATCC® 35218™) biofilms by 20%, 70% and 20%, respectively. However, the materials modified with DB, prevented the adhesion of bacteria by 90% in all cases. The enhanced effect against bacteria might be associated with the WCA of the material. As the wettability properties influence the process of cell adhesion, they also influence the adhesion of bacterial cells. Bacterial adhesion to a substratum is also known to be facilitated by hydrophobic interactions that occur between bacteria and the substratum. Bacteria contain structures that confer them hydrophobic properties which can derive for example from hydrophobic proteins that are covalently bound to the cell wall or to the outer membrane of Gram-negative bacteria. Such hydrophobic areas are in many cases, available to interact with hydrophobic materials and promote adhesion (Doyle, 2000). For instance, in the case of *E. coli*, various fimbriae have been identified as hydrophobic components, while in the case of *S. aureus*, A protein was identified as one of the hydrophobic components. Both fimbriae and A protein have been associated with the virulence of these bacteria as they mediate the process of adhesion and biofilm formation (Rosenberg and Kjelleberg, 1986.). Therefore, the process of bacterial adhesion might be supressed if a material is too hydrophilic. The adsorption of DB led to a sharp decrease in the contact angle values of the P(3HO-co-3HD) discs to a WCA of $53^{o,}$ turning the materials hydrophilic in nature and hence influencing the process of bacterial adhesion.

As mentioned in the introductory section, the goal of this study was to transfer the knowledge obtained with the P(3HO-co-3HD) film structures to P(3HO-co-3HD) fibre-based materials to develop biocompatible and anti-adhesive materials for tissue engineering purposes. The importance of developing P(3HO-co-3HD) based-fibres came with the need to develop new biocompatible platforms based on PHAs for tissue engineering applications, increasing at the

same time the scope of applications of P(3HO-co-3HD). PHA-based fibrous scaffolds are usually obtained from P(3HB) blends with natural or synthetic polymers that have better mechanical properties leading to the production of fibres with decreased crystallinity, improved porosity and permeability (Zonari *et* al., 2012, Azari *et al*., 2014, Fryczkowski and Kowalczyk, 2009, Hinüber *et al*., 2011). However, polymer blends require the synthesis and purification of two or more different polymers, increasing the final costs of the material. Besides using P(3HB) blends, PHA-based fibres can be obtained from P(3HB) copolymers such as (P3HB-co-3HV) (Tong *et al.*, 2011). However, in this study, P(3HO-co-3HD) based-fibres were successfully obtained by electrospinning and are reported here for the first time.

Bead formation is a common problem in the electrospinning process and can affect the quality of the fibres. Besides having a different morphology of that of the ECM, beaded fibres have reduced surface area-to-volume ratio, and therefore reduced contact areas for cells to attach. On the other hand, aligned fibre structures are ideal as they resemble the ECM pattern (Tong and Wang, 2011, Bourget *et al*., 2013). Beadless and slightly aligned fibres were obtained by optimising the electrospinning conditions, resulting in fibres with a suitable morphology for cell attachment, growth and proliferation.

The bioactivation of P(3HO-*co*-3HD) based-fibres was done by employing two different strategies. The first in which the active agents were physically adsorbed to P(3HO-co-3HD) fibres and the second in which the active agents were covalently coupled to P(3HO-co-3HD) fibres by the presence of NCO-sP(EO-stat-PO). As a complementary strategy and in order to see if the combination of different agents with different mechanisms of action against biofilms would enhance the anti-adhesive capacities of a material, Nut2 and DB were combined and physically adsorbed to P(3HO-co-3HD) fibres, whilst AMP3 and DB were combined and covalently coupled to P(3HO-co-3HD) fibres. As this was a preliminary study, the biological properties of the materials as well as wettability properties were the main focus rather than a more detailed chemical characterisation of the materials.

The selection of the above-mentioned AMPs over LL-37 was related to the fact that *S. epidermidis* is one of the most problematic pathogens responsible for tissue-related infections, therefore only the agents that have shown effective activity against *S. epidermidis* (ATCC® 35984™), were selected (Becker *et al*., 2014, Götz, 2002). Apart from that, LL-37 has

been widely used as an antibacterial agent whereas Nut2 and AMP3 are novel synthetic AMPs and are much less explored compared to LL-37.

In this study, it was shown that when P(3HO-co-3HD) was processed to form electrospun fibre meshes, the WCA increased drastically to values of 120^{o} and further increased when processed to form electrospun fibre meshes along with NCO-sP(EO-stat-PO), to a WCA of 132^{o}, granting the materials almost superhydrophobic properties. It is known that roughness has a great influence on the water contact angle of a material, and that hydrophobic materials, when fabricated into highly rough and porous substrates, such as electrospun fibre meshes, become even more hydrophobic. (Law, 2014, Yuan and Lee, 2013, Wilson *et al*., 2005). P(3HO-co-3HD) electrospun fibre meshes with and without the addition of NCO-sP(EO-stat-PO) exhibited similar contact angles, indicating that the additive in this case did not show a strong tendency for surface segregation, and thus not altering the surface characteristics of the original material. On the other hand, and as expected when physically adsorbing or covalently coupling the active agents to the fibres, a much lower WCA was obtained. This evidenced the introduction of hydrophilic groups on the surface of the fibres, derived from the AMPs and DB, causing the fibres to have a significantly lower contact angle. Additionally, in the case of the covalent coupling, the results suggested that these molecules contained enough polar groups to interact with the charges during the spinning process and to promote surface segregation. As expected, fibres containing DB showed a higher hydrophilicity than fibres containing AMPs which as explained before derives from the higher number of hydrophilic amino acids present in DB as compared to the AMPs.

Quantitative cytocompatibility assays revealed cell viability values higher than 70% for all the electrospun fibres prepared in this study when compared to the TCPS control, showing in general, a better cytocompatibility towards L929 murine fibroblasts than P(3HO-co-3HD) materials in a film form as lower cell viabilities were obtained. This supported the well-documented fact that cells can grow better in fibrous scaffolds (Knight and Przyborski, 2015). Nonetheless, the qualitative fluorescent micrographs showed that in case of the materials with higher WCA, that is P(3HO-co-3HD) fibres, P(3HO-co-3HD)/Nut2 and P(3HO-co-3HD)-NCO-sP(EO-stat-PO) fibres, a lower cell density was observed on the fibres, when compared with the remaining fibres, indicating that the increase in hydrophobicity may have influenced the process of cell adhesion. As mentioned before, relatively hydrophilic surfaces are generally

preferred by cells as they tend to promote the attraction of proteins from the media, such as adhesion or growth factors, onto their surfaces, hence facilitating the process of cell adhesion and growth (Wilson *et al*., 2005). For this reason, it was seen that, P(3HO-co-3HD)/DB fibres, P(3HO-co-3HD)/Nut2+DB fibres, P(3HO-co-3HD)-NCO-sP(EO-stat-PO)+AMP and P(HO-co-HD)-NCO-sP(EO-stat-PO)+AMP+DB fibres not only exhibited a higher cell density, but also showed that the cells were able to attach and elongate better along the fibres, indicating that the relatively more hydrophilic properties of the fibres may have promoted the process of cell adhesion.

The colonisation of bioactive fibres by *S. epidermidis* (ATCC® 35984™) was significantly lower than that on the unmodified P(3HO-co-3HD) fibres and unfunctionalised PHA-NCO-sP(EO-stat-PO) fibres, serving as an indicator that the physical adsorption process as well as the covalent coupling of the agents had successfully conferred anti-adhesive properties to the electrospun meshes.

As mentioned above, the idea of combining AMPs with DB was done to see if the anti-adhesive properties of P(3HO-co-3HD) fibres would be enhanced. By comparing the performance of fibres containing only Nut2 with fibres containing both Nut2 and DB, it was possible to visualise a significant reduction in bacterial adhesion, which could have been an indicator that in fact there was a synergistic effect between the two agents against bacterial adhesion. However, the fibres containing only DB showed very similar anti-adhesive effects to the ones observed with the fibres containing both DB and Nut2. The similar performance of the materials suggest that the anti-adhesive action is coming mainly if not only from DB. A hypothesis to explain this could be the fact that when Nut2 and DB are combined, DB acts as an antagonist against Nut2, hence blocking its action. Secondly, it is possible that Nut2 was not adsorbed at all as a consequence of stronger intermolecular forces between DB and P(3HO-co-3HD). Thirdly, perhaps Nut2 was in fact adsorbed, however the presence of DB resulted in Nut2 to re-arrange into a non-active conformation against bacteria. And finally, it might be that after a certain agent concentration, the anti-adhesive effect remains the same. Supporting this last hypothesis are the results obtained by the evaluation of the anti-biofilm properties of AMPs against *S. epidermidis* (ATCC® 35984™) as well as the dispersive properties of DB against pre-established biofilms from *S. epidermidis* (ATCC® 35984™). It was observed

that after a certain concentration, its increase resulted in the same activity towards *S. epidermidis* (ATCC® 35984™) biofilms.

By comparing the performance of fibres containing only AMP3 with fibres containing both AMP3 and DB, it was also possible to visualise a significant reduction in bacterial adhesion, which again could have been an indicator that in fact there was a synergistic effect between the two agents against bacterial adhesion. However, in this case, fibres functionalised only with DB were not fabricated and hence it is not possible to state whether the enhancement in the anti-adhesive effect is derived from a synergistic effect between the agents or, as observed with the physical adsorption method, the activity is only linked to the presence of DB.

The safranin staining allowed to determine whether the bacteria that adhered to the fibres were capable of forming biofilms in a 24-hour bacterial incubation period. The results showed that regardless of the immobilisation method, fibres containing DB were able to prevent biofilm formation, meaning that, although bacterial colonies were recovered from the sonication process, the bacteria that adhered to the DB containing fibres did not develop biofilms. These results suggest that the bacteria recovered are possibly dead bacteria that was not able to proliferate and further develop into sessile communities. Although the results look promising, the presence of a layer of dead bacteria on the surface of a material might constitute a source of nutrients for other bacteria, promoting biofilm formation at a later stage. Additionally, the layer of dead bacteria could also block the action of the active agents by physically protecting them.

6 Chapter 6 Conclusions, outlook and future work

6.1 Conclusions, outlook and future work

The motivation of the research presented in this thesis came with the need to develop alternative and complementary strategies to improve the performance of implantable materials by preventing its early contamination by bacteria. To do so, a class of biopolymers with great potential as biomedical materials, PHAs, were produced with antibacterial, anti-biofilm and/or anti-adhesive features, thus expanding its use in biomedical applications such as tissue engineering and medical device development.

The work developed in this thesis was divided into three major parts:

The first part focused on the production and characterisation of different types of PHAs, that is, a stiff and brittle type of PHA, here identified as P(3HB), and an elastomeric type of PHA, here identified as P(3HO-co-3HD).

The second part consisted in the fabrication and characterisation of bioactive P(3HB) films combined with the small molecule TC and its translation into potential coatings for medical devices.

Finally, the third part included the fabrication and characterisation of bioactive P(3HO-co-3HD) films combined with different bacterial membrane targeting AMPs and biofilm disrupting enzyme DB and its translation into potential scaffolds for tissue engineering applications.

The following sections contain the conclusions, outlook and future work related to each part of the work.

6.1.1 Part 1. Production and characterisation of MCL-PHAs and SCL-PHAs for biomedical applications

In this part of the work, PHAs were successfully produced by batch cultivation using glucose as the carbon source and nitrogen limiting conditions.

Depending on the bacterial strain used, two types of PHAs were produced. SCL-PHAs were produced by fermentation of *B. subtilis* OK2 and MCL-PHAs were produced by fermentation of *P. mendocina* CH50. By carrying out a chemical characterisation of the materials using techniques such as ATR-FTIR, GC-MS and NMR, the produced SCL and MCL-PHAs were later

identified as P(3HB) and P(3HO-co-3HD), respectively. P(3HB) is one of the most studied PHAs, being vastly produced by many research groups and it was the first PHA discovered by the French microbiologist Maurice Lemoigne at the Institute Pasteur in the 1920's (Keshavarz and Roy, 2010). On the other hand, the copolymer of 3-hydroxyoctanoic acid 3-hydroxydecanoic acid produced in this work has unique mole percentages of each monomer unit. Hence, in this sense, by using specific fermentation conditions and *P. mendocina* CH50 as the bacterial strain, a different type of MCL-PHA was produced, which in comparison with other MCL-PHAs produced and described in literature, such as P(3HO) and P(3HO-co-12%3HHx), had better extensibility and flexibility, thus constituting a useful addition to the already existing library of MCL-PHAs.

Although the amount of polymer obtained in this part of the work was enough to carry out the experiments described in this thesis, the production yields were reasonable and could be improved, especially if these polymers are to be explored in biomedical applications. In the past two decades, there has been a considerable increase in the number of studies aiming at the development of biomaterials with antibacterial properties for biomedical applications, however, only few studies proceed to clinical trial stages. One possible reason could be the poor characterisation of the materials developed, which constitutes a barrier for further advancement to clinical trials. Therefore, a more comprehensive chemical, physical, mechanical and biological characterisation of the materials is needed which on one hand, ensures that after each batch cultivation the same properties (e.g., molecular weight) are maintained, and on the other hand confirms the safety and stability of the materials. And for that, considerable amounts of polymer are needed. Indeed, if such high amounts of polymer are needed, one also needs to consider the costs associated with its production. The carbon source is accountable for approximately 50% of the total PHA production costs, with glucose being one of the most expensive carbon sources for PHA production, however, it is also one of the most preferred carbon sources to produce PHAs. This is primarily because many bacterial species can grow and accumulate PHAs with high yield in the presence of glucose but are unable to efficiently grow and accumulate PHAs in the presence of other alternative cheap or renewable carbon sources (Amaro *et al*., 2019). Ultimately this means that with one single carbon source and a collection of different bacterial species it can be possible to produce a library of PHAs with reasonably good yields and different properties such as the ones obtained in this study.

Therefore, if on one hand one wants to keep producing PHAs using glucose as the carbon source but at the same time needs to ensure high polymer yields with no batch-to-batch variation, optimisation strategies need to be applied and are suggested as future work. Traditional optimisation approaches include the use of metabolically engineered strains, different downstream processing, utilisation of cheap carbon sources, improvement of the medium composition and different fermentation strategies (Możejko-Ciesielska *et al*., 2016). However, they are all based on trial-and-error processes and usually involve considerable time, equipment and reagents, contributing for the increase in the process costs and developing time. Therefore, optimisation strategies that can reduce the costs, time, equipment needed and at the same time can contribute for the development of a production strategy that ensures better biomass growth profiles with improved polymer yield accumulation should be explored. To do so, mathematical modelling, an approach used by systems biology can be explored. Mathematical models allow the description of the dynamics of the system in study. Based on these models, one can predict the system's behaviour (e.g., bacterial growth) at any time and also to obtain quantitative knowledge about the importance of different factors, such as the media composition and the range of values in which they are important to improve the yield in polymer production processes (Klamt *et al*., 2007, De Alwis *et al*., 2007). Thus, moving forward and as future work, optimisation strategies focusing on either mathematical models, such as the black box model or even design of experiments should be looked at. These approaches could balance the time, cost and quality of the process and at the same time ensure high yields of PHA accumulation.

6.1.2 Part 2. Development of antibacterial P(3HB) materials: From 2D films to 3D surface coatings

In this part of the work, novel biocidal, anti-adhesive and anti-biofilm materials were developed based on the combination of P(3HB) and small molecule TC.

One of the immediate conclusions of this section has to do with the changes observed in the physical properties of P(3HB) when TC was combined with the polymer. It was observed that when P(3HB) and TC were combined in a film form, the mechanical and thermal properties of P(3HB) showed a tendency to improve as the materials became less brittle and more flexible. The physical properties of a material are one of the most important aspects to consider when targeting an application (Ramakrishna *et al*., 2001). For instance, due to its high mechanical

strength, P(3HB) is mostly considered for hard tissue engineering applications such as bone regeneration, where materials that can resist physiological stress are required. However, because of its mechanical properties, P(3HB) cannot be considered for other applications such as soft tissue engineering applications where soft and elastic materials are typically required. Furthermore, due to its high melting temperatures (170-180^{o}C), P(3HB) is usually processed at higher temperatures (close to 190^{o}C) which are close to its degradation temperatures. This not only causes changes in the molecular weight but also affects greatly the mechanical properties of the polymer (Tanadchangsaeng and Yu, 2015). Blending P(3HB) with other polymers has been a strategy used by many researchers to improve its mechanical properties, however, there is often a problem of miscibility between the components. Here we saw that besides conferring antibacterial properties to P(3HB), the addition of different weight percentages of TC improved significantly the flexibility and extensibility of the material. Additionally, it was also seen that the addition of different weight percentages of TC decreased the melting temperatures to values close to 150^{o}C, suggesting an increase in the window of temperatures in which P(3HB) could be processed. As future work and to enlarge the scope of applications of this material, being that as an antibacterial material or a general material for soft tissue engineering applications, it would be interesting to evaluate the changes in the mechanical and thermal properties of P(3HB) with other TC loadings than the ones used in this study. The main aim would be to explore in more detail the structure-function relationships of P(3HB)/TC materials and to obtain a library of P(3HB) with different mechanical and thermal properties so that they could be used in other applications for which usually these materials are not considered. Using as an example one of the materials developed in this thesis, that is, P(3HB) loaded with 11.5 wt% TC, it was observed that the material had a tensile strength of 14 MPa and an elongation at break of 54%. The tensile stress for articular cartilage ranges from 9 to 18 MPa and the elongation at break from 60 % to 120 %, the tensile stress for tendons and ligaments ranges from 10 to 15 MPa and the elongation at break from 50% to 100%, the tensile stress for skin ranges from 1 to 20 MPa and the elongation at break from 30% to 70% (Martin *et al*., 1998, Holzapfel, 2001). All the mechanical values indicated here suggest that P(3HB) loaded with 11.5 wt% TC could indeed be explored in the above-mentioned soft tissue engineering applications.

Another immediate conclusion was related to the results obtained with the thermal characterisation of the materials, where with higher loadings of TC, the presence of double

melting peaks were observed. Double melting peaks have been reported in many semi-crystalline materials during thermal analysis. This phenomenon can have many origins and a few models have been proposed to explain such findings. Most scientists explain the appearance of multiple melting peaks with the melt-recrystallisation model. This model proposes that at low temperatures, crystal populations that are formed with low degree of perfection can melt and recrystallise to more stable crystals during heating in a DCS thermal scanning, meaning that melting and crystallisation are competing during the heating process while more stable crystal populations are being generated leading to the presence of multiple melting peaks (Yasuniwa *et al*., 2003; Chen and Woo, 1995, Furushima *et al*., 2018). Although this could be an explanation as to why double-melting peaks were observed for P(3HB) materials with high loadings of TC, additional scans would be needed to assess the melting peaks nature. Additionally, a DSC scan of TC would perhaps help clarify these findings. Furthermore, SEM micrographs at higher magnification should be considered as they could provide information on miscibility and phase distribution, as well as on porosity of the materials. Such more in-depth characterisation of the materials would provide more insight to the changes occurring the in the physical properties of the materials.

In conjunction with this, further physicochemical characterisation steps and optimisation of the processing techniques used in this study should also be considered as future work. For instance, an important property when dealing with the synthesis of new polymers has to do with the assessment of the molecular weight of the polymers as it evaluates the reproducibility of the manufacturing techniques used to develop the materials. Therefore, molecular weight analysis should be conducted in each step of development of the materials, that is, since the moment it is synthesised by bacterial fermentation until it has been modified with the antibacterial agents to either ensure that the same properties are maintained in every batch, and if not, what could be the reasons behind such changes. Another way to ensure the reproducibility of the materials produced is to have a better control of the solvent casting process. One of the conclusions of this study was that the process of solvent casting was inconsistent as it was observed that by giving the same percentage of TC to a P(3HB) solution, the amount of TC that was entrapped in each film varied. This outcome suggested to be a consequence of not controlling parameters that greatly influence the solvent casting procedure such as the temperature and humidity. Such parameters will influence the drying rate of the solutions during film formation which in turn will influence for instance, the

thickness of a film. Not only does the thickness have a direct correlation with the mechanical properties, it also correlates with the amount of TC that gets entrapped in the polymer. Therefore, as future work, a precise control and optimisation of such parameters should be looked at in order to avoid variations in film formation and to be able to predict the response of each film, physically and biologically. In addition of having a better control of the solvent casting procedure, the stability of the materials as a function of time should also be looked at. Although a controlled and optimised process can ensure that the materials have the same physical properties after processing, these can inevitably change over time. As already mentioned before, TC is volatile, therefore it is important to consider its evaporation over time. This will not only have an impact in the physical properties as the blend composition will change, but also in the biological properties as the duration of the antibacterial action could be affected. Moreover, future work should also consider the study of sample storage and preservation as this is directly linked with all the above-mentioned aspects, that is, the changes in physical properties over time and its impact in the biological performance of the materials. Hence, a detailed physicochemical characterisation of the materials, the shelf-life of TC, the control of storage and preservation of the materials, as well as stability tests over time should be conducted to have a complete profile of the material for a defined period of time.

Device associated infections such as catheter-related bloodstream infection (CRBSI), VAP, and CAUTIs are the most frequent and costly infections found in healthcare systems. One strategy that has been used to mitigate this problem has been the development of medical devices that could elute antimicrobials, such as rifampicin and minocycline (Zhang and Wagner 2017). Such medical devices are usually designed to kill or inhibit bacterial growth. However, rather than developing a device that ultimately will lead to bacterial death, anti-adhesive and anti-biofilm strategies should also be considered. Firstly, because if medical devices cannot prevent bacterial adhesion, biofilm-growing bacteria will remain intact causing the contamination and infection of the surrounding tissues of the patients, secondly, because many severe chronic infections are related to the presence of biofilms, and thirdly because resistance is less likely to occur as anti-adhesive and anti-biofilm mechanisms of action lead to a lower selective pressure on bacteria than killing mechanisms. Therefore, having a medical device that can elute antimicrobials that are able to prevent bacterial adhesion and biofilm formation are of added value. In this study, it was shown that PU coated with P(3HB)/TC based coatings,

specifically, $PU_{10.13}$, was able to exert not only a biocidal effect, but also an anti-adhesive and anti-biofilm effect against *S. epidermidis* (ATCC® 35984™). Similarly to what was recommended before, a more in depth physicochemical characterisation of the materials assessing its properties over time, as well as the evaluation of the stability, storage and preservation conditions of the materials should be looked at. Likewise, a more detailed antibacterial characterisation should be conducted. For instance, in this work it was shown that the coated PU, more specifically, $PU_{10.13}$, was able to exert not only a biocidal effect, but also an anti-adhesive and anti-biofilm effect against *S. epidermidis* (ATCC® 35984™). However, the test was only performed after a 24-hour incubation period, with one bacterial strain, under static conditions. In order to verify if indeed this material could be used for short-term implantation periods, tests for longer incubation periods, under dynamic conditions and against other relevant pathogens should be done to evaluate if the same biocidal, anti-adhesive and anti-biofilm properties could still be verified because besides coagulase negative Staphylococci (e.g., *S. epidermidis*), there are other types of bacteria that are usually recovered from contaminated medical devices. For instance, *S. aureus* is often recovered from CVC's while *E. coli* is usually recovered from urinary catheters (Zhang and Wagner, 2017). Therefore, the materials developed in this study should also be tested against such relevant bacterial strains to check if these coatings could be applied to a range of medical devices. Additionally, it would be relevant to test the material against a panel of clinical isolates of the same strain to verify possible different susceptibilities. In terms of a more detailed cytotoxic evaluation of the materials there were two examples seen in this study that reinforce the need to re-design the cytotoxicity assessment of the materials in the future. The first example has to do with the fact that the ARROW catheters, which are medical devices used routinely in hospitals, showed cytotoxic and haemolytic effects against mammalian cells and the second example has to do with the contrasting results obtained for the PU coated materials with P(3HB)/TC where an absence of haemolysis as well as a lack of cell viability were observed. Concerning the first aspect, the biological evaluation of the ARROW catheters was done following the International Organisation for Standardisation (ISO) norms for the biological evaluation of cytotoxicity of medical devices and has shown a cytotoxic effect on mammalian cells. Additionally, the same materials caused the destruction of red blood cells when exposed to pre-diluted fresh blood. This automatically questioned the cytotoxicity and haemocompatibility of the material and led to the question of what tests were carried out

that led to the approval and use of such materials in clinics and hospitals. More specifically, what were the criteria for these materials to be tested *in vivo* and to further be explored in clinical trials. These types of questions bring us to the ultimate question that is, what should be the tests that in fact one should follow to ensure that the material is safe and can proceed to more advanced experimental stages? Concerning the second aspect in which PU coated materials with P(3HB)/TC showed that after a 24-hour period there was an absence of haemolysis, but a lack in cell viability, not many conclusions can be taken because of the duration of the assays as well as the limited amount of tests performed. The cell viability test was conducted using resazurin. Resazurin is a non-toxic, cell permeable compound which is actively converted to highly fluorescent compound resorufin by living cells. Although this method is relatively fast and inexpensive, one disadvantage of this method is related to the fact that test compounds can interfere with the fluorescence of the latter compound and hence, the toxicity can be overlooked. Moreover, since both tests were performed only for 24 hours, unclear answers as to the biocompatibility of the materials were obtained. On one hand, although a high cytotoxic signal was given, it could be that a minor percentage of surviving cells remained which would be able to proliferate over time, especially if one considers the volatility of TC. This means that over time, the concentration of TC would be lower and in turn this reduction could increase the chance for cells to survive.

When developing materials for biomedical applications, researchers should follow a compilation of the most relevant and complementary tests to evaluate the cytocompatibility of materials that will be in contact with tissues and blood. These can include, cell testing, haemocompatibility tests and immunomodulatory effects that occur from the interactions between immune cells and the biomaterial. Furthermore, the safety of the biodegradation products should also be examined. And not less important would be to look at protein adsorption on biomaterials as they are also related to platelet adhesion and its activation and consequent thrombus formation (Dawids, 2012). Besides knowing which tests should be performed to ensure that the materials are indeed not cytotoxic to tissue cells, a defined experimental design (e.g., time course) of the cytotoxicity assays should be considered. Also, since the cell type can affect the performance of the assay, more than one cell line should be evaluated. Therefore, as future work, the recommendations described above should be followed to have a compilation of information regarding the antibacterial and cytotoxic

performance of the materials, showing with certainty that it could further be tested in the selected application.

Another conclusion of this section has to do with the selected application and its relevance. Most natural materials are modified with antibacterial properties for wound dressing applications, however the scope of applications of natural-based antibacterial materials needs to be bigger. For instance, each year in the United States more than 2 million people contract infections by antibiotic resistant bacteria, with a minimum of 23,000 deaths as a direct result of such infections. The scenario in Europe is very similar with an average of 25,000 people dying because of resistant strains. This also results in increased economic costs due to longer hospitalisation periods. Multidrug-resistant bacteria in the EU are estimated to cause an economic loss of more than €1.5 billion each year. The Organisation for Economic Co-operation and Development (OECD) predicted a worsening of the situation by 2050 where it was estimated that more than 10 million people could die annually due to antibiotic resistant infections (Blair *et al*., 2015, de Kraker *et al*., 2016). These statistics not only highlight the incredibly high number of people that are affected by bacterial infections in hospital settings, but they also bring attention to the high number of medical devices that might be needed per patient as a result of the long hospitalisation periods. Catheters are used daily in large numbers and can have multiple functions. Catheters can either be used to drain fluids, urine or pus, they can be used as a source of intravenous drug administration, or even to measure blood pressure. Since catheters are used in large numbers and since they are one of the main sources of contamination of patients, focussing on strategies that prevent their contamination and the subsequent development of more serious infections, that for example are mediated by biofilms, should be extensively explored. In this study, we have indeed presented a possible strategy to help minimise this problem, by developing new possible bioactive coatings for medical devices such as catheters. Moreover, and very relevant, was the fact that the material developed had its bioactivity deriving from an agent as cheap as TC. As mentioned earlier, one of the most important aspects regarding the development of materials for biomedical applications is related to their cost. If on one hand we can try to improve the production of PHAs to minimise its associated costs, at the same time we can try to use antibacterial agents which can be easily found, that do not need any pre-treatment or pre-activation and that are cheap.

Finally, another aspect to consider is that, although there have been many attempts to develop antimicrobial coatings for catheters, only few are commercially available and many of them still remain in the clinical trial phase, due to cytotoxic problems, duration of antimicrobial activity, discomfort to patients caused for instance by allergic reactions, and the inherent problem of bacterial resistance (Singha *et al*., 2017). One of the few commercially available CVC catheters is the ARROW catheter used in this part of the work as a control. This catheter contains chlorohexidine and silver sulfadiazine as antimicrobials. On one hand, there have been reports stating that there are bacteria resistant to chlorohexidine and on the other hand, the excessive use of silver in a large number of healthcare products is becoming a great concern as its overuse might contribute for the emergence of bacterial resistance to silver (Kampf, 2016, Cieplik *et al*., 2019, Percival *et al*., 2005). Therefore, considering the rise of antimicrobial resistant bacteria it is always necessary to have either complementary or backup materials to aid in the fight of bacterial infection in medical settings. Our proof of principle study demonstrated that the idea of using P(3HB)/TC based materials for the development of bioactive releasing coatings for devices with short-term implantation periods could be a promising complementary approach to the existing strategies.

6.1.3 Part 3. Development of antibacterial P(3HO-co-3HD) materials: From 2D films to 3D fibrous scaffolds

In this part of the work, novel anti-adhesive and anti-biofilm materials were obtained by combining P(3HO-co-3HD) with different AMPs, termed AMP3, Nut2 and LL-37, and biofilm disrupting enzyme DB.

Overall, the anti-biofilm screening showed and confirmed the different behaviours of the agents against biofilms. On one hand, AMPs were capable of preventing biofilm formation and on the other hand, DB was capable of destroying pre-established biofilms. As mentioned before, bacterial adhesion and biofilm formation are closely related and one way to prevent biofilm formation is by interfering with bacterial adhesion. Therefore, having two classes of agents that acted effectively but differently against biofilms was of most interest to further explore the anti-adhesive properties of these agents.

One of the first conclusions that could be taken from this section was the fact that the initial antibacterial and cytotoxicity evaluation of the agents allowed to find the range of

concentrations of agents that should be adsorbed to the surface of P(3HO-co-3HD) allowing for cytocompatibility as well as effectiveness against bacteria. Additionally, the physicochemical characterisation, although limited, showed that the surface of P(3HO-co-3HD) had indeed been changed by the presence of the agents. Such promising results led to the development of P(3HO-co-3HD) fibres and its modification to yield antibacterial materials and indeed, by optimising the electrospinning conditions, slightly aligned P(3HO-co-3HD) based-fibres were successfully obtained and were reported here for the first time.

Additionally, further modification of the fibres, either by physical adsorption or by covalent coupling resulted in anti-adhesive and anti-biofilm P(3HO-co-3HD) based-fibres. Notwithstanding, a far more detailed characterisation of the fibres needs to be performed and it is here suggested as future work. For instance, SEM would allow to observe the morphology, fibre alignment as well as fibre diameter, which for some areas of TE are highly relevant. Furthermore, a mechanical and thermal characterisation of the fibres would also be of great importance to evaluate the strength of the material and to evaluate the maximum temperatures that this material could withstand before melting. For instance, chemical characterisation methods such as XPS or ATR-FTIR should be employed to detect the presence of the AMPs or DB on the fibres as well as its spatial topographical distribution. Surely a quantification of the amount of agent present in the fibres would also be very important to calculate. *In vitro* screening of the biodegradation profile would also be very important to evaluate the stability of the materials and finally an *in vitro* release profile of the antimicrobials should also be investigated. The compilation of information regarding the amounts of agent adsorbed plus the release kinetics would provide an idea of the durability of the action of the materials and would improve the interpretation of the biological results. Furthermore, this information would be crucial when optimising the process of agent adsorption as in fact a synergistic effect between the AMPs and DB could be achieved because as seen in this section, one of the outcomes was that the fibres modified with Nut2+DB did not show an enhancement in the anti-adhesive properties of the materials as the reduction in bacterial adhesion was similar to the one obtained for the fibres modified only with DB. However, in a study conducted by Gawande *et al*., it was observed that DB was in fact capable of enhancing the susceptibility of biofilm-forming bacteria to the synthetic AMP, KSL-W (Gawande *et al*., 2014). This shows the importance of having as much information as possible regarding the characterisation of the materials which could help define the correct ratio of AMPs and DB

that would result in the enhancement of the antibacterial properties of materials containing both types of agents. Moreover, such information could be of much use to develop materials with other agent combinations such as DB and LL-37 to act on Gram-negative bacteria as well as thus, increase the spectrum of activity of the materials.

A more in-depth chemical characterisation of the fibres coupled with NCO-sP(EO-stat-PO) would also be beneficial to understand the differences observed in the wettability of the materials. In the work described by Grafahrend *et al*., it was shown that when PLGA, a hydrophobic, synthetic and biodegradable polyester material, and NCO-sP(EO-stat-PO) were combined, the electrospun fibres resulting from this combination were hydrophilic. This change in wettability was explained by a surface segregation of the hydrophobic end-groups of the star-shaped polymer to the surface of the fibres (Grafahrend *et al*., 2011). However in our case, P(3HO-co-3HD) fibres, which were naturally hydrophobic, when combined with NCO-sP(EO-stat-PO) became even more hydrophobic. There are two possible explanations for this. On one hand, the additive in this case did not show a strong tendency for surface segregation, possibly due to a good miscibility of the additive with P(3HO-co-3HD). Or, on the other hand, in this case the deactivation of the isocyanate groups occurred. Isocyanate groups, NCO, are highly moisture-sensitive (Rolph *et al.,* 2016). The fact that the samples containing NCO-sP(EO-stat-PO) were prepared in acetone instead of dry acetone could have caused the deactivation of the NCO groups resulting in a material with similar wettability properties of P(3HO-co-3HD) fibres. Thus, as future work, the formation of urethane linkages should be characterised. This would not only confirm that the covalent grafting approach was successful but also that the NCO groups of the amphiphilic polymer were not deactivated. Additionally, blending directly the agents with P(3HO-co-HD) and then produce fibres out of this solution could be prepared to be used as control materials and to indeed verify if the presence of NCO-sP(EO-stat-PO) is dispensable or not. Another suggestion for future work comes with the need to explore the role of the wettability of a material with bacterial adhesion and biofilm formation. As mentioned before, tissue related cells tend to prefer hydrophilic surfaces while bacterial cells tend to prefer hydrophobic surfaces. Here it was seen that in fact the fibres with higher hydrophilicity yielded higher cell viabilities and at the same time prevented bacterial adhesion more efficiently, such as the case of P(3HO-co-3HD) fibres either modified with DB or functionalised with DB. It might be that the presence of DB on the fibres was not the sole aspect that contributed for these results, but it might be that the wettability characteristics of

the materials might have played a part in it too. Therefore, it could be that, in spite of using DB, which is an expensive enzyme, one could adsorb or couple less expensive relevant proteins, like cell adhesion mediators such as Gly-Arg-Gly-Asp-Ser-Pro (GRGDSP) peptide sequences which would not only promote cell attachment but in principle would render the materials more hydrophilic as a consequence of the introduction of polar groups. By modulating the ratio of the peptide to the polymer one could improve the biocompatibility of a material and at the same time possibly hinder bacterial adhesion due to the hydrophilic characteristics of the materials.

Another conclusion of this section was that indeed cells grew better when exposed to materials with a fibrous arrangement than when exposed to materials with a flat arrangement, supporting what has already been described in literature.

The development of anti-adhesive and anti-biofilm natural-based fibres derived from a novel biocompatible polymer opened the possibility of targeting new biomedical applications. These materials could be used in the form of patches or even medical device coatings. For instance, osteomyelitis is a condition where bones get infected and it is one of the most challenging chronic infections found in patients with open fractures and in patients requiring orthopaedic procedures. Usually, its treatment includes high doses of antibiotics for long periods of time, surgery and debridement. As an example, when bacteria infect a bone, the blood flow of the infected area decreases and necrotic bone or dead bone is formed, called the sequestrum. In cases where a sequestrum is formed, surgical debridement is carried out to remove the sequestrum but often other tissues are affected and can get damaged such as the periosteum. The periosteum is a membrane covering the bone structure which provides nutrients and also serves as a reservoir of mesenchymal stem cells. If the periosteum is not repaired after surgery, there is a delay in the healing process accompanied with lack of nutrients and a much slower and compromised regeneration process. Therefore, one of the applications of such anti-adhesive and anti-biofilm P(3HO-co-3HD) based-fibres meshes could be as a periosteum patch which would aid in the regenerative process and at the same time prevent further bacterial contaminations. Additionally, it sometimes happens that after the removal of the sequestrum, a large bone defect is present which is usually compensated by the introduction of intermedullary titanium nails. However, the prevention of infections is compromised as because of the absence of vacularisation, the antibiotics cannot reach this area (Berebichez-

Fridman *et al*., 2017). Therefore, one of the applications of the materials developed here could be as a coating of such nails.

The overall performance of the fibres showed that by exploring both techniques, that is, physical adsorption of the agents and covalent coupling of the agents, fibres with similar anti-adhesive, anti-biofilm and possibly cytocompatible properties were produced. Comparing both processes, on one hand, the process of chemical immobilisation is a one-step procedure that uses less amounts of active agents while the process of physical adsorption is a more time-consuming process which uses higher amounts of active agents. Another aspect is that perhaps since the agents are covalently coupled to the fibres in the first process, it might be that the washing-out of the agents is less likely to occur, which in turn might increase the antibacterial action of the materials. On the other hand, the process of physical adsorption process precludes the need of amphiphilic NCO-sP(EO-stat-PO) as a coupling mediator which might decrease the cost of the process. However, in order to verify which of the processes was in fact better, the characterisation steps mentioned earlier, such as the durability of the antibacterial action of the materials would need to be further explored in order to identify which of the processes yielded better results.

One of the premises considered in this part of the work was the "race for the surface" introduced by Anthony Gristina. Gristina suggested that tissue cells and bacterial cells compete for the surface of the implanted materials either to promote tissue cell integration or bacterial adhesion, respectively (Gristina, 1987). Therefore, to have a material that would effectively promote tissue cell adhesion and at the same time would impede bacterial adhesion would be extremely advantageous, especially when developing TE scaffolds. Therefore, based on our findings as future work it would be interesting to perform a co-culture of tissue cells and bacterial cells to observe whether the race would be won by the former type of cells.

In light of this, significant research still needs to be performed in order to develop ideal systems that are able to prevail over the intelligent bacterial machinery and to fight infections without triggering bacterial resistance. In addition to this, more *in vivo* studies should be conducted to get a better understanding of the biological behaviour of such materials in complex living models. Nonetheless, with our proof of principle study it was possible to develop a new class of polyhydroxyalkanoates with antibacterial properties and with different

structural designs that could be applied in clinical and medical settings for a more selective type of application. On one hand, P(3HB)/TC materials which appear to be cheaper to produce due to the cost of TC could be applied to improve or develop medical devices that are used daily but constitute a high source of bacterial contamination. On the other hand, materials with a more complex design and incorporated with more costly ingredients could be applied as scaffolds for the regeneration of tissues which not only are damaged but have a high chance of being contaminated by bacteria, serving as a support for tissue regeneration and at the same time prevention of bacterial adhesion and further tissue contamination.

7 References

A

- Absolom, D.R. and Neumann, A.W., 1987. Modification of substrate surface properties through protein adsorption. Colloids and surfaces, 30(1), pp.25-45.
- Absolom, D.R., Van Oss, C.J., Zingg, W. and Neumann, A.W., 1981. Determination of surface tensions of proteins II. Surface tension of serum albumin, altered at the protein-air interface. Biochimica et Biophysica Acta (BBA)-Protein Structure, 670(1), pp.74-78.
- Adochitei, A. and Drochioiu, G., 2011. Rapid characterization of peptide secondary structure by FT-IR spectroscopy. Rev Roum Chim, 56(8), pp.783-791.
- Affrossman, S., Jérôme, R., O'neill, S.A., Schmitt, T. and Stamm, M., 2000. Surface structure of thin film blends of polystyrene and poly (n-butyl methacrylate). Colloid and Polymer Science, 278(10), pp.993-999.
- Agarwal, S., Wendorff, J.H. and Greiner, A., 2008. Use of electrospinning technique for biomedical applications. Polymer, 49(26), pp.5603-5621.
- Albano, M., Crulhas, B.P., Alves, F.C.B., Pereira, A.F.M., Andrade, B.F.M.T., Barbosa, L.N., Furlanetto, A., da Silveira Lyra, L.P., Rall, V.L.M. and Júnior, A.F., 2019. Antibacterial and anti-biofilm activities of cinnamaldehyde against S. epidermidis. Microbial pathogenesis, 126, pp.231-238.
- Albuquerque, M.G.E., Eiroa, M., Torres, C., Nunes, B.R. and Reis, M.A.M., 2007. Strategies for the development of a side stream process for polyhydroxyalkanoate (PHA) production from sugar cane molasses. Journal of biotechnology, 130(4), pp.411-421.
- Allen, A.D., Anderson, W.A., Ayorinde, F.O. and Eribo, B.E., 2010. Biosynthesis and characterization of copolymer poly (3HB-co-3HV) from saponified Jatropha curcas oil by Pseudomonas oleovorans. Journal of industrial microbiology & biotechnology, 37(8), pp.849-856.
- Allesen-Holm, M., Barken, K.B., Yang, L., Klausen, M., Webb, J.S., Kjelleberg, S., Molin, S., Givskov, M. and Tolker-Nielsen, T., 2006. A characterization of DNA release in

Pseudomonas aeruginosa cultures and biofilms. *Molecular microbiology*, *59*(4), pp.1114-1128.

- Akaraonye, E., Keshavarz, T. and Roy, I., 2010. Production of polyhydroxyalkanoates: the future green materials of choice. Journal of Chemical Technology and Biotechnology, 85(6), pp.732-743.
- Amache, R., Sukan, A., Safari, M., Roy, I. and Keshavarz, T., 2013. Advances in PHAs production. *CHEMICAL ENGINEERING*, *32*.
- Amaro, M.M., Miguel, T., Rosa, F., Comi, G. and Iacumin, L., 2019. Prospects for the use of whey for polyhydroxyalkanoate (PHA) production. Frontiers in microbiology, 10, p.992.
- Anjum, A., Zuber, M., Zia, K.M., Noreen, A., Anjum, M.N. and Tabasum, S., 2016. Microbial production of polyhydroxyalkanoates (PHAs) and its copolymers: a review of recent advancements. International journal of biological macromolecules, 89, pp.161-174.
- Arjunan, N., Kumari, H.L.J., Singaravelu, C.M., Kandasamy, R. and Kandasamy, J., 2016. Physicochemical investigations of biogenic chitosan-silver nanocomposite as antimicrobial and anticancer agent. International journal of biological macromolecules, 92, pp.77-87.
- Avan, I., Hall, C.D. and Katritzky, A.R., 2014. Peptidomimetics via modifications of amino acids and peptide bonds. Chemical Society Reviews, 43(10), pp.3575-3594.
- Azari, P., Yahya, R., Wong, C.S. and Gan, S.N., 2014. Improved processability of electrospun poly [(R)-3-hydroxybutyric acid] through blending with medium-chain length poly (3-hydroxyalkanoates) produced by Pseudomonas putida from oleic acid. Materials Research Innovations, 18(sup6), pp.S6-345.

B

- Babinot, J., Guigner, J.M., Renard, E. and Langlois, V., 2012. A micellization study of medium chain length poly (3-hydroxyalkanoate)-based amphiphilic diblock copolymers. Journal of colloid and interface science, 375(1), pp.88-93.
- Bagdadi, A.V., Safari, M., Dubey, P., Basnett, P., Sofokleous, P., Humphrey, E., Locke, I., Edirisinghe, M., Terracciano, C., Boccaccini, A.R. and Knowles, J.C., 2018. Poly (3-

hydroxyoctanoate), a promising new material for cardiac tissue engineering. Journal of tissue engineering and regenerative medicine, 12(1), pp.e495-e512.

- Balouiri, M., Sadiki, M. and Ibnsouda, S.K., 2016. Methods for in vitro evaluating antimicrobial activity: A review. Journal of pharmaceutical analysis, 6(2), pp.71-79.
- Basnett, P., Ching, K.Y., Stolz, M., Knowles, J.C., Boccaccini, A.R., Smith, C., Locke, I.C. and Roy, I., 2013. Aspirin-loaded P (3HO)/P (3HB) blend films: potential materials for biodegradable drug-eluting stents. Bioinspired, Biomimetic and Nanobiomaterials, 2(3), pp.141-153.
- Basnett, P., 2014. Biosynthesis of polyhydroxyalkanoates, their novel blends and composites for biomedical applications (Doctoral dissertation, University of Westminster).
- Basnett, P., Lukasiewicz, B., Marcello, E., Gura, H.K., Knowles, J.C. and Roy, I., 2017. Production of a novel medium chain length poly (3-hydroxyalkanoate) using unprocessed biodiesel waste and its evaluation as a tissue engineering scaffold. Microbial biotechnology, 10(6), pp.1384-1399.
- Basnett, P., Mahalingam, S., Lukasiewicz, B., Harding, S., Edirisinghe, M. and Roy, I., 2016. Evaluation of porous polyhydroxyalkanoate (PHA) fibres as tissue engineering scaffold. Front. Bioeng. Biotechnol.
- Batoni, G., Maisetta, G. and Esin, S., 2015. Antimicrobial peptides and their interaction with biofilms of medically relevant bacteria. *Biochimica et Biophysica Acta (BBA)-Biomembranes*.
- Bazaka, K., Jacob, M.V., Chrzanowski, W. and Ostrikov, K., 2015. Anti-bacterial surfaces: natural agents, mechanisms of action, and plasma surface modification. Rsc Advances, 5(60), pp.48739-48759.
- Becker, K., Heilmann, C. and Peters, G., 2014. Coagulase-negative staphylococci. Clinical microbiology reviews, 27(4), pp.870-926.
- Berebichez-Fridman, R., Montero-Olvera, P., Gómez-García, R. and Berebichez-Fastlicht, E., 2017. An intramedullary nail coated with antibiotic and growth factor nanoparticles: An individualized state-of-the-art treatment for chronic osteomyelitis with bone defects. Medical hypotheses, 105, pp.63-68.
- Beveridge, T.J., 1999. Structures of gram-negative cell walls and their derived membrane vesicles. Journal of bacteriology, 181(16), pp.4725-4733.

- Blair, J.M., Webber, M.A., Baylay, A.J., Ogbolu, D.O. and Piddock, L.J., 2015. Molecular mechanisms of antibiotic resistance. Nature reviews microbiology, 13(1), p.42.
- Bocchinfuso, Gianfranco, Antonio Palleschi, Barbara Orioni, Giacinto Grande, Fernando Formaggio, Claudio Toniolo, Yoonkyung Park, Kyung-Soo Hahm, and Lorenzo Stella. "Different mechanisms of action of antimicrobial peptides: insights from fluorescence spectroscopy experiments and molecular dynamics simulations." Journal of peptide science: an official publication of the European Peptide Society 15, no. 9 (2009): 550-558.
- Bouhdid, S., Abrini, J., Amensour, M., Zhiri, A., Espuny, M.J. and Manresa, A., 2010. Functional and ultrastructural changes in Pseudomonas aeruginosa and Staphylococcus aureus cells induced by Cinnamomum verum essential oil. Journal of applied microbiology, 109(4), pp.1139-1149.
- Bourget, J.M., Guillemette, M., Veres, T., Auger, F.A. and Germain, L., 2013. Alignment of cells and extracellular matrix within tissue-engineered substitutes. Advances in biomaterials science and biomedical applications.
- Brancatisano, F.L., Maisetta, G., Di Luca, M., Esin, S., Bottai, D., Bizzarri, R., Campa, M. and Batoni, G., 2014. Inhibitory effect of the human liver-derived antimicrobial peptide hepcidin 20 on biofilms of polysaccharide intercellular adhesin (PIA)-positive and PIA-negative strains of Staphylococcus epidermidis. Biofouling, 30(4), pp.435-446.
- Brogden, K.A., 2005. Antimicrobial peptides: pore formers or metabolic inhibitors in bacteria?. Nature Reviews Microbiology, 3(3), pp.238-250.
- Brundle, C.R., Evans, C.A. and Wilson, S., 1992. Encyclopedia of materials characterization: surfaces, interfaces, thin films. Gulf Professional Publishing.
- Bueno, J., 2014. Anti-biofilm drug susceptibility testing methods: looking for new strategies against resistance mechanism. Journal of Microbial & Biochemical Technology S, 3(2).
- Bumgardner, J., Wiser, R., Elder, S.H., Jouett, R., Yang, Y. and Ong, J.L., 2003. Contact angle, protein adsorption and osteoblast precursor cell attachment to chitosan coatings bonded to titanium. Journal of Biomaterials Science, Polymer Edition, 14(12), pp.1401-1409.
- Busscher, H.J., van der Mei, H.C., Subbiahdoss, G., Jutte, P.C., van den Dungen, J.J., Zaat, S.A., Schultz, M.J. and Grainger, D.W., 2012. Biomaterial-associated infection:

locating the finish line in the race for the surface. Science translational medicine, 4(153), pp.153rv10-153rv10.

C

- Campoccia, D., Montanaro, L. and Arciola, C.R., 2013. A review of the biomaterials technologies for infection-resistant surfaces. *Biomaterials*,*34*(34), pp.8533-8554.
- Cao, Z. and Sun, Y., 2008. N-halamine-based chitosan: Preparation, characterization, and antimicrobial function. *Journal of Biomedical Materials Research Part A*, *85*(1), pp.99-107.
- Carretero, M., Escámez, M.J., García, M., Duarte, B., Holguín, A., Retamosa, L., Jorcano, J.L., Del Río, M. and Larcher, F., 2008. In vitro and in vivo wound healing-promoting activities of human cathelicidin LL-37. Journal of Investigative Dermatology, 128(1), pp.223-236.
- Cech, N.B., Junio, H.A., Ackermann, L.W., Kavanaugh, J.S. and Horswill, A.R., 2012. Quorum quenching and antimicrobial activity of goldenseal (Hydrastis canadensis) against methicillin-resistant Staphylococcus aureus (MRSA). *Planta medica*, *78*(14), pp.1556-1561.
- Cerca, N. and Jefferson, K.K., 2008. Effect of growth conditions on poly-N-acetylglucosamine expression and biofilm formation in Escherichia coli. FEMS microbiology letters, 283(1), pp.36-41.
- Chang, C.Y., Krishnan, T., Wang, H., Chen, Y., Yin, W.F., Chong, Y.M., Tan, L.Y., Chong, T.M. and Chan, K.G., 2014. Non-antibiotic quorum sensing inhibitors acting against N-acyl homoserine lactone synthase as druggable target. *Scientific reports*, *4*, p.7245.
- Chaudhry, W.N., Jamil, N., Ali, I., Ayaz, M.H. and Hasnain, S., 2011. Screening for polyhydroxyalkanoate (PHA)-producing bacterial strains and comparison of PHA production from various inexpensive carbon sources. Annals of microbiology, 61(3), pp.623-629.
- Chen, F., Gao, Y., Chen, X., Yu, Z. and Li, X., 2013. Quorum quenching enzymes and their application in degrading signal molecules to block quorum sensing-dependent infection. *International journal of molecular sciences*,*14*(9), pp.17477-17500.

- Chen, G.Q. and Wang, Y., 2013. Medical applications of biopolyesters polyhydroxyalkanoates. Chinese Journal of Polymer Science, 31(5), pp.719-736.
- Chen, W. and Tong, Y.W., 2012. PHBV microspheres as neural tissue engineering scaffold support neuronal cell growth and axon–dendrite polarization. Acta Biomaterialia, 8(2), pp.540-548.
- Chen, G.Q. and Wu, Q., 2005. The application of polyhydroxyalkanoates as tissue engineering materials. Biomaterials, 26(33), pp.6565-6578.
- Chen, G.Q., Hajnal, I., Wu, H., Lv, L. and Ye, J., 2015. Engineering biosynthesis mechanisms for diversifying polyhydroxyalkanoates. *Trends in biotechnology*, *33*(10), pp.565-574.
- Chen, C., Yu, C.H., Cheng, Y.C., Peter, H.F. and Cheung, M.K., 2006. Biodegradable nanoparticles of amphiphilic triblock copolymers based on poly (3-hydroxybutyrate) and poly (ethylene glycol) as drug carriers. Biomaterials, 27(27), pp.4804-4814.
- Chen, C.Y. and Woo, E.M., 1995. Some new evidence for polymorphism in cold-crystallized and melt-crystallized poly (ether ether ketone). Polymer journal, 27(4), pp.361-370.
- Chessa, D., Ganau, G., Spiga, L., Bulla, A., Mazzarello, V., Campus, G.V. and Rubino, S., 2016. Staphylococcus aureus and Staphylococcus epidermidis virulence strains as causative agents of persistent infections in breast implants. PloS one, 11(1), p.e0146668.
- Cho, K., Li, F. and Choi, J., 1999. Crystallization and melting behavior of polypropylene and maleated polypropylene blends. Polymer, 40(7), pp.1719-1729.
- Chu, Y.Y., Nega, M., Wölfle, M., Plener, L., Grond, S., Jung, K. and Götz, F., 2013. A new class of quorum quenching molecules from Staphylococcus species affects communication and growth of Gram-negative bacteria. *PLoS Pathog*, *9*(9), p.e1003654.
- Cieplik, F., Jakubovics, N.S., Buchalla, W., Maisch, T., Hellwig, E. and Al-Ahmad, A., 2019. Resistance Toward Chlorhexidine in Oral Bacteria–Is There Cause for Concern?. Frontiers in Microbiology, 10.
- Ciofu, O., Rojo-Molinero, E., Macià, M.D. and Oliver, A., 2017. Antibiotic treatment of biofilm infections. Apmis, 125(4), pp.304-319.

- Costerton, J.W., Stewart, P.S. and Greenberg, E.P., 1999. Bacterial biofilms: a common cause of persistent infections. Science, 284(5418), pp.1318-1322

D

- Dai, X., Guo, Q., Zhao, Y., Zhang, P., Zhang, T., Zhang, X. and Li, C., 2016. Functional Silver Nanoparticle as a Benign Antimicrobial Agent That Eradicates Antibiotic-Resistant Bacteria and Promotes Wound Healing. ACS applied materials & interfaces, 8(39), pp.25798-25807.
- Dal Pozzo, M., Silva Loreto, É., Flores Santurio, D., Hartz Alves, S., Rossatto, L., Castagna de Vargas, A., Viegas, J. and Matiuzzi da Costa, M., 2012. Antibacterial activity of essential oil of cinnamon and trans-cinnamaldehyde against Staphylococcus spp. isolated from clinical mastitis of cattle and goats. Acta scientiae veterinariae, 40(4).
- Darouiche, R.O., Mansouri, M.D., Gawande, P.V. and Madhyastha, S., 2009. Antimicrobial and antibiofilm efficacy of triclosan and DispersinB® combination. Journal of antimicrobial chemotherapy, 64(1), pp.88-93.
- Dawids, S. ed., 2012. Test procedures for the blood compatibility of biomaterials. Springer Science & Business Media.
- De Alwis, D.M., Dutton, R.L., Scharer, J. and Moo-Young, M., 2007. Statistical methods in media optimization for batch and fed-batch animal cell culture. Bioprocess and biosystems engineering, 30(2), pp.107-113.
- de la Fuente-Núñez, C., Reffuveille, F., Haney, E.F., Straus, S.K. and Hancock, R.E., 2014. Broad-spectrum anti-biofilm peptide that targets a cellular stress response. *PLoS Pathog*, *10*(5), p.e1004152.
- De Geyter, N., Morent, R. and Leys, C., 2008. Surface characterization of plasma-modified polyethylene by contact angle experiments and ATR-FTIR spectroscopy. Surface and Interface Analysis: An International Journal devoted to the development and application of techniques for the analysis of surfaces, interfaces and thin films, 40(3-4), pp.608-611.
- de Kraker, M.E., Stewardson, A.J. and Harbarth, S., 2016. Will 10 million people die a year due to antimicrobial resistance by 2050?. PLoS medicine, 13(11), p.e1002184.

- Delcour, A.H., 2009. Outer membrane permeability and antibiotic resistance. Biochimica et Biophysica Acta (BBA)-Proteins and Proteomics, 1794(5), pp.808-816.
- Dias, J., Pardelha, F., Eusébio, M., Reis, M.A. and Oliveira, R., 2009. On-line adaptive metabolic flux analysis: Application to PHB production by mixed microbial cultures. Biotechnology progress, 25(2), pp.390-398.
- Dinjaski, N., Fernández-Gutiérrez, M., Selvam, S., Parra-Ruiz, F.J., Lehman, S.M., San Román, J., García, E., García, J.L., García, A.J. and Prieto, M.A., 2014. PHACOS, a functionalized bacterial polyester with bactericidal activity against methicillin-resistant Staphylococcus aureus. *Biomaterials*,*35*(1), pp.14-24.
- Domadia, P., Swarup, S., Bhunia, A., Sivaraman, J. and Dasgupta, D., 2007. Inhibition of bacterial cell division protein FtsZ by cinnamaldehyde. Biochemical pharmacology, 74(6), pp.831-840.
- Donelli, G., Francolini, I., Romoli, D., Guaglianone, E., Piozzi, A., Ragunath, C. and Kaplan, J.B., 2007. Synergistic activity of dispersin B and cefamandole nafate in inhibition of staphylococcal biofilm growth on polyurethanes. Antimicrobial agents and chemotherapy, 51(8), pp.2733-2740.
- Donlan, R.M. and Costerton, J.W., 2002. Biofilms: survival mechanisms of clinically relevant microorganisms. Clinical microbiology reviews, 15(2), pp.167-193.
- Donlan, R.M., 2002. Biofilms: microbial life on surfaces. Emerging infectious diseases, 8(9), p.881.
- Dowben, P.A., Miller, A.H. and Vook, R.W., 1987. Surface segregation from gold alloys. *Gold Bulletin*, *20*(3), pp.54-65.
- Doyle, R.J., 2000. Contribution of the hydrophobic effect to microbial infection. Microbes and infection, 2(4), pp.391-400.

E

- Ebbensgaard, A., Mordhorst, H., Overgaard, M.T., Nielsen, C.G., Aarestrup, F.M. and Hansen, E.B., 2015. Comparative evaluation of the antimicrobial activity of different antimicrobial peptides against a range of pathogenic bacteria. *PloS one*, *10*(12), p.e0144611.

- Escapa, I.F., Morales, V., Martino, V.P., Pollet, E., Avérous, L., García, J.L. and Prieto, M.A., 2011. Disruption of β-oxidation pathway in Pseudomonas putida KT2442 to produce new functionalized PHAs with thioester groups. Applied microbiology and biotechnology, 89(5), pp.1583-1598.
- ESCAPA, I.F., Ruiz, M.D.V.M., Lopez, J.L.G. and Jimenez, M.A.P., Consejo Superior De Investigaciones Científicas (Csic), 2011b. Synthesis of polyhydroxyalkanoates (pha) with thioester groups in the side chain. U.S. Patent Application 13/825,447.
- Estrela, A.B., Heck, M.G. and Abraham, W.R., 2009. Novel approaches to control biofilm infections. *Current medicinal chemistry*, *16*(12), pp.1512-1530.
- Etienne, O., Picart, C., Taddei, C., Haikel, Y., Dimarcq, J.L., Schaaf, P., Voegel, J.C., Ogier, J.A. and Egles, C., 2004. Multilayer polyelectrolyte films functionalized by insertion of defensin: a new approach to protection of implants from bacterial colonization. *Antimicrobial agents and chemotherapy*,*48*(10), pp.3662-3669.
- Everett, J.A. and Rumbaugh, K.P. (2015) 'Biofilms, quorum sensing and Crosstalk in medically important microbes', in Molecular Medical Microbiology. Elsevier BV, pp. 235–247.

F

- Foster, T., 1996. Staphylococcus. In Medical Microbiology. 4th edition. University of Texas Medical Branch at Galveston.
- Fryczkowski, R. and Kowalczyk, T., 2009. Nanofibres from polyaniline/polyhydroxybutyrate blends. Synthetic Metals, 159(21-22), pp.2266-2268.
- Fuller, F.W., 2009. The side effects of silver sulfadiazine. Journal of burn care & research, 30(3), pp.464-470.
- Furushima, Y., Schick, C. and Toda, A., 2018. Crystallization, recrystallization, and melting of polymer crystals on heating and cooling examined with fast scanning calorimetry. Polymer Crystallization, 1(2), p.e10005.

G

- García-Contreras, R., Maeda, T. and Wood, T.K., 2016. Can resistance against quorum-sensing interference be selected&quest. *The ISME journal*,*10*(1), pp.4-10.

- García-García, J.M., López, L., París, R., Núñez-López, M.T., Quijada-Garrido, I., de la Peña Zarzuelo, E. and Garrido, L., 2012. Surface modification of poly (3-hydroxybutyrate-co-3-hydroxyvalerate) copolymer films for promoting interaction with bladder urothelial cells. Journal of Biomedical Materials Research Part A, 100(1), pp.7-17.
- Gawande, P.V., Leung, K.P. and Madhyastha, S., 2014. Antibiofilm and antimicrobial efficacy of DispersinB®-KSL-W peptide-based wound gel against chronic wound infection associated bacteria. Current microbiology, 68(5), pp.635-641.
- Gomes, C., Moreira, R.G. and Castell-Perez, E., 2011. Poly (DL-lactide-co-glycolide)(PLGA) nanoparticles with entrapped trans-cinnamaldehyde and eugenol for antimicrobial delivery applications. Journal of Food Science,76(2), pp.N16-N24.
- González, J.E. and Keshavan, N.D., 2006. Messing with bacterial quorum sensing. *Microbiology and Molecular Biology Reviews*, *70*(4), pp.859-875.
- Götz, F., 2002. Staphylococcus and biofilms. Molecular microbiology, 43(6), pp.1367-1378.
- Grafahrend, D., Heffels, K.H., Beer, M.V., Gasteier, P., Möller, M., Boehm, G., Dalton, P.D. and Groll, J., 2011. Degradable polyester scaffolds with controlled surface chemistry combining minimal protein adsorption with specific bioactivation. Nature materials, 10(1), p.67.
- Grage, K., Jahns, A.C., Parlane, N., Palanisamy, R., Rasiah, I.A., Atwood, J.A. and Rehm, B.H., 2009. Bacterial polyhydroxyalkanoate granules: biogenesis, structure, and potential use as nano-/micro-beads in biotechnological and biomedical applications. Biomacromolecules, 10(4), pp.660-669.
- Gottenbos, B., Busscher, H.J., Van Der Mei, H.C. and Nieuwenhuis, P., 2002. Pathogenesis and prevention of biomaterial centered infections. Journal of Materials Science: Materials in Medicine, 13(8), pp.717-722.
- Gristina, A.G., 1987. Biomaterial-centered infection: microbial adhesion versus tissue integration. Science, 237(4822), pp.1588-1595.
- Gristina, A.G., Naylor, P. and Myrvik, Q., 1988. Infections from biomaterials and implants: a race for the surface. Medical progress through technology, 14(3-4), pp.205-224.

H

- Hacker, M.C., Krieghoff, J. and Mikos, A.G., 2019. Synthetic polymers. In Principles of regenerative medicine (pp. 559-590). Academic Press.
- Hacking, A.J., Taylor, I.W.F., Jarman, T.R. and Govan, J.R.W., 1983. Alginate biosynthesis by Pseudomonas mendocina. Microbiology, 129(11), pp.3473-3480.
- Hanai, K., Kuwae, A., Takai, T., Senda, H. and Kunimoto, K.K., 2001. A comparative vibrational and NMR study of cis-cinnamic acid polymorphs and trans-cinnamic acid. Spectrochimica Acta Part A: Molecular and Biomolecular Spectroscopy, 57(3), pp.513-519.
- Hancock, R.E. and Sahl, H.G., 2006. Antimicrobial and host-defense peptides as new anti-infective therapeutic strategies. Nature biotechnology, 24(12), pp.1551-1557.
- Hayati, A.N., Hosseinalipour, S.M., Rezaie, H.R. and Shokrgozar, M.A., 2012. Characterization of poly (3-hydroxybutyrate)/nano-hydroxyapatite composite scaffolds fabricated without the use of organic solvents for bone tissue engineering applications. Materials Science and Engineering: C, 32(3), pp.416-422.
- Hazer, D.B., Kılıçay, E. and Hazer, B., 2012. Poly (3-hydroxyalkanoate) s: diversification and biomedical applications: a state of the art review. Materials Science and Engineering: C, 32(4), pp.637-647.
- He, Y., Hu, Z., Ren, M., Ding, C., Chen, P., Gu, Q. and Wu, Q., 2014. Evaluation of PHBHHx and PHBV/PLA fibers used as medical sutures. Journal of Materials Science: Materials in Medicine, 25(2), pp.561-571.
- Heilborn, J.D., Nilsson, M.F., Sørensen, O., Ståhle-Bäckdahl, M., Kratz, G., Weber, G. and Borregaard, N., 2003. The cathelicidin anti-microbial peptide LL-37 is involved in re-epithelialization of human skin wounds and is lacking in chronic ulcer epithelium. Journal of Investigative Dermatology, 120(3), pp.379-389.
- Hinüber, C., Häussler, L., Vogel, R., Brünig, H., Heinrich, G. and Werner, C., 2011. Hollow fibers made from a poly (3-hydroxybutyrate)/poly-ε-caprolactone blend. Express Polymer Letters, 5(7), pp.643-652.
- Hlady, V. and Buijs, J., 1996. Protein adsorption on solid surfaces. Current Opinion in Biotechnology, 7(1), pp.72-77.

- Hogan, C.M., 2010. Bacteria. *Encyclopaedia of Earth. Washington DC: National Council for Science and the Environment.*
- Hogan, S., Zapotoczna, M., Stevens, N.T., Humphreys, H., O'Gara, J.P. and O'Neill, E., 2017. Potential use of targeted enzymatic agents in the treatment of Staphylococcus aureus biofilm-related infections. Journal of Hospital Infection, 96(2), pp.177-182.
- Hoefer, P., 2010. Activation of polyhydroxyalkanoates: functionalization and modification. Frontiers in bioscience (Landmark edition), 15, pp.93-121.
- Holzapfel, G.A., 2001. Biomechanics of soft tissue. The handbook of materials behavior models, 3, pp.1049-1063.
- Hu, S.G., Jou, C.H. and Yang, M.C., 2003. Antibacterial and biodegradable properties of polyhydroxyalkanoates grafted with chitosan and chitooligosaccharides via ozone treatment. Journal of Applied Polymer Science, 88(12), pp.2797-2803.
- Hufenus, R., Reifler, F.A., Maniura-Weber, K., Zinn, M., Spierings, A. and Hänggi, U.J., Biodegradable Fibers from Renewable Sources: Melt Spinning of Polyhydroxyalkanoates (PHAs).
- Humblot, V., Yala, J.F., Thebault, P., Boukerma, K., Héquet, A., Berjeaud, J.M. and Pradier, C.M., 2009. The antibacterial activity of Magainin I immobilized onto mixed thiols Self-Assembled Monolayers. Biomaterials, 30(21), pp.3503-3512.
- Hume, E.B.H., Baveja, J., Muir, B., Schubert, T.L., Kumar, N., Kjelleberg, S., Griesser, H.J., Thissen, H., Read, R., Poole-Warren, L.A. and Schindhelm, K., 2004. The control of Staphylococcus epidermidis biofilm formation and *in vivo* infection rates by covalently bound furanones.Biomaterials, 25(20), pp.5023-5030.

I

- Inouye, S., Takizawa, T. and Yamaguchi, H., 2001. Antibacterial activity of essential oils and their major constituents against respiratory tract pathogens by gaseous contact. Journal of antimicrobial chemotherapy, 47(5), pp.565-573.
- ISO 20776-1:2006(E), First edition 2006-11-15. Clinical laboratory testing and in vitro diagnostic test systems — Susceptibility testing of infectious agents and evaluation of performance of antimicrobial susceptibility test devices.

- ISO 10993-5:2009(E), Third edition 2009-06-01. Biological evaluation of medical devices.
- Itoh, Y., Wang, X., Hinnebusch, B.J., Preston, J.F. and Romeo, T., 2005. Depolymerization of β-1, 6-N-acetyl-D-glucosamine disrupts the integrity of diverse bacterial biofilms. Journal of bacteriology, 187(1), pp.382-387.
- Izano, E.A., Wang, H., Ragunath, C., Ramasubbu, N. and Kaplan, J.B., 2007. Detachment and killing of Aggregatibacter actinomycetemcomitans biofilms by dispersin B and SDS. Journal of dental research, 86(7), pp.618-622.
- Izano, E.A., Amarante, M.A., Kher, W.B. and Kaplan, J.B., 2008. Differential roles of poly-N-acetylglucosamine surface polysaccharide and extracellular DNA in Staphylococcus aureus and Staphylococcus epidermidis biofilms. Applied and environmental microbiology, 74(2), pp.470-476.

J

- Jakobsen, T.H., van Gennip, M., Phipps, R.K., Shanmugham, M.S., Christensen, L.D., Alhede, M., Skindersoe, M.E., Rasmussen, T.B., Friedrich, K., Uthe, F. and Jensen, P.Ø., 2012. Ajoene, a sulfur-rich molecule from garlic, inhibits genes controlled by quorum sensing. Antimicrobial agents and chemotherapy, 56(5), pp.2314-2325.
- Junyu, Z., Shishatskaya, E.I., Volova, T.G., da Silva, L.F. and Chen, G.Q., 2018. Polyhydroxyalkanoates (PHA) for therapeutic applications. Materials Science and Engineering: C.
- Jurasek, L. and Marchessault, R.H., 2002. The role of phasins in the morphogenesis of poly (3-hydroxybutyrate) granules. Biomacromolecules, 3(2), pp.256-261.

K

- K Bhardwaj, A., Vinothkumar, K. and Rajpara, N., 2013. Bacterial quorum sensing inhibitors: attractive alternatives for control of infectious pathogens showing multiple drug resistance. *Recent patents on anti-infective drug discovery*, *8*(1), pp.68-83.
- Kabilan, S., Ayyasamy, M., Jayavel, S. and Paramasamy, G., 2012. Pseudomonas sp. as a source of medium chain length polyhydroxyalkanoates for controlled drug delivery: perspective. International journal of microbiology, 2012.

- Kalia, S. and Avérous, L., 2016. *Biodegradable and Biobased Polymers for Environmental and Biomedical Applications*. John Wiley & Sons
- Kalia, V.C., 2013. Quorum sensing inhibitors: an overview. *Biotechnology advances*, *31*(2), pp.224-245.
- Kampf, G., 2016. Acquired resistance to chlorhexidine–is it time to establish an 'antiseptic stewardship'initiative?. Journal of Hospital Infection, 94(3), pp.213-227.
- Kannan, L.V. and Rehacek, Z., 1970. Formation of poly-beta-hydroxybutyrate by Actinomycetes. Indian journal of biochemistry, 7(2), pp.126-129.
- Kaplan, J.B., Ragunath, C., Ramasubbu, N. and Fine, D.H., 2003. Detachment of Actinobacillus actinomycetemcomitans biofilm cells by an endogenous β-hexosaminidase activity. Journal of bacteriology, 185(16), pp.4693-4698.
- Kaplan, J.B., 2009. Therapeutic potential of biofilm-dispersing enzymes. The International journal of artificial organs, 32(9), pp.545-554.
- Kaplan, J.Á., 2010. Biofilm dispersal: mechanisms, clinical implications, and potential therapeutic uses. Journal of dental research, 89(3), pp.205-218.
- Kaplan, J.B., Ragunath, C., Velliyagounder, K., Fine, D.H. and Ramasubbu, N., 2004. Enzymatic detachment of Staphylococcus epidermidis biofilms. Antimicrobial agents and chemotherapy, 48(7), pp.2633-2636.
- Karahaliloğlu, Z., Demirbilek, M., Şam, M., Sağlam, N., Mızrak, A.K. and Denkbaş, E.B., 2016. Surface-modified bacterial nanofibrillar PHB scaffolds for bladder tissue repair. Artificial cells, nanomedicine, and biotechnology, 44(1), pp.74-82.
- Katsikogianni, M. and Missirlis, Y.F., 2004. Concise review of mechanisms of bacterial adhesion to biomaterials and of techniques used in estimating bacteria-material interactions. Eur Cell Mater, 8(3), pp.37-57.
- Kenar, H., Kose, G.T. and Hasirci, V., 2010. Design of a 3D aligned myocardial tissue construct from biodegradable polyesters. Journal of Materials Science: Materials in Medicine, 21(3), pp.989-997.
- Keshavarz, T. and Roy, I., 2010. Polyhydroxyalkanoates: bioplastics with a green agenda. Current opinion in microbiology, 13(3), pp.321-326.
- Khanna, S. and Srivastava, A.K., 2005. Recent advances in microbial polyhydroxyalkanoates. Process Biochemistry, 40(2), pp.607-619.

- Kim, Y.S., Kim, H.W., Lee, S.H., Shin, K.S., Hur, H.W. and Rhee, Y.H., 2007. Preparation of alginate–quaternary ammonium complex beads and evaluation of their antimicrobial activity. International journal of biological macromolecules, 41(1), pp.36-41.
- Kim, Y.G., Lee, J.H., Kim, S.I., Baek, K.H. and Lee, J., 2015. Cinnamon bark oil and its components inhibit biofilm formation and toxin production. International journal of food microbiology, 195, pp.30-39.
- Kiran, M.D., Adikesavan, N.V., Cirioni, O., Giacometti, A., Silvestri, C., Scalise, G., Ghiselli, R., Saba, V., Orlando, F., Shoham, M. and Balaban, N., 2008. Discovery of a quorum-sensing inhibitor of drug-resistant staphylococcal infections by structure-based virtual screening. Molecular pharmacology, 73(5), pp.1578-1586.
- Klamt, S., Saez-Rodriguez, J. and Gilles, E.D., 2007. Structural and functional analysis of cellular networks with CellNetAnalyzer. BMC systems biology, 1(1), p.2.
- Knight, E. and Przyborski, S., 2015. Advances in 3D cell culture technologies enabling tissue-like structures to be created in vitro. Journal of anatomy, 227(6), pp.746-756.
- Koleske, J.V., 2006. Mechanical properties of solid coatings. Encyclopedia of Analytical Chemistry: Applications, Theory and Instrumentation.
- Koller, M., 2018. Biodegradable and biocompatible polyhydroxy-alkanoates (PHA): Auspicious microbial macromolecules for pharmaceutical and therapeutic applications. Molecules, 23(2), p.362.
- Köse, G.T., Kenar, H., Hasırcı, N. and Hasırcı, V., 2003. Macroporous poly (3-hydroxybutyrate-co-3-hydroxyvalerate) matrices for bone tissue engineering. Biomaterials, 24(11), pp.1949-1958.
- Krimm, S. and Bandekar, J., 1986. Vibrational spectroscopy and conformation of peptides, polypeptides, and proteins. In Advances in protein chemistry (Vol. 38, pp. 181-364). Academic Press.

L

- Lampin, M., Warocquier-Clérout, R., Legris, C., Degrange, M. and Sigot-Luizard, M.F., 1997. Correlation between substratum roughness and wettability, cell adhesion, and

cell migration. Journal of Biomedical Materials Research: An Official Journal of The Society for Biomaterials and The Japanese Society for Biomaterials, 36(1), pp.99-108.

- Landel, R.F. and Nielsen, L.E., 1993. Mechanical properties of polymers and composites. CRC press.
- LaSarre, B. and Federle, M.J., 2013. Exploiting quorum sensing to confuse bacterial pathogens. *Microbiology and Molecular Biology Reviews*, *77*(1), pp.73-111.
- Law, K.Y., 2014. Definitions for hydrophilicity, hydrophobicity, and superhydrophobicity: getting the basics right.
- Lebeaux, D., Ghigo, J.M. and Beloin, C., 2014. Biofilm-related infections: bridging the gap between clinical management and fundamental aspects of recalcitrance toward antibiotics. Microbiology and Molecular Biology Reviews, 78(3), pp.510-543.
- Lee, W. and Lee, D.G., 2014. Magainin 2 induces bacterial cell death showing apoptotic properties. Current microbiology, 69(6), pp.794-801.
- Lee, J. and Lee, D.G., 2015. Antimicrobial Peptides (AMPs) with Dual Mechanisms: Membrane Disruption and Apoptosis. *Journal of microbiology and biotechnology*, *25*(6), pp.759-764.
- Lee, S.Y., 1996. Bacterial polyhydroxyalkanoates. Biotechnology and bioengineering, 49(1), pp.1-14.
- Lee, M.S., Lee, S.H., Ma, Y.H., Park, S.K., Bae, D.H., Ha, S.D. and Song, K.B., 2005. Effect of plasticizer and cross-linking agent on the physical properties of protein films. Preventive Nutrition and Food Science, 10(1), pp.88-91.
- Leng, Y., 2009. Materials characterization: introduction to microscopic and spectroscopic methods. John Wiley & Sons.
- Levy, S.B. and Marshall, B., 2004. Antibacterial resistance worldwide: causes, challenges and responses. Nature medicine, 10(12s), p.S122.
- Lewis, K., 2001. Riddle of biofilm resistance. Antimicrobial agents and chemotherapy, 45(4), pp.999-1007.
- Li, Z., Yang, J. and Loh, X.J., 2016. Polyhydroxyalkanoates: opening doors for a sustainable future. NPG Asia Materials, 8(4), p.e265.
- Lin, Y.H., Xu, J.L., Hu, J., Wang, L.H., Ong, S.L., Leadbetter, J.R. and Zhang, L.H., 2003. Acyl-homoserine lactone acylase from Ralstonia strain XJ12B represents a novel and

potent class of quorum-quenching enzymes. Molecular microbiology, 47(3), pp.849-860.

- Lin, M.H., Shu, J.C., Lin, L.P., yu Chong, K., Cheng, Y.W., Du, J.F. and Liu, S.T., 2015. Elucidating the crucial role of poly N-acetylglucosamine from Staphylococcus aureus in cellular adhesion and pathogenesis. PloS one, 10(4), p.e0124216.
- Linthorne, J.S., Chang, B.J., Flematti, G.R., Ghisalberti, E.L. and Sutton, D.C., 2015. A Direct Pre-screen for Marine Bacteria Producing Compounds Inhibiting Quorum Sensing Reveals Diverse Planktonic Bacteria that are Bioactive. *Marine Biotechnology*, *17*(1), pp.33-42.
- Lister, J.L. and Horswill, A.R., 2015. Staphylococcus aureus biofilms: recent developments in biofilm dispersal. *Biofilm formation by staphylococci and streptococci: Structural, functional and regulatory aspects and implications for pathogenesis*.
- Liu, Y., Li, L., Li, X., Wang, Y., Ren, X. and Liang, J., 2015. Antibacterial Modification of Microcrystalline Cellulose by Grafting Copolymerization. BioResources, 11(1), pp.519-529.
- Lu, X.F. and Hay, J.N., 2001. Isothermal crystallization kinetics and melting behaviour of poly (ethylene terephthalate). Polymer, 42(23), pp.9423-9431.
- Lui, L.T., Xue, X., Sui, C., Brown, A., Pritchard, D.I., Halliday, N., Winzer, K., Howdle, S.M., Fernandez-Trillo, F., Krasnogor, N. and Alexander, C., 2013. Bacteria clustering by polymers induces the expression of quorum-sensing-controlled phenotypes. Nature chemistry, 5(12), pp.1058-1065.
- Lukasiewicz, B., Basnett, P., Nigmatullin, R., Matharu, R., Knowles, J.C. and Roy, I., 2018. Binary polyhydroxyalkanoate systems for soft tissue engineering. Acta biomaterialia, 71, pp.225-234.

M

- Maathuis, P.G.M., Bulstra, S.K., Van der Mei, H.C., van Horn, J.R. and Busscher, H.J., 2007. Biomaterial-associated surgery and infection a review of literature. Detection, prevention and direct post-operative intervention in orthopaedic implant infection, p.17.

- Magana, M., Sereti, C., Ioannidis, A., Mitchell, C.A., Ball, A.R., Magiorkinis, E., Chatzipanagiotou, S., Hamblin, M.R., Hadjifrangiskou, M. and Tegos, G.P., 2018. Options and Limitations in Clinical Investigation of Bacterial Biofilms. Clinical microbiology reviews, 31(3), pp.e00084-16.
- Marcano, A., Ba, O., Thebault, P., Crétois, R., Marais, S. and Duncan, A.C., 2015. Elucidation of innovative antibiofilm materials. *Colloids and Surfaces B: Biointerfaces*, *136*, pp.56-63.
- Martin, R.B., Burr, D.B., Sharkey, N.A. and Fyhrie, D.P., 1998. Skeletal tissue mechanics (Vol. 190). New York: Springer.
- Mathuriya, A.S. and Yakhmi, J.V., 2017. Polyhydroxyalkanoates: Biodegradable Plastics and Their Applications. Handbook of Ecomaterials, pp.1-29.
- Matsuyama, H., Takida, Y., Maki, T. and Teramoto, M., 2002. Preparation of porous membrane by combined use of thermally induced phase separation and immersion precipitation. Polymer, 43(19), pp.5243-5248.
- Matuschek, E., Brown, D.F. and Kahlmeter, G., 2014. Development of the EUCAST disk diffusion antimicrobial susceptibility testing method and its implementation in routine microbiology laboratories. Clinical Microbiology and Infection, 20(4), pp.O255-O266.
- McDougald, D., Rice, S.A., Barraud, N., Steinberg, P.D. and Kjelleberg, S., 2012. Should we stay or should we go: mechanisms and ecological consequences for biofilm dispersal. Nature Reviews Microbiology, 10(1), pp.39-50.
- Meireles, A., Borges, A., Giaouris, E. and Simões, M., 2016. The current knowledge on the application of anti-biofilm enzymes in the food industry. Food Research International, 86, pp.140-146.
- Meyers, M.A. and Chawla, K.K., 2008. Mechanical behavior of materials. Cambridge university press.
- Miller, G.L., 1959. Use of dinitrosalicylic acid reagent for determination of reducing sugar. Analytical chemistry, 31(3), pp.426-428.
- Mohammed Sakr, M., Mohamed Anwar Aboshanab, K., Mabrouk Aboulwafa, M. and Abdel-Haleem Hassouna, N., 2013. Characterization and complete sequence of lactonase enzyme from Bacillus weihenstephanensis isolate P65 with potential activity against acyl homoserine lactone signal molecules.BioMed research international, 2013.

- Mohanna, P.N., Young, R.C., Wiberg, M. and Terenghi, G., 2003. A composite poly-hydroxybutyrate–glial growth factor conduit for long nerve gap repairs. Journal of anatomy, 203(6), pp.553-565.
- Możejko-Ciesielska, J. and Kiewisz, R., 2016. Bacterial polyhydroxyalkanoates: still fabulous?. Microbiological research, 192, pp.271-282.
- Muangwong, A., Boontip, T., Pachimsawat, J. and Napathorn, S.C., 2016. Medium chain length polyhydroxyalkanoates consisting primarily of unsaturated 3-hydroxy-5-cis-dodecanoate synthesized by newly isolated bacteria using crude glycerol. Microbial cell factories, 15(1), p.55.
- Murugan, R. and Ramakrishna, S., 2007. Design strategies of tissue engineering scaffolds with controlled fiber orientation. Tissue engineering, 13(8), pp.1845-1866.
- Muszanska, A.K., Busscher, H.J., Herrmann, A., van der Mei, H.C. and Norde, W., 2011. Pluronic–lysozyme conjugates as anti-adhesive and antibacterial bifunctional polymers for surface coating. Biomaterials, 32(26), pp.6333-6341.

N

- Navarre, W.W. and Schneewind, O., 1999. Surface proteins of gram-positive bacteria and mechanisms of their targeting to the cell wall envelope. Microbiol. Mol. Biol. Rev., 63(1), pp.174-229.
- Nieto-Bobadilla, M.S., Siepmann, F., Djouina, M., Dubuquoy, L., Tesse, N., Willart, J.F., Dubreuil, L., Siepmann, J. and Neut, C., 2015. Controlled delivery of a new broad spectrum antibacterial agent against colitis: In vitro and in vivo performance. European Journal of Pharmaceutics and Biopharmaceutics, 96, pp.152-161.
- Nigmatullin, R., Thomas, P., Lukasiewicz, B., Puthussery, H. and Roy, I., 2015. Polyhydroxyalkanoates, a family of natural polymers, and their applications in drug delivery. Journal of Chemical Technology and Biotechnology, 90(7), pp.1209-1221.
- Nikaido, H., 1988. Bacterial resistance to antibiotics as a function of outer membrane permeability. Journal of Antimicrobial Chemotherapy, 22(Supplement_A), pp.17-22.
- Niu, C., Afre, S. and Gilbert, E.S., 2006. Subinhibitory concentrations of cinnamaldehyde interfere with quorum sensing. Letters in applied microbiology, 43(5), pp.489-494.

- Nostro, A., Scaffaro, R., D'Arrigo, M., Botta, L., Filocamo, A., Marino, A. and Bisignano, G., 2012. Study on carvacrol and cinnamaldehyde polymeric films: mechanical properties, release kinetics and antibacterial and antibiofilm activities. Applied microbiology and biotechnology, 96(4), pp.1029-1038.
- Novikov, L.N., Novikova, L.N., Mosahebi, A., Wiberg, M., Terenghi, G. and Kellerth, J.O., 2002. A novel biodegradable implant for neuronal rescue and regeneration after spinal cord injury. Biomaterials, 23(16), pp.3369-3376.

O

- O'grady, N.P., Alexander, M., Burns, L.A., Dellinger, E.P., Garland, J., Heard, S.O., Lipsett, P.A., Masur, H., Mermel, L.A., Pearson, M.L. and Raad, I.I., 2011. Summary of recommendations: guidelines for the prevention of intravascular catheter-related infections. Clinical Infectious Diseases, 52(9), pp.1087-1099.
- Onaizi, S.A. and Leong, S.S., 2011. Tethering antimicrobial peptides: current status and potential challenges. Biotechnology advances, 29(1), pp.67-74.
- Otto, M., 2009. Staphylococcus epidermidis—the'accidental'pathogen. Nature reviews microbiology, 7(8), p.555.
- Overhage, J., Campisano, A., Bains, M., Torfs, E.C., Rehm, B.H. and Hancock, R.E., 2008. Human host defense peptide LL-37 prevents bacterial biofilm formation. Infection and immunity, 76(9), pp.4176-4182.

P

- Panchal, B., Bagdadi, A. and Roy, I., 2013. Polyhydroxyalkanoates: the natural polymers produced by bacterial fermentation. In Advances in natural polymers (pp. 397-421). Springer, Berlin, Heidelberg.
- Park, S.J., Kim, T.W., Kim, M.K., Lee, S.Y. and Lim, S.C., 2012. Advanced bacterial polyhydroxyalkanoates: towards a versatile and sustainable platform for unnatural tailor-made polyesters. Biotechnology advances, 30(6), pp.1196-1206.
- Pavlukhina, S.V., Kaplan, J.B., Xu, L., Chang, W., Yu, X., Madhyastha, S., Yakandawala, N., Mentbayeva, A., Khan, B. and Sukhishvili, S.A., 2012. Noneluting enzymatic antibiofilm coatings. ACS applied materials & interfaces, 4(9), pp.4708-4716.

- Percival, S.L., Bowler, P.G. and Russell, D., 2005. Bacterial resistance to silver in wound care. Journal of hospital infection, 60(1), pp.1-7.
- PeŠŠková, V., Kubies, D., Hulejova, H. and Himmlova, L., 2007. The influence of implant surface properties on cell adhesion and proliferation. Journal of Materials Science: Materials in Medicine, 18(3), pp.465-473.
- Pfalzgraff, A., Brandenburg, K. and Weindl, G., 2018. Antimicrobial peptides and their therapeutic potential for bacterial skin infections and wounds. Frontiers in pharmacology, 9, p.281.
- Pramanik, N., Mitra, T., Khamrai, M., Bhattacharyya, A., Mukhopadhyay, P., Gnanamani, A., Basu, R.K. and Kundu, P.P., 2015. Characterization and evaluation of curcumin loaded guar gum/polyhydroxyalkanoates blend films for wound healing applications. RSC Advances, 5(78), pp.63489-63501.
- Philip, S., Keshavarz, T. and Roy, I., 2007. Polyhydroxyalkanoates: biodegradable polymers with a range of applications. Journal of Chemical Technology and Biotechnology, 82(3), pp.233-247.
- Piras, A.M., Maisetta, G., Sandreschi, S., Gazzarri, M., Bartoli, C., Grassi, L., Esin, S., Chiellini, F. and Batoni, G., 2015. Chitosan nanoparticles loaded with the antimicrobial peptide temporin B exert a long-term antibacterial activity in vitro against clinical isolates of Staphylococcus epidermidis.Frontiers in microbiology, 6, p.372.
- Poblete-Castro, I., Binger, D., Rodrigues, A., Becker, J., dos Santos, V.A.M. and Wittmann, C., 2013. In-silico-driven metabolic engineering of Pseudomonas putida for enhanced production of poly-hydroxyalkanoates. Metabolic engineering, 15, pp.113-123.
- Ponnusamy, K., Kappachery, S., Thekeettle, M., Song, J.H. and Kweon, J.H., 2013. Anti-biofouling property of vanillin on Aeromonas hydrophila initial biofilm on various membrane surfaces. World Journal of Microbiology and Biotechnology, 29(9), pp.1695-1703.
- Powers, J.P.S. and Hancock, R.E., 2003. The relationship between peptide structure and antibacterial activity. Peptides, 24(11), pp.1681-1691.
- Prabuseenivasan, S., Jayakumar, M. and Ignacimuthu, S., 2006. In vitro antibacterial activity of some plant essential oils. BMC complementary and alternative medicine, 6(1), p.39.

Q

- Qin, Y., Yang, J. and Xue, J., 2015. Characterization of antimicrobial poly (lactic acid)/poly (trimethylene carbonate) films with cinnamaldehyde. Journal of materials science, 50(3), pp.1150-1158.

R

- Rahmati, M., Pennisi, C.P., Budd, E., Mobasheri, A. and Mozafari, M., 2018. Biomaterials for Regenerative Medicine: Historical Perspectives and Current Trends.
- Rai, R., Keshavarz, T., Roether, J.A., Boccaccini, A.R. and Roy, I., 2011. Medium chain length polyhydroxyalkanoates, promising new biomedical materials for the future. Materials Science and Engineering: R: Reports, 72(3), pp.29-47.
- Rai, R., Boccaccini, A.R., Knowles, J.C., Mordon, N., Salih, V., Locke, I.C., Moshrefi-Torbati, M., Keshavarz, T. and Roy, I., 2011b. The homopolymer poly (3-hydroxyoctanoate) as a matrix material for soft tissue engineering. Journal of Applied Polymer Science, 122(6), pp.3606-3617.
- Rai, R., Yunos, D.M., Boccaccini, A.R., Knowles, J.C., Barker, I.A., Howdle, S.M., Tredwell, G.D., Keshavarz, T. and Roy, I., 2011c. Poly-3-hydroxyoctanoate P (3HO), a medium chain length polyhydroxyalkanoate homopolymer from Pseudomonas mendocina. Biomacromolecules, 12(6), pp.2126-2136.
- Ramakrishna, S., Mayer, J., Wintermantel, E. and Leong, K.W., 2001. Biomedical applications of polymer-composite materials: a review. Composites science and technology, 61(9), pp.1189-1224.
- Ramasubbu, N., Thomas, L.M., Ragunath, C. and Kaplan, J.B., 2005. Structural analysis of dispersin B, a biofilm-releasing glycoside hydrolase from the periodontopathogen Actinobacillus actinomycetemcomitans. Journal of molecular biology, 349(3), pp.475-486.
- Ramos, H.C., Hoffmann, T., Marino, M., Nedjari, H., Presecan-Siedel, E., Dreesen, O., Glaser, P. and Jahn, D., 2000. Fermentative metabolism of Bacillus subtilis: physiology and regulation of gene expression. Journal of Bacteriology, 182(11), pp.3072-3080.
- Reis, R.L., Neves, N.M., Mano, J.F., Gomes, M.E., Marques, A.P. and Azevedo, H.S., 2008. Natural-based polymers for biomedical applications. Elsevier.

- Ren, D., Sims, J.J. and Wood, T.K., 2001. Inhibition of biofilm formation and swarming of Escherichia coli by (5Z)-4-bromo-5-(bromomethylene)-3-butyl-2 (5H)-furanone. Environmental Mic
- Renard, E., Versace, D.L., Babinot, J. and Langlois, V., 2015. tAIlorIng Surface ProPertIeS of degradable Poly (3-HydroxyalkanoateS) for bIologIcal aPPlIcatIonS. Surface Modification of Biopolymers, p.150.
- Repanas, A., Andriopoulou, S. and Glasmacher, B., 2016. The significance of electrospinning as a method to create fibrous scaffolds for biomedical engineering and drug delivery applications. Journal of Drug Delivery Science and Technology, 31, pp.137-146.
- Rojas, J., Bedoya, M. and Ciro, Y., 2015. Current Trends in the Production of Cellulose Nanoparticles and Nanocomposites for Biomedical Applications.
- Rosenberg, M. and Kjelleberg, S., 1986. Hydrophobic interactions: role in bacterial adhesion. In Advances in microbial ecology (pp. 353-393). Springer, Boston, MA.
- Ruer, S., Pinotsis, N., Steadman, D., Waksman, G. and Remaut, H., 2015. Virulence-targeted Antibacterials: Concept, Promise, and Susceptibility to Resistance Mechanisms. Chemical biology & drug design, 86(4), pp.379-399.
- Ryan, L., Lamarre, B., Diu, T., Ravi, J., Judge, P.J., Temple, A., Carr, M., Cerasoli, E., Su, B., Jenkinson, H.F. and Martyna, G., 2013. Anti-antimicrobial Peptides FOLDING-MEDIATED HOST DEFENSE ANTAGONISTS. Journal of Biological Chemistry, 288(28), pp.20162-20172.

S

- Sánchez, C.J., Mende, K., Beckius, M.L., Akers, K.S., Romano, D.R., Wenke, J.C. and Murray, C.K., 2013. Biofilm formation by clinical isolates and the implications in chronic infections. BMC infectious diseases, 13(1), p.47.
- Sanhueza, C., Acevedo, F., Rocha, S., Villegas, P., Seeger, M. and Navia, R., 2018. Polyhydroxyalkanoates as biomaterial for electrospun scaffolds. International journal of biological macromolecules.
- Schaeffer, C.R., Woods, K.M., Longo, G.M., Kiedrowski, M.R., Paharik, A.E., Büttner, H., Christner, M., Boissy, R.J., Horswill, A.R., Rohde, H. and Fey, P.D., 2015. Accumulation-

associated protein enhances Staphylococcus epidermidis biofilm formation under dynamic conditions and is required for infection in a rat catheter model. Infection and immunity, 83(1), pp.214-226.

- Segev-Zarko, L.A., Saar-Dover, R., Brumfeld, V., Mangoni, M.L. and Shai, Y., 2015. Mechanisms of biofilm inhibition and degradation by antimicrobial peptides. Biochemical Journal, 468(2), pp.259-270.
- Sengha, S.S., Anderson, A.J., Hacking, A.J. and Dawes, E.A., 1989. The production of alginate by Pseudomonas mendocina in batch and continuous culture. Microbiology, 135(4), pp.795-804.
- Shah, S.R., Tatara, A.M., D'Souza, R.N., Mikos, A.G. and Kasper, F.K., 2013. Evolving strategies for preventing biofilm on implantable materials. Materials Today, 16(5), pp.177-182.
- Shamala, T.R., Divyashree, M.S., Davis, R., Kumari, K.L., Vijayendra, S.V.N. and Raj, B., 2009. Production and characterization of bacterial polyhydroxyalkanoate copolymers and evaluation of their blends by fourier transform infrared spectroscopy and scanning electron microscopy. Indian journal of microbiology, 49(3), pp.251-258.
- Sharma, P., Munir, R., Blunt, W., Dartiailh, C., Cheng, J., Charles, T. and Levin, D., 2017. Synthesis and physical properties of polyhydroxyalkanoate polymers with different monomer compositions by recombinant Pseudomonas putida LS46 expressing a novel PHA synthase (PhaC116) enzyme. Applied Sciences, 7(3), p.242.
- Shen, S., Zhang, T., Yuan, Y., Lin, S., Xu, J. and Ye, H., 2015. Effects of cinnamaldehyde on Escherichia coli and Staphylococcus aureus membrane. Food Control, 47, pp.196-202.
- Singha, P., Locklin, J. and Handa, H., 2017. A review of the recent advances in antimicrobial coatings for urinary catheters. Acta biomaterialia, 50, pp.20-40.
- Smith, B.C., 1998. Infrared spectral interpretation: a systematic approach. CRC press.
- Song, Z., Borgwardt, L., Høiby, N., Wu, H., Sørensen, T.S. and Borgwardt, A., 2013. Prosthesis infections after orthopedic joint replacement: the possible role of bacterial biofilms. Orthopedic reviews, 5(2).
- Stefani, S., Campana, S., Cariani, L., Carnovale, V., Colombo, C., Lleo, M.M., Iula, V.D., Minicucci, L., Morelli, P., Pizzamiglio, G. and Taccetti, G., 2017. Relevance of multidrug-

resistant Pseudomonas aeruginosa infections in cystic fibrosis. International Journal of Medical Microbiology, 307(6), pp.353-362.

- Steinstraesser, L., Tack, B.F., Waring, A.J., Hong, T., Boo, L.M., Fan, M.H., Remick, D.I., Su, G.L., Lehrer, R.I. and Wang, S.C., 2002. Activity of novispirin G10 against Pseudomonas aeruginosa in vitro and in infected burns. Antimicrobial agents and chemotherapy, 46(6), pp.1837-1844.
- Stange, T.G., Evans, D.F. and Hendrickson, W.A., 1997. Nucleation and growth of defects leading to dewetting of thin polymer films. Langmuir, 13(16), pp.4459-4465.
- Stock, U.A., Sakamoto, T., Hatsuoka, S., Martin, D.P., Nagashima, M., Moran, A.M., Moses, M.A., Khalil, P.N., Schoen, F.J., Vacanti, J.P. and Mayer, J.E., 2000. Patch augmentation of the pulmonary artery with bioabsorbable polymers and autologous cell seeding. The Journal of thoracic and cardiovascular surgery, 120(6), pp.1158-1167.
- Su, Z., Li, P., Wu, B., Ma, H., Wang, Y., Liu, G., Zeng, H., Li, Z. and Wei, X., 2014. PHBVHHx scaffolds loaded with umbilical cord-derived mesenchymal stem cells or hepatocyte-like cells differentiated from these cells for liver tissue engineering. Materials Science and Engineering: C, 45, pp.374-382.
- Subbiahdoss, G., Fernández, I.C.S., da Silva Domingues, J.F., Kuijer, R., Van der Mei, H.C. and Busscher, H.J., 2011. In vitro interactions between bacteria, osteoblast-like cells and macrophages in the pathogenesis of biomaterial-associated infections. PLoS One, 6(9), p.e24827.
- Szewczyk, P., Ura, D., Metwally, S., Knapczyk-Korczak, J., Gajek, M., Marzec, M., Bernasik, A. and Stachewicz, U., 2019. Roughness and Fiber Fraction Dominated Wetting of Electrospun Fiber-Based Porous Meshes. Polymers, 11(1), p.34.

T

- Thakor, N., Trivedi, U. and Patel, K.C., 2005. Biosynthesis of medium chain length poly (3-hydroxyalkanoates)(mcl-PHAs) by Comamonas testosteroni during cultivation on vegetable oils. Bioresource technology, 96(17), pp.1843-1850.
- The European Committee on Antimicrobial Susceptibility Testing. Breakpoint tables for interpretation of MICs and zone diameters.Version 9.0, 2019. http://www.eucast.org.

- Tamada, Y. and Ikada, Y., 1993. Effect of preadsorbed proteins on cell adhesion to polymer surfaces. Journal of colloid and interface science, 155(2), pp.334-339.
- Tanadchangsaeng, N. and Yu, J., 2015. Thermal stability and degradation of biological terpolyesters over a broad temperature range. Journal of Applied Polymer Science, 132(13).
- Tenover, F.C., 2006. Mechanisms of antimicrobial resistance in bacteria. The American journal of medicine, 119(6), pp.S3-S10.
- Tian, W., Hong, K., Chen, G.Q., Wu, Q., Zhang, R.Q. and Huang, W., 2000. Production of polyesters consisting of medium chain length 3-hydroxyalkanoic acids by Pseudomonas mendocina 0806 from various carbon sources. Antonie van Leeuwenhoek, 77(1), pp.31-36.
- Tiso, T., Wierckx, N. and Blank, L., 2014. Non-pathogenic Pseudomonas as platform for industrial biocatalysis. Industrial biocatalysis. Pan Stanford, Singapore, pp.323-372.
- Tong, H.W. and Wang, M., 2011. Electrospinning of poly (hydroxybutyrate-co-hydroxyvalerate) fibrous scaffolds for tissue engineering applications: effects of electrospinning parameters and solution properties. Journal of Macromolecular Science, Part B, 50(8), pp.1535-1558.
- Tong, H.W. and Wang, M., 2011. An investigation into the influence of electrospinning parameters on the diameter and alignment of poly (hydroxybutyrate-co-hydroxyvalerate) fibers. Journal of Applied Polymer Science, 120(3), pp.1694-1706.

V

- Valappil, S.P., Misra, S.K., Boccaccini, A.R. and Roy, I., 2006. Biomedical applications of polyhydroxyalkanoates, an overview of animal testing and in vivo responses. Expert Review of Medical Devices, 3(6), pp.853-868.
- Valappil, S.P., Boccaccini, A.R., Bucke, C. and Roy, I., 2007. Polyhydroxyalkanoates in Gram-positive bacteria: insights from the genera Bacillus and Streptomyces. *Antonie van leeuwenhoek*, *91*(1), pp.1-17.
- Van de Velde, K. and Kiekens, P., 2002. Biopolymers: overview of several properties and consequences on their applications. Polymer testing, 21(4), pp.433-442.

- Van de Witte, P., Dijkstra, P.J., Van den Berg, J.W.A. and Feijen, J., 1996. Phase separation processes in polymer solutions in relation to membrane formation. Journal of membrane science, 117(1-2), pp.1-31.
- Van Oeveren, W., 2013. Obstacles in haemocompatibility testing. Scientifica, 2013.
- Ventola, C.L., 2015. The antibiotic resistance crisis: part 1: causes and threats. Pharmacy and Therapeutics, 40(4), p.277.
- Versace, D.L., Ramier, J., Grande, D., Andaloussi, S.A., Dubot, P., Hobeika, N., Malval, J.P., Lalevee, J., Renard, E. and Langlois, V., 2013. Versatile photochemical surface modification of biopolyester microfibrous scaffolds with photogenerated silver nanoparticles for antibacterial activity. Advanced healthcare materials, 2(7), pp.1008-1018.
- Vieira, M.G.A., da Silva, M.A., dos Santos, L.O. and Beppu, M.M., 2011. Natural-based plasticizers and biopolymer films: A review. European Polymer Journal, 47(3), pp.254-263.
- Vollmer, W., Blanot, D. and De Pedro, M.A., 2008. Peptidoglycan structure and architecture. FEMS microbiology reviews, 32(2), pp.149-167.
- Volova, T., Goncharov, D., Sukovatyi, A., Shabanov, A., Nikolaeva, E. and Shishatskaya, E., 2014. Electrospinning of polyhydroxyalkanoate fibrous scaffolds: effects on electrospinning parameters on structure and properties. Journal of Biomaterials Science, Polymer Edition, 25(4), pp.370-393.

W

- Walsh, C., 2000. Molecular mechanisms that confer antibacterial drug resistance. Nature, 406(6797), p.775.
- Wang, X., Preston, J.F. and Romeo, T., 2004. The pgaABCD locus of Escherichia coli promotes the synthesis of a polysaccharide adhesin required for biofilm formation. Journal of bacteriology, 186(9), pp.2724-2734.
- Wang, J., He, Y., Maitz, M.F., Collins, B., Xiong, K., Guo, L., Yun, Y., Wan, G. and Huang, N., 2013. A surface-eroding poly (1, 3-trimethylene carbonate) coating for fully biodegradable magnesium-based stent applications: toward better biofunction, biodegradation and biocompatibility. Acta biomaterialia, 9(10), pp.8678-8689.

- Wang, Y., Jayan, G., Patwardhan, D. and Phillips, K.S., 2017. Antimicrobial and anti-biofilm medical devices: public health and regulatory science challenges. In Antimicrobial Coatings and Modifications on Medical Devices (pp. 37-65). Springer, Cham.
- Ward, I.M. and Hadley, D.W., 1993. An introduction to the mechanical properties of solid polymers.
- Welch, M., Mikkelsen, H., Swatton, J.E., Smith, D., Thomas, G.L., Glansdorp, F.G. and Spring, D.R., 2005. Cell–cell communication in Gram-negative bacteria. Molecular BioSystems, 1(3), pp.196-202.
- Wilson, C.J., Clegg, R.E., Leavesley, D.I. and Pearcy, M.J., 2005. Mediation of biomaterial–cell interactions by adsorbed proteins: a review. Tissue engineering, 11(1-2), pp.1-18.
- Wu, J., Xue, K., Li, H., Sun, J. and Liu, K., 2013. Improvement of PHBV scaffolds with bioglass for cartilage tissue engineering. PloS one, 8(8), p.e71563.
- Wu, H., Moser, C., Wang, H.Z., Høiby, N. and Song, Z.J., 2015. Strategies for combating bacterial biofilm infections. International journal of oral science, 7(1), p.1.

Y

- Yang, L., Liu, Y., Wu, H., Song, Z., Høiby, N., Molin, S. and Givskov, M., 2012. Combating biofilms. FEMS Immunology & Medical Microbiology, 65(2), pp.146-157.
- Yasir, M., Willcox, M. and Dutta, D., 2018. Action of Antimicrobial Peptides against Bacterial Biofilms. Materials, 11(12), p.2468.
- Yasuniwa, M., Tsubakihara, S. and Fujioka, T., 2003. X-ray and DSC studies on the melt-recrystallization process of poly (butylene naphthalate). Thermochimica acta, 396(1-2), pp.75-78.
- Yoo, H.S., Kim, T.G. and Park, T.G., 2009. Surface-functionalized electrospun nanofibers for tissue engineering and drug delivery. Advanced drug delivery reviews, 61(12), pp.1033-1042.

- Yuan, Y. and Lee, T.R., 2013. Contact angle and wetting properties. In Surface science techniques (pp. 3-34). Springer, Berlin, Heidelberg.

Z

- Zhang, Z. and Wagner, V.E. eds., 2017. Antimicrobial Coatings and Modifications on Medical Devices. Springer.
- Zhang, J., Rui, X., Wang, L., Guan, Y., Sun, X. and Dong, M., 2014. Polyphenolic extract from Rosa rugosa tea inhibits bacterial quorum sensing and biofilm formation. Food control, 42, pp.125-131.
- Zhang, J., Shishatskaya, E.I., Volova, T.G., da Silva, L.F. and Chen, G.Q., 2018. Polyhydroxyalkanoates (PHA) for therapeutic applications. Materials Science and Engineering: C, 86, pp.144-150.
- Zhang, H., Zhou, W., Zhang, W., Yang, A., Liu, Y., Jiang, Y., Huang, S. and Su, J., 2014. Inhibitory effects of citral, cinnamaldehyde, and tea polyphenols on mixed biofilm formation by foodborne Staphylococcus aureus and Salmonella enteritidis. Journal of food protection, 77(6), pp.927-933.
- Zhao, K., Deng, Y., Chen, J.C. and Chen, G.Q., 2003. Polyhydroxyalkanoate (PHA) scaffolds with good mechanical properties and biocompatibility. Biomaterials, 24(6), pp.1041-1045.
- Zhou, X. and Li, Y. eds., 2015. Atlas of Oral Microbiology: From Healthy Microflora to Disease. Academic Press.
- Zhu, C., Tan, H., Cheng, T., Shen, H., Shao, J., Guo, Y., Shi, S. and Zhang, X., 2013. Human b-defensin 3 inhibits antibiotic-resistant Staphylococcus biofilm formation. journal of surgical research 183(1), pp.204-213.
- Zhu, M. and Dai, X., 2019. Growth suppression by altered (p) ppGpp levels results from non-optimal resource allocation in Escherichia coli. Nucleic acids research.
- Zonari, A., Noviöoff, S., Electo, N.R., Breyner, N.M., Gomes, D.A., Martins, A., Neves, N.M., Reis, R.L. and Goes, A.M., 2012. Endothelial differentiation of human stem cells seeded onto electrospun polyhydroxybutyrate/polyhydroxybutyrate-co-hydroxyvalerate fiber mesh. *PLoS One*, *7*(4), p.e35422.f

8 Appendix

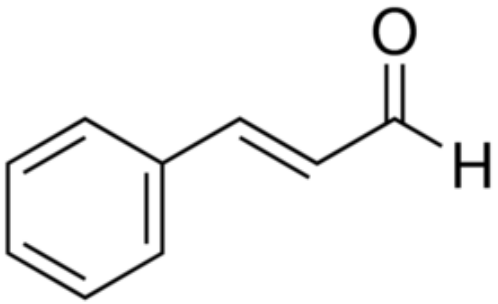

Figure 64: Chemical structure of TC.

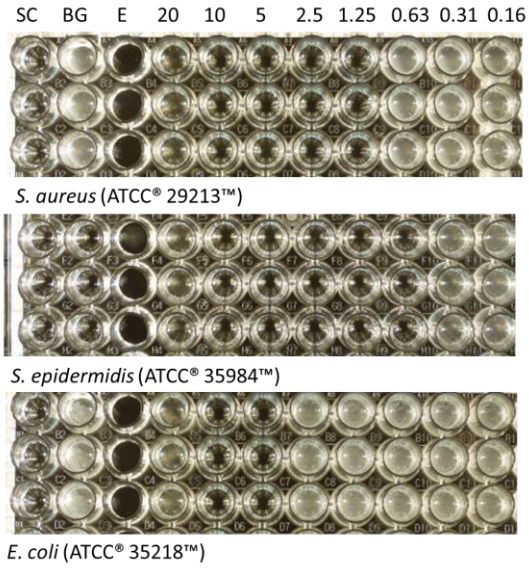

Figure 65: From top to bottom, appearance of wells of 96 TCPS microplates inoculated with *S. aureus* (ATCC® 29213™), *S. epidermidis* (ATCC® 35984™) and *E. coli* (ATCC® 35218™) after the exposure to increasing concentrations of TC for a period of 24 hours. Column 1 represents the sterility control (SC); column 2 represents the bacterial growth control (BG); column 3 represents an empty well (E); columns 4-11 represent wells with serial two-fold dilutions of TC.

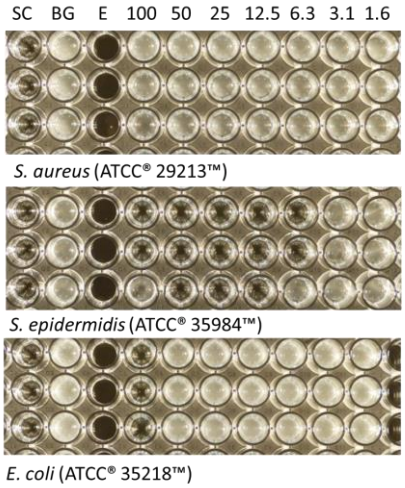

Figure 66: From top to bottom, appearance of wells of 96 TCPS microplates inoculated with *S. aureus* (ATCC® 29213™), *S. epidermidis* (ATCC® 35984™) and *E. coli* (ATCC® 35218™) after the exposure to increasing concentrations of Nut2 for a period of 24 hours. Column 1 represents the sterility control (SC); column 2 represents the bacterial growth control (BG); column 3 represents an empty well (E); columns 4-11 represent wells with serial two-fold dilutions of Nut2.

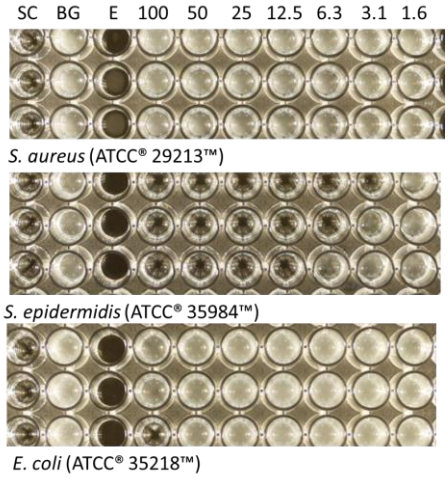

Figure 67: From top to bottom, appearance of wells of 96 TCPS microplates inoculated with *S. aureus* (ATCC® 29213™), *S. epidermidis* (ATCC® 35984™) and *E. coli* (ATCC® 35218™) after the exposure to increasing concentrations of AMP3 for a period of 24 hours. Column 1 represents the sterility control (SC); column 2 represents the bacterial growth control (BG); column 3 represents an empty well (E); columns 4-11 represent wells with serial two-fold dilutions of AMP3.

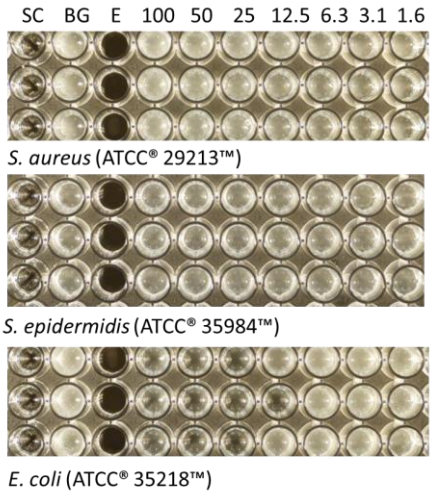

Figure 68: From top to bottom, appearance of wells of 96 TCPS microplates inoculated with *S. aureus* (ATCC® 29213™), *S. epidermidis* (ATCC® 35984™) and *E. coli* (ATCC® 35218™) after the exposure to increasing concentrations of LL-37 for a period of 24 hours. Column 1 represents the sterility control (SC); column 2 represents the bacterial growth control (BG); column 3 represents an empty well (E); columns 4-11 represent wells with serial two-fold dilutions of LL-37.

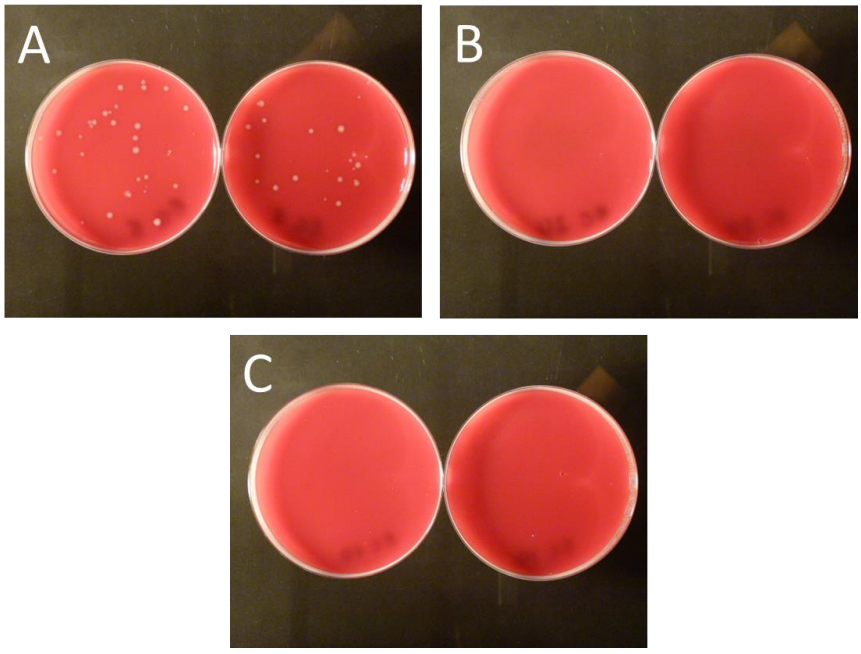

Figure 69: Appearance of blood agar plates after being incubated with 100 µL of the supernatant corresponding to the MIC and of two concentrations above the MIC of TC against *E. coli* (ATCC® 35218™) for a period of 24 hours A – 5 mM TC; B – 10 mM TC; C – 20 mM TC.

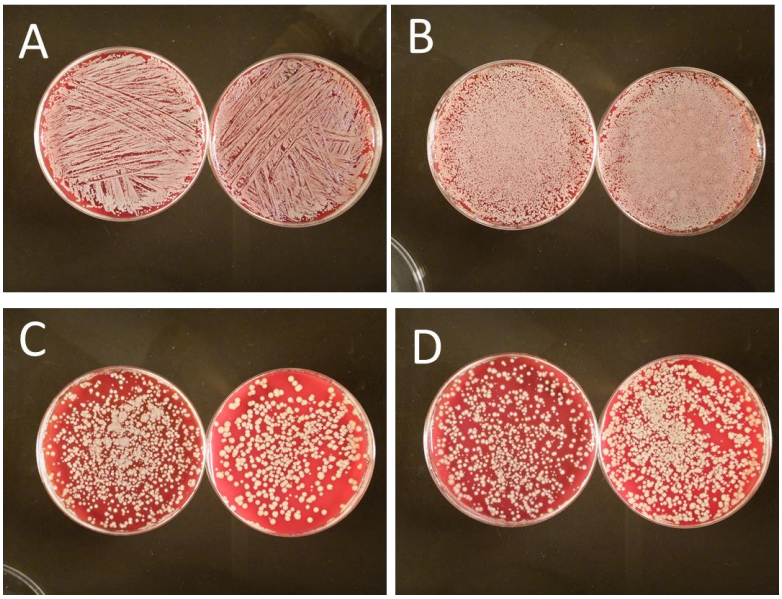

Figure 70: Appearance of blood agar plates after being incubated with 100 µL of the supernatant corresponding to the MIC and of three concentrations above the MIC of TC against *S. aureus* (ATCC® 29213™) for a period of 24 hours A – 1.25 mM TC; B – 2.5 mM TC; C – 5 mM TC; D – 10 mM TC.

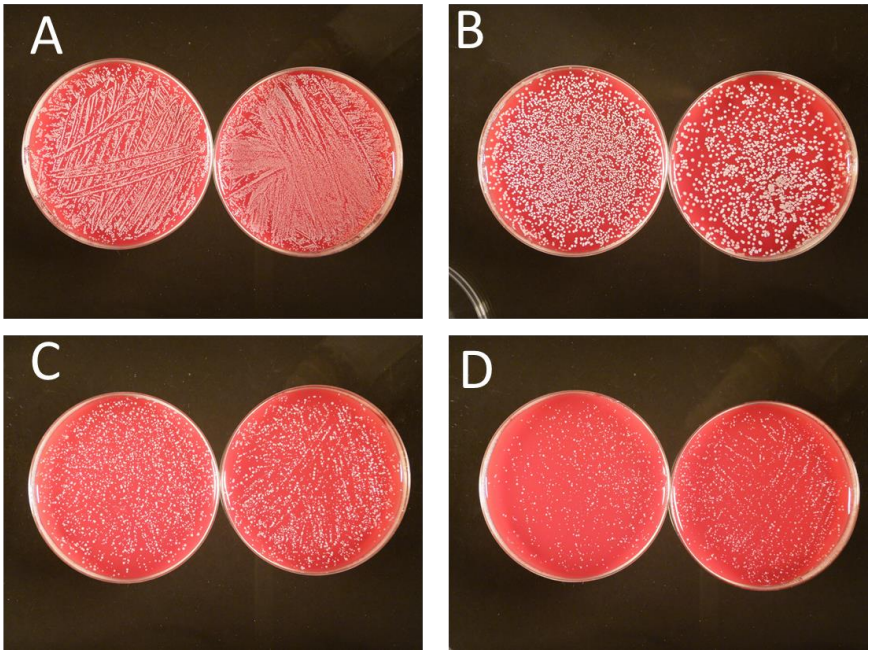

Figure 71: Appearance of blood agar plates after being incubated with 100 µL of the supernatant corresponding to the MIC and of three concentrations above the MIC of TC against *S. epidermidis* (ATCC® 35984™) for a period of 24 hours A – 0.63 mM TC; B – 1.25 mM TC; C – 2.5 mM TC; D – 5 mM TC.

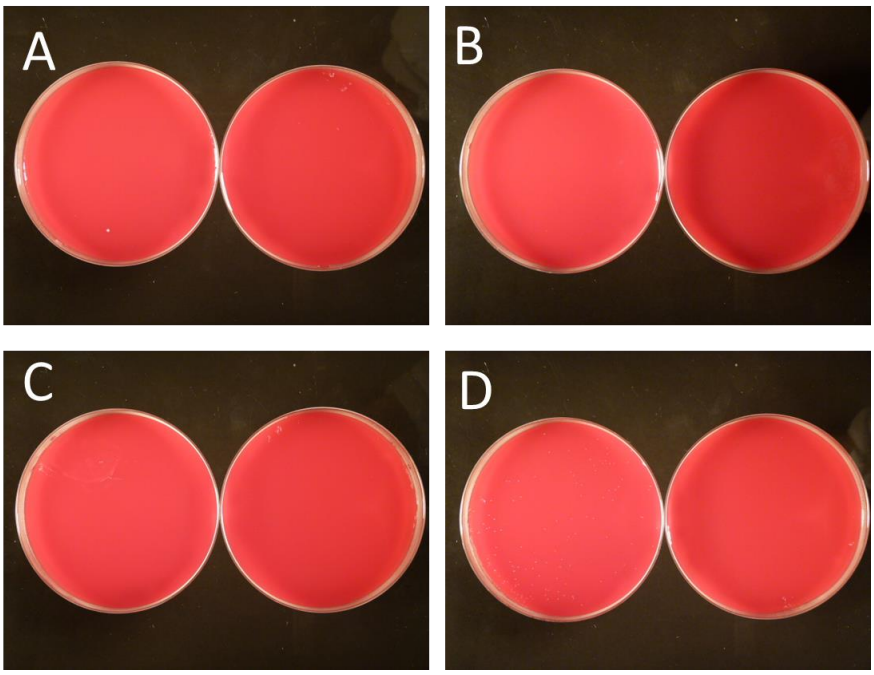

Figure 72: Appearance of blood agar plates after being incubated with 100 µL of the supernatant corresponding to the MIC and of three concentrations above the MIC of Nut2 against *S. epidermidis* (ATCC® 35984™) for a period of 24 hours A – 12.5 µg/mL Nut2; B – 25 µg/mL Nut2; C – 50 µg/mL Nut2; D – 100 µg/mL Nut2.

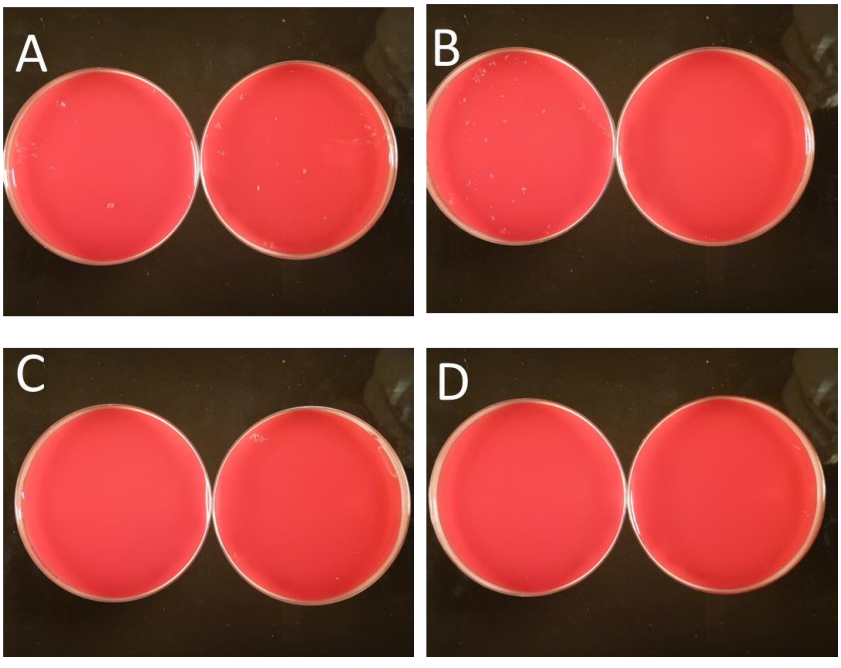

Figure 73: Appearance of blood agar plates after being incubated with 100 µL of the supernatant corresponding to the MIC and of three concentrations above the MIC of AMP3 against *S. epidermidis* (ATCC® 35984™) for a period of 24 hours A – 6.3 µg/mL AMP3; B – 12.5 µg/mL AMP3; C – 25 µg/mL AMP3; D – 50 µg/mL AMP3.

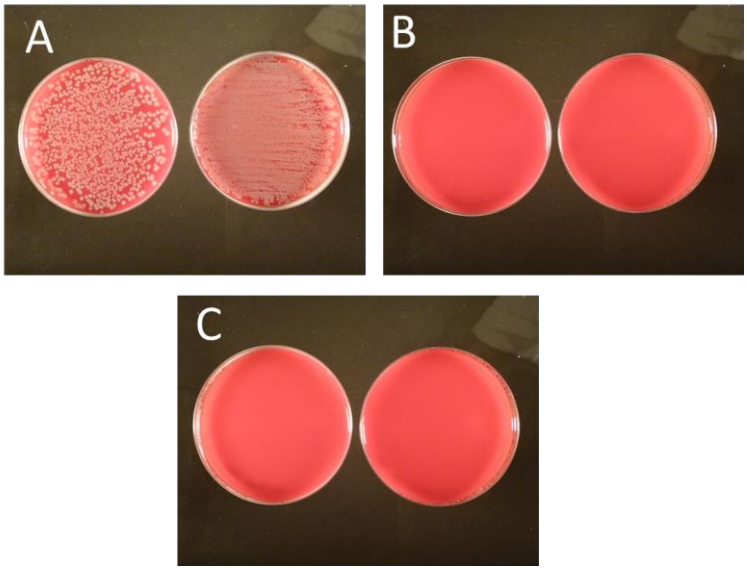

Figure 74: Appearance of blood agar plates after being incubated with 100 µL of the supernatant corresponding to the MIC and of two concentrations above the MIC of LL-37 against *E. coli* (ATCC® 35218™) for a period of 24 hours A – 25 µg/mL LL-37; B – 50 µg/mL LL-37; C – 100 µg/mL LL-37.

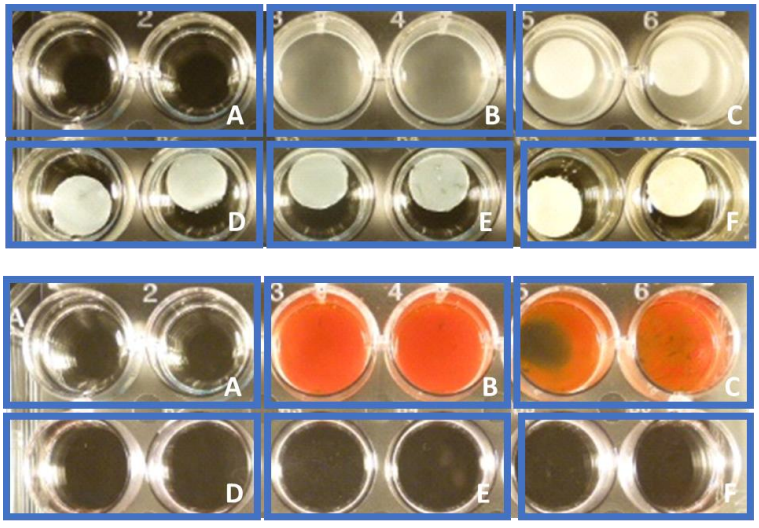

Figure 75: Upper picture, differences in the supernatant present on wells of 24 TCPS microplates inoculated with *S. epidermidis* (ATCC® 35984™) after the exposure to non-loaded and loaded P(3HB) films with TC for a period of 7 consecutive days. Bottom picture, appearance of the same wells of 24 TCPS microplates after removal, washing, fixation and staining of biofilms with safranin. A – Sterility control; B – Bacterial growth control; C – P(3HB); D – P(3HB) 11.5 wt% TC; E – P(3HB) 13 wt% TC; F – P(3HB) 16.7 wt% TC.

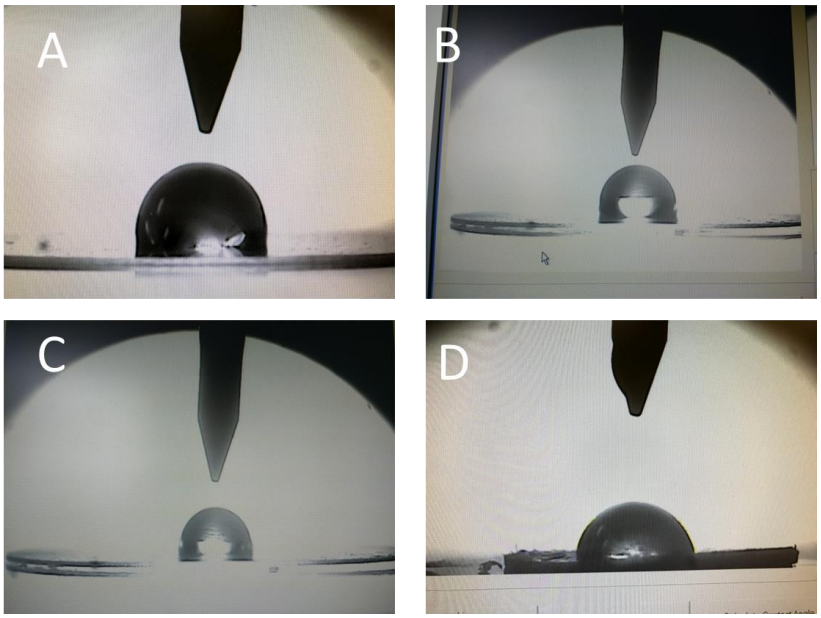

Figure 76: Images of water droplets on different fibre mesh surfaces. A – P(3HO-co-3HD); B - P(3HO-co-3HD)/Nut2; C- P(3HO-co-3HD)/Nut2+DB; D - P(3HO-co-3HD)/DB.

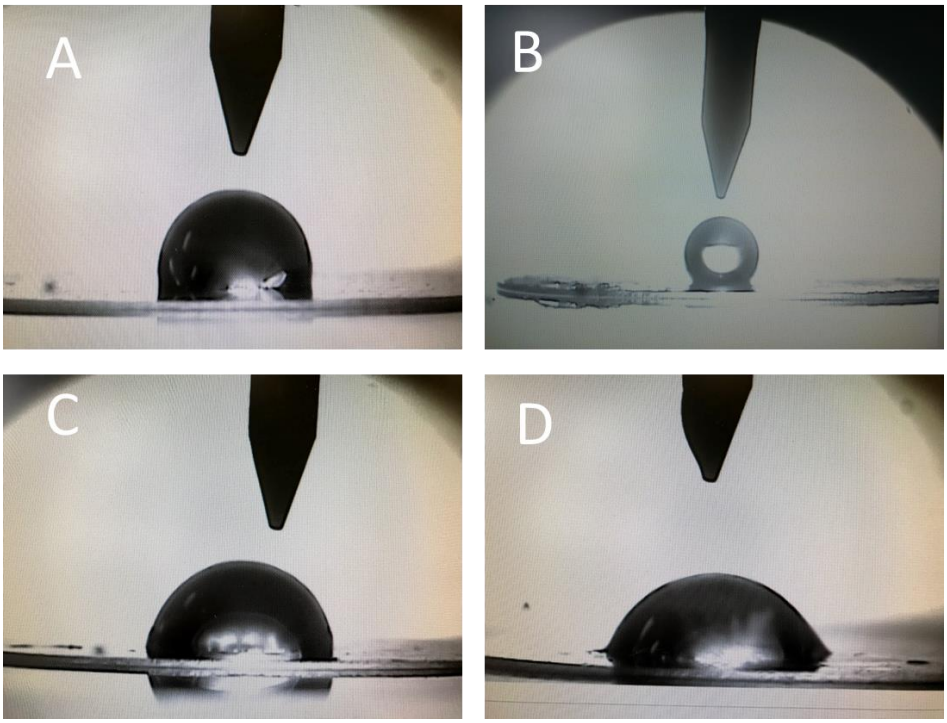

Figure 77: Images of water droplets on different fibre mesh surfaces. A – P(3HO-co-3HD); B - P(3HO-co-3HD)-NCO-sP(EO-stat-PO); C- P(3HO-co-3HD)-NCO-sP(EO-stat-PO)-AMP3; D - P(3HO-co-3HD)-NCO-sP(EO-stat-PO)AMP3+DB.

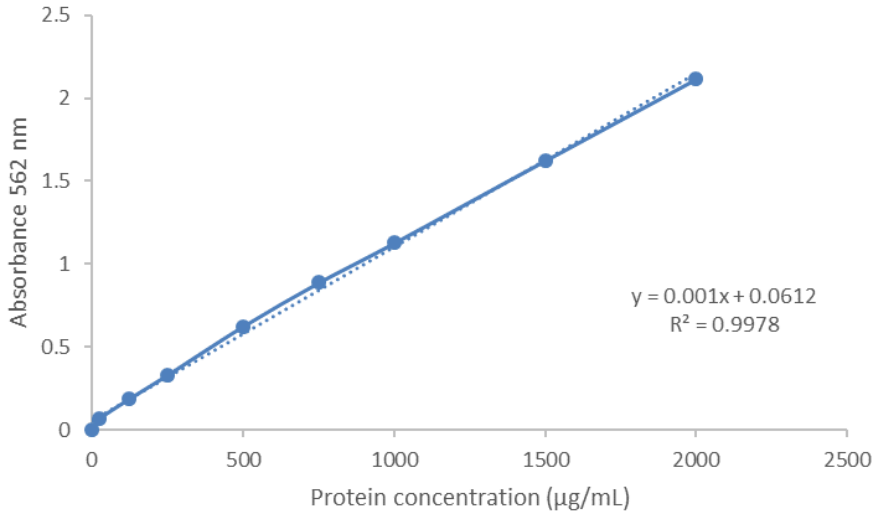

Figure 78: BCA calibration curve made from bovine serum albumin standards.

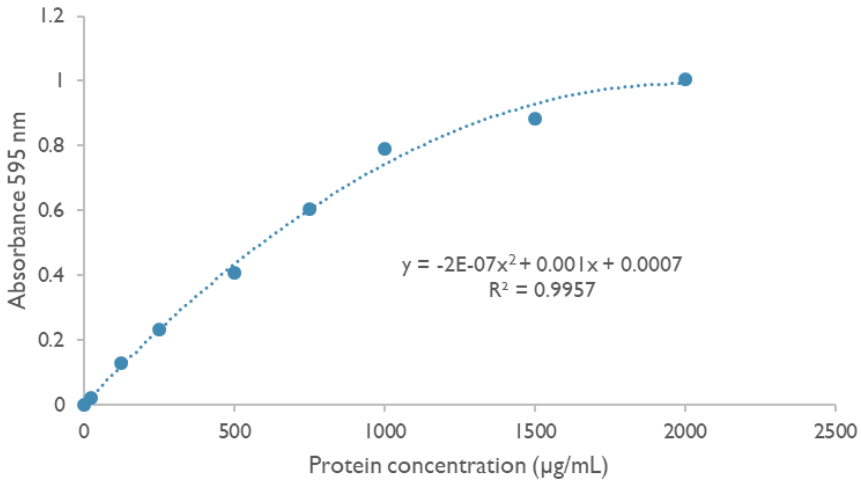

Figure 79: Bradford calibration curve made from bovine serum albumin standards.

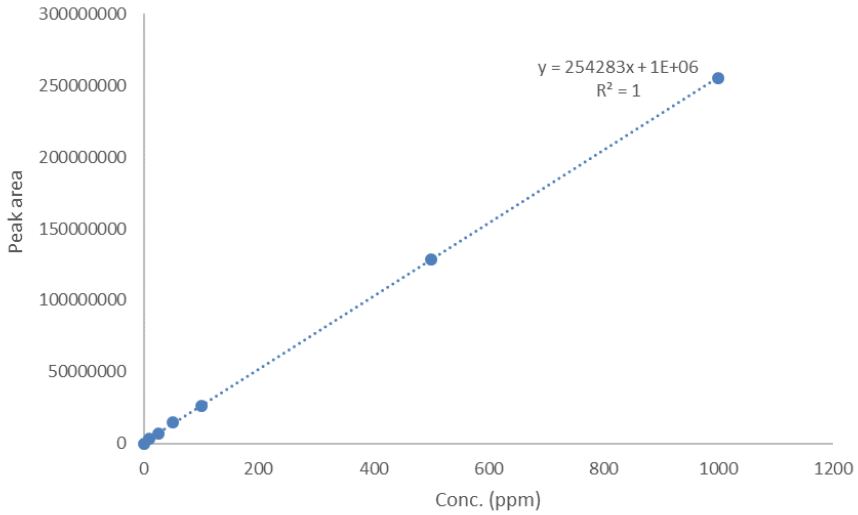

Figure 80: TC calibration curve made from serial dilutions of TC in chloroform.